http://eprints.soton.ac.uk

UNIVERSITY OF SOUTHAMPTON

FACULTY OF ENGINEERING, SCIENCE AND MATHEMATICS

INSTITUTE OF SOUND AND VIBRATION RESEARCH

A METHODOLOGY FOR DEVELOPING HIGH DAMPING MATERIALS WITH APPLICATION TO NOISE REDUCTION OF RAILWAY TRACK

by

NAZIRAH AHMAD

Thesis submitted for the degree of Doctor of Philosophy

February 2009

UNIVERSITY OF SOUTHAMPTON

ABSTRACT

FACULTY OF ENGINEERING, SCIENCE AND MATHEMATICS
INSTITUTE OF SOUND AND VIBRATION RESEARCH

Doctor of Philosopy

A METHODOLOGY FOR DEVELOPING HIGH DAMPING MATERIALS WITH
APPLICATION TO NOISE REDUCTION OF RAILWAY TRACK

by NAZIRAH AHMAD

For application in damping treatments, elastomeric materials should have a high damping loss factor, but this is inevitably linked to a strong temperature-dependence of the dynamic properties. A methodology is developed that allows a material to be formulated for a particular damping application where temperature-dependence has to be taken into account. The methodology is applied to the case of a tuned absorber system used for damping the vibration of a railway track. This is required to be effective over a temperature range -20℃ to 40℃.

To investigate the effect of the temperature on the performance of a rail damper, a simple Timoshenko beam model of the track vibration is used, to which are added single-frequency and dual-frequency tuned absorbers. The results show that a high noise reduction can be achieved for the optimum stiffness, provided that the loss factor is between about 0.25 and 0.4.

In order to study the generic effects of high damping versus constant stiffness, the time-temperature superposition principle is used to convert frequency-dependence to temperature-dependence for a notional material with constant loss factor. This is used in the prediction of decay rates and thereby noise reduction. In addition, a weighted noise reduction is studied by using measured rail temperature distributions. This temperature-weighted noise reduction allows a single number measure of performance to be obtained which can be used to assess various elastomeric materials in order to determine the optimum material for a given situation.

Two types of viscoelastic material, butyl and EPDM rubbers with various amount of fillers and plasticisers are investigated. The properties of both rubbers have been measured over the range of temperatures for frequencies 300-3000 Hz. For this a test rig had to be modified. For butyl, the best combination of filler and plasticiser gives temperature weighted noise reductions up to 5.9 dB(A). Butyl rubber is suitable for use in the rail absorber giving high noise reductions between 0℃ and 40℃. The best EPDM compound gives a temperature-weighted noise reduction up to 6.2 dB(A). Comparing these two rubbers, EPDM is more suitable for low temperatures below 10℃ and butyl is more suitable for higher temperatures above 10℃.

Acknowledgements

First of all, I would especially like to thank my main supervisor, Prof. David Thompson for his patience and for supporting this work with ideas, criticism, etc. I sincerely can not help expressing how I should credit this thesis to his excellent support and guidance whenever I dropped into his office, his encouragement and stimulation throughout the duration of my research work and writing up.

I am really grateful to my other supervisors, Dr Chris Jones and Dr Alan Muhr for their invaluable support, guidance, help and comments in my research work, particularly in relation to the experimental work. Dr Chris Jones helped me to learn and understand the test rig behaviour as well as the method of testing the rubber samples to determine the dynamic properties required. Dr Alan Muhr provided me with good hints for the development and design of high damping materials for particular applications.

I am also thankful to Tun Abdul Razak Research Centre (TARRC) for providing me with an environment and support for my work. I want to thank all its staff members with whom I had numerous discussions, more or less related to this thesis, especially Hamid Ahmadi, Dr Andy Chapman, Dr Stuart Cook, Judith Picken and Roy Brown, and the mixing room staff who helped me mixing the materials.

I wish to thank all my colleagues in the Dynamics Group and ISVR staff whose names are too numerous to mention for giving me support and warm friendship during my life in the UK.

My appreciation is also addressed to Lembaga Getah Malaysia for its Scholarship throughout my study. Thanks also for their support and understanding.

Finally but most importantly, I would like to express my gratitude to my beloved husband Bardol Hussin and my children Emira, Emirol and Al-Phil who have supported, helped and loved me constantly during these years. Special thanks are also due to my parents, Ahmad and Kalthum for their unlimited love and prayers in these remarkable days.

Contents

Nomenclature

Roman Symbols

A	Beam cross-sectional area
a	Length of the sample
b	Width of the sample
c	Wave speed; $c = \sqrt{E/\rho}$
ΔH	Activation for viscous flow
ΔL	Change in length
E^*	Complex Young's modulus
F	Force
G'	The in-phase, 'storage' shear modulus
G''	The out-of-phase, 'loss' shear modulus
G^*	Complex shear modulus
$G(t - \tau)$	Relaxation modulus
h	Thickness of the sample
I	Second moment of area
$i = \sqrt{-1}$	Imaginary unit
$J(t - \tau)$	Creep compliance function
k	Wavenumber; $k = \omega/c$
K	Bulk modulus
kT	Thermal energy in degree per molecule
L_f	Frequency

L_0	Original length
S	Stiffness per unit length
S_a	Stiffness per unit length of absorber
S_p	Support stiffness per unit length
t	Time
T	Absolute temperature
T_s	Reference temperature
T_g	Glass transition temperature
$\ddot{u}$	Vertical acceleration
U	The complex amplitude
$U\Psi$	The corresponding amplitude of ϕ
V	Volume
$\triangle V$	Change of volume

Greek Symbols

α	Stress
$\alpha(T)$	Shift factor as a function of temperature
δ	Phase angle between stress and strain
Δ	Decay rate
η	Loss factor
ε	Strain
γ_0	Shear strain amplitude
κ	Shear coefficient
μ_a	Mass per unit length of absorber
μ	Viscosity
ν	Poisson's ratio
ϕ	Rotation of beam cross section

ρ	Density
τ	Time delay
τ_0	Shear stress amplitude
φ	Ratio of rotation to displacement in beam model shape
ω	Angular frequency, $\omega = 2\pi f$
ω_n	Natural frequency

Abbreviations

BR	Butadiene Rubber
CCD	Centre Composite Design
CCI	inscribed central composite design
CR	Chloroprene Rubbers
DCP	DiCumyl Peroxide
DMTA	Dynamic mechanical thermal analysis
DOF	Degree of Freedom
DSC	Differential scanning calorimetry
END	Environmental Noise Directive
EPDM	Ethylene Propylene Diene Monomer
ERRI	European Rail Research Institute
IIR	Isobutylene Isoprene (Butyl) Rubber
ISVR	Institute of Sound and Vibration Research
MBT	2-Mercapto Benzothiazole
NBR	Nitrile Butadiene Rubber
NR	Natural Rubbers
OFWHAT	Optimised Freight Wheel And Track
pphr	Part Per Hundred Rubber
PU	Polyurethane

SBR	Styrene Butadiene Rubber
SDOF	Single Degree Of Freedom
SR	Synthetic Rubbers
TARRC	Tun Abdul Razak Research Centre
TMTD	Tetramethylthiuram Disulfide
TRD	Tuned Rail Damper
TSI	Technical Specifications for Interoperability
TSM	Thermorheologically Simple Material
TTSP	Time-temperature superposition principle
TWINS	Track-Wheel Interaction Noise Software package
WLF	Williams Landel and Ferry

Chapter 1

Introduction

1.1 Background

Nowadays, people face noise problems in the work place, on the street, at home, in the shops and everywhere in their daily lives. Noise is defined as an unwanted sound, which is disturbing or annoying. There are many sources of noise, most of which are associated with urban developments such as road, air and rail transport, industrial activity, neighbourhood and recreational noise. As the population increases so do volumes of road, rail and air traffic. Hence, noise control measures are increasingly important to keep the noise to comfortable levels.

Many methods for solving noise problems are available commercially. These include damping treatments, vibration isolation, acoustic absorption and shielding. Elastomeric materials are widely used as damping treatments to reduce the vibration of components which otherwise may radiate excessive sound. Vibration isolation is also extensively based on elastomers. Their dynamic properties are therefore very important for noise control applications, but they depend strongly on temperature and also on frequency. The damping is greatest in the 'transition region' where the stiffness varies most rapidly with temperature and frequency, making it difficult to find materials with suitable properties for particular applications, especially where effectiveness is required over a range of temperatures.

One method of reducing railway noise, which becomes the main focus in this study, is to damp rail vibrations using a rail absorber. This can give a significant reduction in the component of noise radiated by the rails, as shown in Thompson *et al.* (2007). A typical absorber consists of steel masses embedded in an elastomer, which acts to dissipate vibrational energy in the rail.

To determine the most suitable elastomer for an application such as the rail absorber, it is vital to establish a design method. The approach proposed here is summarised in Figure 1.1. This design methodology is used to determine suitable high damping materials for application in damping devices, in this case, the rail absorber. Within this methodology several models are required in order to achieve the right level of performance in improving the reduction of noise. The process begins with material selection, where the dynamic properties of the material are compared to a rough target requirement. Then, the dynamic properties can be refined by modifications to the chemical formulation of the polymers. The dynamic properties are measured for an appropriate range of frequencies and temperatures, requiring a test rig. A prediction model is required to determine the noise reduction and how it is affected by the dynamic properties of the elastomer. Next, distributions of environmental temperatures are required, which can be used as weighting functions for noise reduction. This can be used to assess various elastomeric materials for the application focusing on the temperatures that occur most commonly at a given location. Based on the information gathered from those methods, suitable materials can be developed using an iterative process.
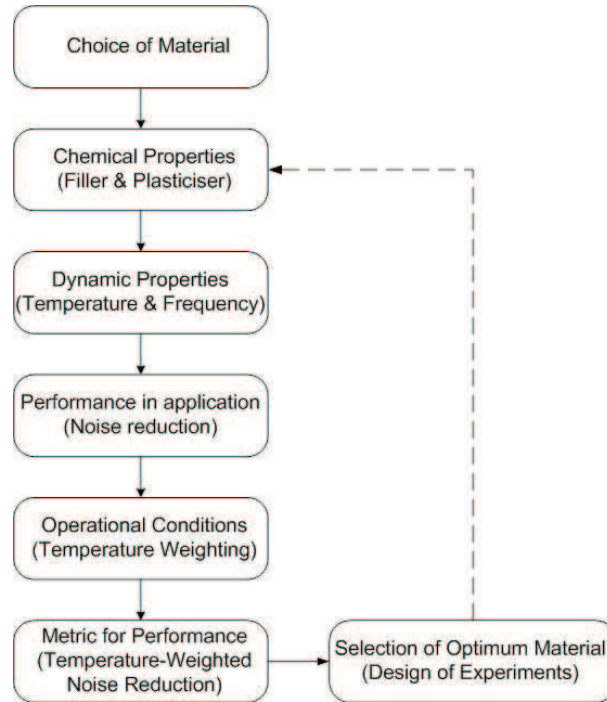
Figure 1.1: *The design method for determining suitable high damping materials for use in damping device applications.*

1.2 Railway noise

Railway transportation systems need to develop and grow as the rail passenger and freight traffic increase. In line with that, the European authorities also want to increase the usage

of railway transport relative to road transport. This policy of encouraging modal shift was also supported by the railway manufacturer association (UNIFE), whose stated aim was to double the volume of passenger and triple the freight tonne kilometers between the years 2000 to 2020 (UNIFE *et al.*, 2001). If the railway traffic volume increases that much, this will require expansion of the network with new lines and increased traffic on existing lines, which will cause considerable problems in terms of noise nuisance and will have a large impact on the environment. It can be roughly estimated that the overall noise emission will increase by 5 dB(A) unless appropriate countermeasures are taken. This may also affect human health as annoyance and sleep disturbance may increase (Miedema & Vos, 1998; UNIFE *et al.*, 2001). Annoyance and sleep disturbance are the most important health effects of environmental noise exposure.

The European Community has already acted on the transport and environmental issues above. With Directive 2002/49/EC on the assessment and management of environmental noise (END), they required noise maps from all transport and industrial sources for all conurbations in Europe by 2007. Moreover, Action Plans for major railways ($\geq$ 60,000 trains per year) and large agglomerations ($\geq$ 250,000 inhabitants) had to be drawn up by 2008 (Directive-2002/49/EC, 2002). The aim of these plans is to prevent or reduce environmental noise at exposure levels that might have harmful effects on human health as well as to preserve quieter areas.

Besides that, the European Community has also introduced noise legislation applying emission limits for new vehicles through the Technical Specifications for Interoperability (TSI) relating to the subsystem 'rolling stock noise'. In 2002, the TSI for high-speed rolling stock was introduced and later followed by conventional rolling stock. These noise limits also apply for freight wagons, in effect requiring low-noise brake blocks to be used thereby reducing the noise of these wagons by about 10 dB.

The major source of railway noise is rolling noise. It is produced by vibration of the wheel, rails and sleepers. The irregularities (roughness) of the surfaces of both wheels and rail are responsible for the generation of these vibrations. The noise radiated by the wheels is dominant at high frequency, usually above about 1.5 kHz. The spectrum of the noise emitted by the sleepers is concentrated at lower frequencies below about 400 Hz. The rail is usually the greatest source of rolling noise in the frequency range 500 to 2000 Hz and often forms the most important contribution overall (Thompson *et al.*, 2007), as shown in the example in Figure 1.2.

In order to study rolling noise, a theoretical model has been developed which has been implemented in the computer program TWINS (Track-Wheel Interaction Noise Software package) (Thompson *et al.*, 1996b) and (Thompson *et al.*, 1996a). Figure 1.3 shows an overview of the TWINS model. With this model it is possible to evaluate the rolling noise
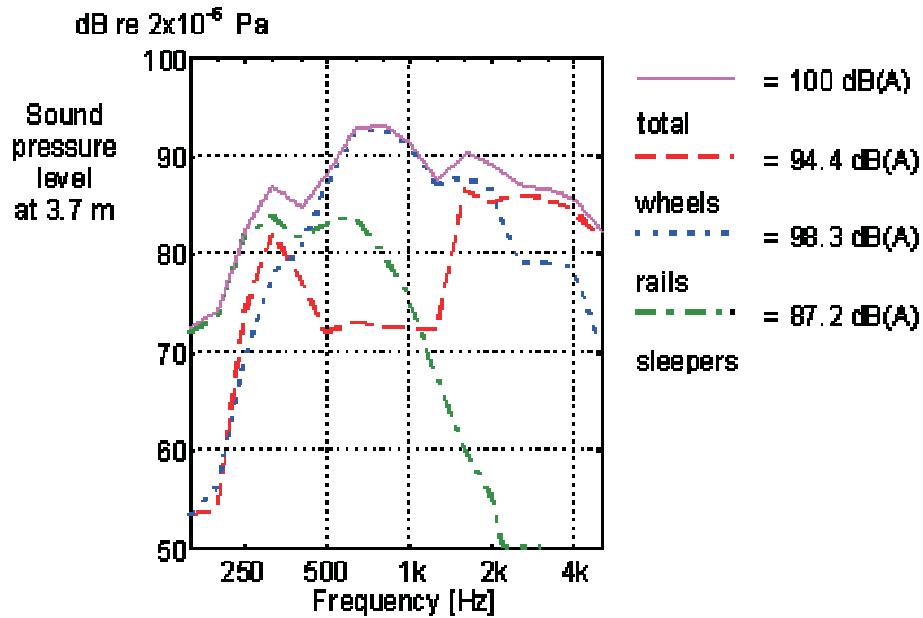
Figure 1.2: *Typical noise spectrum showing wheel, rail and sleeper noise components calculated using TWINS (Thompson* et al.*, 1996a).*

behaviour of various wheel and track designs, based on the wheel/rail roughness. There are several models available within TWINS for wheel and track analysis as shown in Figures 1.4 and 1.5. These models can be used to predict the noise from the wheel and track design at various train speeds. In validation results compared with field measurements the agreement was within 2 dB (Thompson *et al.*, 1996b).

It is known from previous research that measures to reduce the noise at source can be more attractive than the installation of high trackside barriers and increased window insulation because these are expensive. Apart from this, noise barriers cause visual nuisance, particularly because of their height. The maintenance of the barriers is also costly. Studies by Swiss Federal Railways have found that in Switzerland control of noise at source, for example by rolling stock improvements, is more effective and efficient than noise barriers and insulation of windows. They therefore spend 2/3 of the funding available on improving the rolling stock and only 1/3 on barriers and window insulation (Oertli, 2000).

Since controlling noise at source is more cost-effective and acceptable to society, it becomes a priority of significant fundamental research to satisfy enviromental needs. One example of measures that can be applied at source, is the rail damper. Rail dampers are applied to the existing railway track and have proved to be effective (Thompson *et al.*, 2007; van den Dool, 2007). Therefore, reducing the rolling noise, especially noise from the rail, by reducing its response forms the motivation for this study. In the following section the development of rail dampers, or absorbers, is described. In section 1.4 the implications for elastomeric materials are discussed.
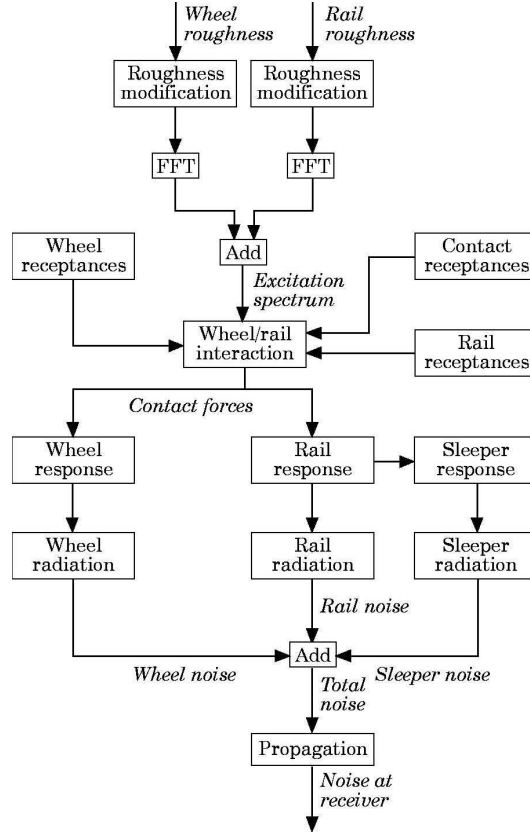
Figure 1.3: *Flow chart of the TWINS calculation method for rolling noise (Thompson et al., 1996b).*
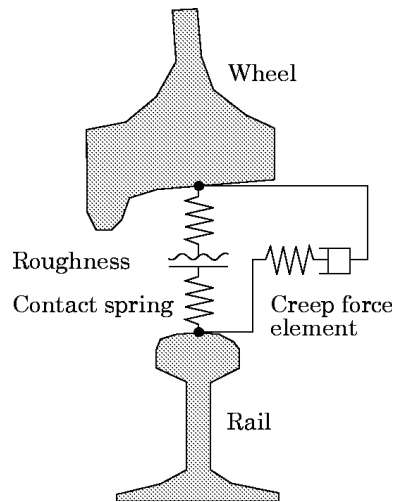
Figure 1.4: *Details of the wheel-rail interaction in the TWINS model (Thompson et al., 1996b).*
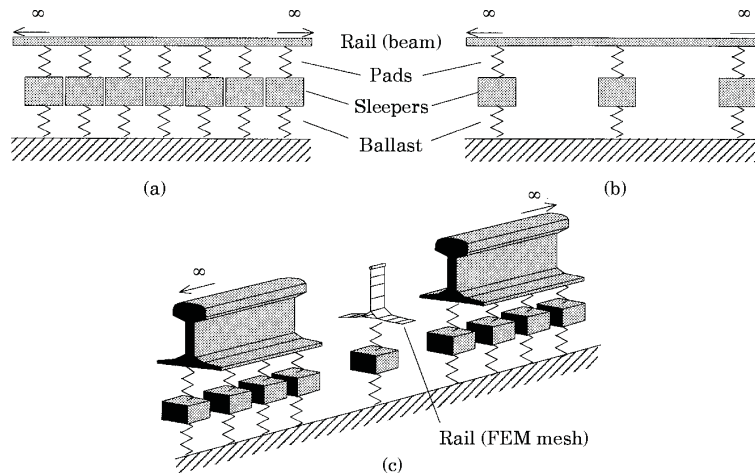
Figure 1.5: *Models for track vibration: a) continuously supported beam model; (b) periodically supported beam model; (c) continuously supported rail model including cross-sectional deformation (Thompson et al., 1996b).*

1.3   Rail absorbers

A number of different rail dampers or absorbers have been developed in recent years which are intended to reduce the rolling noise. The purpose of rail dampers is to increase the attenuation of vibration with distance along the track and thereby reduce the noise radiated by the rail. The rail damper acts as a tuned mass-spring absorber system, to damp the vibration along the track. An early prototype was developed in the OFWHAT project (Optimised Freight Wheel And Track) in 1993. This project was set up by Committee C163 of ERRI with the aim of using calculations and prototype tests to define a specification of wheel and track components for freight traffic as well as establishing an optimized solution for wheel and track (Jones & Edwards, 1996). Figure 1.6 shows the geometry of the rail damper developed in this project. These rail dampers were attached at the ends of the rail foot and fastened with bolts. They were positioned mid way between sleepers. This absorber was specified to act over the frequency range 600 Hz to 2800 Hz, (Jones & Edwards, 1996) and (Beaubatie, 1997). The experiments carried out in this project demonstrated a reduction in noise from 3 to 7 dB(A) from a combination of measures on the wheel and track as shown in Figure 1.7 and this result also validated the TWINS predictions (Fodiman, 1996). However, the effect of the absorber was only determined in combination with an optimised (stiffer) rail pad, giving an added benefit of 1 to 2 dB.

Further investigation into potential designs for both wheel and track to reduce the rolling noise was continued in the Silent Freight and Silent Track projects. The objectives of these two European projects were to develop solutions for lower noise vehicles and lower noise track. To achieve the objective, particularly for the Silent Track project, a rail damper was developed to be applied on existing or new tracks. The work began in February
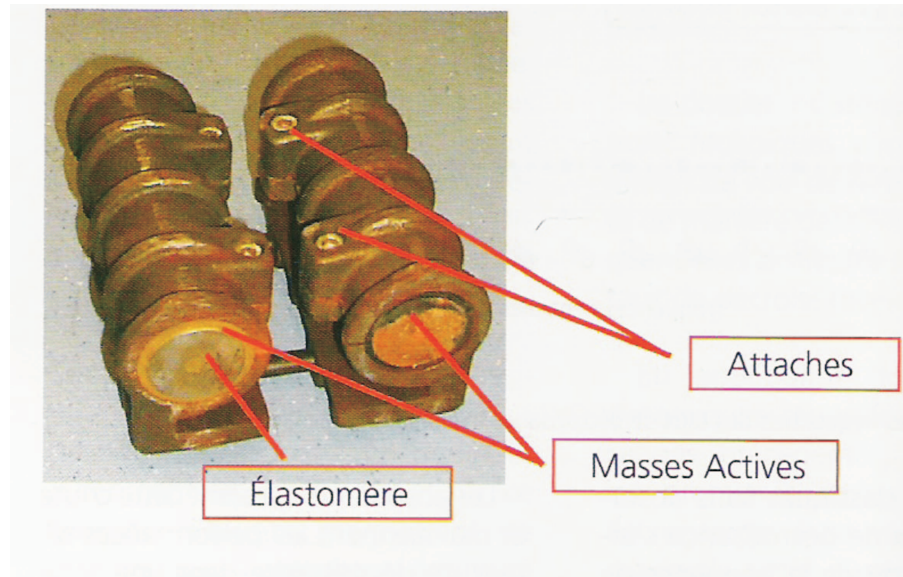
Figure 1.6: *Cross-section of OFWHAT absorber arrangement fitted to UIC60 rail (Gautier, 2000).*
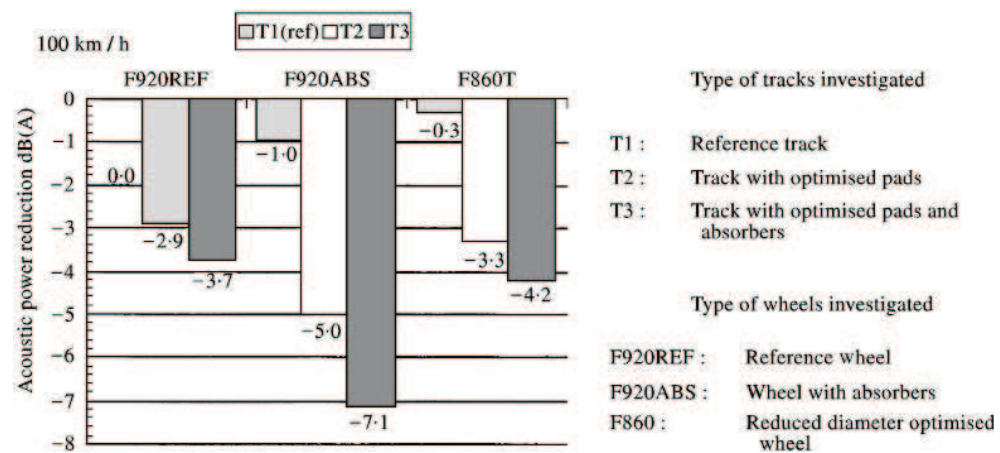
Figure 1.7: *Noise reduction obtained within the OFWHAT project of freight vehicles on different tracks (100 km/h) (Gautier, 2000).*

1996 and was completed in December 1999. The projects were both co-ordinated by ERRI and each had 11 partners including the Institute of Sound and Vibration Research (ISVR) (Hemsworth *et al.*, 2000).

In the Silent Track project, the rail damper (or tuned absorber) was designed as a 'stacked' system, as shown in Figure 1.8. It was tuned to two frequencies, 630 Hz and 1350 Hz. A validation test was carried out on a track with the prototype rail damper in the Czech Republic in 1999. The test was carried out at rail temperature of 30℃ and with a soft rail pad. The high temperature led to a lower tuning frequency, around 500 Hz. Figure 1.9 shows the sound pressure level measured with and without the rail absorber. This measurement shows an overall reduction of 5.6 dB(A); the corresponding reduction in rail noise was about 6 dB(A) (Thompson *et al.*, 2007).
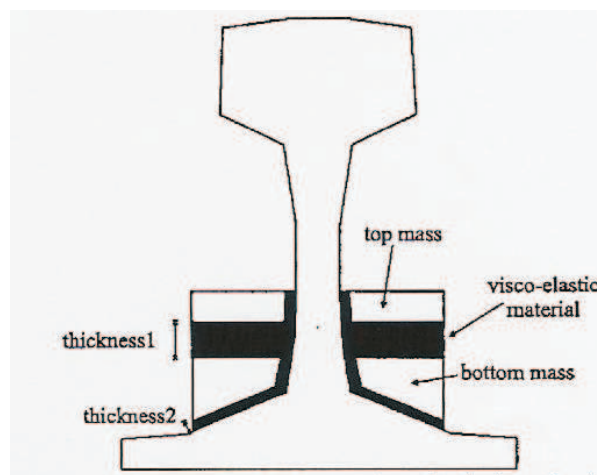
Figure 1.8: *Cross-section of Silent Track absorber arrangement fitted to UIC60 rail (Thompson* et al.*, 2000)*
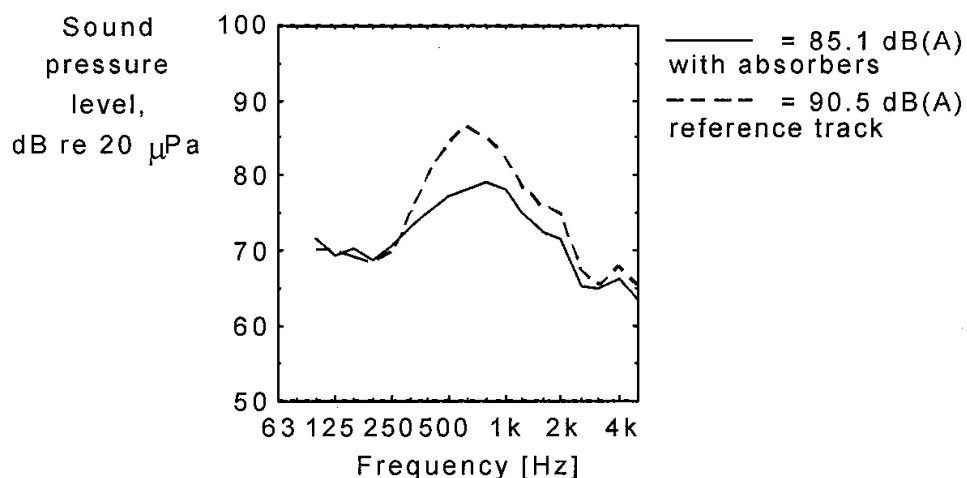
Figure 1.9: *Measurement of total rolling noise at 100 km/h with and without rail absorbers. The influence of wheel noise is minimized by using a vehicle fitted with a noise-reducing wheel. Average from three microphones at 3 m from near rail (Thompson* et al.*, 2007)*

In the development of this rail damper, an initial study was carried out using a simple track model, to identify the appropriate parameters (Thompson *et al.*, 2007). In this

model, the rail is represented by a Timoshenko beam on a continuous spring-mass-spring foundation representing the rail pad, sleeper and ballast. The mass per unit length of the absorber was 17.5 kg/m. The noise reduction was shown to increase in proportion to the added mass but this is limited by practical considerations. It was shown that the damping loss factor of the absorber should be at least 0.35. This study considered systems with one or more tuning frequencies to determine the maximum reduction of noise. A single tuning frequency was found to give significant reduction of noise when set to 800 Hz. Using two tuning frequencies at 630 Hz and 1350 Hz a slightly higher noise reduction was found, for the same overall mass. A three-frequency system was found to give only very small improvements over the two-frequency system. From this study, it was also concluded that the reduction of noise is similar for an optimum two-DOF system as for the optimum pair of SDOF systems.

In the process of development, elastomeric materials from several suppliers were tested over a frequency range 300 Hz to 3000 Hz. The materials selected from this process were satisfactory but their dynamic properties vary considerably with temperature. The frequency and temperature dependence of the elastomer properties were also included in a detailed FE model in this study. Ideally, however, the selected material should maintain a particular stiffness and sufficiently high damping over a temperature range -20℃ to 40℃ and a frequency range 100 to 3000 Hz. Therefore, further study is required to investigate the dynamic properties of elastomers in order to develop an improved material for application in this rail absorber.

Further investigation to improve the performance of the rail damper is carried out in the present project. A similar rail damper to that which was developed by Institute of Sound and Vibration Research (ISVR) and Corus Rail in the Silent Track project is studied. It consists of steel masses embedded in an elastomer, attached to the rail on either side of the lower part of the rail web and the upper surface of the rail foot (Hodgson *et al.*, 2000). A similar clip-on rail damper has more recently been developed by Corus and has been tested in France, the Netherlands, Germany and Sweden (van den Dool, 2007) and (Poisson *et al.*, 2006). This form of damper has been installed on 22 km of track in the Netherlands and France in various tests (van den Dool, 2007) achieving about 3 dB noise reduction.

Besides these rail dampers a number of other types of rail damper are available on the market which are intended to reduce rolling noise. They include Schrey and Veit (S&V) (type: VICON– AMSA 5RQ), James Walker (type: @10u8), Edilon Sedra tuned rail damper (TRD), as presented in Figure 1.10. The S&V rail dampers (as shown in Figure 1.10(a)) have been applied to the south of Rotterdam in the section of high speed line (van den Dool, 2007). Using this rail damper, a reduction of about 2.5 dB(A) was achieved. The James Walker rail damper has also been tested in the Netherlands and

consists of a pad of 24 cm including 3 viscoelastic elements with steel and a constrained layer as shown in Figure 1.10(c). Only one test has so far been carried out and the benefits were limited (van den Dool, 2007).

Another damper is the TRD from Edilon Sedra. This damper as shown in Figure 1.10(d) is fabricated from polymer containing a steel mass and intended to work in the frequency range 400-1500 Hz. The TRD is glued in the webs of the rail at both sides by using adhesive and installed between the sleepers (Edilon, 2007).

(a)

(b)

(c)

(d)
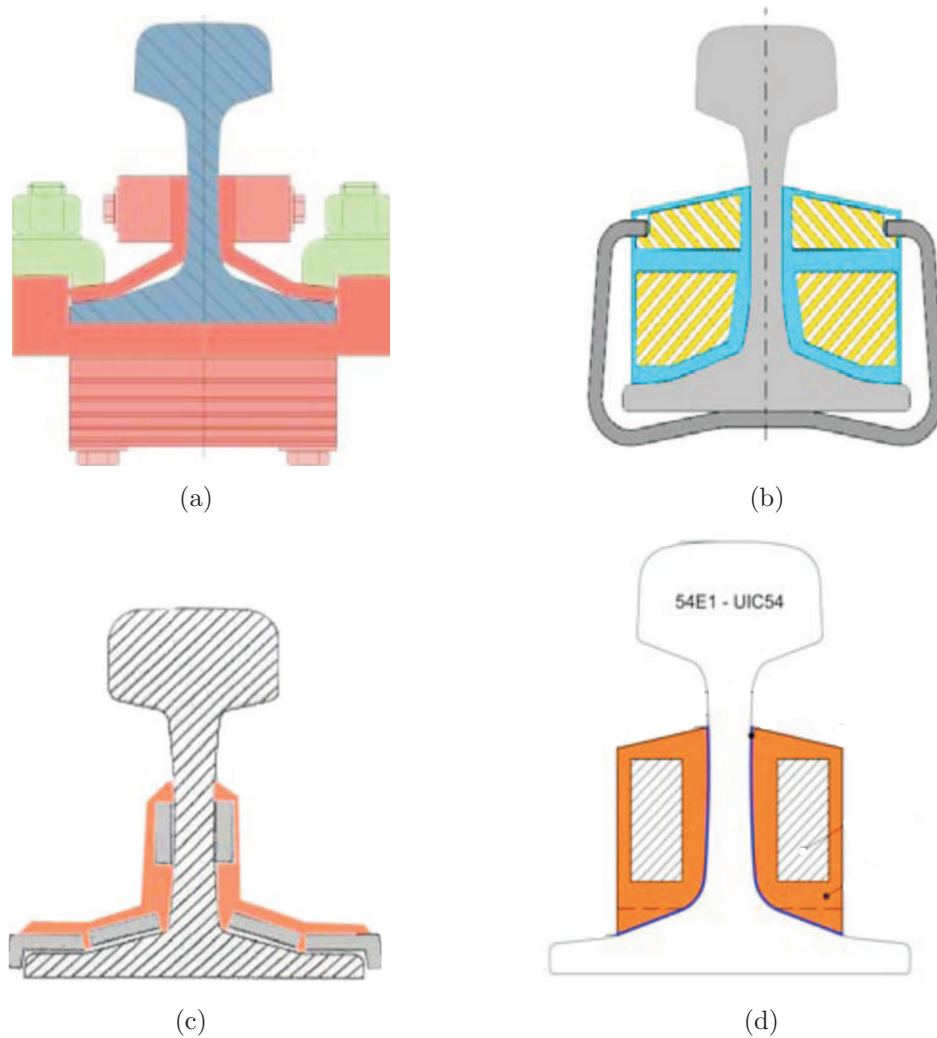
Figure 1.10: *Several available dampers (a) S&V rail damper type VICON–AMSA 5RQ, (b) Corus type clip-on rail damper, (c) James Walker type @10u8 and (d) Edilon Sedra tuned rail damper (Jones & Edwards, 1996) and (Edilon, 2007).*

1.4 Elastomeric materials

It was found in previous studies by Jones *et al.* (2001a), that to achieve a suitable noise reduction using the ISVR/Corus rail damper, the elastomeric material should have a damping loss factor of at least 0.35 (at 1000 Hz) and a Young's modulus close to 14×10^6 Nm^{-2}. However, the current materials used for the rail damper have dynamic properties which vary considerably with temperature. Therefore, this work will concentrate on developing suitable materials to be used in the ISVR/Corus rail absorber for various environmental temperatures in the range -20℃ to 40℃.

Loss factor and dynamic stiffness are two important properties in developing suitable materials for many damping applications. Both properties can be very sensitive to changes in the temperature, which may reduce the performance of the device, if it is required to operate in a range of environmental temperatures. The requirement for both properties are in conflict with each other. If the requirement for a high damping loss factor is met, this means that the material is usually in its transition region, and the modulus falls steeply with increasing temperature. As well as temperature, these dynamic properties also depend significantly on vibration frequency. They can be affected by types and amounts of filler, compounding chemicals such as plasticisers and environmental humidity (Payne, 1996).

In the following a brief description is given of the dynamic properties required for the rail absorber.

1.4.1 Dynamic properties

The modulus is the rate of change of strain as a function of stress in a specimen subjected to a particular form of loading. For example, in shear the modulus is the shear stress amplitude divided by the shear strain amplitude. For harmonic motion, the complex modulus can be expressed in terms of the in-phase response (elastic) and out-of-phase response (viscous).

$$G^* = G' + iG'' \tag{1.1}$$

where G' is the in-phase, 'storage' modulus and G'', the out-of-phase, 'loss' modulus and G^* is complex modulus (N/m^2). The magnitude of the modulus, $\mid G^* \mid$ is related to G' and G'' by $\mid G^* \mid = \sqrt{G'^2 + G''^2} = \tau_0/\gamma_0$, where τ_0 is the shear stress amplitude and γ_0 is the shear strain amplitude. The Young's modulus can similarly be defined for extensional strain and stress.

The loss factor is the ratio of the imaginary and real components of the complex modulus. The term is used in connection with dynamic tests to determine the damping capacity of materials and combinations of materials. An alternative term is tangent delta, where δ is the phase angle between stress and strain,

$$\eta = \frac{G''}{G'} = \tan \delta \qquad (1.2)$$

The complex modulus can be written as $G^* = G'(1 + i\eta)$.

1.4.2 Effect of temperature

The temperature is the most important environmental factor affecting the dynamic properties of damping materials. This effect is shown in Figure 1.11 for a typical polymeric material, having four distinct regions (Nashif *et al.*, 1985). The first region is the glassy state where the material has very large storage modulus (dynamic stiffness) but very low damping. The storage modulus in this region changes slowly with temperature, while the loss factor increases with increasing temperature. After a transition regions, the rubbery region is reached where both modulus and loss factor take somewhat low values and vary very slowly with temperature. In the flow region, the material continues to soften as temperature increases, depending on the molecular weight of the polymer.

The transition region is very important for damping applications because it is in this region that the loss factor is high. However, the material modulus decreases rapidly with increasing temperature. This is linked to the high loss factor in this region. The so-called glass transition temperature, T_g, at which, as the temperature is raised, there is a sudden increase in the volume expansion coefficient of the polymer, corresponds with the start of the transition in the dynamic properties. The damping loss factor usually peaks at or around the centre of the transition region of the material. The location and shape of the transition curves are dependent on the frequency at which the dynamic properties are measured. Some polymers can be made to have more than one transition region by adapting the polymeric structure and composition to take advantage of the peak damping capacity in this region.

1.4.3 Effect of frequency

Experiments have shown that vibration frequency also has a significant effect on the damping and dynamic modulus of elastomeric materials. The variation of the modulus and loss factor of a typical high damping material with frequency over a range of three to
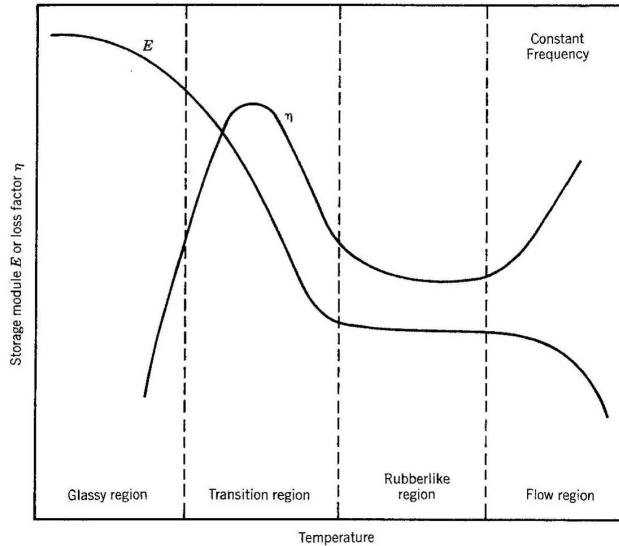
Figure 1.11: *Variation of the storage modulus and loss factor with temperature (Nashif et al., 1985)*

five decades shows that, for a material away from the flow region, the effect of increasing frequency on the modulus is similar to the effect of reducing temperature. This behaviour provides the basis for the temperature-frequency superposition principle that is used to transform material properties from the frequency domain to the temperature domain, and vice versa (Jones, 1990). Results at different temperatures can be transformed to a reference temperature and plotted against 'reduced frequency' in the form of a 'master curve'.

1.4.4   Test method

Selected materials will be tested to obtain their shear modulus and loss factor, as input parameters for further prediction of the noise reduction. Several methods of testing have been compared by Ahmad (2005) to build up the appropriate methodology and ensure that reliable test methods are available for evaluating these properties. Each of these methods (ISVR test rig, Schenck servohydraulic and DMTA (GABO)) have their limitations. For example the Schenck servohydraulic testing machine can measure frequencies between 0.1 Hz and 700 Hz and DMTA (GABO) machine can only measure frequencies up to 100 Hz, while the required frequency range in this work is 300-3000 Hz. Therefore, the ISVR test rig is the most appropriate to test the material. In addition, this test rig is small, compact, mobile and simple to use. For measuring the material at various temperatures, an additional temperature cabinet will be used.

The ISVR test rig was used in developing the desired material for use in the original Silent Track absorber (Thompson *et al.*, 1998). The tests are performed dynamically

to determine the complex shear modulus, G^*, under low amplitude excitation at high frequency. The loss factor can be derived from the phase angle of the modulus.

Figure 1.12 shows the test set up used to measure the shear modulus of the samples and Figure 1.13 shows a close up diagram of the test set up. Four rectangular samples (20 mm × 15 mm × 10 mm thickness) were used in the tests. They are held between a central steel shaft and an outer steel yoke. A bolt, connected to the yoke on either side, allows a pre-compression to be applied. The excitation is applied by means of an electrodynamic shaker (coil and magnet) and the input acceleration and the force transmitted to a high impedance foundation are measured.

The stiffness is derived from the transfer function between the vertical acceleration, $\ddot{u}$ of the central shaft and the force, F, transmitted to the high impedance foundation.
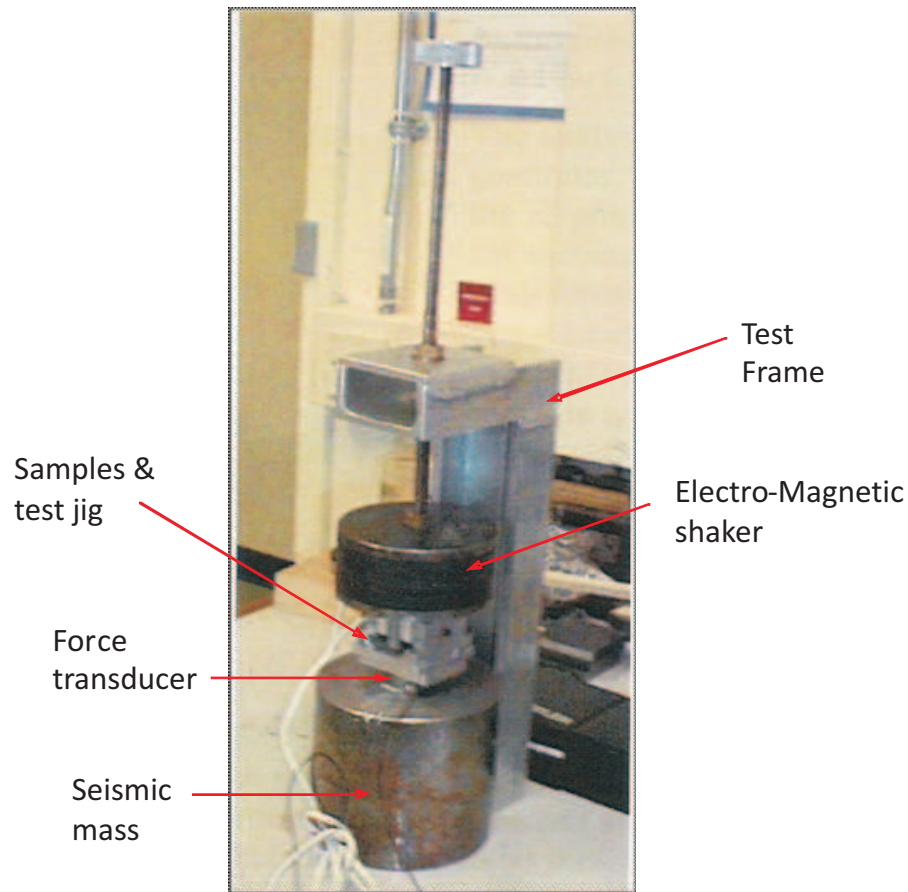
Figure 1.12: *Experimental arrangement for measuring shear modulus (Jones, 2003)*
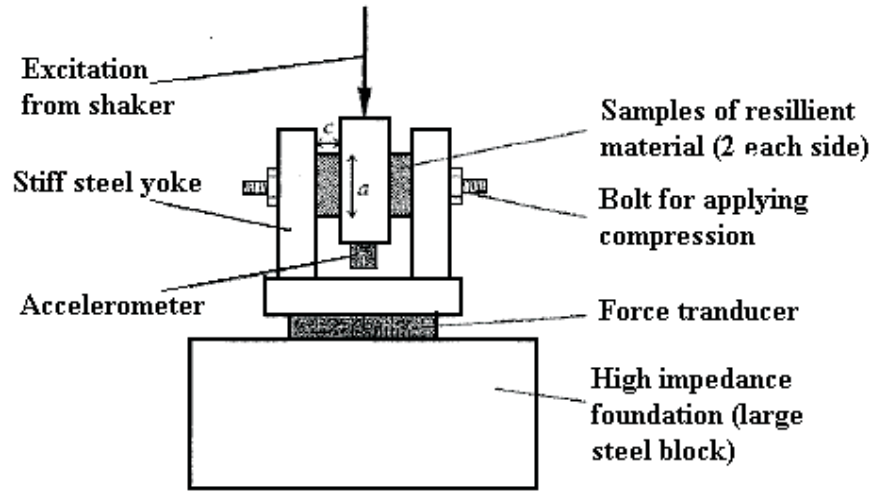
Figure 1.13: *Sketch of the details of experimental arrangement for measuring shear modulus.*

1.5   Objectives and contribution of the thesis

The objective of this thesis is to develop a methodology by which a suitable high damping elastomeric material can be designed to meet specific dynamic properties over a range of temperatures. In particular, this methodology is demonstrated by application to the development of a suitable elastomeric material for use in the ISVR/Corus rail absorber that provides acceptable performance on track over a range of environmental temperatures from -20℃ to 40℃.

The main contributions of the thesis are:

- A detailed literature review into the relationship between the polymer structure and the dependence on temperature and frequency of its dynamic properties. From analysis of this information suitable candidate materials for use in the rail damper application are identified (Chapter 2).

- Development of an analysis method for studying the trade-off between high damping and temperature-dependent stiffness of elastomers for use in the rail damper. This is based on a simple dynamic model of the track, which is shown to give similar trends to a more detailed model. The temperature-dependence of the elastomer is included in a physically-consistent manner by making use of the Williams-Landel-Ferry (WLF) (Williams *et al.*, 1955) equations (Chapter 3).

- Implementation of a method of weighting the effect of temperature on the performance of a rail damper, based on an annual distribution of rail temperatures. Where only air temperature data is available a method is developed to estimate the weighting function using this (Chapter 4).

15

- Improved design of a test rig for measuring the dynamic properties of elastomers using dynamic models and demonstration that improved results are obtained by means of suitable modifications to the rig (Chapter 5).

- Development of a range of materials designed according to a systematic approach and measurements of their dynamic properties. The analysis method based on the simple track model and the temperature weighting is used to assign a single number to the performance of particular elastomers from which the optimum configuration can be identified (Chapters 6/7).

1.6   Layout of the thesis

This thesis is organized as follows. This chapter has given a brief introduction to railway noise, especially the use of absorbers to reduce the rail noise and the dynamic properties of elastomers. However, as seen, the properties of the elastomer depend on the temperature and frequency.

Chapter 2 provides a detailed literature review which will discuss possible materials suitable for the rail absorber. Results for a wide range of materials will be assessed for compliance with a target specification of adequate damping, η at least 0.25, and a permissible range for the shear modulus which should not vary too widely in the temperature range -20℃ to 40℃. Polymer behaviour and the link between physical and dynamic properties will be investigated. The concept of a thermorheologically simple material will be introduced as well as the importance of transition temperature and how the polymer structure, fillers, plasticisers and polymer blends will affect the transition temperature.

Chapter 3 deals with the prediction of noise reduction, which is based on the numerical analysis of the rail damper. The influence of the stiffness and damping of the rail absorber on the noise reduction is studied as well as how they are affected by the temperature. The relative merits of high damping and a low variation of stiffness with temperature are investigated, in order to establish a more practical target for new materials. In Chapter 4, based on the temperature distribution at a site in the UK, an estimate for the rail temperature distribution at this and other locations in Europe is established. This is used to provide a suitable weighting of noise reduction at different temperatures that can be used in assessing materials for the rail absorber.

Chapter 5 describes and seeks to understand the behaviour of the test rig system for the measurement of dynamic properties (shear modulus and loss factor). This chapter discusses the limitations of the test rig and the influence of its design parameters on the reliability of the dynamic properties obtained. Having understood the problems of the

test rig, some modifications are proposed and implemented to improve the results from the test rig within the frequency range of interest.

In Chapter 6, butyl rubbers are investigated as potential materials for the rail absorber. The dynamic properties of the selected materials are investigated experimentally. The effects of fillers, plasticisers and other chemicals are determined by using a design of experiments (DOE) approach. The experimental results for butyl rubber are used to predict the noise reduction, from which an optimum formulation is identified.

Chapter 7 discusses another potential material, Ethylene Propylene Diane Monomer (EPDM). The detailed characteristics and behaviour of the EPDM rubber are discussed. The experimental design approach is again used to evaluate the performance of EPDM for different formulations. The results are compared with those for butyl and for other materials studied previously.

Chapter 8 presents the conclusions of the work and gives recommendations for future work.

Chapter 2

Elastomers and their dynamic properties

2.1 Introduction

Elastomers are increasingly utilized as engineering materials and are unique in the materials spectrum. Their ability simultaneously to store and dissipate energy via their characteristic large strain behaviour is called viscoelasticity. The dynamic properties of viscoelastic materials depend strongly on temperature and frequency. This can be shown in a 'master curve' of modulus and loss factor against 'reduced frequency' (Nashif *et al.*, 1985). The aim of this chapter is to review from the literature what chemical properties determine the shape of the master curve of a viscoelastic material.

For the rail damper application it is desirable to develop a damping material which has a broad loss factor peak and minimal change of modulus over the temperature and frequency range of interest. However, these requirements for the dynamic properties are in conflict with each other, as high damping in polymers occurs in the transition region, where the modulus changes most rapidly (Sperling, 1990).

Nevertheless, by tailoring the polymer structure so that the transition region is in the required temperature and frequency range, it is possible for a polymer to become an effective material for use as a damping treatment and a suitable compromise can be sought. Therefore, this chapter will review the effect of temperature, frequency and amplitude on the stiffness and damping properties of rubbery polymers with the emphasis on the relationship with the polymer structure.

This literature review is organized as follows. Firstly, a brief review is given of polymer behaviour and characteristics, particularly in terms of dynamic properties. The concept

of a thermorheologically simple material is introduced. The effect of polymer structure, fillers, plasticisers and polymer blends on the transition temperatures and shape of the master curve is discussed, as illustrated with reference to particular materials such as polyurethane. Finally, results for a wide range of materials are assessed for compliance with the target specification of adequate damping (loss factor should be greater than 0.25) and a permissible range for the shear modulus which should not vary too widely in the temperature range -20℃ to 40℃.

2.2   Rubbers and elastomers

Commercially available rubbers may be divided into Natural Rubber and around 20 classes of Synthetic Rubber. Natural Rubber (NR) is extracted from the tree Hevea Brasiliensis, while Synthetic Rubbers (SR) are synthesized from petroleum, coal, or natural gas. By changing the composition of SR, it is possible to achieve specific properties desired for particular applications. The earliest synthetic rubbers were acryolonitrile–butadiene rubber (NBR) (1934), chloroprene rubber (CR) (1935), styrene–butadiene rubber (SBR) (1939) and butadiene rubber (BR) (1967).

Natural Rubber has a large deformability capacity. Its high resilience, which is responsible for a very low heat build-up in flexing, and its high strength, make NR a prime candidate for use under shock and severe dynamic load. NR also has low compression set, stress relaxation, and low level of damping. Its properties at room temperature remain fairly constant over the range 1 to 200 Hz, and show only slight increase up to 1000 Hz. It also has excellent low temperature properties with a glass transition temperature (T_g) of approximately -70℃ (Robert, 1990) (T_g will be described in Section 2.3.3). Unfortunately it has a relatively high reactivity with its environment, such as with ozone. Natural Rubber remains the best choice for tyres, shock mounts, seals, isolators, couplings, bearings, springs and many dynamic applications.

Although Natural Rubber has satisfactory properties for many applications, it has relatively poor ageing resistance. SR can cope with high and low temperatures, contact with fluids of various types (including at high pressure), and aggressive or corrosive environments (Morton, 1995). Synthetic materials have been developed to replace Natural Rubber in a wide range of applications. The main synthetic rubbers are Styrene Butadiene Rubber (SBR) (T_g is higher at about -55℃), Butadiene Rubber (BR) (T_g approximately -80℃), Isobutylene Isoprene (Butyl) Rubber (IIR) (low T_g but has very little 'bounce'), Polyurethane (PU), Nitrile Rubber (NBR), Ethylene Propylene Rubber (EPDM or EPR), Chloroprene Rubber (CR), Neoprene and Silicone Rubber (Whitby *et al.*, 1954).

Each of these synthetic rubbers has interesting properties. For example, NBR rubbers have excellent oil resistance and are widely used for flexible couplings, hoses, and washing machine parts. Butyl rubbers, which are copolymers of isobutylene and 1.3% isoprene, have good resistance to abrasion, low gas permeability, and high dielectric strength. Neoprene (polychloroprene) is particularly useful at elevated temperatures and is used for heavy-duty applications. Ethylene-propylene rubbers (EPDM) with their high resistance to weathering and sunlight are used for automobile parts, hoses, electrical insulation, and footwear. Polyurethane elastomers are the most versatile elastomer family because of their hardness, strength, oil resistance, and ageing characteristics (Blow, 1971).

2.2.1 Structure of polymers

Elastomers are a subset of polymers, i.e. high molecular weight materials, consisting of long chains of one or more types of molecules, known as monomers. These long-chain molecules are made up of repeating units usually on a backbone of carbon atoms (Blow, 1971).

Long-chain molecules occur commonly in nature and may also be synthetically produced by polymerization. The two broad classes of polymerization are shown in Figure 2.1 (Vollmert, 1973). The first is defined as chain addition polymerization (addition; Figure 2.1(a)). Addition polymers are created from one or more monomers, and their polymeric sequences are identical to the monomers. Condensation polymers result when two or more difunctional molecules (not necessarily monomers) combine to create long-chain molecules releasing by-products such as water, or CO_2, which have to be removed.
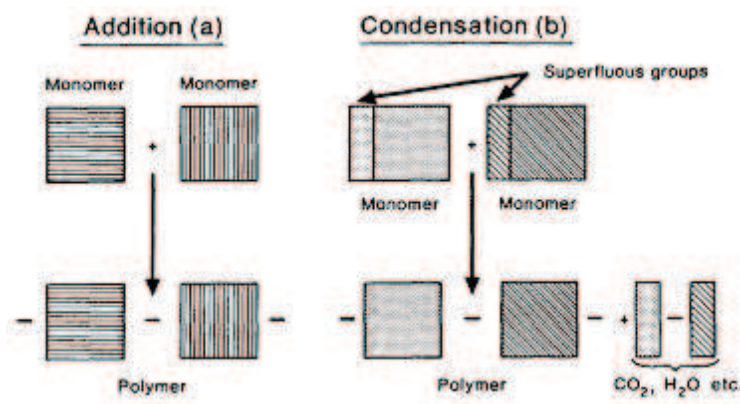
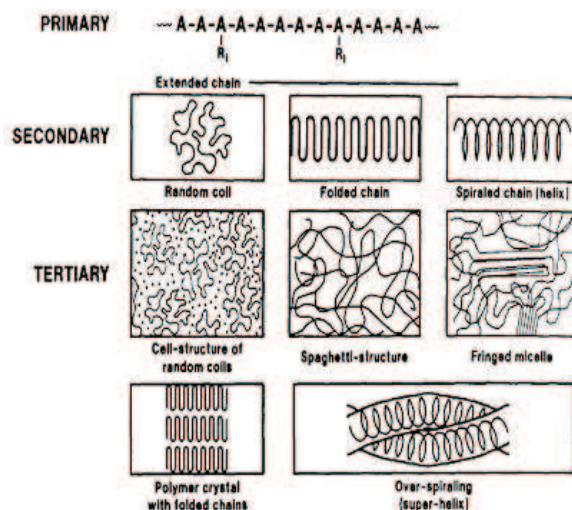**Figure 2.1:** *Polymeric structure (Vollmert, 1973) .*

The long-chain molecule forms the primary structure of any polymeric material (Figure 2.2), Vollmert (1973). The secondary (micro) structure is dictated by the molecule, which in turn influences the development of the tertiary (macro) structure.

Materials can generally be considered as crystalline (solids) or amorphous (liquids or gases). Non-gaseous amorphous polymeric materials may therefore be regarded as liquids. However, as the temperature is reduced the thermal energy associated with each degree of freedom, such as a segment of the polymer chain, falls. This means that fewer segments have sufficient energy for rearrangement which makes the molecular movement more sluggish and increases the viscosity. Below a certain temperature, flow is effectively prevented and the material appears brittle, like glass. In this 'glassy' regime, deformation occurs only by distortion of chemical bonds and changes in interatomic distances, rather than by rearrangement of the polymer segments, so that the shear and bulk moduli have similar magnitudes (roughly 2000 MPa). This 'glass transition' temperature (T_g) is a characteristic of the particular material, depending on the chemical structure in a way that is examined later in this chapter.

Above their T_g amorphous polymers exhibit both viscous and elastic characteristics, and so are said to be 'viscoelastic'. If the polymer chains are particularly long and the temperature is well above T_g, they have very high elasticity and deformability: such materials are termed 'elastomers'. Elastomers have remarkably low elastic shear moduli (0.3 - 3 MPa) and a remarkably high elastic extension capability (several hundred percent) imparted by their long-chain structure and the entropic mechanism of elastic deformation. The typical elastomer has a random coil microphase and a spaghetti structure macrophase.

The chemical structure not only determines the value of T_g. Depending on the chemical structure, the polymer molecules may be able to rearrange themselves into a crystal lattice above the T_g (see Figure 2.2). This can only happen if the polymer chains are sufficiently regular and enough heat energy enters the material. The extent of crystallinity and the temperature up to which it is the stable phase (the melting temperature, T_m) depend on the strength of the chemical bonds formed when the material crystallises: stronger bonds mean that T_m will be higher and the extent of crystallisation will be greater. Polymers are generally not regular or mobile enough to crystallise more than partially. Hence 'crystalline' polymers (e.g. polypropylene, polyethylene, Nylon and PTFE) generally have shear moduli significantly less than 2000 MPa, the typical value for amorphous glassy polymers, although much greater than the range 0.3 - 3 MPa typical of amorphous polymers well above their T_g.

Elastomers can be enhanced by introducing crosslinks between the long chain molecules. This is normally achieved by a chemical process called "vulcanization" or "curing", but physical entanglements and co-engagement of chains in microcrystalline regions have a similar if less permanent effect. The term "rubber" implies a vulcanized elastomer. This is the process of chemical reaction (cross-linking elastomer molecules) to make the bulk material harder, less soluble and more durable (Blow, 1971). Usually, the actual chemical

Figure 2.2: *Polymeric structure (Vollmert, 1973) .*

cross-linking is done with sulphur, but there are other technologies, including peroxide-based systems. The vulcanization system in a typical rubber compound comprises the cure agent itself, sulphur or peroxide, together with accelerators and retarding agents.

Unvulcanized rubber is soluble in appropriate solvents, but such solvents merely swell rather than dissolve rubber. Highly swollen elastomers are too weak to be useful for most engineering applications, hence the need to choose a rubber which is solvent/oil resistant rubber in some applications.

2.3   Dynamic properties of elastomers

One of the main applications of rubber is to control vibration, and the key physical properties that determine how well it does this are the dynamic mechanical properties, in particular the elastic modulus and damping. These in turn are determined by the molecular mobility, and hence the structure of the polymer.

The dynamic properties of viscoelastic materials are influenced by frequency, temperature, dynamic strain rate, static pre-load, time effects such as creep and relaxation, ageing and other irreversible effects. The complex modulus (stiffness and damping properties) will be discussed in section 2.3.1.

Polymers with a high molecular weight behave in a rubbery fashion in a certain temperature region. These are termed visco–elastic. At low temperatures they become 'glassy' while at high temperatures they eventually become liquid. The glass transition

temperature, T_g, marks the point where glassy behaviour gives way to the start of the rubbery behaviour (section 2.3.3).

The physical properties of rubber are generally temperature and frequency dependent and these effects will be described in section 2.3.4. An increase in frequency affects the rubber in the same manner as a decrease in temperature.

2.3.1 Dynamic modulus and damping

Viscoelastic materials are characterized by a combination of viscous and elastic behaviour. When they are deformed, energy is stored by the elastic elements and released in the process of strain recovery, while the viscous elements dissipate energy and retard the elastic deformation. The viscous elements, or internal friction, are thus responsible for the energy difference or hysteresis, between work recovered and expended (Blow, 1971). The superimposed elastic and viscous behaviour of rubber is clearly demonstrated during oscillatory deformations as shown in Figure 2.3 (Macioce, 2003).

Referring to Figure 2.3, the stress and strain of a purely elastic material move in phase because all the energy stored during the loading is returned when the load is removed. In this case, the stress is proportional to strain and the modulus is defined as a ratio of stress to strain. On the other hand, a purely viscous material does not return any of the energy stored during loading because all the energy is lost as 'pure damping' during motion. Therefore, the stress is proportional to the rate of strain and the ratio of the stress to strain rate is known as viscosity, μ. As a result, these materials have no stiffness component, only damping (Macioce, 2003). A viscoelastic material is characterized by possessing both viscous and elastic behaviour where some of the energy stored in a viscoelastic system is recovered upon removal of the load, and the remainder is dissipated in the form of heat. The stress and strain are these out of phase by some phase lag.

For a harmonic applied shear strain, for example, the complex shear modulus, G^*, can be defined as $G^*(\omega) = \dfrac{\sigma(\omega)}{\varepsilon(\omega)}$ where σ and ε are complex amplitudes at frequency, ω . This can be separated into its real part, which is related to elastic behaviour, and its imaginary part, which is related to viscous behaviour,

$$G(i\omega) = G'(\omega) + iG''(\omega) = G'(\omega)[1 + i\eta(\omega)] \tag{2.1}$$

where G' is the in-phase (storage) modulus, G'' is the out-of-phase (loss) modulus, $i = \sqrt{-1}$ is the imaginary unit and $\omega = 2\pi f$ is the circular frequency in rad/s (f is the

23
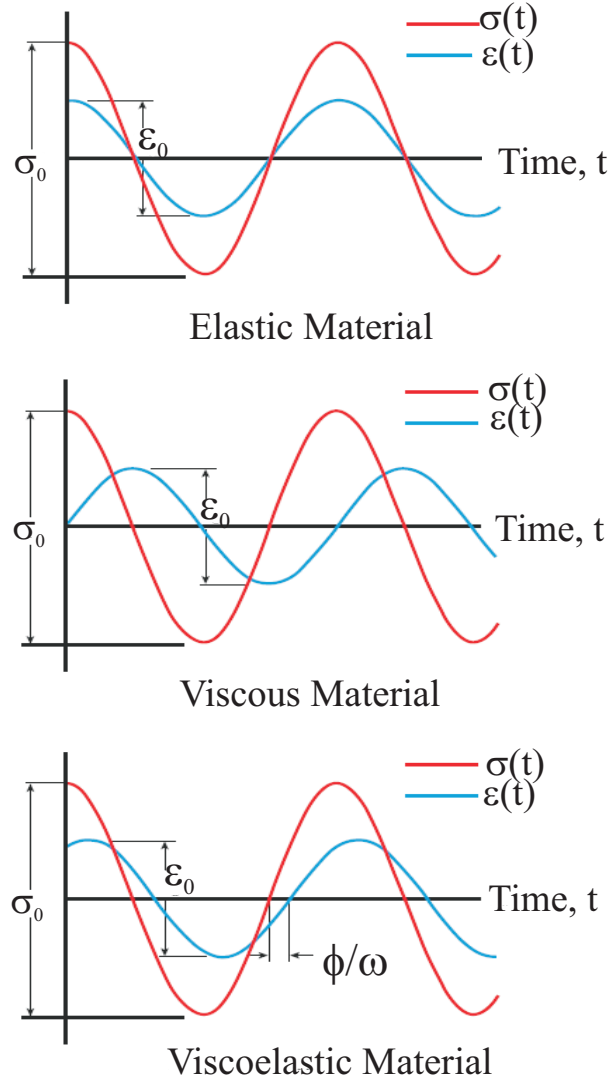
Figure 2.3: *(a) elastic material– the stress and strain curves move completely in phase, where the stress is proportional to the strain, and modulus is defined at the ratio of stress to strain. (b) viscous material– the stress is proportional to the rate of strain, and the ratio of stress to strain rate is viscosity, μ. This material has no stiffness component, only damping. (c) viscoelastic material (Macioce, 2003).*

frequency in Hz). The loss factor is given by

$$\eta(\omega) = \tan\delta = \frac{G''(\omega)}{G'(\omega)} \tag{2.2}$$

where δ is the phase angle between stress and strain.

The shear modulus can be measured, for example using non-resonance techniques, using a variety of test rigs (Ahmad, 2005). This complex modulus describes the material's stiffness and damping properties. Damping is caused by the conversion of mechanical energy of a vibrating structure into thermal energy. For viscoelastic material, the cyclic stress at a loading frequency is out of phase with the strain by some angle, δ (where $0<\delta<\pi/2$). The angle is a measure of the material's damping level; the larger the angle the larger the damping (Macioce, 2003).

The stress and strain over one deformation cycle (Figure 2.3) form a closed 'hysteresis' loop, as shown in Figure 2.4. The area within the loop, 'D', represents the energy loss per unit volume of material during each cycle. The relationship between material damping and loop area is given by the following equation (Ahmadi & Fuller, 1994).

$$\eta = \frac{D}{\pi\sigma_0\varepsilon_0} \tag{2.3}$$
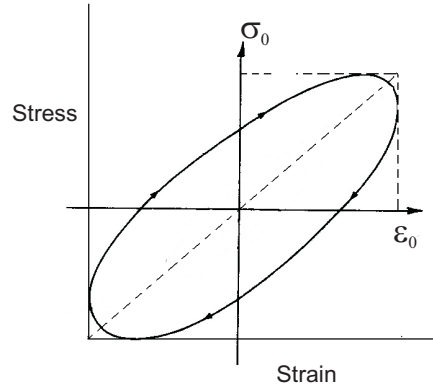
Figure 2.4: *Hysteresis loops of the stress-strain cycle for linear viscoelastic material (Ahmadi & Fuller, 1994)*

Furthermore, the complex Young's modulus, E^* can be estimated in terms of shear and bulk modulus as shown in the following equations.

$$E^* = 2G^*(1+\nu) \tag{2.4}$$

$$E^* = \frac{9K^*G^*}{3K^* + G^*} \tag{2.5}$$

where ν is Poisson's ratio, which lies between 0 and 0.5. K is the bulk modulus, which describes volumetric stress over volumetric strain. For many engineering purposes, it is adequate to take a typical default value of K for rubber–like materials as 2000 MPa. Therefore, from equation (2.4) and (2.5) and for rubber–like materials $K^* >> G^*$, which allows E^* to be estimated as $E^* \approx 3G^*$ (Ahmadi & Fuller, 1994) and hence $\nu \approx 0.5$.

A characteristic feature of polymers is the way in which their response to an applied stress or strain depends on the rate, temperature or time period of loading. These are extremely important effects, which will be discussed in detail in this chapter. For example, the modulus of natural rubber does not vary strongly with frequency below 1000 Hz at room temperature (Lindley, 1992). At frequencies above 1000 Hz, the dependence of modulus on frequency becomes stronger although raising the temperature will lower the frequency sensitivity (section 2.3.4). A strong dependence exists between frequency and temperature effects due to the direct relationship between temperature and molecular motion (Nashif *et al.*, 1985).

Viscoelastic materials typically exhibit the type of behaviour already shown in Figure 1.11, where four distinct regions can be observed (Nashif *et al.*, 1985). The first is the so-called glassy region at low temperature or high frequency. Here the polymer chains cannot move relative to each other, resulting in glass-like behaviour. The material is therefore stiff in this region; the storage modulus shows its highest value but the damping level is typically low. The second region is the transition region. In this region, the viscoelastic material has a rapid rate of change in stiffness and possesses its highest level of damping loss factor (as discussed in section 2.3.3). In the third region, the rubbery region, the material reaches a lower stiffness and lower damping, but these values change less rapidly. The fourth, flow region is typical of a few damping materials such as vitreous enamels and thermoplastics. In this region the material continues to soften with increasing temperature but the storage modulus diminishes more rapidly than the loss modulus, so the loss factor becomes very high.

Adding fillers to the rubber will increase the modulus and lower the peak of the loss factor. Besides that, the dynamic modulus of filled rubbers decreases as the amplitude increases (Lindley, 1992). More detailed discussion on fillers will be presented in section 2.4.3.

2.3.2 Stress relaxation and creep

Some results in the literature of the effect of temperature are given in terms of relaxation or creep functions. These are therefore introduced here.

Stress relaxation is the gradual decrease of stress when the material is held at a constant strain. Suppose a shear strain (e) is imposed over a brief period of time t at a constant rate of strain $\dot{e}$ and the stress, $\sigma(t)$ is measured as shown in Figure 2.5. Then, the relaxation modulus can be expressed as

$$G(t) = \frac{\sigma(t)}{e} \tag{2.6}$$
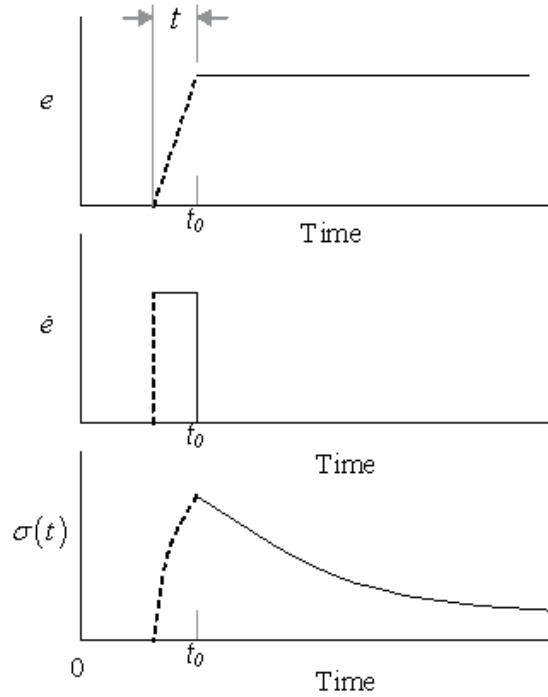
Figure 2.5: *A typical stress relaxation experiment.*

Creep is the slow progressive deformation under constant stress. It results from the viscoelastic flow of the polymer with time. A shear stress σ may be applied within a very brief period of time and then maintained constant as shown in Figure 2.6. The creep, $e(t)$ at a constant stress σ is given by $e(t) = \frac{\triangle x(t)}{l_0}$. The creep compliance is given by

$$J(t) = \frac{e(t)}{\sigma} \tag{2.7}$$
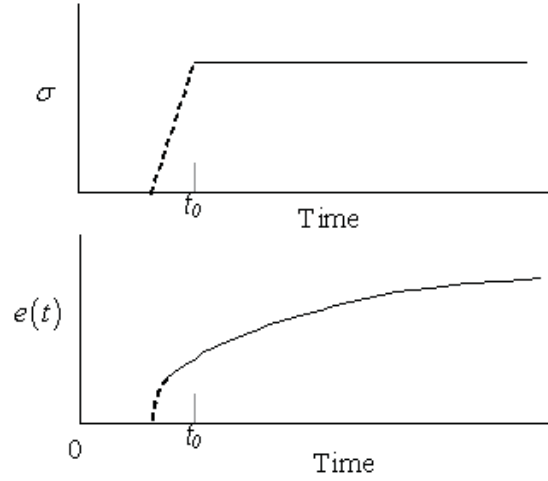
Figure 2.6: *Time profile of a creep experiment.*

2.3.2.1 Boltzmann superposition principle

The Boltzmann superposition principle allows the general linear response of a system to be determined allowing for details of loading history. In the linear viscoelastic regime the stress responses to successive deformations are additive. Similarly, the strain responses to successive stresses are additive. Boltzmann proposed (Ward, 1983) that creep is a function of the whole sample loading history and each loading step makes an independent contribution to a total loading history. Thus, the total final deformation is the sum of each contribution.

In general, for a creep experiment, the increment of stress $\triangle\sigma_1$, $\triangle\sigma_2$, $\triangle\sigma_3$, etc at times τ_1, τ_2, τ_3, etc respectively may be shown as in Figure 2.7. The total strain at time t is given by

$$e(t) = \triangle\sigma_1 J(t - \tau_1) + \triangle\sigma_2 J(t - \tau_2) + \triangle\sigma_3 J(t - \tau_3) + \ldots \quad (2.8)$$

where $J(t - \tau)$ is the creep compliance function. The above equation may be written in integral form as

$$e(t) = \int_{-\infty}^{t} J(t - \tau) \, d\sigma(\tau) \quad (2.9)$$

The Boltzmann superposition principle can also be applied to the stress relaxation behaviour. The increment of stress relaxation in which incremental strains $\triangle e_1$, $\triangle e_2$, $\triangle e_3$, etc, are added at times τ_1, τ_2, τ_3, etc respectively, the total stress at time t is then given

$$\sigma(t) = \triangle e_1 G(t - \tau_1) + \triangle e_2 G(t - \tau_2) + \triangle e_3 G(t - \tau_3) + \ldots \quad (2.10)$$

where $G(t-\tau)$ is the relaxation modulus. The above equation may be written in integral form as

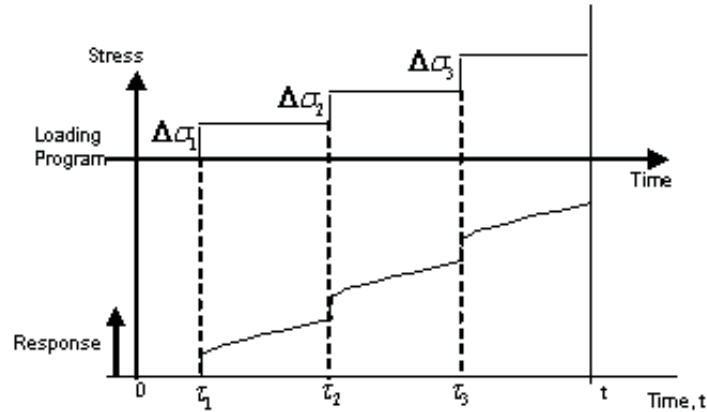$$\sigma(t) = \int_{-\infty}^{t} G(t - \tau) \, de(\tau) \qquad (2.11)$$

Figure 2.7: *The creep behaviour of a linear viscoelastic solid (Ward, 1983).*

2.3.3 Glass transition temperature

The concept of the glass transition temperature is of broad significance and usefulness in many applications of viscoelastic materials under changing temperature conditions. It represents the boundary between the glassy and transition regions.

In the glassy region at low temperature (or high frequency), there is not enough free volume for the molecules to move past each other. In other words, kT, the thermal energy in Joule/K, is small compared with the activation energy required for a molecule or segment of a molecule to move past its neighbours. In the transition region this restriction no longer applies because the polymer has enough free volume available for the molecules to move from one position to another with respect to their neighbours.

The glass transition temperature can be defined in terms of volume change $(\triangle V)$ as shown in Figure 2.8 (Christensen, 1971). The temperature at which the slope dV/dT has a discontinuity is defined as the glass transition temperature (T_g). At high temperature, the volume expands considerably and results in increasing molecular mobility, which gives a lower modulus. On the other hand, at low temperature, the molecular mobility decreases due to the volumetric shrinkage that leads to a high modulus or relatively stiff material.
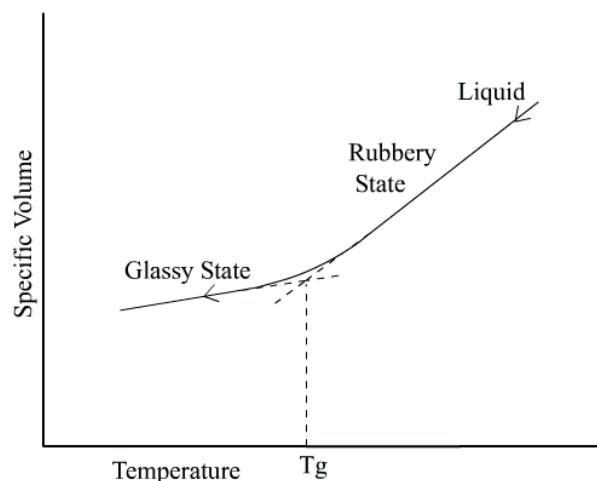
Figure 2.8: T_g– *volume change versus temperature (Christensen, 1971)*

An alternative means of defining a transition temperature can also be mentioned. The region where the modulus has its greatest dependence upon temperature (maximum magnitude of slope) and the loss factor has its maximum value defines the centre of the transition region and can be designated as the transition temperature. However, this is not the same as T_g and will be denoted $T_{g,mech}$ in order to distinguish them. The transition region in terms of volume change will be used here to define T_g because it can be determined more accurately.

There are several methods available to measure the glass transition temperature such as the volume method (as shown in Figure 2.8), differential scanning calorimetry (DSC), mechanical methods and dynamic mechanical thermal analysis DMTA. Since the value of the glass transition temperature depends on the strain rate and cooling or heating rate, there cannot be a unique value for T_g.

Thermal methods such as differential scanning calorimetry (DSC) can be used to measure T_g. This method uses the fact that the enthalpy of a polymer decreases as the temperature decreases, but with a change in slope in the graph at T_g. Taking the derivative of this graph with respect to temperature, the specific heat capacity can be plotted, as shown in Figure 2.9 (Turi, 1981).

It is possible to calculate T_g using the mechanical method by measuring the elastic modulus of the polymer as a function of the temperature. DMTA measures the energy absorbed when a specimen is deformed cyclically as a function of the temperature and a plot of energy loss per cycle as a function of temperature shows a maximum at $T_{g,mech}$ (Turi, 1981).

The value of T_g for a polymer is important because it determines the temperature range in which a material can be used effectively as a damping material (Ferry, 1970). There are
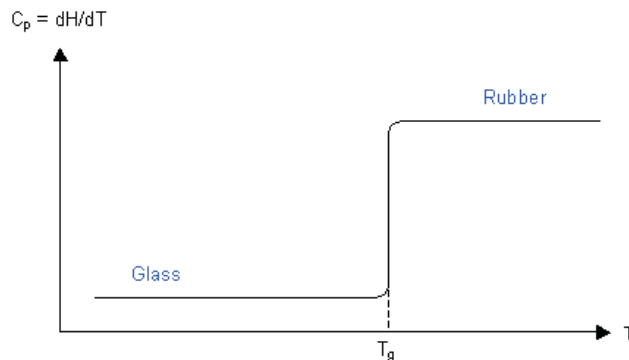
Figure 2.9: *Thermal method to measure T_g (Turi, 1981)*

several factors that affect the glass transition temperature such as the chemical structure, molecular weight, and copolymerization (Brandrup & Immergut, 1989) (section 2.4.1).

In general, concerning the glass transition temperatures, the material structure, not only for polymers but also a variety of organic and inorganic glass-forming liquids (Williams *et al.*, 1955) will also affect the T_g. The breadth of the loss factor peak may be determined by the randomness or blockiness of the polymer structure. These properties will be discussed in section 2.4.5.

2.3.4 Effect of temperature and frequency

As shown in Figure 1.11, the complex modulus varies with temperature. As indicated above, the reduction in volume on cooling at low temperature increases the shear modulus, resulting in a progressive stiffening and loss of resilience. As the temperature increases, the vulcanizate material becomes rubbery (Figure 2.10 (a)).

This reversible behaviour occurs provided that there are no chemical changes in the rubber (Payne, 1996). Rubber tends to be degraded by oxygen, especially at high temperature. The maximum operational temperature depends on how long the rubber component stays at the increased temperature. For most rubbers short-term temperatures up to at least 150℃ can be sustained, but for longer term temperatures over about 100℃ 'ageing' of the rubber is caused.

Besides temperature, frequency also has a significant effect on the dynamic properties as illustrated in Figure 2.10. An increase in frequency generally has a similar effect to a reduction in temperature. The modulus increases with frequency, especially in the transition region (Figure 2.10 (d)). The loss factor increases with frequency in the rubbery region and decreases with frequency in glassy region and takes its maximum value in the transition region (Nashif *et al.*, 1985), see also Figure 1.11.
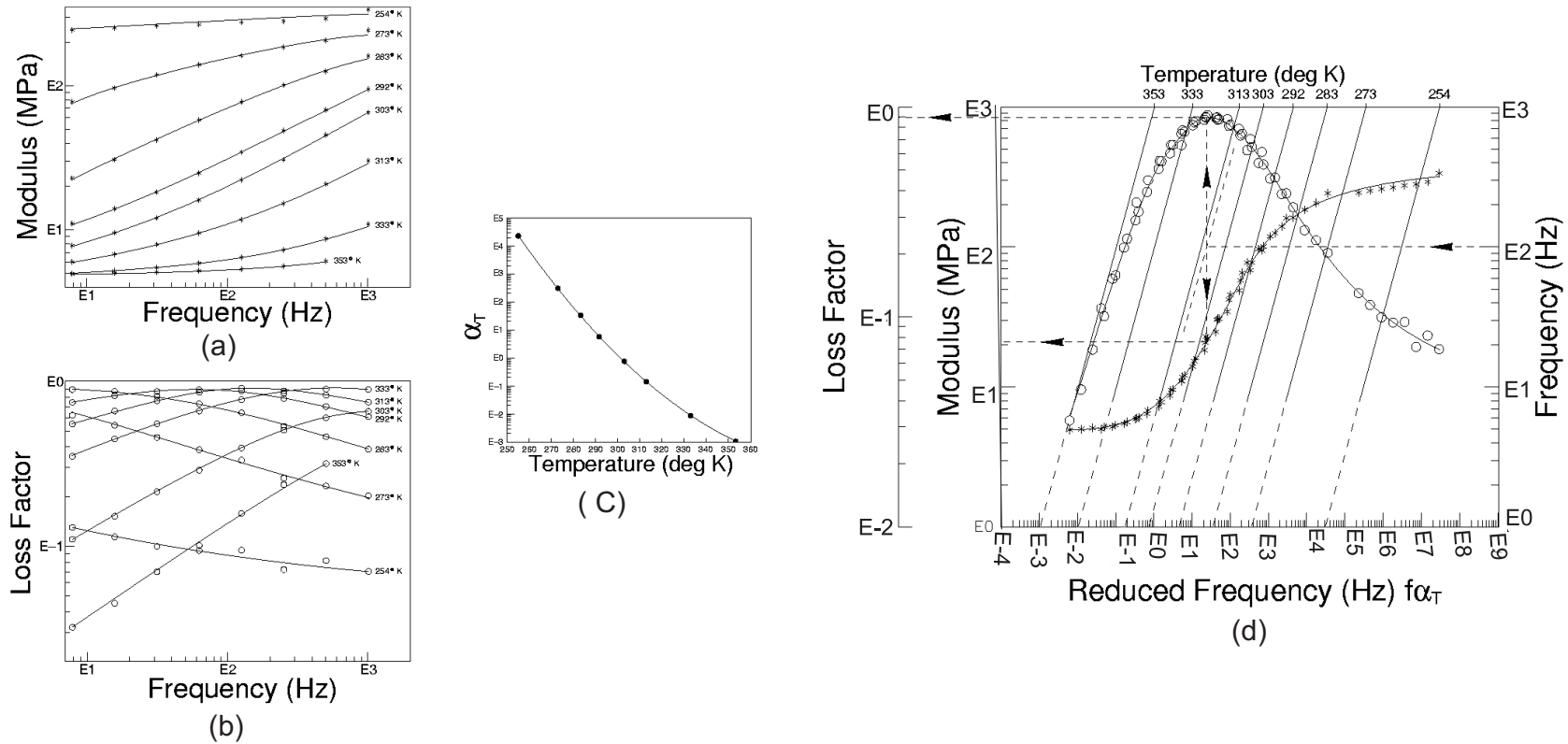
Figure 2.10: *Effect of temperature and frequency on modulus and loss factor (Ferry, 1970; Nashif et al., 1985). (a) Modulus versus frequency at various temperatures of -20°C to 80°C (from top to bottom curve). (b) Loss factor versus frequency at various temperatures of -20°C to 80°C (from bottom to top curve). (c) A temperature shift curve, α_T as a function of temperature (-23°C to 77°C). (d) Master curves of modulus and loss factor versus reduced frequency, temperature nomogram on the top scale and experimental frequency on the right hand scale.*

2.3.4.1   Time-temperature superposition principle

The time-temperature superposition principle (TTSP) is a procedure frequently applied, either to determine the temperature dependence or to expand the time or frequency regime at a given temperature at which the material behaviour is studied. It is also known as frequency-temperature superposition or the method of reduced variables. This TTSP works properly for unfilled rubbers consisting of a single polymer, which have a well-defined 'glass transition' temperature T_g (Ferry, 1970; Nashif *et al.*, 1985). Materials which satisfy the TTSP are also known as Thermorheologically Simple Materials (TSM).

As shown by Ferry (1970) and Nashif *et al.* (1985), dynamic mechanical data taken near the glass-transition temperature at different frequencies as a function of temperature can be 'shifted' along the frequency (or temperature) axis to yield a 'master-curve' as shown in Figure 2.10. For a single phase polymer, the modulus is large below the T_g, but it falls from just above the T_g eventually reaching a very low value around T_g +100℃. Within this region T_g to T_g +100℃, the viscous behaviour is pronounced.

The amount (and direction) that each frequency, taken at temperature T, is shifted can be tabulated and is given the symbol $\alpha(T)$ and called 'the shift factor'. This is constructed for each particular set of complex modulus data, as shown in Figure 2.10 (c). Williams, Landel and Ferry showed that $\alpha(T)$ can be written in the form

$$\log_{10} \alpha(T) = -c_1 \frac{(T - T_s)}{(c_2 + T - T_s)} \tag{2.12}$$

where c_1 and c_2 are constants that can be determined empirically (Williams *et al.*, 1955). This is known as the WLF equation. From experimental data it has been shown that for a range of polymers a good fit is obtained using c_1=8.86 and c_2=101.6 (Williams *et al.*, 1955). T_s is a reference temperature and may be estimated as $T_s \approx T_g + 50$. This relationship has been found to work reliably in the range $T_s \pm 50$ (Ahmadi *et al.*, 1992).

The shift factor can be used to give an empirical relationship between the frequencies f_2 at which dynamic properties measured at temperature T_2 are equal to those measured at frequency f_1 and temperature T_1:

$$\log_{10} f_2 = \log_{10} f_1 - \alpha(T_1) + \alpha(T_2) \tag{2.13}$$

Thus, the Williams, Landel and Ferry (WLF) model (equation 2.12) will be used in this work to generate the 'master curves'. This model relies on the observation that time and temperature have equivalent effects on the properties of a viscoelastic material. The frequency shifts required are superimposed on the curves to form the final master

curves. One advantage of TTSP is that the master curves allow the dynamic behaviour of materials to be determined at frequencies beyond the practical measurement ranges. This can be done by using the frequency-temperature equivalence principle to superimpose lines of constant temperature on the plot.

2.4 Material types

2.4.1 Factors affecting the glass transition temperature (T_g)

The value of T_g for a polymer is important because it affects mechanical properties at particular temperatures and determines the temperature range in which a material can be used effectively for a particular purpose. Several factors affect the T_g such as bond interaction, molecular weight, functionality, branching, and chemical structure (Sartomer, 2005). Polymer chains that do not easily undergo bond rotation would be expected to have difficulty in changing their configuration, resulting in a high T_g. High intra- and inter-molecular secondary force, such as high hydrogen bonding and dipole interaction would also be expected to decrease the mobility of the polymer chains and hence increase the T_g (Brandrup & Immergut, 1989).

Factors affecting T_g are:

(I). *The effect of chain stiffness.* Figure 2.11 shows an example of how chain stiffness of the polymer affects T_g. If there are bulky groups, such as benzene rings, in the backbone of the polymer chain, there is a high energy barrier to rotations, which then only occur at higher temperatures. Polymer chains with pendant groups, for example polystyrene, have decreased mobility of polymer chains, increased chain rigidity, and a resulting high T_g (Ferry, 1970). Polymers with highly flexible components have lower values of T_g. The chain stiffness is thus a major determinator of T_g.

(II). *The effect of bulky side groups.* The presence of bulky pendant groups attached to the polymer backbone raises the T_g, through steric interference to bond rotations, as shown in Figure 2.12. The glass transition temperature, T_g increases as the pendant group gets larger, until at some point the attached groups no longer get in the way of bond rotations because they are too far away from the chain.

The effect of attaching a methyl group to the main chain of the polymer structure, to give poly (-methyl styrene), is greater than increasing the size of the aromatic unit, because the close proximity of this group to the polymer backbone introduces a higher degree of steric hindrance.
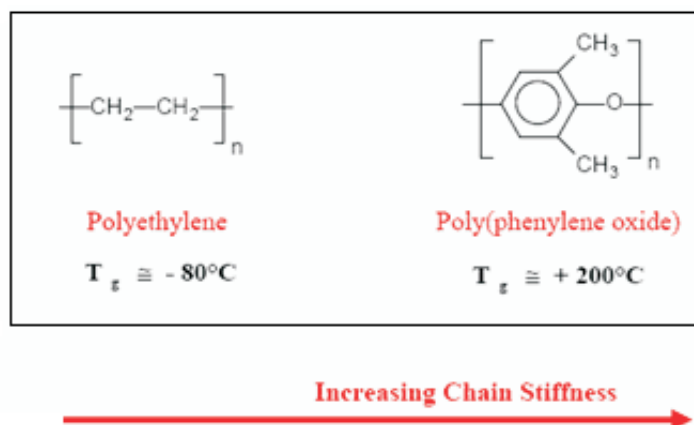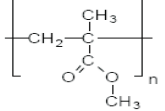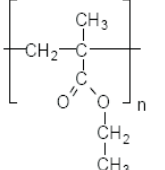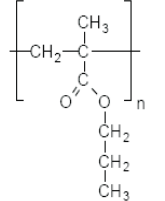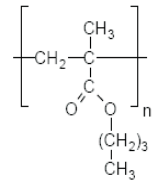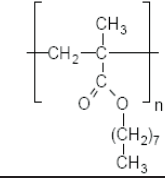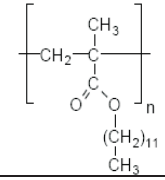
Figure 2.11: *Example of polymer structure showing the effect of chain stiffness on T_g (Brandrup & Immergut, 1989; Vollmert, 1973).*

Figure 2.12: *Examples of polymers which have bulky side groups, show the increasing of T_g (Brandrup & Immergut, 1989) and (Vollmert, 1973).*

(III). *The effect of flexible side groups.* T_g decreases with increasing side-chain length as shown in Figure 2.13. Substituents closest to the chain, such as the methyl and ester group, provide the bulk of the steric hindrance. The rest of the attached side chain can 'get out of the way' of motions of the main chain through rotations around side-chain bonds. Because these side chains increase the free volume through their effect on the packing of the chains, the T_g is lowered (Sartomer 2005).

(IV). *The effect of molecular weight.* T_g increases with increasing molecular weight. This can be expressed in the following equation given by Fox and Flory (1950).

Figure 2.13: *Examples of polymers show the effect of flexible side groups on T_g (Brandrup & Immergut, 1989) and (Vollmert, 1973).*

$$T_g = T_g(\infty) - \frac{K}{M} \tag{2.14}$$

where $T_g(\infty)$ is the limiting T_g at high molecular weight, K is a constant and M is molecular weight.

This equation was obtained by simple volume arguments. Low molecular weight chains have more ends per unit volume than long chains, hence a higher free volume, and a lower T_g. This can be seen with products, for example polystyrene, where a plot of molecular weight versus T_g (data according to equation (2.14) is shown in Figure 2.14 (Fox & Flory, 1950)).
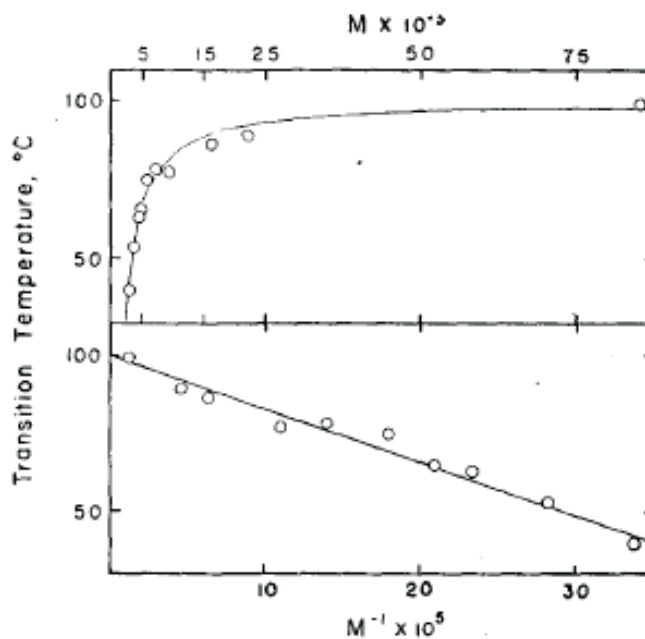
Figure 2.14: *Glass transitions of polystyrene fractions plotted as a function of molecular weight, M (bottom) and 1/M (top) (Fox & Flory, 1950).*

(V). *The effect of intermolecular attraction and crosslinking.* In theory, when the free volume is less, T_g is higher. T_g will therefore increase when there are strong intermolecular attractions in the polymer structure. For example, the chlorine atom and methyl group have approximately the same effect on bond rotations, but the polar character of the chlorine atom leads to stronger forces of attraction between chains, so that on average these groups are closer. Similarly, cross-linking decreases free volume, because parts of the chain are tied more closely together and hence T_g increases. Figure 2.15 illustrates the influence of intermolecular attraction on T_g.
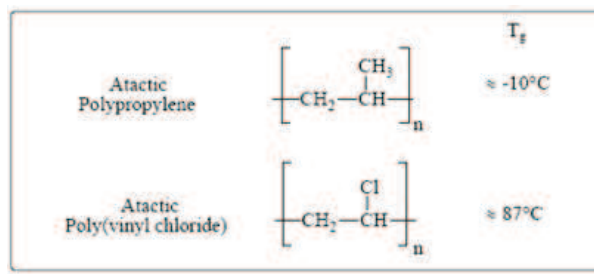
Figure 2.15: *Example of polymers that have a strong intermolecular attraction will increase the T_g (Vollmert, 1973).*

2.4.2 Single-phase elastomer

Many commonly used elastomers are amorphous homopolymers, that is the polymer chains include only one type of monomer. Such a material will be homogeneous with no phase separation. Examples are given in Table 2.1.

Table 2.1: *Examples of single-phase polymers with their T_g values.*

Elasytomer	Monomer	T_g (°C)
Butadiene rubber (BR)	Butadiene	-85
Butyl rubber (IIR)	98% Isobutylene	-74
Natural rubber (NR)	Isoprene	-70
ENR25	Epoxidised natural rubber	-23
ENR50	Epoxidised natural rubber	-48
Chloroprene Rubber (CR)	Chloroprene	-48

Single-phase elastomers have the same constituents (or ratio of constituents) down to the scale of the monomer units, so homopolymers will be single-phase. Copolymers (section 2.4.5) may be single-phase, if either of the monomers is very small in concentration, for example butyl rubber. This is because the percentage of isoprene to isobutylene is very small. If two types of monomer are completely random along the chain such as ENR, the material may also be single-phase, separation into two phases being prevented by the monomers being tied into long chains. Some copolymers are borderline between single-phase and two phase materials because the chain may have regions with a relatively high proportion of one polymer to the other, for instance SBR and NBR. Block copolymers (see section 2.4.5) are very likely to be two-phase, since the blocks will tend to clump together, giving microphases rich in each type of monomer (Smith, 1978).

Normally, single–phase elastomers will have one sharp glass–to–rubber transition, whereas materials tending towards clumping of monomers result in a broader transition, arising from smeared contributions of the transitions for regions of different monomer mixture ratios. The true two-phase elastomers will give two separate transition peaks and will be inhomogeneous in microstructure.

Butyl rubber is an exception; it is near to being a homopolymer (98% isobutylene), yet it has a broad transition. The explanation cannot be that there are clumps rich in polyisoprene and polyisobutylene, because these two polymers have similar T_g. Instead, the broadness of the transition is believed to be because of the steric hindrance for the chain motion (Williams *et al.*, 1955).

Homopolymers are usually able to crystallise because of the regularity of their molecules. If crystallisation is thermodynamically favourable in the temperature range typical of engineering applications they are not elastomeric, but can nevertheless can be very useful materials, examples being polyethylene, polypropylene and polytetrafluoroethylene. Elastomers that are homopolymers are normally completely amorphous, but will tend to partially crystallise if either the temperature is very low or they are subjected to very high strain; examples are NR and CR. Strain crystallisation gives a very important characteristic to these elastomers: because strains are very high at crack tips, the rubber there strain-crystallises, blunting the crack tip and greatly enhancing the resistance of the elastomer to tearing. IIR also fits into this category, suggesting that the 2% of isoprene units is not high enough to suppress crystallisation altogether, and so it may be thought of as a homopolymer with occasional foreign units in the chains, rather than as a copolymer.

2.4.3 Filler reinforcement

Fillers are added to rubber compounds to impart changes to their processing behaviour or to the physical properties of the vulcanization or simply to increase their bulk with a cheaper ingredient. There are many types of filler on the market such as silica, calcium carbonate, clay and carbon black. They are classified in terms of their ability to enhance the physical properties of rubber. This ability is termed reinforcement and depends on characteristics of the fillers such as their surface area, morphology and surface activity. There is a wide spectrum of fillers from non-reinforcing to high-reinforcing.

The non-reinforcing fillers, for example, calcium carbonate, clays and the largest particle size of carbon black, are used as cheap diluents which slightly increase the stiffness of a rubber but drastically reduce its resistance to fatigue. On the other hand, reinforcing fillers such as carbon black with small particle size and silica are used in both natural and synthetic rubber to improve their physical properties. Rubber containing reinforcing filler exhibits some non-linear characteristics (Fletcher & Gent, 1973). The hysteresis loops (Figure 2.4) are not perfectly elliptical while their modulus shows a reasonably strong dependence on amplitude, as shown in Figure 2.16.
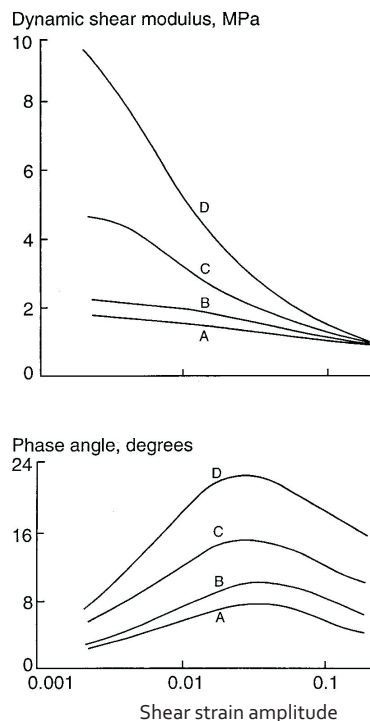
Figure 2.16: *Effect of strain amplitude on the dynamic properties (measured at 5 Hz) of various filled rubber vulcanizates. The types and amounts of carbon black per hundred parts of rubber are A, N762 45 pphr; B, N330 30 pphr; C, N330 50 pphr plus oil 20 pphr; D, N330 75 pphr plus oil 40 pphr (Lindley, 1992).*

There are several factors that influence the behaviour of filled rubber, in particular the particle size and the amount of filler. Finer particle sizes and greater content of filler will increase the 'reinforcement' of a particular product.

The behaviour of filled rubber in the transition region between the rubberlike and glasslike behaviour, is illustrated by storage and loss modulus data from (Ecker 1968) as shown in Figure 2.17. This shows results for unfilled styrene–butadiene and with two levels of loading of carbon black. It is shown that both moduli are substantially increased in the rubbery zone and the transition zone is broadened (Ferry, 1970). The effects of carbon black depend not only on the extent of loading but also the structure of the black and they are found to correlate with its surface area as measured by adsorption (Kraus, 1978).

Choi *et al.* (2004) reported the effect of filler type on the tensile modulus, for example comparing carbon black and silica. The modulus was found to increase linearly with the filler content. Carbon black gives a better increment to the modulus than silica. This is because of the relative dispersion of the different fillers in the particular compound. The dispersion of silica is much worse than for carbon black because silica has strong filler–filler interaction by hydrogen bonding of silinol groups (Choi *et al.*, 2004).

Besides that, fillers and materials with strain-crystallisation can increase strength and perhaps can increase the breadth of the transition. Studies from George & Ival (1966)
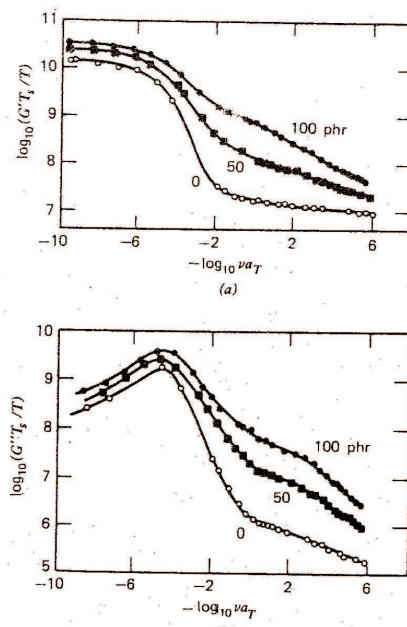
Figure 2.17: *Logarithmic plots of (a) storage and (b) loss shear modulus against frequency reduced to 263K for styrene–butadiene rubber unfilled (open circles) and with two loadings of carbon black. Number (phr) denotes parts carbon black per hundred parts rubber by weight (Ecker, 1968).*

show that graphite has the effect of both increasing damping and broadening the operable temperature and frequency range of the damping system.

2.4.4   Plasticisers

Plasticisers are additives used to soften or 'plasticise' polymers (usually a glassy polymer like PVC) by virtue of their compatibility and high free volume (hence low T_g). Plasticisers behave like a solvent when mixed into a polymer and lower the glass transition temperature T_g. Plasticisers are used in many types of materials but the main usage of organic plasticisers is in polymeric materials. For example dioctyl phthalate (DOP) is extensively used as a plasticiser for PVC (Turi, 1981). Besides lowering the T_g value, it may also serve to lower the melt viscosity, thus making the fabrication process easier at a lower temperature.

Most plasticisers have a glass transition temperature (T_g) in the range from -50℃ to 150℃. The lower the T_g of the plasticiser the more efficient it is at lowering the T_g of the polymer–plasticiser mixture. Plasticisers not only lower the T_g but also increase the width of the transition region (Nielsen, 1962). Efficient plasticisers generally have low viscosities which are only weakly dependent on temperature (Nielsen, 1962).

A mixture of two compatible substances should yield a homogeneous, molecularly inter-dispersed blend with a single glass transition temperature. The T_g can be shifted to higher

or lower values by blending with other compatible elastomers or plasticisers (Nielsen, 1962). The T_g can be approximated by a simple relationship as shown in equation (2.15) which is based on the concept of free volume.

$$T_g = V_1 T_{g1} + V_2 T_{g2} \tag{2.15}$$

where T_{g1} and T_{g2} are the glass transition temperatures in degrees Kelvin (273.15°K = 0°C) for component 1 and 2, and V_1 and V_2 are the volume fraction. Similarly, Fox & Flory (1956) and Wood (1958) derived the resulting T_g based on weight fraction:

$$T_g = w_1 T_{g1} + w_2 T_{g2} \tag{2.16}$$

where w_1 and w_2 are their respective weight fractions. In fact, it would seem more justifiable to base the law of mixture based on volume fraction rather than weight fraction, since T_g is governed by the free volume (Fox & Flory, 1956).

One common deficiency of low molecular weight plasticisers is their susceptibility to migration and volatilization, and yet a very low molecular weight polymer can be used as a plasticiser (Paul & Newman, 1978). Either way, the plasticiser must interact on the molecular scale with the segments of the polymer to speed up the viscoelastic response and increase the molecular mobility, thereby lowering the glass transition temperature (T_g).

2.4.5   Behaviour of copolymers

A polymer derived from more than one species of monomer is called a copolymer (Moore & Kline, 1984). Copolymers that are obtained by copolymerization of two monomer species are sometimes termed bipolymers, those obtained from three monomers terpolymers, those obtained from four monomers quaterpolymers, etc. The properties of resulting products depend on the specific polymerization process that was used leading for example to random or block copolymers. Although the overall composition of block copolymers and random copolymers can be the same, their physical properties will differ significantly (Hofmann, 1989). Examples of polymer structure are shown in Figure 2.18.

Copolymerisation usually results in molecules that are insufficiently regular to allow the material to crystallise. This feature can be exploited to synthesise elastomers using different monomers, such as ethylene (PE) and propylene (PP), which on their own would result in crystalline homopolymers. Thus PE and PP are both crystalline polymers, whereas their random copolymer yields EPR - ethylene propylene rubber. EPDM,
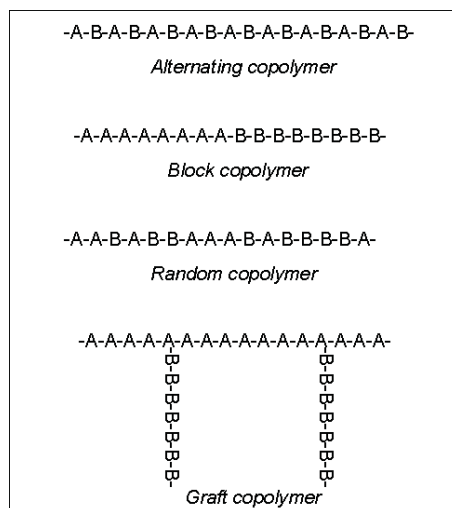
Figure 2.18: *Several types of copolymers (Hofmann, 1989).*

ethylene-propylene-diene monomer, is a form of EPR with some diene monomers to enable it to be vulcanized with sulphur. Similarly, the fluoroelastomer family may be thought of as arising from the introduction of sufficient irregularity into Polytetrafluoroethylene (PTFE) to suppress crystallisation.

Random copolymers occur when one of the monomers polymerized together to form a polymer is in a random or statistical distribution in the polymer chain. Therefore, they have no long blocks of identical units, as shown in Figure 2.18. Examples are styrene-butaniene copolymers and butyl methacrylate-ethylene glycol monomethacry. Their transition regions can be shifted several decades of logarithmic time (or frequency) according to the proportions of their monomers, with very little change in shape of the curve, as discussed by Kraus & Rollman (1971), using results reported using stress relaxation and creep tests.

However, if the two comonomers have relaxation spectra that are different in shape, for example poly (methyl methacrylate) and poly (methyl acrylate), their random copolymers show a change of shape as well as position on the time or frequency scale as the composition is varied, as illustrated in Figure 2.19. It can be expected that the composition will produce similar behaviour in the elastic moduli on a frequency scale although the shift factor may be different (Ferry, 1970).

The molecules in random copolymers are heterogeneous. Studies by Nielsen (1953) found that increasing the degree of this kind of molecular heterogeneity caused a broadening of the transition region on the temperature scale where G' decreased less steeply near its inflection, and the maximum in tan δ was lower.

Block copolymers are composed of long sequences ('blocks') of the same monomer unit, covalently bonded to sequences of unlike type as shown in Figure 2.18. There are three main categories: diblock copolymers, sometimes referred to as AB block copolymers,
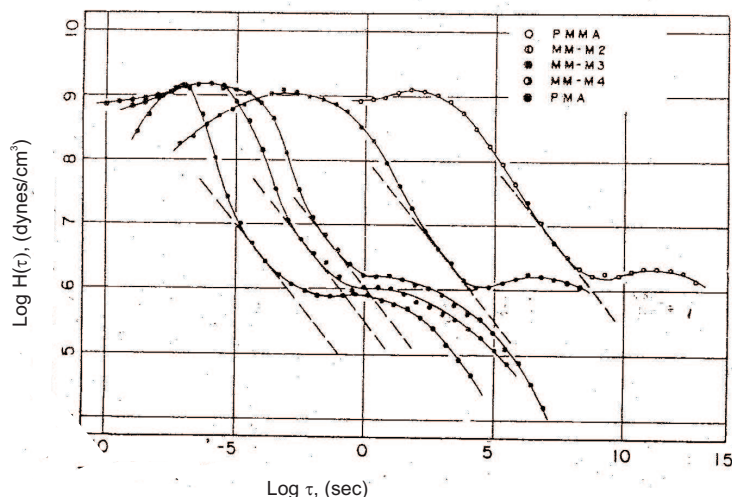
Figure 2.19: *Relaxation spectra of in extension of poly (methyl acrylate), poly (methyl methacrylate) and three copolymers with compositions indicated, reduced to 100℃ (Fujino et al., 1961).*

triblock copolymers of the ABA type, and multiblock copolymers of the $(AB)_n$ type. Diblock copolymers are macromolecules comprising two chemically distinct and mutually incompatible segments (monomers) that are covalently bonded together.

The blocks can sometimes intermix freely at sufficiently high temperatures, or when sufficiently diluted with solvent, generating a 'disordered' structure. However, it is common for the blocks spontaneously to self-assemble ('order') into a diversity of mesophases, with the size scale governed by the chain dimensions (order of tens of nanometers).

The 'order-disorder' temperature is the term used for the temperature of phase separation in the block copolymer as shown in Figure 2.20. Most block copolymers are phase separated, that is, the two kinds of blocks are immiscible. (Most of the important properties of block copolymers, including thermoplastic elastomers, elastic fibres, and surfactant applications, depend on phase separation). On the other hand, most polymer blends exhibit lower critical solution temperatures (LCST). This means that the two polymers become more miscible as the temperature is lowered.

Polyurethane elastomer is an example of a block copolymer, formed by reacting diisocyanate with a hydroxy-terminated prepolymer. The glass transition of this polymer is increased as the concentration of the diisocyanate is increased. This phenomenon results from the high polarity of short segments of each macromolecule, called 'hard' segments. They are formed from the diisocyanate and the short chains diol and diamine (Smith, 1978). The urethane linkages form at the end of the hard segments leading to long chains of low polarity called 'soft' segments.

Similar to block copolymers, **triblock** elastomers contain long sequences of identical units

44
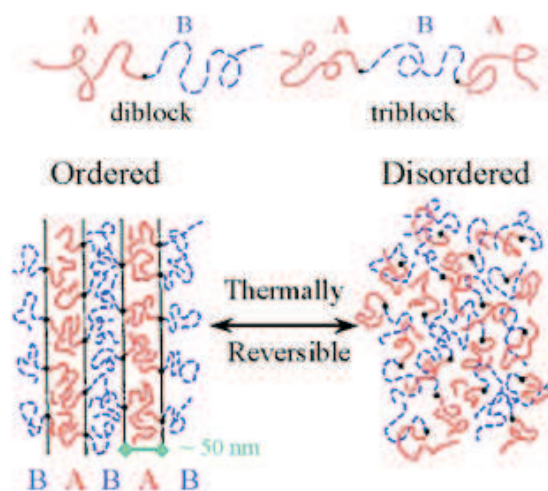
Figure 2.20: *The structure of copolymers showing phase separation at low temperature and miscibility at high temperature (Kraus, 1978).*

where all the molecules have a similar pattern of block (i.e often three, ABA). Some examples of triblock elastomers are styrene-isoprene-styrene (SIS), methyl styrene–isoprene–α-methylstyrene (mSImS) and styrene–butadiene–styrene (SBS) rubber which is used for the soles of shoes and for tyre treads.

Experiments at 110 Hz at various temperatures of a styrene–butadiene triblock copolymer showed two transition zones, as illustrated in Figure 2.21 (Ferry, 1970). Two peaks are observed in the loss modulus, at -100℃ and +120℃. This phenomenon occurs due to the degree of 'blockiness' from random to long block which will affect the steady flow viscosity and its shear rate dependence. In contrast, if the block is quite long, a single transition zone will be observed.

The number of transition zones of a copolymer material can also be determined by studying the compatibility or incompatibility of the combination of different monomer units in the mixtures. Incompatibility occurs when physical blending leaves moderately large regions of homogeneous composition. This will lead to the occurrence of several transition zones. For example, results for a mixture of poly (methyl methacrylate) and poly (vinyl acetate) are illustrated in Figure 2.22 (in plots of G^* and tan δ), which are reported from data of Jenckel & Herwig (1956). This shows transition regions at 40℃ and 110℃. Similar behaviour can be found for mixtures of polystyrene with butadiene–styrene copolymer (Nielsen, 1953). In exceptional cases such as poly (vinyl chlorite) and butadiene–acrylonitrile rubber (Nielsen, 1953), a compatible mixture is produced which leads to a single transition zone.

Polystyrene–polyisobutylene–polystyrene (PS–PIB–PS) is a triblock copolymer made by
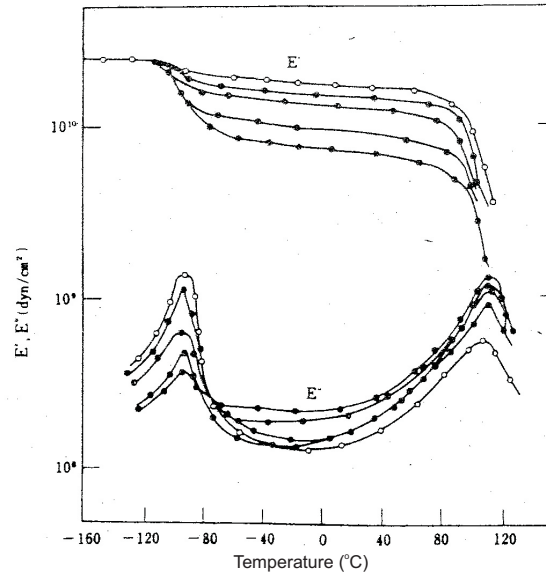
Figure 2.21: *Storage and loss Young's modulus (on a logarithmic scale) at a frequency of 110 Hz against temperature for styrene – butadiene triblock copolymers. Decreasing values of **E**' correspond to decreasing styrene/butadiene ratio (Ferry, 1970).*
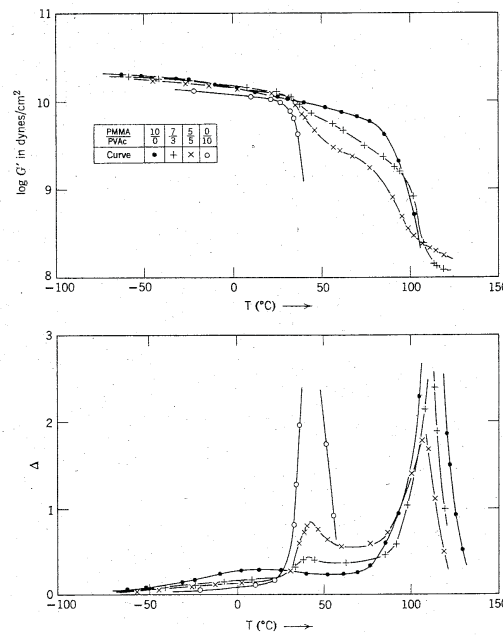
Figure 2.22: *Storage modulus and logarithmic decrement (approximately propotional to loss tangent) plotted against temperature, for physical mixtures of poly(methyl methacylate) and poly(vinyl acetate) with compositions as indicated (Jenckel & Herwig, 1956).*

46

different processes. Its dynamic properties were determined by dynamic mechanical analysis (DMA) in Reauschle *et al.* (1997). The PS–PIB–PS films were composed of approximately 30% polystyrene end–blocks. Figure 2.23 shows the tensile storage modulus E', loss modulus E'', and tan δ as a function of temperature. E' shows a distinct drop at the glass transition temperature of the PIB matrix (the T_g of pure PIB is -70℃ (Sperling, 1992)) and another decrease that begins at approximately 93℃ associated with onset of the glass transition of the PS domains. The tan δ curve exhibits a low–temperature shoulder at approximately -60℃ that may be a contribution from less–restricted PIB chains. The low–temperature shoulder seems to correspond with the peak of E''. In this particular exercise, the transition temperature is defined as the temperature corresponding with the maxima in the E'' data and was measured at approximately -63℃ for the PS–PIB–PS copolymers. The transition temperature was previously reported for non–commercial PS–PIB–PS polymers to be approximately -65℃ using differential scanning calorimetry (DSC), which is in good agreement with the DMA data.
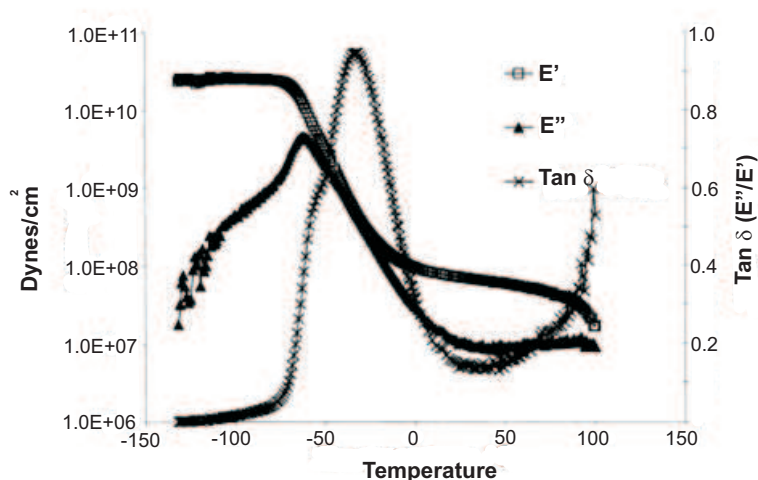
Figure 2.23: *Mechanical analysis of PS-PIB-PS (Reauschle* et al.*, 1997).*

2.4.5.1   Polyurethane

Based on the above information, polyurethane is an example of a segmented copolymer which gives two peaks in the tan δ. This section discusses this polymer further.

Polyurethanes are linear segmented copolymers which consist of alternating soft (flexible) and hard (rigid) segments as shown in Figure 2.24. The soft segment is commonly a low molecular weight polyether or polyester with long (1000 - 2000nm) flexible segments, where polyester is prone to hydrolysis and this will limit its uses in water contact applications. The hard segments are based on diisocyanate and a low molecular weight diol (Schneider *et al.*, 1975) which have shorter (150nm) rigid units that are chemically and hydrogen bonded. Each molecule contains a number of hard segments attached

to long flexible chains of soft segments (Figure 2.25). Thermodynamic immiscibility of the hard and soft segments at low temperature results in a micro-phase separation (or mircosegregation) and consequently a domain structure (Wang & Luo, 2004).
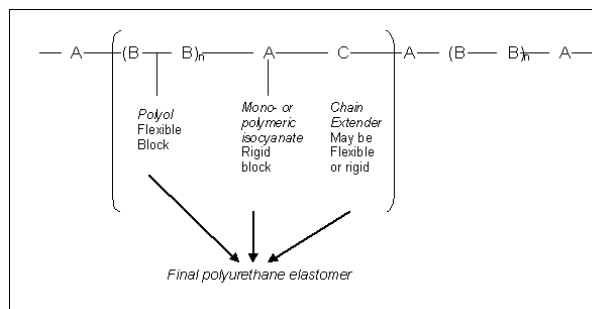
Figure 2.24: *The basic unit in a urethane block copolymer (Hepburn, 1982).*
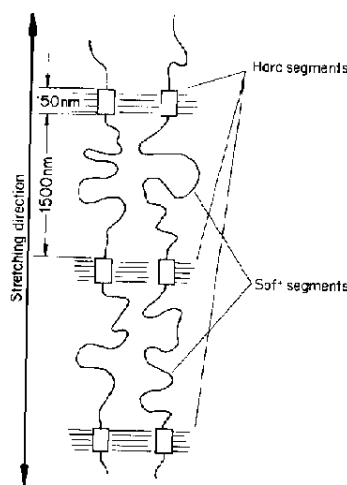
Figure 2.25: *Flexible and rigid segments in a polyurethane elastomer (Hepburn, 1982).*

Polyurethane will remain flexible between temperatures -70℃ and 200℃. This can be seen in Figure 2.26 where the modulus–temperature curve of an elastomeric polyurethane block copolymer shows at least two major drops in the modulus over the temperature range. The material undergoes a change from stiff to rubbery character at the low temperature transition (below room temperature), related to segmental flexibility of the polyol. The higher temperature transition (above 100℃), corresponds to the thermal dissociation of hydrogen bonds and breakdown of van der Waal's forces between hard blocks in rigid units (Hepburn, 1982). Between these two transition regions the modulus is much less affected by temperature. The two transition temperatures for the curve in Figure 2.26 are -40℃ for the lower temperature and 10℃. These values were measured using differential scanning calorimetry (DSC) (Hepburn, 1982). This type of modulus-temperature dependence is typical of elastomeric block copolymers containing both flexible (soft) and rigid (hard) segments.

The chemical formulation of polyurethane is illustrated in Figure 2.27. It is referred to as the prepolymer route which is formed from several steps.
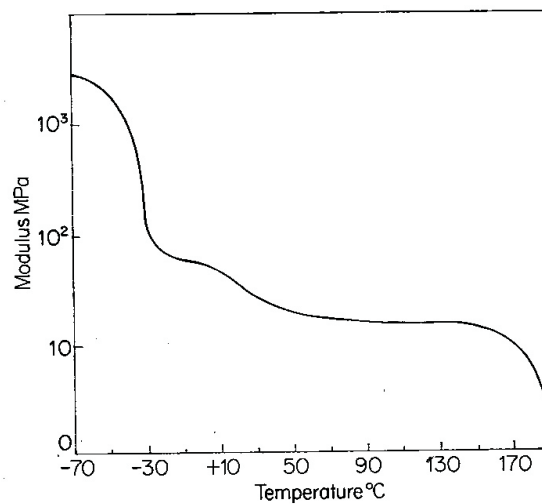
Figure 2.26: *Torsional modulus–temperature relationship for polyurethane based on poly(tetramethylene adipate) (PTMA) (Hepburn, 1982).*
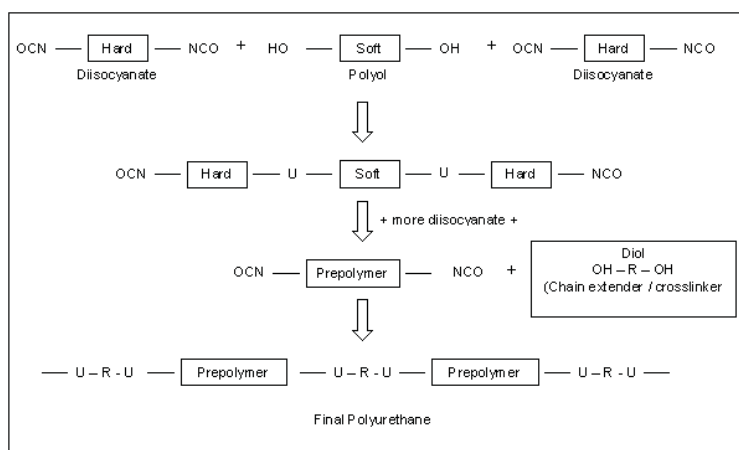
Figure 2.27: *Prepolymer route for the formation of a polyurethane elastomer where 'U' is a urethane group and 'R' is a chain extender.*

49

Polyurethane can contain a high concentration of polar groups. The interactions between the polar groups are very important in determining the properties of the polyurethane block copolymer. The rigid segments in polyurethane block copolymers affect the modulus, hardness and tear strength, and determine the upper usable temperature. The flexible blocks influence the elastic nature of the product and its low temperature performance.

The flexible block segment contains an aliphatic polyester material. These have a glass transition temperature below room temperature and a low melting point. They are amorphous and the molecular weight range used is from 600 to 3000. Poorer physical properties occur at low molecular weight (less than 600). As the molecular weight of the flexible block increases, the modulus falls and the elongation at break increases (Hepburn, 1982).

The rigid block segments are formed by reaction of diisocyanate with a glycol or a di-amine and sometimes another chain extender. The rigid segments have greater interchain attractive forces than the flexible blocks, due to high concretration of polar groups and hydrogen bonding, which affect the modulus, hardness and tear strength.

Figures 2.28, 2.29 and 2.30 are examples of the modulus and loss factor (tan δ) of polyurethane polymers. These figures show the storage modulus and tan δ of poly (urethane–imide)s copolymer prepared using different isocyanate and polyol based prepolymer and pyromellitic dianhydride(PMDA) (Gnanarajan *et al.*, 2002). Gnanarajan *et al.* (2002) reported that all the storage modulus curves shown (Figure 2.28 and 2.30) plateau up to -50℃.

Polymers prepared with different isocyanates uniformly showed a sharp decline in modulus around -56℃ due to the glass transition of the polymer (Figure 2.28). On the other hand, the effect of different polyol on the polymer (Figure 2.29) showed that T_g decreases from polypropyleneoxy glycol (PPG-2000) to polytetramethyleneoxy glycol (PTMG-2000) and hydroxyl terminated polybutadiene (HTPB-2500) based polymers due to the absence of side groups and hence the latter have a greater segmental mobility (Gnanarajan *et al.*, 2002).

According to Gnanarajan *et al.* (2002), the imide content will also affect the T_g of the polymer. The imide content of the resulting copolymer will be increased as the amount of free isocyanate groups present in the prepolymer increases. This causes the T_g gradually to shift towards higher values as seen in Figure 2.30. This is due to the increase in the hard segments content and rigidity which restricts the segmental mobility. Polyimides are preferred for their good thermal stability and high T_g while PU has low T_g. Therefore the combination of these two materials will give an intermediate T_g.
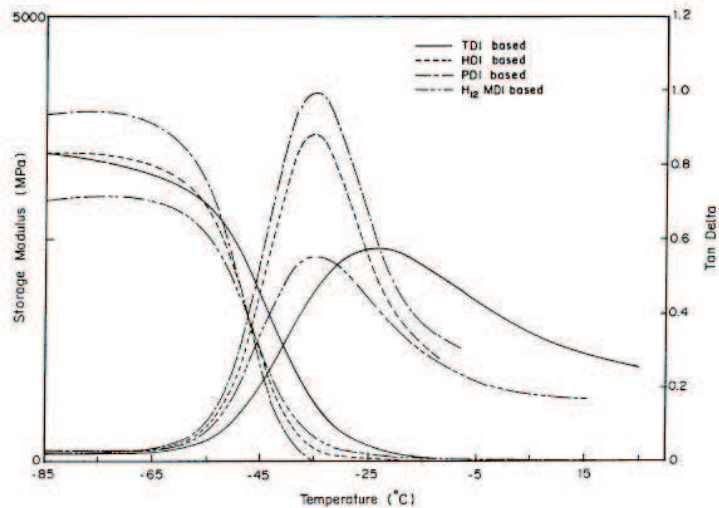
Figure 2.28: *Storage modulus and tan δ profiles of poly (urethane–imide)s copolymer prepared using prepolymer having different isocyanate (NCO) content and pyromellitic di-anhydride (PMDA) (Gnanarajan* et al., *2002).*
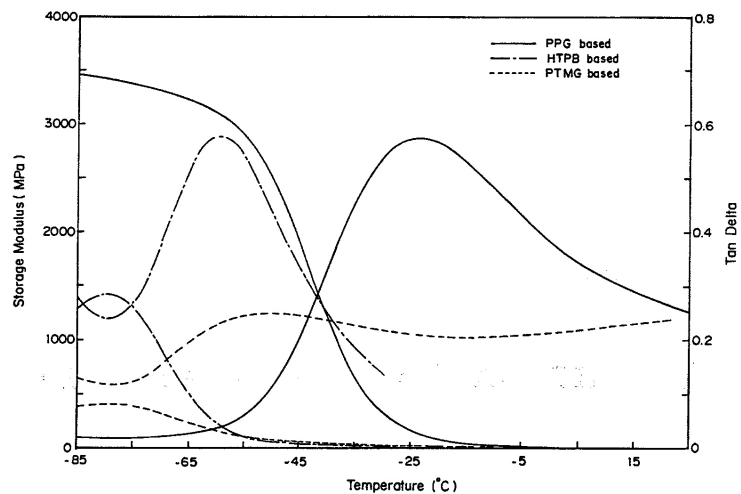
Figure 2.29: *Storage modulus and tan δ profiles of poly (urethane–imide)s copolymer prepared using different polyol based prepolymer and PMDA (Gnanarajan* et al., *2002).*

51
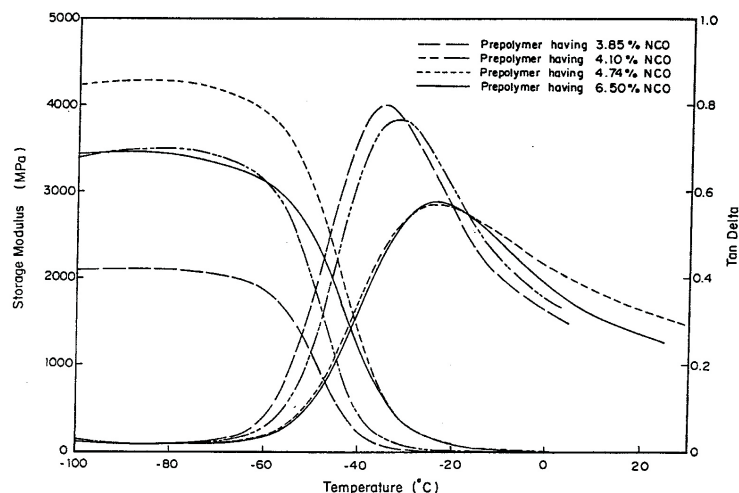
Figure 2.30: *Storage modulus and tan δ profiles of poly (urethane–imide)s copolymer prepared using prepolymer having different NCO content and PMDA (Gnanarajan* et al., *2002).*

2.4.6 Polymer blend

A polymer blend may be defined as a combination of two polymers without any chemical bonding between them. Blending of two or more polymers is used to obtain new products that can solve a particular problem, in this case to have a polymer that can maintain suitable properties over the temperature range of interest. When blending polymers together, one of question concerns the miscibility or compatibility of the polymeric components in a blend. In the following, results are given for examples of polymer blends which show the modulus and loss factor in the temperature or frequency domain.

An elastomer formed of Thermoplastic Polyurethane (TPU) and Ethylene-propylene-diene elastomer (EPDM) is an example of a polymer blend which can be prepared via melt blending. Wang & Luo (2004) found using dynamic mechnical thermal anaysis (DMTA) that EPDM was thermodynamically miscible with the soft segment of TPU and incompatible with the hard segments. Results are shown in Figure 2.31 for TPU, EPDM and their blends determined by DMTA. This shows the loss factor (tan δ) versus temperature. The transition temperature (maximum tan δ) of TPU is at -45.8℃, whereas EPDM exhibits a value of -52.6℃. The transition of TPU arises from the polyester-based soft segment because the T_g of poly(diisocyanates-diol) based on the hard segments is usually -75℃ to -120℃ (Wang & Luo, 2004). The plot also shows that by increasing the EPDM content in the blend, the peak shifts to the left and reduces in height. Besides that, Figure 2.31 shows only a single peak in each curve.

Another example of polymer blends is shown in Figure 2.32, which shows loss factor (tan δ) versus temperature. Styrene-butadiene (SBR) (T_g=-67℃) diblock polymer containing
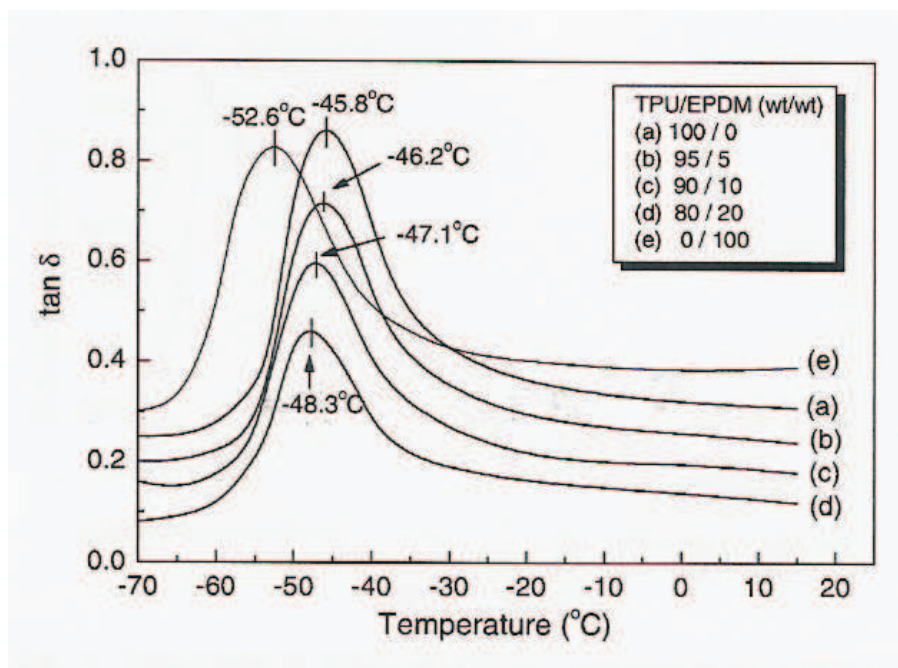
Figure 2.31: *Plots of tan δ vs. temperature for TPU/EPDM blend at frequency 1 Hz (Wang & Luo, 2004).*

25% styrene was blended in a ratio of 30/70 with natural rubber (NR) (T_g=-70℃), polychloroprene (CR) (T_g=-54.5℃), or EPDM (T_g=-60℃) (Paul & Newman, 1978). In all cases the polybutadiene (PB)(T_g=-110℃) and polystyrene (PS) (T_g=+90℃) glass transitions are detected. The resolution suffers when the T_g values lie close together as shown in the figures for the example of the natural rubber and butadiene block polymer.

2.5 Candidate Materials

In seeking to develop an elastomeric material for use in the ISVR/Corus rail absorber, the material should ideally have the following dynamic properties (Thompson *et al.*, 1998, 2000):

- tan δ > 0.35

- G' = 5 MPa at 1000 Hz and 20℃, with as small a variation as possible over the working range of temperature and frequency.

These should be satisfied for temperatures between -20℃ and 40℃ and frequencies between 300 Hz and 3000 Hz. Material will therefore be sought with tan δ > 0.25 and G' between 1.7 and 8.3 MPa.

Based on the information reviewed in section 2.4 and the aims to have a material with a broad loss factor over the temperature range of interest, several interesting polymers are
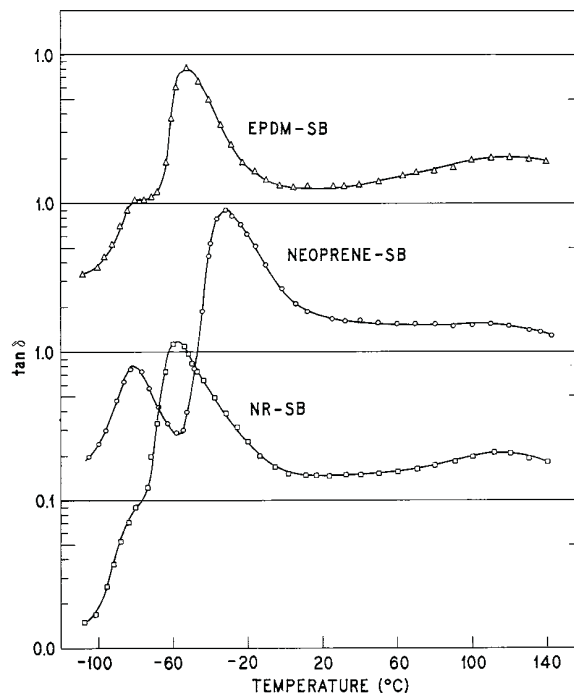
Figure 2.32: *Loss factor (35 Hz) of cross-linked polyblends of 30% SB block polymer (25% styrene) with 70% of another rubber. Curves are displaced by one decade each (Paul & Newman, 1978).*

selected to be discussed in more detail in this section. Polyurethane, for example, is a segmented copolymer which gives two peaks of T_g. It is believed that this polymer can be modified to suit the requirements. Another example is butyl rubber. This rubber is a random copolymer which gives a very broad peak of loss factor.

Table 2.2 shows data for a number of different rubbers gathered from the literature. The materials are selected based on their broad loss factor across the temperature range of interest. The properties such as shear modulus and loss factor have been calculated using interpolation and time temperature superposition methods to determine the properties at the specific temperature and frequency required. The value of $T_{g,mech}$ is derived from the maximum peak of loss factor as discussed in section 2.3.3.

Figure 2.33 plots the loss factor against shear modulus (at either 500 or 1000 Hz) for the temperatures -20, 0, 20 and 40℃. Also shown is a region defining the specification (the range of allowable values for G' and loss factor). As can be seen, most of the materials considered fall outside the specified area. Moreover, where the loss factor is very high the shear modulus varies too rapidly.

Figure 2.34 shows the results for seven selected viscoelastic materials (five materials from Table 2.2 and two other materials from Ahmad (2005) and Jones *et al.* (2001b)), where most of their properties fall within the targeted area. They are polyphosphazene, butyl, polysulphide, 3M ISD-113, EPDM, NBR sample 23 and PU sample 7*f*. A description of

Table 2.2: *Shear modulus and loss factor of different materials at various temperatures.*

| No	Material	Freq. Hz	$T_{g,mech}$ ℃	$G'_{T_g,mech}$ MPa	$\eta_{T_g,mech}$	-20℃ G'/MPa	η	0℃ G'/MPa	η	20℃ G'/MPa	η	40℃ G'/MPa	η
1	SBR[3]	500	-73	60.0	0.90	15.0	0.40	10.0	0.32	6.7	0.26	4.7	0.20
2	EPDM[3]	500	-55	33.3	0.50	16.7	0.30	10.0	0.28	8.3	0.25	6.7	0.20
3	Polynorbornene[3]	500	-40	16.7	1.50	3.2	0.80	1.0	0.40	0.8	0.20	0.7	0.18
4	Natural rubber[3] (NR)	500	-28	10.0	2.50	3.0	2.00	0.6	1.00	0.5	0.40	0.5	0.20
5	Barry Controls H-326[1]	1000	-26	62.1	0.90	37.9	0.80	11.8	0.35	6.9	0.19	6.2	0.10
6	Shell Kraton[1]	1000	-20	9.2	1.20	9.2	1.20	1.2	0.60	0.9	0.40	0.9	0.20
7	Fluorosilicon[3]	500	-20	3.5	0.80	3.5	0.80	1.7	0.55	1.0	0.35	0.8	0.25
8	neoprene[3]	500	-20	80.0	0.40	80.0	0.40	25.0	0.30	15.0	0.20	10.0	0.18
9	Polyphosphazene[3]	500	-20	20.0	1.00	20.0	1.00	8.0	0.90	4.0	0.70	2.0	0.50
10	Butyl (IIR)[3]	500	-20	16.7	0.80	16.7	0.80	8.3	0.60	6.7	0.50	3.0	0.40
11	polyacrylate[3]	500	-17	70.0	0.90	100.0	0.80	40.0	0.40	25.0	0.20	15.0	0.20
12	Urethane[3]	500	-15	12.0	0.40	18.0	0.30	7.0	0.25	4.5	0.15	4.0	0.10
13	Polysulfide[3]	500	-15	30.0	1.30	15.0	1.00	5.0	0.50	3.5	0.30	2.2	0.30
14	3M ISD-113[1]	1000	-12	2.8	1.04	13.1	0.80	4.8	1.00	2.1	1.02	1.4	1.03
15	ENR25[2]	1000	-12	20.0	2.90	200.0	1.60	2.2	1.50	0.6	0.48	N/a	N/a
16	VAMAC Ethylene acrylic[3]	500	-11	60.0	0.80	116.7	0.60	26.7	0.70	10.0	0.40	6.7	0.30
17	Paracril-BJ with 0 phr C[1]	1000	-5	10.2	4.30	291.0	0.68	6.9	4.70	1.9	0.60	1.8	0.30
18	Paracril-BJ with 25 phr C[1]	1000	-4	31.4	1.90	413.7	0.39	19.5	1.80	4.6	0.88	3.7	0.30
19	Paracril-BJ with 50 phr C[1]	1000	-2	76.7	1.50	842.7	0.20	64.3	1.40	16.5	0.65	10.3	0.35
20	TPFE elastmer[3]	500	0	120.0	0.70	420.0	0.50	120.0	0.70	51.0	0.47	27.0	0.26
21	Polyurethane[4] (PU)	1000	0	3.8	0.65	N/a	N/a	15.7	0.88	4.7	0.40	2.7	0.35
22	Nitrile (NBR)[5] blend	1000	5	20.0	1.10	254.0	0.24	23.5	0.99	3.5	0.64	2.1	0.32
23	Polyisobutylene[1] (PIB)	1000	10	10.3	1.64	69.0	0.80	8.0	1.50	1.6	1.36	0.8	0.68
24	3M ISD-112[1]	1000	31	1.6	1.30	68.9	0.28	11.5	0.65	3.1	1.20	1.1	1.00
25	EAR C-1002[1]	1000	35	6.2	1.83	661.9	0.17	206.8	0.50	26.2	1.33	4.1	1.67
26	EAR C-2003[1]	1000	38	68.9	1.10	2413	0.02	1723	0.20	413.7	0.70	41.4	1.00
27	Down Corning Sylgard[1]	1000	44	5.5	0.60	N/a	N/a	37.9	0.30	17.2	0.45	6.9	0.50
28	Antiphon-13[1]	1000	48	41.4	1.70	689.5	0.67	413.7	0.40	172.4	1.00	55.2	1.70
29	EC 2216 with graphite [1]	1000	49	551.6	0.40	3792	0.01	3585	0.05	2757	0.12	827.4	0.35
30	GE SMRD[1]	1000	52	34.5	0.90	689.5	0.00	551.6	0.04	206.8	0.20	48.3	0.70
31	Lord LD-400[1]	1000	52	413.7	0.65	6205	0.01	5515	0.05	3447	0.25	827.4	0.58
32	Blachford Aquaaplus[1]	1000	53	1034	0.50	3792	0.00	3447	0.03	3447	0.15	1723	0.40
33	Soundcoat DYAD[1] 606	1000	59	17.2	1.00	689.5	0.01	620.5	0.09	310.3	0.33	55.2	0.80
34	3M ISD-110[1]	1000	66	2.1	1.67	68.9	0.08	55.2	0.30	19.0	0.70	6.2	1.20
33	Soundcoat DYAD 609[1]	1000	85	6.9	1.00	N/a	N/a	482.6	0.03	413.7	0.16	172.4	0.38

[1](Nashif *et al.*, 1985), [2](Ahmadi & Muhr, 1994), [3](Nashif & Lewis, 1991), [4](Jones, 2005), [5](Ahmad, 2005).
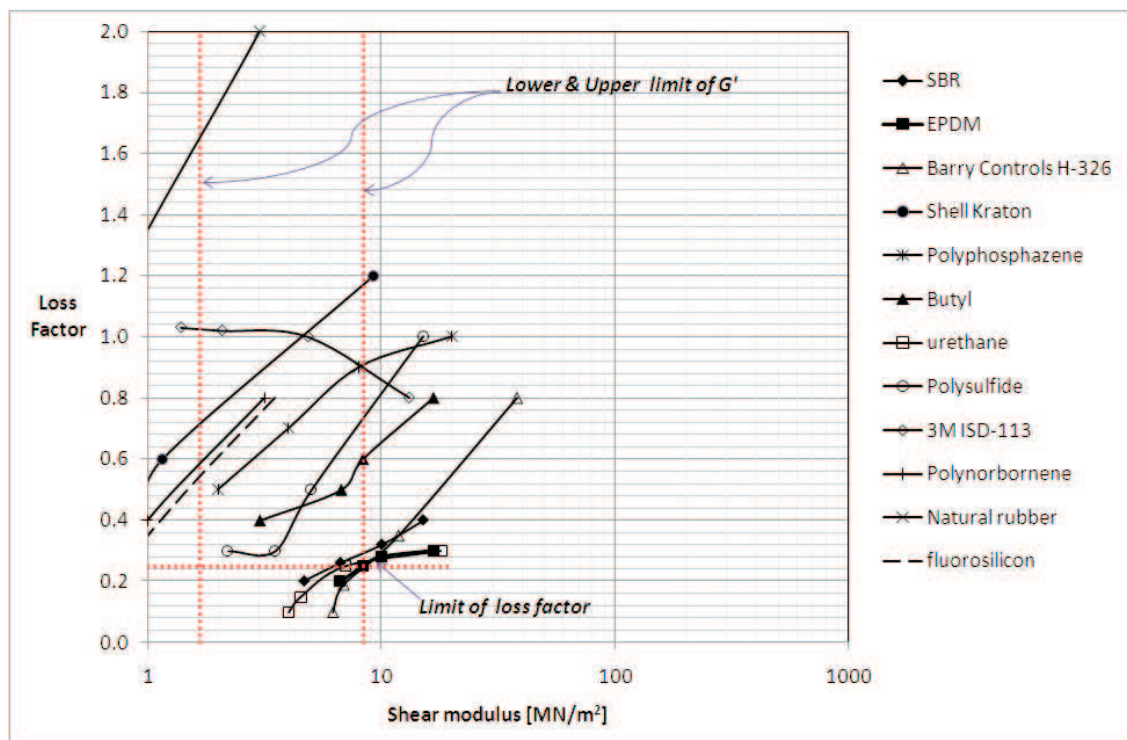
(a)
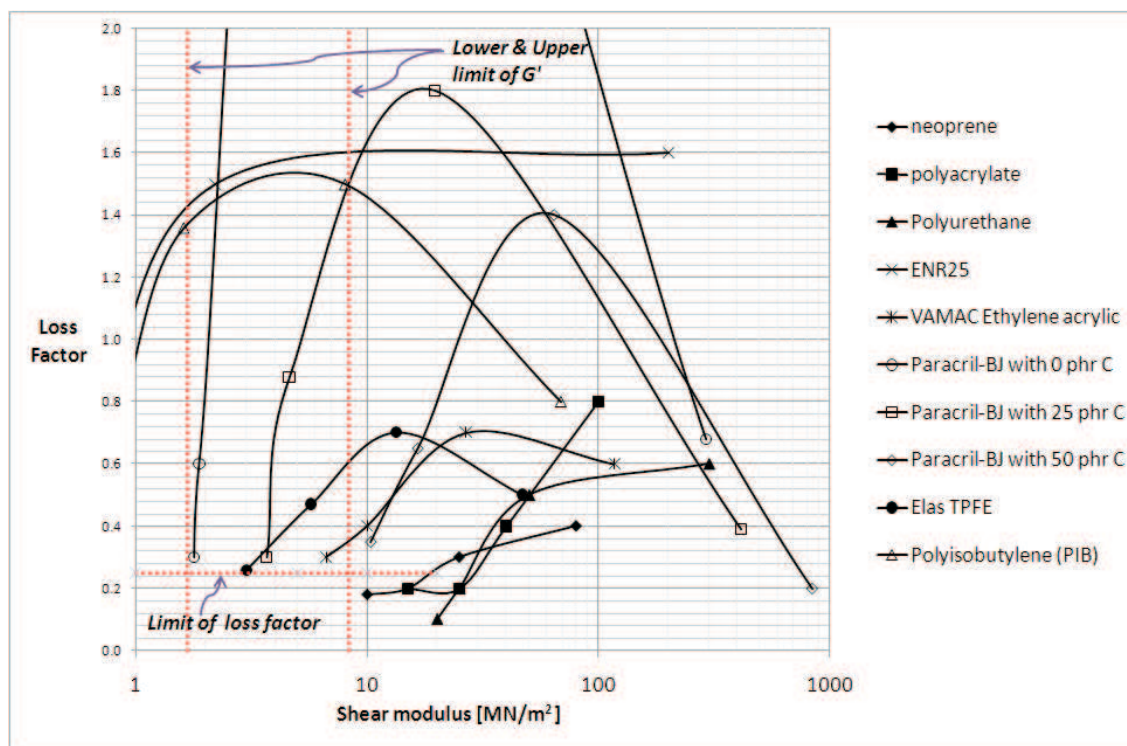
(b)

Figure 2.33: *The dynamic properties of rubbers (at either 500 or 1000 Hz: see Table 2.2) compound with the requirement for the rail absorber as marked by red lines.*
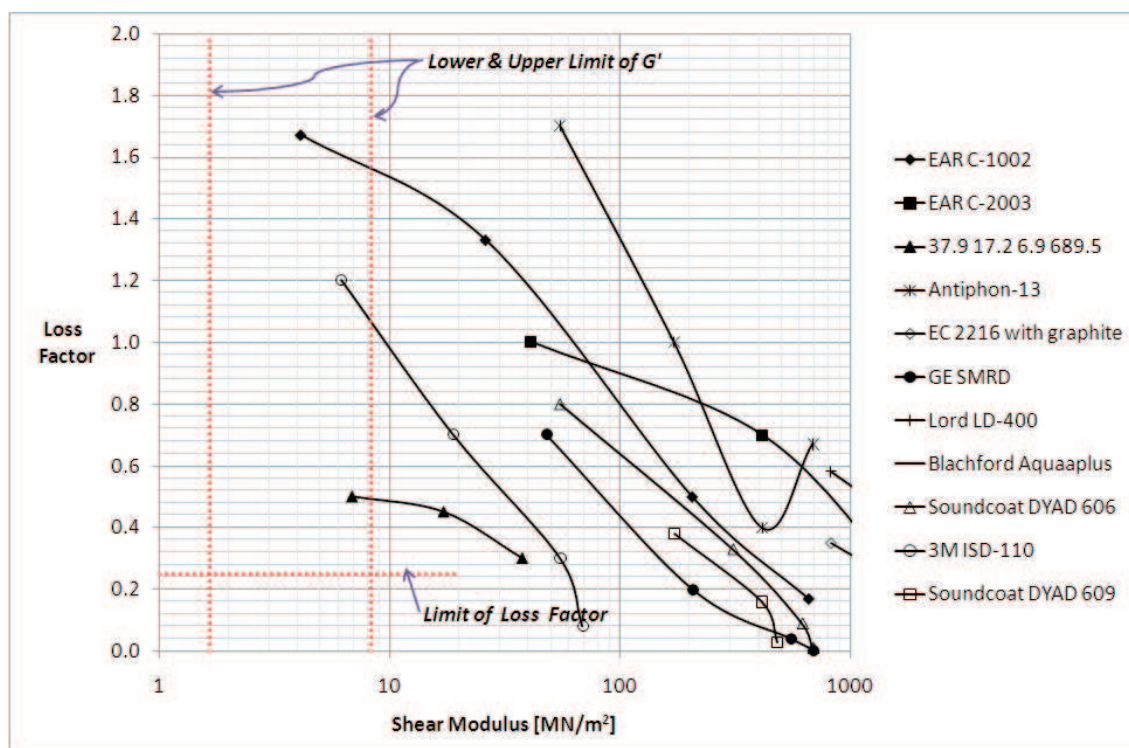
(b)

Figure 2.33: (Continued).

each material is given below.

2.5.1 Polyphosphazene

The Polyphosphazene family covers a broad range of compositions. They are semi-organic polymers having a backbone composed of alternating phosphorous and nitrogen atoms with each phosphorous atom attached to two organic or organometallic side groups (Allcock, 2002) and (Jones, 1991). The general structure of polyphosphazenes is shown in Figure 2.35, where 'R' can be organic/organometallic side group (Allcock, 2002) and (Laurencin & Nair, 2003). The side groups on phosphorous atoms play a crucial role in determining the properties. Many of these polymers have been identified as excellent candidates for biomedical, oil field and high technology applications such as aerospace and automotive. According to Jones (1991), they are available commercially from a company called Ethyl and commercialised under the trade name Eypel-F elastomer.

The key property of polyphosphazene is it backbone flexibility, due to the -P-N- skeletal system, which offers the opportunity for synthesizing polymers with a wide spectrum of properties in terms of crystallinity, solubility, processability etc, depending on the nature of the side groups. Moreover, this phosphorus-nitrogen backbone also gives the polyphosphazene elastomer its inherent fatigue resistance, low-temperature performance

57
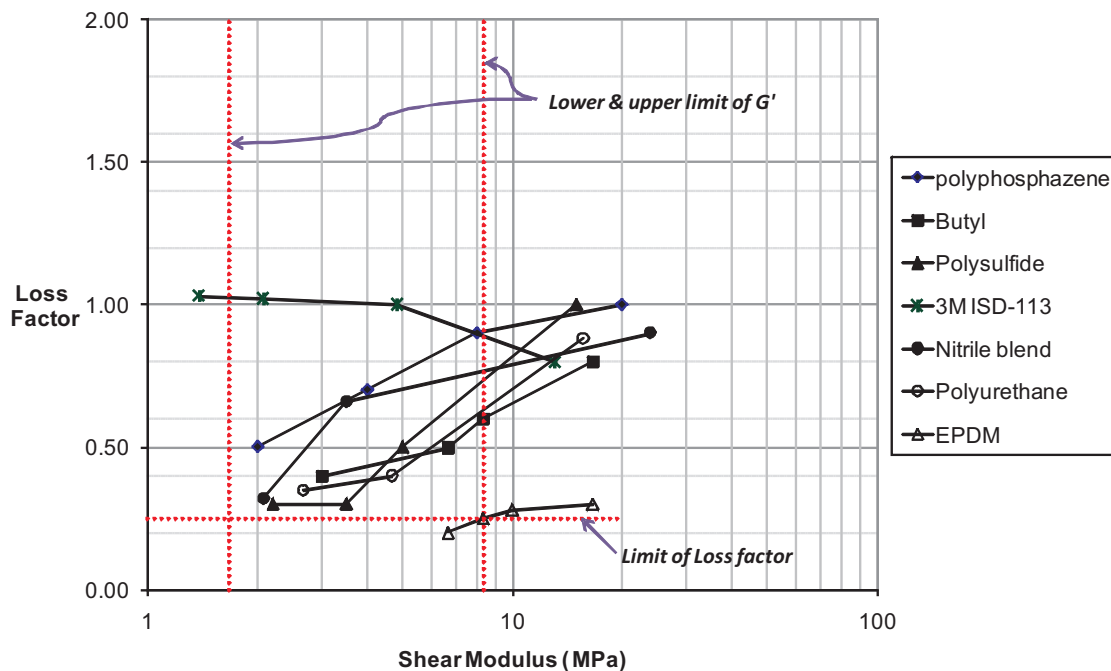
Figure 2.34: *Selection of materials to be investigated in detail.*

and thermal stability characteristics (Jones, 1991). Another property of polyphosphazene is the ability to incorporate two or more different side groups which could add another dimension to fine tuning the properties of the polymer (Allcock, 1977). Fluorination imparts good resistance to hydrocarbon, oils, water, amine corrosion inhibitors, diesel fuel and greases.

The choice of side groups can vary the T_g of the polyphosphazene polymer. For example, poly[bis(trifluoroethoxy)phosphazene] as shown in Figure 2.36(a) has a T_g of -66℃ due to the presence of fluorinated side groups. This polymer can be converted to a useful elastomer by introduction of other fluor-alcohols along with trifluoroethoxy groups by simultaneous substitution or using metathetical ligand exchange reaction. This elastomer is used in developing gaskets, O-rings and low temperature fuel lines. Similarly, fluorinated polyphosphazene described by Jones (1991) has a T_g value of -65℃ and is used in oil field applications. The T_g of the polyphosphazene can be increased as high as 93℃ by incorporating rigid, bulky side groups which will restrict the main chain mobility (Figure 2.36(b)). By mixing other side groups such as phenoxy along with phenyl phenoxy side groups the T_g can be reduced to 43℃ (Figure 2.36(c)) (Allcock *et al.*, 1989).

Jones (1991) shows that the hardness of a particular polyphosphazene studied is 35 to 95 Shore A, tensile strength of 6.89×10^6 N/m^2 to 13.79×10^6 N/m^2, elongation of 75 to 250% and compression sets of 15 to 55% after 70 hours at 150℃. The tensile strength of polyphosphazene elastomer changes less across the temperature range than NBR-nitrile and fluorocarbon. The ultimate elongation of polyphosphazene elastomer is relatively constant regardless of the temperature in the range -30℃ to 175℃. Due to the

R= alkoxy, aryloxy or amino groups
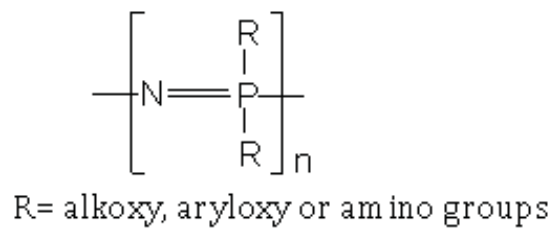
Figure 2.35: *General structure of polyphosphazenes (Allcock, 2002).*
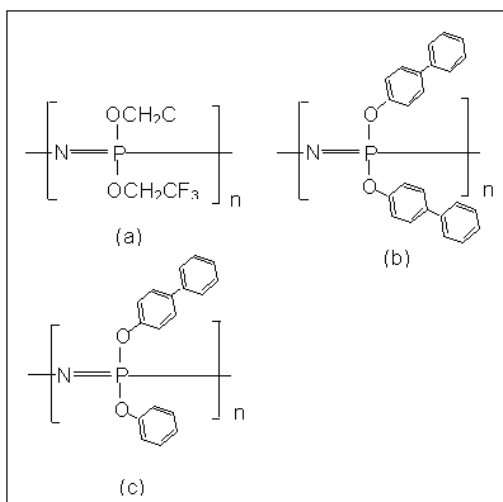
Figure 2.36: *Structure of various polyphosphazenes (Allcock, 2002). (a) T_g=-65℃, (b) T_g=93℃ and (c) T_g=43℃*

phosphorus-nitrogen backbone, the polyphosphazene elastomers do not require addition of plasticiser to have excellent low temperature performance.

Based on the properties discussed, this material is suitable for the rail absorber. However, it may be very expensive and more information needs to be sought in terms of the processing method.

2.5.2 Polysulphide

Polysulphide rubber was discovered in 1926 by the American chemist, Joseph Cecil. This elastomer was commercialised under the trade name Thiokol. Polysulphide rubber is prepared from ethylene dichlorides and sodium tetrasulphide which is manufactured by Thiokol Chemical Corporation (Britannica, 2005) and commercialised by trade names FA Polysulfide Rubber and ST Polysulfide Rubber (Robert, 1990). Commercial grades vary in sulphur content from 37 to 84% and are available in viscosities ranging from pourable liquids to millable gum stock. Typcal application of polysulphide rubbers are sealants, rubber washers, propellant binders and window glazing.

Polysulphide rubbers have high sulphur content of the polymer backbone. This results in a very flexible and virtually impermeable rubber. The polymer is mainly used in the form of a low-molecular-weight liquid that cures in place to create an elastomeric sealant. It consists of sulphur-sulphur linkages connecting short sequences of ethylene, the molecular chain being terminated by reactive mercaptan groups that are also used for interlinking (Britannica, 2005). The polysulphide rubber has a good combination of solvent resistance, low temperature flexibility, flex-crack resistance and oxygen and ozone resistance. However, heat resistance, mechanical strength and compression set are not outstanding. The useful temperature range is -54℃ to 107℃. Polysulphide is used for seals and recommended for services involving contact with solutions of petroleum solvent.

This rubber is not considered for further investigation because it has a very steep slope of shear modulus in the temperature range of interest, especially below +10℃. Furthermore, polysulphide rubber has a strong odour and it is difficult to process.

2.5.3 Nitrile rubber (NBR)

Ahmad (2005) considered a series of materials based on NBR, of which the material labelled sample 23 was found to be a good candidate material for the rail vibration absorber. NBR offers a wide range of material properties, depending on the acrylonitrile content, and a very broad glass transition range. This material has extremely low mould fouling properties combined with fast curing characteristics. It has a high modulus, high

resilience, good abrasion resistance and good balance between oil resistance and low temperature performance (Hofmann, 1989). Nitrile rubber is an unsaturated copolymer of acrylonitrile and butadiene. By selecting an elastomer with the appropriate acrylonitrile content in balance with other properties, NBR can be used for a wide variety of applications in a temperature range of -40℃ to +125℃.

NBR requires formulating with added ingredients, and further processing to make useful articles. Since the materials required for the rail absorber should perform effectively over a wide temperature range, blending of NBRs according to their acrylonitrile content was carried out (Ahmad, 2005). The loss factor - temperature curve can be broadened by blending grades of NBR. Although blending reduces the maximum loss factor, it goes some way to extending the effective temperature range. By increasing the number of incompatible components in the blend, a material should be obtained with a broad loss factor peak, as shown in Figure 2.37 (Ramirez, 1995).

The acrylonitrile content also affects the glass transition temperature. By increasing the acrylonitrile content in the polymer, the T_g of NBR rises as shown in Figure 2.38. Besides that, an increase in the acrylonitrile content will also give less swell, poorer gas permeability, elasticity and low temperature flexibility, but improve the compatibility with polar plasticisers and polar plastics (Hofmann, 1963) and (Mackey & Jorgensen, 1999).
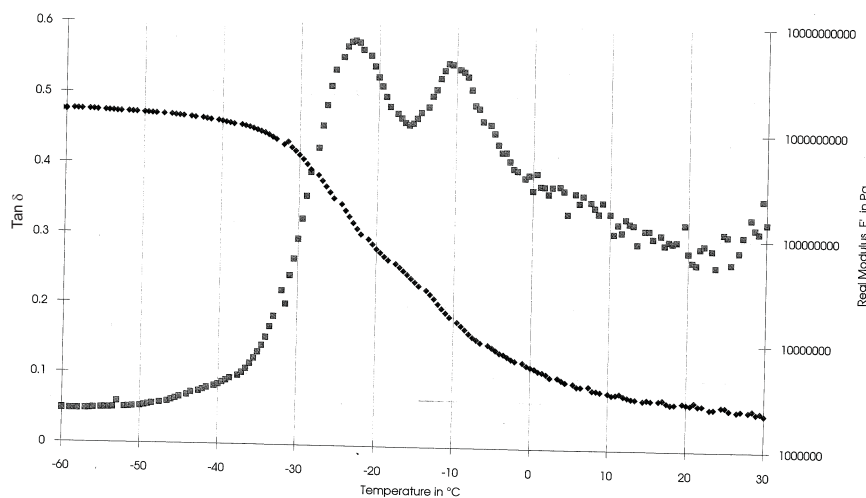
Figure 2.37: *Plot of (□) tan δ and (◇) Young's modulus over wide range of temperature at 1 Hz for unvulcanized rubber blend (Ramirez, 1995).*

Based on the analysis done by (Ahmad, 2005), the results from sample 23 are close to the requirement. Figure 2.39 shows the shear modulus and loss factor of the sample averaged over the range 500 to 800 Hz. The shear modulus shown is about 3.5 MPa at 20℃ which is close to the target value and the change of G^* with temperature is considered small. The loss factor of this material is above 0.35 for 85% of the temperature range (it falls
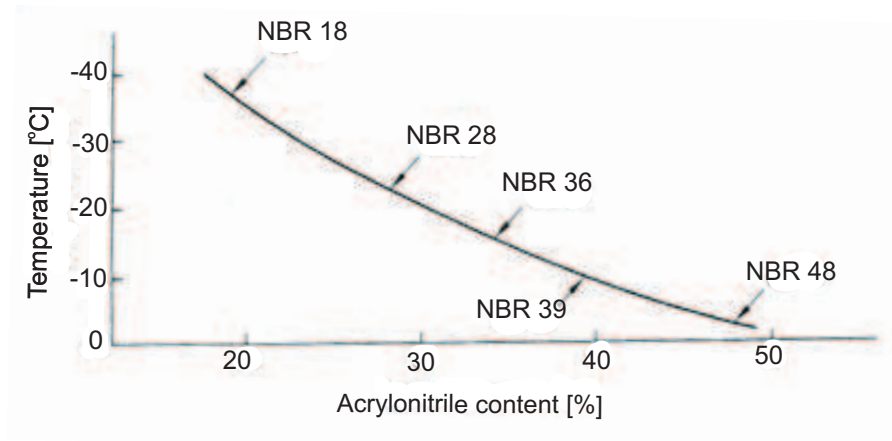
Figure 2.38: *The influence of the acrylonitrile content on the glass transition temperature of NBR (Hofmann, 1989).*

below 0.35 at -20℃ and 40℃). However the material is too stiff below 0℃. If the peak in loss factor could be reduced and broadened this stiffening effect could perhaps be reduced.
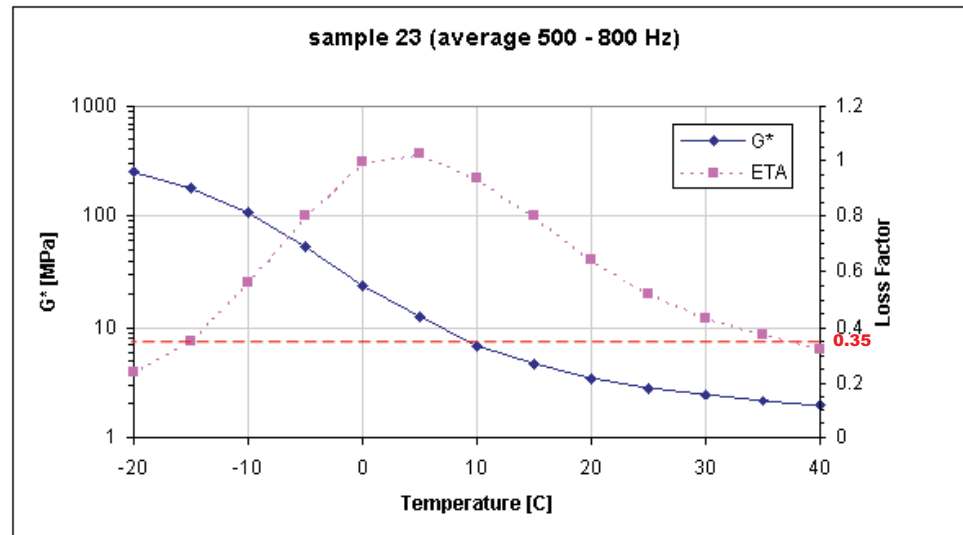
Figure 2.39: *Shear modulus and loss factor of NBR sample 23 (Ahmad, 2005).*

2.5.4 Polyurethane (PU)

Polyurethane has already been described in some detail in Section 2.4.5.1.

A series of PU materials have been tested by the ISVR for the Silent Track project. The results for sample 7*f* are very suitable as shown in Figure 2.40 (Jones, 2005). This material has been used in the prototype absorber. Unfortunately, the tests were limited to the range 0℃ to 40℃. The Young's modulus at 20℃ and 1000 Hz is about 14 MPa while the loss factor is 0.35.

Figure 2.40 also illustrates the properties of sample 23 (NBR) in comparison to PU. Sample 23 is slightly stiffer than PU sample 7*f* except at 3000 Hz at 40℃. On the other hand, the loss factor of NBR sample 23 at 1000 Hz is higher than that of PU sample 7*f* at 20℃ and slightly lower at 40℃.
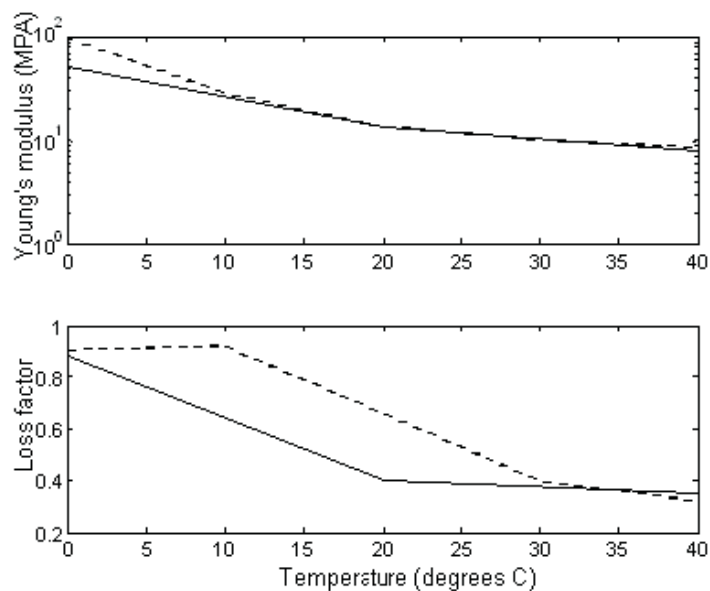
Figure 2.40: *Temperature dependent material properties of the two elastomers PU sample 7f (solid line) and NBR sample 23 (dash line) at 1000 Hz (Jones, 2005).*

However, PU was not considered further here, the focus being on broadening the search for the most cost-effective material to other classes of elastomers.

2.5.5 Butyl rubber (IIR)

Butyl rubber was developed in the 1940's and commercialised in 1943 (Salamore, 1996). To extend the usefulness of butyl for fast curing rates, in the 1950's and 1960's halogenated butyl rubber (halobutyl) was invented, which is composed of both chlorinated (chlorobutyl) and brominated (bromobutyl) butyl rubber. Butyl is crosslinked with sulphur or resin cures. A sulphur cure is most widely used for butyl and gives good physical properties. Most common applications of butyl rubber are tyre inner tubes because of its low permeability to air, resulting from low levels of unsaturation between long polyisobutylene segments. Besides this, the high damping characteristics of butyl are used in automotive components like exhaust hangers.

Butyl rubber is a synthetic rubber predominantly formed of polyisobutylene. A few (about 2%) isoprene monomer units, containing a double bond, provide sites for crosslinking during vulcanization, hence its designation as a copolymer of isobutylene and isoprene (IIR). Butyl rubber has a sufficiently regular chain structure to crystallize at low temperature.

It also crystallizes on stretching and therefore possesses good strength even in the unfilled state. Butyl rubber has a lower polarity and more paraffinic character than unsaturated rubbers, such as NR, IR, BR and SBR.

Because of its lower polarity, interaction of IIR with carbon black is weaker than for unsaturated hydrocarbon rubbers such as NR and SBR (Medalia, 1978). Furthermore, its lower polarity, associated with lower cohesion and symmetrical structure, mean that butyl rubber has a relatively low glass transition temperature (about -70℃). Butyl rubber has a very broad transition region because of the presence of a large number of methyl substituents (shown in Figure 2.41) that represent steric hindrance for the shape changes of the chains (Salamore, 1996). Presumably the steric hindrance is not high enough to counteract the low T_g associated with the high rotational ability of the main chain bonds, but increases the internal friction and hence damping when the elastomer is sheared.
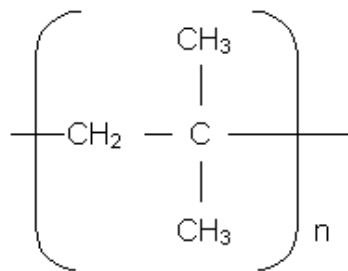
Figure 2.41: *Chemical structure of butyl rubber (Ward, 1983).*

The primary attributes of butyl rubber are good resistance to weather and ozone, resulting from low levels of unsaturation, impermeability/air retention because of the steric hindrance, and good flex properties because of its capability to strain-crystallize. Butyl also has good, thermal stability, chemical and moisture resistance, vibration damping and a high coefficient of friction.

The dynamic properties of butyl rubber in the ranges of temperature and frequency mentioned previously for the rail absorber are given by Fletcher & Gent (1973); Nashif *et al.* (1985). Figure 2.42 shows the dynamic properties from Nashif *et al.* (1985) and Fletcher & Gent (1973) at 1000 Hz for temperatures -20℃ to 40℃. Results from Nashif & Lewis (1991) are also compared in the figure but the curves were read at 500 Hz. The G' value of Nashif *et al.* (1985) is higher by a factor of 3 than that from Fletcher & Gent (1973). The loss factors also differ considerably but all are well above the required minimum.

Although they are nominally the same rubber, the dynamic properties from these sources are significantly different especially at low temperature. The shear modulus from (Nashif *et al.*, 1985) and Nashif & Lewis (1991) were calculated using interpolation from the master curve, while the shear modulus from Fletcher & Gent (1973) is calculated using time temperature superposition. Ideally they should give similar behaviour; the source of

this discrepancy is not known. They would be expected to give similar results, suggesting the source of the discrepancy lies with the experimental technique.

Butyl rubber is considered to have potential for application in the rail absorber. However, further investigation is required to confirm the dynamic properties.
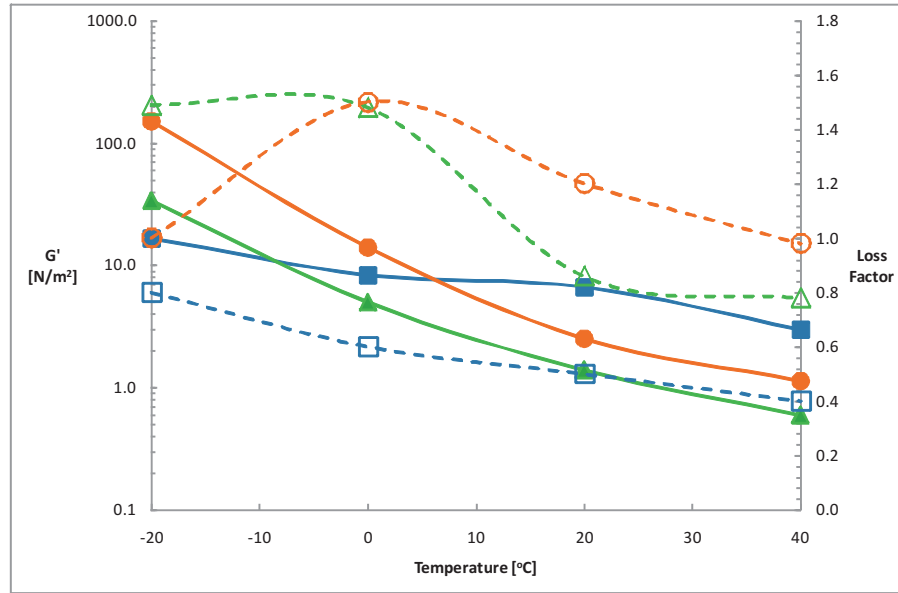
Figure 2.42: *The dynamic modulus and loss factor of butyl rubbers from Fletcher & Gent (1973); Nashif et al. (1985) at 1000 Hz and Nashif & Lewis (1991) at 500 Hz. The shear modulus curves are (▲) Nashif et al. (1985), (●) Fletcher & Gent (1973), (■) Nashif & Lewis (1991) and the loss factor curves are (△) Nashif et al. (1985), (○) Fletcher & Gent (1973), (□) Nashif & Lewis (1991).*

2.5.6 Polyacrylate (ACM)

The 3M company has developed a material, 3M ISD 113 which is based on polyacrylic material (ACM). From Table 2.2, this material has dynamic properties which has potential for use in the rail absorber. However, detailed information on this rubber is not reported in Nashif & Lewis (1991).

Since it is based on polyacrylate rubber, some information of similar rubber was obtained from Robert (1990). According to Robert (1990) ACM rubber has tan δ about 0.17 at 20℃ and it is close to 0 at 100℃. The value of complex Young's modulus decreases with increasing temperature from 21 MPa at 20℃ to 8.2 MPa at 100℃. It has a hardness of 67 Shore A and has a range of T_g from -54℃ to 24℃. It is suitable for continuous use at temperatures up to 150℃ but is not suitable much below -10℃. It has poor resistance to water and acids. It has only modest dynamic properties and rather poor compression set.

These dynamic properties of polyacrylate rubber differ significantly from those listed in Table 2.2 for ISD 113. These ACM rubbers probably have different formulation, which is unknown. Although 3M ISD 113 rubbers exhibit encouraging dynamic properties, they are only available in cured form (ready made product), which is expensive and difficult to process. Therefore, this material is not selected.

2.5.7 Ethylene propylene diene monomer (EPDM)

In contrast with the above candidate materials, the EPDM material presented in Table 2.2 has a lower loss factor, around 0.2 to 0.3. EPDM rubber is one of the most widely used thermoplastic elastomers. It is denoted a terpolymer, based on three monomers: ethylene, propylene and a non-conjugated diene (double bonds) in order to cross link the material. It was discovered in 1956 (Morton, 1995) and the largest market for EPDM is the automotive field because of its low cost, low density, and good weather resistance. EPDM can be cured by using peroxide and sulphur cures.

This polymer has an amorphous structure, except for grades with greater than 55% weight ethylene monomer content. In general, the polymer itself is weak because the rubber does not crystallize on stretching. It must therefore be reinforced to achieve useful properties. EPDM rubber can be reinforced with various fillers such as carbon black. Besides that, EPDM is compatible with either paraffinic or naphthenic process oil as a plasticiser. A high viscosity oil can be used to enhance the physical properties, improve heat resistance and minimise shrinkage. Conversly, a low viscosity oil improves both resilience and low temperature flexibility. Although this rubber has a low loss factor which is slightly lower than the target requirement, it is worth further investigation. In addition, this rubber is cheaper and easy to process compared to the current material for rail absorber, PU.

2.5.8 Styrene butadiene (SBR) rubber and natural rubber(NR)

Besides the seven candidate materials considered above, SBR and NR are materials that will also be used for the comparative purposes.

Styrene butadiene rubber (SBR) was developed by a German chemist in 1929. It is a synthetic elastomer by copolymerisation of two compounds (25% styrene and 75% butadiene). Most of the applications of SBR are in the automotive field. SBR is very weak unless reinforced fillers are incorporated to create a stronger rubber. It has good abrasion resistance. SBR has similar chemical and physical properties as natural rubber, except its low temperature flexibility and tensile strength are less than that of natural rubber (Morton, 1995). The properties of SBR given in Table 2.2 are similar to those

of EPDM, but detailed information is not available from the Nashif & Lewis (1991) so more investigation is required. Further investigation is not considered here because of time limitations in this study.

Whilst the previous rubbers are synthetic, which are mostly produced from petroleum, natural rubber comes from the tree known as Hevea Brasiliensis. NR was developed over 100 years ago and is most widely used in tyres, engineering products and latex products. NR has properties such as good tensile strength and tear with outstanding resistance to fatigue, but it deteriorates when exposed to sunlight, ozone and oxygen. In addition, NR has low level of damping and ageing properties make it less suitable for the rail absorber application. Due to these properties, NR is not pursued for further study here.

2.5.9 Discussion and strategy for development of a suitable material

Table 2.3 shows the estimated price of each polymer involved in this literature survey.

For the rail application cost is an important factor, and materials that are expensive or difficult to process are unlikely to be acceptable; polyacrylate, polysulphide and polyphosphazine are rejected on this account, despite the possibility that they may have useful damping and stiffness values over the requisite temperature range. Butyl rubber (IIR), EPDM and NBR have a reasonable price compared with the common rubber NR or SBR. Therefore, the use of this rubber will be efficient.

Table 2.3: *Estimated price for the polymer (Rubbermill, 2006).*

Polymer	$1 \cong £/kg$	Notes
Styrene butadiene rubber (SBR)	1	
Natural rubber (NR)		
Ethylene propylene diene monomer (EPDM)		
Butyl rubber (IIR)	2	
Polychloroprene (CR)		
Nitrile rubber (NBR)		
Polyurethane (PU)	3	
Hydrogenated nitrile rubber (HNBR)	5	
Acrylic rubber (ACM)	N/a	Same level as HNBR[1]
Polyphosphazene (PZ)	N/a	N/a
Fluoroelastomers (FKM)	10	

[1]comparison made based on the performance of the material Dupont (2006)

The key difficulty in finding an elastomer with suitable values of damping and modulus over the requisite temperature range (-20℃ to +40℃) is to have adequate damping and yet minimise the sensitivity of the modulus to temperature. This is because, if the

damping is high, the frequency and temperature sensitivity will be higher, as shown in the literature review. The theoretical basis for this relationship is discussed further in Chapter 3, in an attempt to answer the question as to whether the goal of the specification is feasible, since Figure 2.34 shows that none of the materials reviewed meet it fully.

It is clear that if an elastomer with a single T_g is chosen, this would need to be in the right range (much lower than -20℃). In addition, it would also appear to be very beneficial if the material has a very broad transition, so that the damping is reasonably high over a wide temperature range and the modulus may be less sensitive to temperature than for a material with a sharp transition. Butyl rubber has these attributes although the published data for its dynamic properties reveal significant discrepancies, showing that a careful new investigation is called for. Chapter 5 describes the method used to measure dynamic properties in this project, and the care taken to ensure its reliability. By formulating butyl rubber with filler and oil it may be possible to fine-tune and optimise its dynamic properties; such work is described in Chapter 6. No other elastomer appears to rival butyl rubber in having both a very broad transition and a suitably low T_g, but alternative strategies also exist for developing a material to meet the specification.

An incompatible blend of materials with different T_g values would appear to be a sensible approach to achieving a broad transition between rubbery and glassy regions. This has previously been pursued (Ahmad, 2005), by blending a range of NBR elastomers with differing acrylonitrile: butadiene monomer ratios, which are readily commercially available and not too expensive. The results were good but not outstanding. Therefore, further investigation was suggested and would be justified. The original PU material used was the outcome of a substantial development effort, albeit carried out in a confidential project, details of which are not available for the purposes of the present project. The PU family clearly provides a versatile tool kit of possibilities, it being feasible to choose at will different values of T_g for the constituent parts, and presumably also a range of T_g within one system. However, as this has already been done, the objective was set here of seeking an alternative and possibly more cost-effective material, possibly coming even nearer to meeting the specification.

Finally, the use of reinforcing fillers would appear to provide another strategy that could help to reduce the difficulty of compromise between achievement of damping and avoidance of excessive sensitivity of the modulus to temperature. Such an approach, using NR as the elastomer to carry the high loading of reinforcing carbon black, has proved very useful in providing the high damping and low temperature sensitivity required of seismic isolation bearings for buildings (Derham *et al.*, 1985). However, that application concerns properties at low frequency (about 0.5 Hz) and high amplitude (about 100% shear strain). It is less clear if the damping would be adequate under the present conditions of high frequency (300 to 3000Hz) and low amplitude (0.01% shear strain). There is

reason to believe that as the strain is reduced the shear modulus reaches a high plateau, perhaps suggesting that the loss factor falls towards that of the unfilled elastomer (Payne, 1962). Nevertheless, a decision was made to investigate this approach, as it seems that the damping due to reinforcing filler is quite distinct from the viscoelastic properties of the matrix elastomer, in particular not being very rate-sensitive. EPDM is well known for its ease of processing when highly loaded with carbon black and oil, so that it was chosen for the matrix elastomer to be used in the investigation of this approach, which is reported in Chapter 7. The oil is necessary to reduce the mix viscosity to a processable level, and can also be used to control the modulus of the filled rubber.

2.6 Conclusions

The glass transition temperature, T_g, is a very useful physical property that can be measured and reflects the behaviour of a polymer. Single phase polymers are thermorheologically simple materials with a single glass transition but the breadth and position of the master curve on the temperature axis varies. Similar behaviour is also found in miscible blends of polymers or plasticisers with the transition temperature occurring between those of the ingredients.

On the other hand, immiscible blends and phase separated copolymers have multiple transitions giving the impression of a single broad transition. They would not be expected to be TSMs. Many such materials have good strength and a typical example is thermoplastic elastomer (TPE).

From the number of candidate rubbers investigated, butyl rubber, EPDM, poly-urethane and NBR appear to be practical for the rail vibration absorber. They are selected based on their dynamic properties, as well as other criteria like cost-effectiveness, material availability and processing method.

Within this thesis butyl rubber and EPDM will be investigated in detail. Results for NBR are available from (Ahmad, 2005) and will be reconsidered in the light of improved analysis methods developed here. PU will not be considered further due to the difficult processing required and higher cost relative to butyl and EPDM.

Chapter 3

Numerical analysis of the noise reduction due to a rail damper

3.1   Introduction

In this present chapter a simple dynamic model of a rail damper attached to a railway track is introduced and used to study the influence of the stiffness and damping in the absorber on the noise reduction.

The rail damper considered is based on an elastomeric material which is used with steel masses to form a tuned mass-spring system. The loss factor and stiffness of the elastomer are very important for the performance of the system. Both properties are very sensitive to changes in the temperature which must be taken into account as this device is required to operate in a range of environmental temperatures between about -20℃ and 40℃.

Ideally the elastomer in the absorber should have a relatively high loss factor and a stiffness which does not vary strongly with temperature but these are known to be conflicting requirements for practical elastomers. The present analysis therefore aims to derive more realistic specifications for the material, taking into account the physical connection between stiffness variation and damping.

The properties of actual materials are not considered at this stage but rather a generic material is considered with a constant loss factor. By assuming such a constant loss factor, an estimate is made of the frequency-dependence of the stiffness. Then, by using the time-temperature superposition principle, this can be expressed as a temperature-dependence of the stiffness. Finally, this is used to estimate the noise reduction as a function of temperature. The aim is to determine the relative merits of high damping and a low variation in stiffness, in order to establish a more practical target for a new

material.

3.2 Predicted decay rate

3.2.1 Model for track vibration

The noise from the track depends on the rate of decay of waves propagating along the rail (Jones *et al.*, 2006). The sound power radiated by the rail is proportional to $1/\triangle$, where Δ is the decay rate in dB/m. This in turn is given by,

$$\triangle = -8.686 Im(k) \tag{3.1}$$

where k is the complex wavenumber of waves in a rail (Thompson, 2007; Wu & Thompson, 1999).

A simple track model is introduced and used to identify the effect of varying the properties of the elastomer. The untreated track is modelled as a Timoshenko beam on an elastic foundation (representing the rail pad) as shown in Figure 3.1(a). By introducing the mass-spring system (absorber) to the untreated beam, as shown in Figure 3.1(b), an estimate is obtained for the decay rate of the track fitted with absorbers. The ratio of the decay rates of the treated and untreated tracks is used to determine the effect of the damping device. This neglects the sound radiation from the absorber masses themselves but due to their relatively small dimensions this is a reasonable assumption especially where the loss factor of the absorber is relatively high (Thompson, 2007).
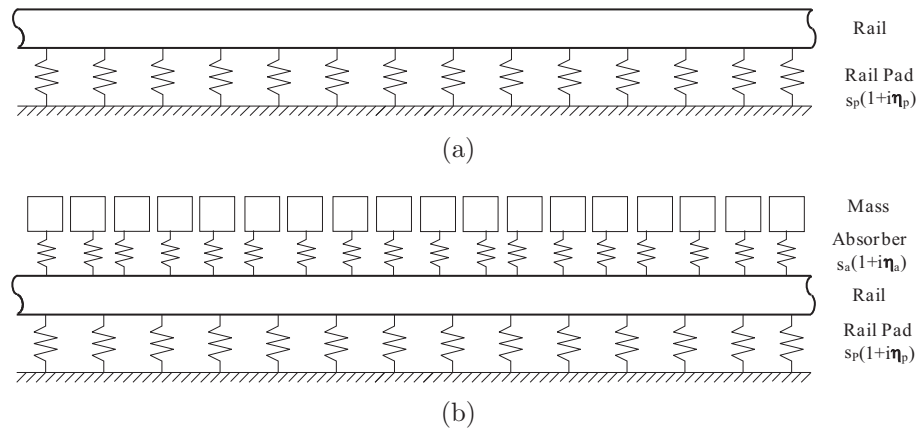
Figure 3.1: Schematic diagram of (a) untreated track and (b) treated track.

3.2.2 Timoshenko beam model

The Timoshenko beam theory constitutes an improvement over the Euler-Bernoulli theory, by including shear deformation and rotational inertia effects (Graff, 1997). The Timoshenko beam model is more appropriate at high frequency, typically where the wavelength is less than about six times the height of the beam. For a rail section, significant differences between Euler-Bernoulli and Timoshenko beam models occur for frequencies above about 500 Hz (Thompson, 2007).

Adding the effect of the elastic foundation of stiffness per unit length S_p (see Figure 3.1(a)), the equations of motion of a Timoshenko beam on the elastic foundation is (Thompson, 2008).

$$GA\kappa\frac{\partial}{\partial x}\left(\phi - \frac{\partial u}{\partial x}\right) + S_p u + \rho A\frac{\partial^2 u}{\partial t^2} = F\delta(x)e^{i\omega t} \tag{3.2}$$

$$GA\kappa\left(\phi - \frac{\partial u}{\partial x}\right) - EI\frac{\partial^2 \phi}{\partial x^2} + \rho I\frac{\partial^2 \phi}{\partial t^2} = 0 \tag{3.3}$$

where u is the vertical deflection, ϕ is the rotation of the cross-section relative to the undeformed axis, κ is the shear coefficient, $\kappa < 1$, ρ is the density, A is the cross-sectional area, I is the second moment of area and E is the Young's modulus, and G is the shear modulus.

To find the dispersion relation, free wave solutions are sought of the form $u(x,t) = Ue^{ikx}e^{i\omega t}$ and $\phi(x,t) = U\Psi e^{ikx}e^{i\omega t}$. U is the complex amplitude of u and $U\Psi$ is the corresponding amplitude of ϕ from equation (3.3) and Ψ is given by

$$\Psi = \frac{-ikGA\kappa}{\rho I\omega^2 - GA\kappa - EIk^2} \tag{3.4}$$

The dispersion relation can be obtained by substituting this equation into Eq. (3.2) giving

$$k^4 + C_2(\omega)k^2 + C_3(\omega) = 0 \tag{3.5}$$

where (Thompson, 2008)

$$C_2(\omega) = \left(\frac{S_p - \rho A\omega^2}{GA\kappa}\right) - \left(\frac{\rho I\omega^2}{EI}\right) \tag{3.6}$$

$$C_3(\omega) = \left(\frac{S_p - \rho A \omega^2}{EI}\right)\left(1 - \frac{\rho I \omega^2}{GA\kappa}\right) \tag{3.7}$$

Damping can be introduced by making E, G and S_p complex with the form $E(1 + i\eta_r)$, $G(1 + i\eta_r)$ and $S_p(1 + i\eta_p)$, where η_r is the loss factor of the rail and η_p is the loss factor of the rail pad.

For the treated track, a similar procedure is followed except that the absorber is introduced onto the existing beam as shown in Figure 3.1(b). Its dynamic stiffness is

$$S_{dyn}(\omega) = \left(\frac{1}{S_a} - \frac{1}{\mu_a \omega^2}\right)^{-1} = S_a - \frac{S_a^2}{S_a - \mu_a \omega^2} \tag{3.8}$$

where μ_a is the mass of the absorber per unit length of rail and S_a is the absorber stiffness per unit length. The stiffness can be chosen according to the 'tuning' frequency of the absorber, which is obtained from $\omega_a = \sqrt{\frac{S_a}{\mu_a}}$. S_{dyn} should be added to S_p, giving a modified value of C_2 and C_3.

Similarly, damping can be introduced into the absorber by making S_a complex with the form $S_a(1 + i\eta_r)$.

3.2.3   Comparison between models

First, a comparison is presented between the above Timoshenko beam model and an Euler-Bernoulli beam model in which shear deformation and rotational inertia are neglected. The decay rate, $\triangle$=-8.686 Im(k), and the wavenumbers $Re(k)$ are determined from the above equations, using the parameters listed in Table 3.1, which represent a typical track, as used by Jones (2005). (The sleeper mass and ballast stiffness are not used in the present calculations).

The wavenumbers are shown in Figure 3.2. At lower frequencies the wavenumbers of the Timoshenko and Euler-Bernoulli beam models are reasonably close, although at 500 Hz the additional flexibility of the Timoshenko beam is noticeable. At 1000 Hz the behaviour of the Timoshenko beam is markedly different from that of the Euler-Bernoulli beam. This is caused mainly by the shear deformation terms in the Timoshenko beam model.

Similarly, the decay rates are shown in Figure 3.3. Again differences are found between the results above 500 Hz. This is because the Timoshenko beam has a shorter wavelength so for the same loss factor its decay rate is higher (Thompson, 2007).
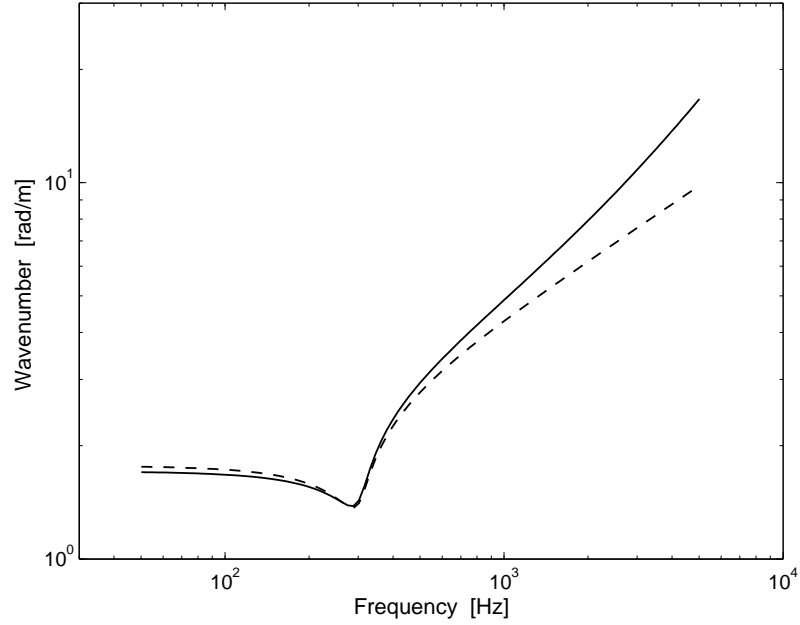
Figure 3.2: *Comparison of real part of wavenumber between Timoshenko (—) and Euler-Bernoulli (− − −) beam models as in Table 3.1.*

Table 3.1: *Parameters used for railway track from Jones (2005) which includes rail pad, sleeper and ballast.*

Rail		
Cross-sectional area	A	7.68×10^{-3} m^2
Second moment of area	I	3.0×10^{-5} m^4
Young's modulus for steel	E	2.11×10^{11} Nm^{-2}
Density for steel	ρ	7850 kgm^{-3}
Timoshenko shear coefficient for rail	κ	0.4
Poisson's ratio	ν	0.3
Damping loss factor of rail	η_r	0.02
Pad		
Support stiffness per unit length	S_p	2.17×10^8 Nm^{-2}
Damping loss factor of support	η_p	0.16
Ballast		
Stiffness of ballast per unit length	S_b	8.33×10^7 Nm^{-2}
Damping loss factor of ballast	η_b	1.0
Sleeper		
Sleeper mass per unit length of rail	m_s	233 kg/m
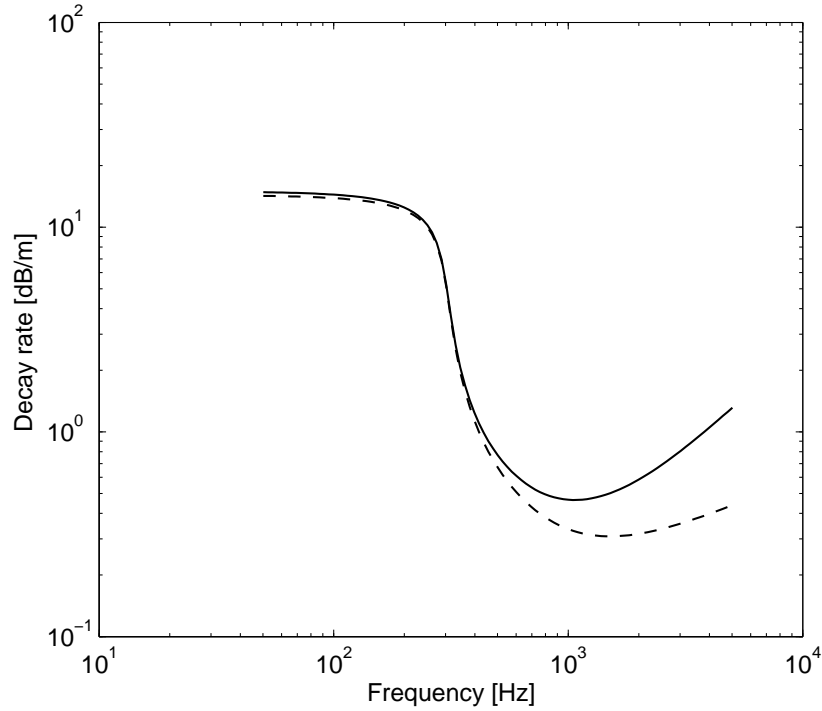
Figure 3.3: *The decay rate of the untreated beam predicted using Timoshenko (—) and Euler-Bernoulli (− − −) beam models. The input parameters for both models are as in Table 3.1.*

Below 300 Hz the decay rate is high (more than 10 dB/m) and waves cannot propagate freely due to the influence of the foundation (Thompson, 2007). Above 300 Hz free waves 'cut on' and the decay rate falls to a level determined by the rail pad damping and, at high frequencies, by the rail damping (Thompson, 2007).

In Figures 3.4 and 3.5, the results obtained from this study are compared with the results from the track model in TWINS (Thompson *et al.*, 1996b), presented by Jones (2005). Both results use a Timoshenko beam model but in TWINS two springs and an intermediate mass are used to represent the foundation. The two springs represent the rail pad and the ballast while the mass represents the sleepers. As shown in Figure 3.4, the wavenumbers agree above about 500 Hz. However, at low frequency the curve predicted by TWINS shows a peak at 200 Hz which is the effect of the sleeper mass vibrating between the two springs.

Similar effects are found in the decay rate curves in Figure 3.5. The decay rate curve from the TWINS model falls around 100 Hz before rising to a peak at 250 Hz. Above this frequency free waves cut on in both models. Sleeper vibration becomes negligible at high frequency and the model with a single layer foundation is sufficient.

Although the curves show differences at low frequencies, this does not affect the current analysis, as the rail damper only influences the decay rate above the cut-on frequency.

However, a suitable value of S_p is needed to give the correct cut-on frequency. For example, the curve in Figure 3.5, which has the same value of S_p as the TWINS model, gives a lower cut-on frequency. By increasing S_p to 3.80×10^8 N/m^2 the cut-on frequency is similar to that found in the two-layer model and the decay rates match more closely.
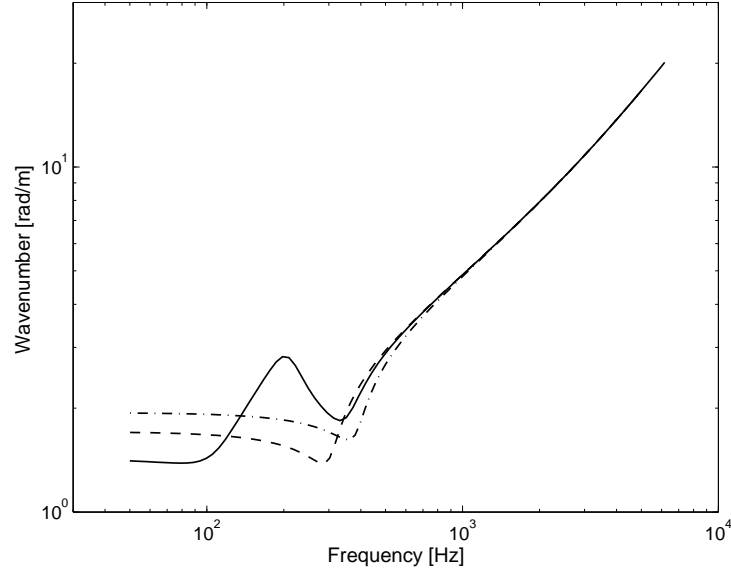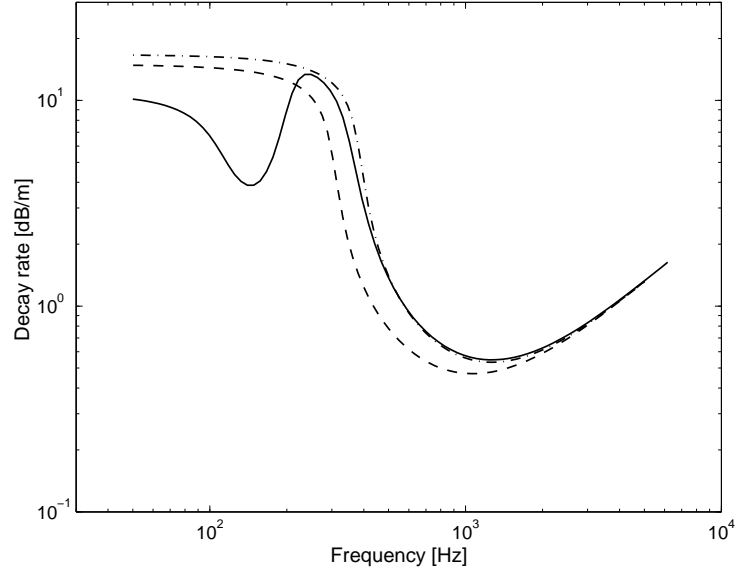

Figure 3.4: *Wavenumbers predicted using Timoshenko beam models. Single layer support $(---)$ $S_p = 2.17 \times 10^8 N/m^2$, single layer support $(-\cdot-)$ $S_p = 3.80 \times 10^8$ N/m^2, double layer support $(—)$ $S_p = 2.17 \times 10^8$ N/m^2, sleeper mass 233 kg/m, ballast stiffness $S_b = 8.33 \times 10^7$ N/m^2, $\eta_b = 1.0$. Other parameters as in Table 3.1.*

Predicted decay rates are compared with measured decay rates from (Thompson, 2007) in Figure 3.6. Because of the influence of temperature, the rail pad measured at Velim at 30℃ is softer than the similar one measured in Belgium at 5℃. The decay rate from Velim is therefore lower than the predicted curve and that for the stiffer pad is higher. This also illustrates that the cut-on frequency is shifted to higher frequencies as temperature decreases.
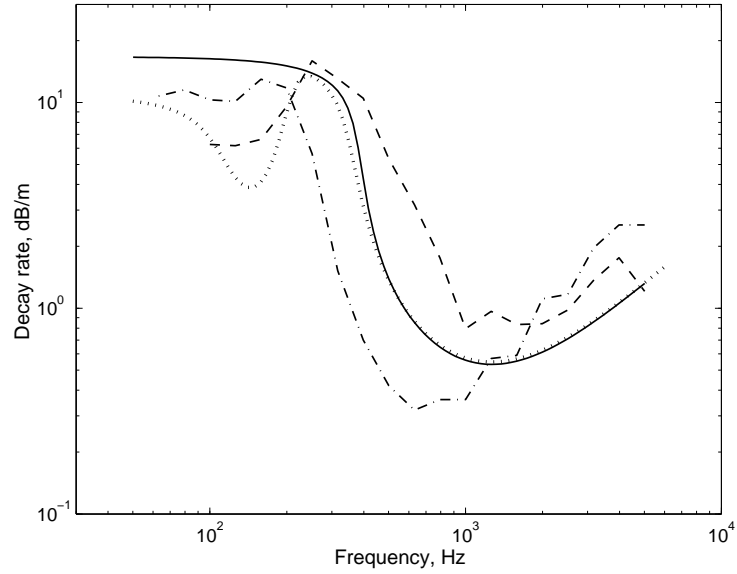
In the track model, damping is added to the rail to ensure that the predictions follow measured curves, especially above 1 kHz (see Figure 3.6). Otherwise, the curve would continue to fall at high frequency. However it is known that, in practice, this damping is not associated with the rail itself, but with the rail pad, the damping effect of which is increased at high frequencies due to cross-sectional deformation of the rail (Thompson, 2007).

3.2.4 Results with absorber

Figure 3.7 shows the wavenumber $Re(k)$ of the treated and untreated track for the parameters given in Table 3.2. The tuning frequency of the absorber is set to 1000 Hz.

Figure 3.5: *The decay rate predicted from Timoshenko model and TWINS. Single layer support $(---)$ $S_p = 2.17 \times 10^8$ N/m^2, single layer support $(-\cdot-)$ $S_p = 3.80 \times 10^8$ N/m^2 , double layer support $(—)$ $S_p = 2.17 \times 10^8$ N/m^2, sleeper mass 233 kg/m, ballast stiffness $S_b = 8.33 \times 10^7$ N/m^2, η_b=1.0. Other parameters as in Table 3.1.*

Figure 3.6: *Predicted and measured decay rates of a track without absorber. $(—)$ Timoshenko beam model (single layer foundation); $(\cdots)$, TWINS model (two layer foundation); $(---)$, measured at 5℃; $(-\cdot-)$, measured at 30℃ (measured results from Thompson (2007)).*

Below this frequency the wavenumber is increased in the presence of the absorber due to the effect of its added mass (Thompson, 2007).

Figure 3.8 shows the corresponding decay rate ($\triangle$=-8.686 $Im(k)$). The absorber introduces a large peak between 500 and 3000 Hz with its maximum around the tuning frequency of 1000 Hz, which corresponds to the region where the rail noise component is dominant (see Section 3.3 below). The added mass of the absorber reduces the cut-on frequency and hence reduces the decay rate between 200 and 500 Hz.

Table 3.2: Parameters used for railway track including absorber.

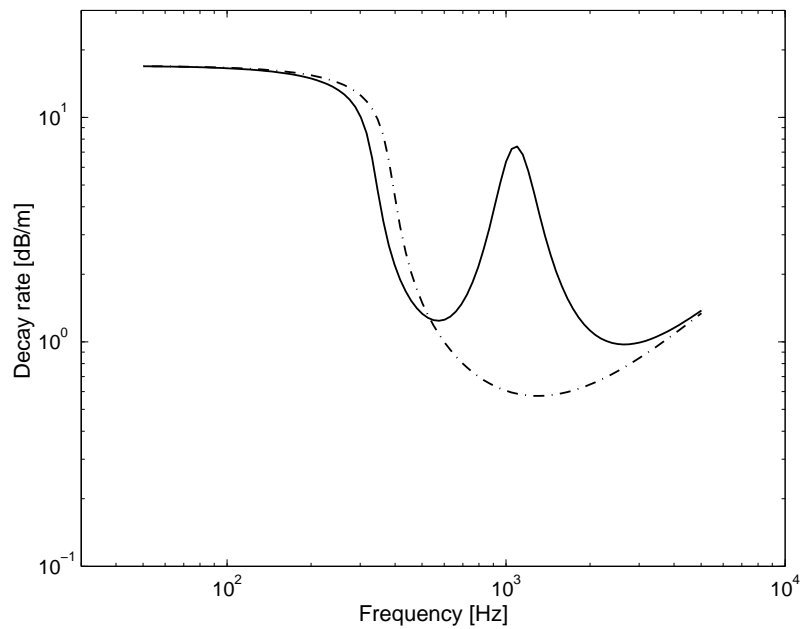| Rail			
Cross-sectional area	A	7.68×10^{-3}	m^2
Second moment of area	I	3.0×10^{-5}	m^4
Young's modulus for steel	E	2.11×10^{11}	Nm^{-2}
Density for steel	ρ	7850 kgm^{-3}	
Timoshenko shear coefficient for rail	κ	0.4	
Poisson's ratio	ν	0.3	
Damping loss factor of rail	η_r	0.02	
Pad			
Support stiffness per unit length	S_p	3.80×10^8	Nm^{-2}
Damping loss factor of support	η_p	0.16	
Absorber			
Stiffness per unit length	S_a	6.91×10^8	Nm^{-2}
Mass per unit length	μ_a	17.5 kg/m	
Damping loss factor	η_a	0.35	

Next, the decay rate behaviour is illustrated for various values of rail pad stiffness. Figure 3.9 shows that increasing the rail pad stiffness will also increase the cut-on frequency of free wave propagation. As shown in Figure 3.10, for a high rail pad stiffness, the cut-on frequency occurs near to the tuning frequency and the absorber has much less effect, as the decay rate is already high.

Figure 3.11 shows the effect of increasing the stiffness of the absorber. This increases its tuning frequency. This effect is important because, in practice, its stiffness is sensitive to changes in the temperature.

Figure 3.12 shows that increasing the loss factor of the absorber will increase the breadth but decrease the peak of the decay rate. Moreover, for high loss factors, the peak of the decay rate is shifted slightly towards higher frequencies. In order to determine the relative merits of the breadth and height of the peak, these results need to be combined with noise predictions, which are considered in the next section.
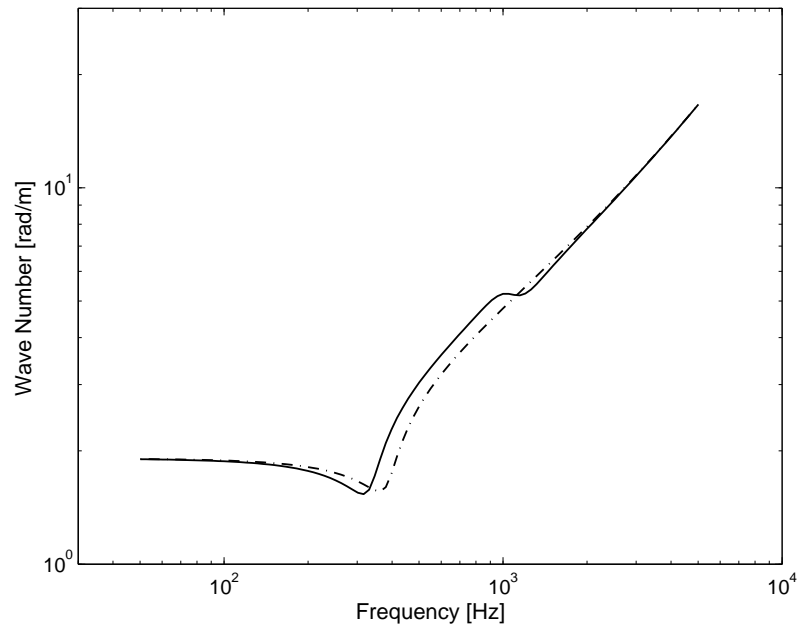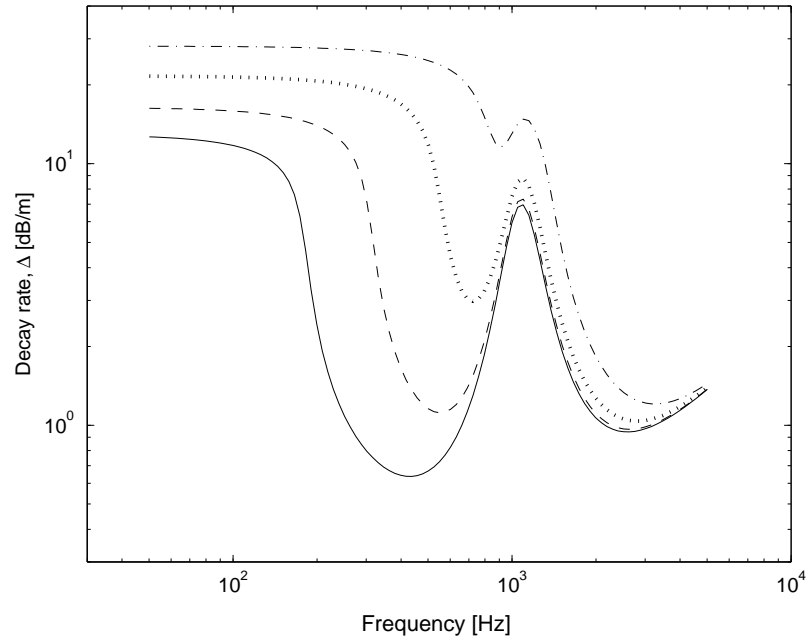
Figure 3.7: *The real part of wavenumber of untreated* $(- \cdot -)$ *and treated track* $(—)$*. The parameters used are listed in Table 3.2.*

Figure 3.8: *The decay rate of the untreated* $(- \cdot -)$ *and treated* $(—)$ *track. The parameters used are listed in Table 3.2.*
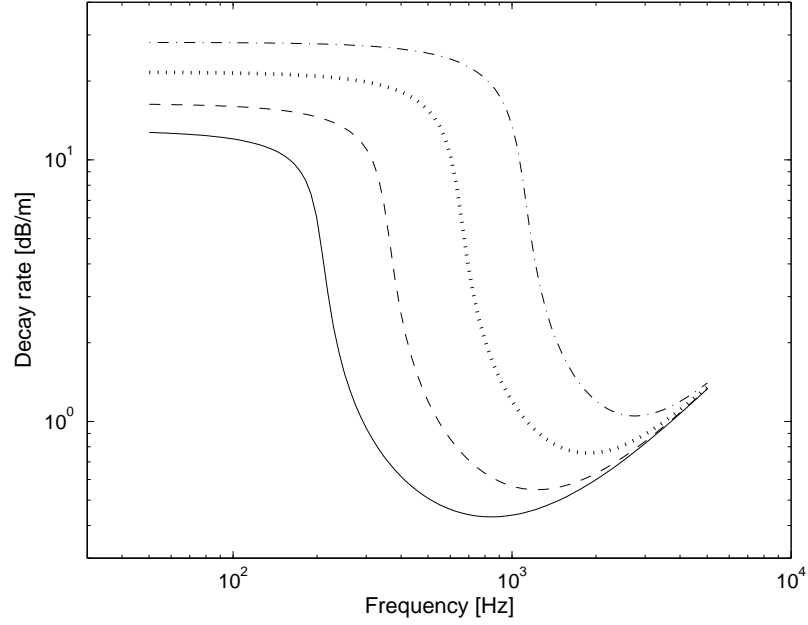
Figure 3.9: *The decay rate of the rail with no absorber for various rail pad stiffnesses. (a) (—) $S_p = 1.0 \times 10^8 N/m^2$; (b) (− − −) $S_p = 3.0 \times 10^8 N/m^2$; (c) (· · ·) $S_p = 1.0 \times 10^9 N/m^2$'; (d) (− · −) $S_p = 3.0 \times 10^9 N/m^2$.*
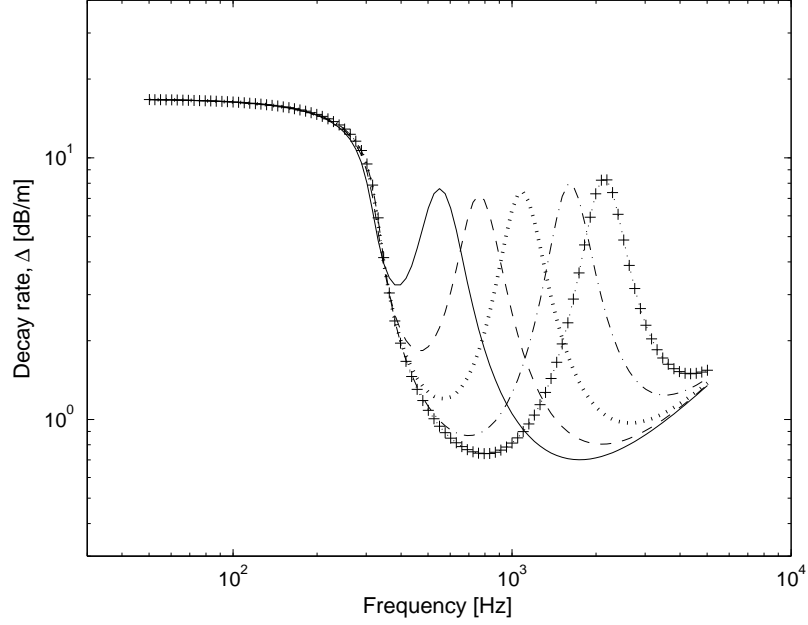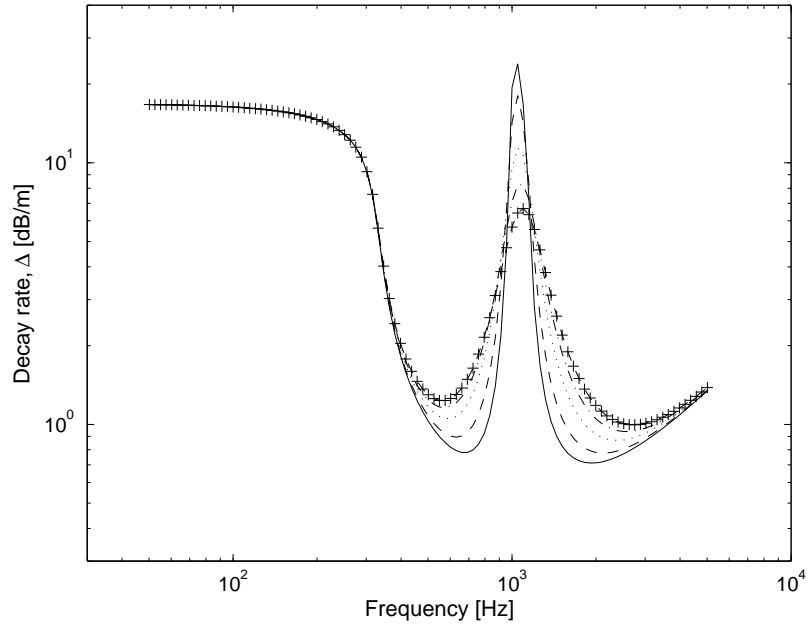

Figure 3.10: *The decay rate of the rail with absorber for various rail pad stiffnesses. (a) (—) $S_p = 1.0 \times 10^8 N/m^2$; (b) (− − −) $S_p = 3.0 \times 10^8 N/m^2$; (c) (· · ·) $S_p = 1.0 \times 10^9 N/m^2$; (d) (− · −) $S_p = 3.0 \times 10^9 N/m^2$.*

Figure 3.11: *The decay rate of the rail with absorber for various values of absorber stiff-ness. (a) (—) $S_a = 1.73 \times 10^8$ N/m^2 (500 Hz); (b) ($- - -$) $S_a = 3.39 \times 10^8$ N/m^2 (700 Hz); (c) ($\cdots$) $S_a = 6.91 \times 10^8$ N/m^2 (1000 Hz); (d) ($- \cdot -$) $S_a = 15.5 \times 10^8$ N/m^2 (1500 Hz); (e) (+) $S_a = 27.6 \times 10^8$ N/m^2 (2000 Hz).*

Figure 3.12: *The decay rate of the rail with absorber for various absorber loss factors: (a) (—) η=0.05; (b) ($- - -$) η=0.1; (c) ($\cdots$) η=0.2; (d) ($- \cdot -$) η=0.4; (e) (+) η=0.8.*
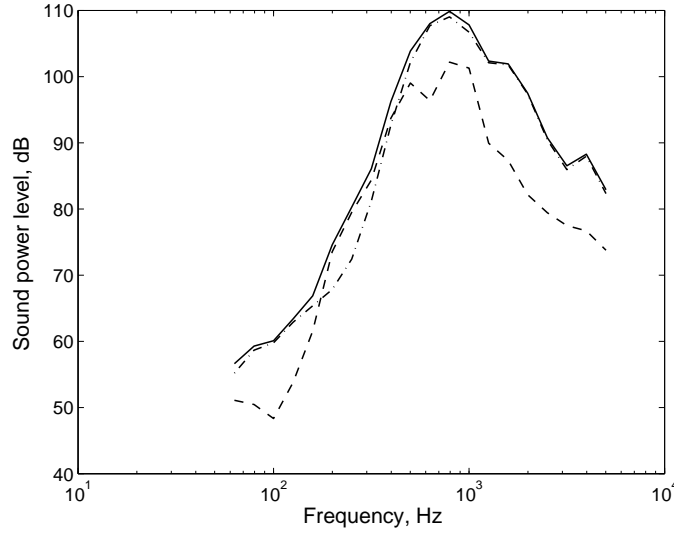
3.3   Predicted rail noise

In order to estimate the effect on the radiated sound, use is made of an existing pre-
diction (Jones, 2005) using the TWINS model (Thompson *et al.*, 1996a,b). The sound
power of the damped track is then calculated by modifying the component associated
with the vertical rail vibration, as predicted using the TWINS model. Figure 3.13 shows
the initial sound power spectrum predicted using TWINS, separated into wheel, rail and
sleeper components. This initial situation represents a typical modern track with rela-
tively soft rail pads, as in Table 3.1, a train speed of 100 km/h and a roughness spectrum
corresponding to cast-iron block tread brakes.
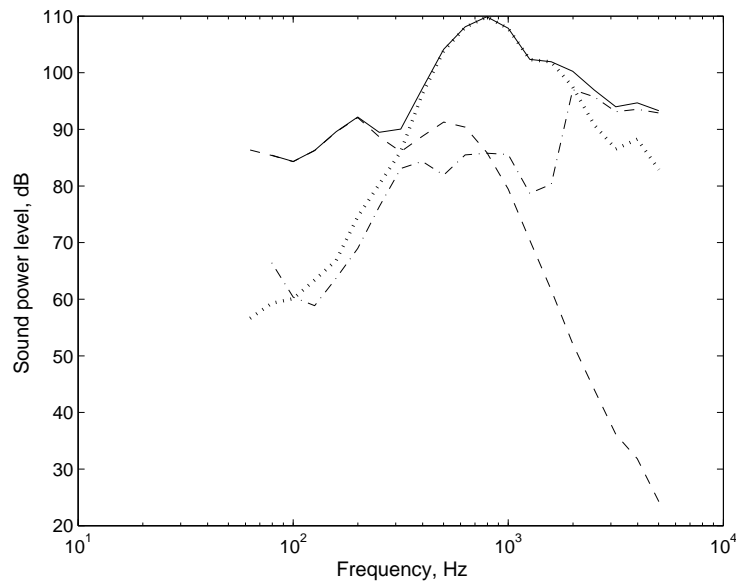
Figure 3.13: *The initial sound power level from one wheel and associated track predicted
using TWINS (Jones, 2005). (a) (—) total; (b) (− · −) wheel; (c) (· · ·) rail; (d) (− − −)
sleeper.*

In reality, the noise from the rail is composed of components due to vertical and lateral
vibration. This is shown in Figure 3.14, where the contributions due to vertical and
lateral components are compared with the total rail noise. In this untreated situation the
vertical component is 7.5 dB(A) greater than the lateral component. Even in the treated
situation, shown in Figure 3.15, if the vertical component is modified by the effect of the
rail absorbers but the lateral component is left unaffected, the vertical component is still
greater than the lateral component. In practice, the absorber will also introduce some
damping to the lateral direction.

However, from these comparisons it can be concluded that the lateral component can be
neglected in optimising the effect of the absorber, due to the dominance of the vertical
motion.

Figure 3.14: *The sound power level of vertical and lateral waves compared with total rail noise for the untreated tracks. (a) (—) Total (113.9 dB(A)); (b) (– · –) vertical-untreated (113.2 dB(A)); (c) (– – –) lateral-untreated (105.7 dB(A)).*

The predicted noise reduction will therefore be calculated in terms of the reduction in the vertical component. Using the decay rate obtained from the parameters given in Table 3.2, the predicted sound power level is shown in Figure 3.16. Results are shown for an absorber with a loss factor of 0.35 and stiffness of 6.91×10^8 N/m^2, corresponding to a tuning frequency of 1000 Hz. These results are calculated from the ratio of the decay rates shown in Figure 3.8. The absorber is found to give a reduction of 4.0 dB(A) in this component of rail noise. The maximum effect, in the 1000 Hz band, is about 10 dB. Note that the vertical component of rail noise consists of a propagating wave and a nearfield wave; only the decay rate of the propagating wave is modified in this calculation.

Figure 3.17 shows the predicted noise reduction based on a range of values of the loss factor (between of 0.01 and 2.0) and stiffness (corresponding to a range of tuning frequency from 250 to 2000 Hz). This is also shown as a contour plot in Figure 3.18. This shows that the optimum values, corresponding to the maximum noise reduction, are for loss factors in the range 0.3 and above and a stiffness of about 4.0×10^8 N/m^2 (tuning frequency of about 800 Hz). As the loss factor is increased beyond 0.3, the noise reduction also increases but only slightly. It is also observed that the maximum noise reduction shifts to a slightly lower stiffness as loss factor increases. This corresponds to the shift in the decay rate peak for a given stiffness towards higher frequencies seen in Figure 3.13. On the other hand, materials with a higher loss factor will have a stiffness that varies more significantly with temperature (and frequency). The two parameters cannot be considered to be independent. This effect will therefore be considered in the next sections.
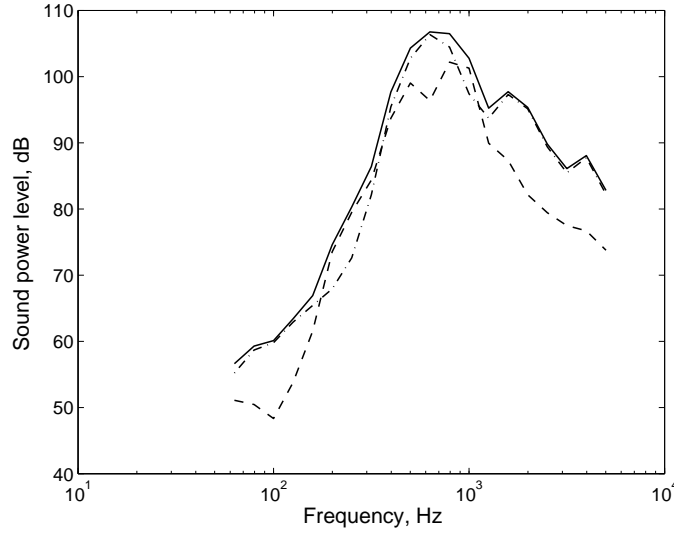
Figure 3.15: *The sound power level of the vertical and lateral waves with absorber added according to parameters in Table 3.2. The tuning frequency is 1000 Hz, η_a=0.35. (a) (—) Total (110.8 dB(A)); (b) ($- \cdot -$) vertical-damped (109.2 dB(A)); (c) ($- - -$) lateral-undamped (105.7 dB(A)).*

## 3.4 Temperature dependence of loss factor and stiffness

It is known that the dynamic properties of the absorber will vary with temperature: the higher the loss factor, the bigger the change in the stiffness over a range of temperatures. If the stiffness varies too much, then the absorber will be less effective at extremes of temperature. Conversely if the loss factor is too low, the effect of the absorber is reduced, as seen above. Therefore, the balance between these two effects over the range of temperature required will be investigated.

It is known from Schwarzl & Struik (1968) that, for a general elastomer, the slope of the shear storage modulus G' with log frequency is related to the loss modulus, G'' by
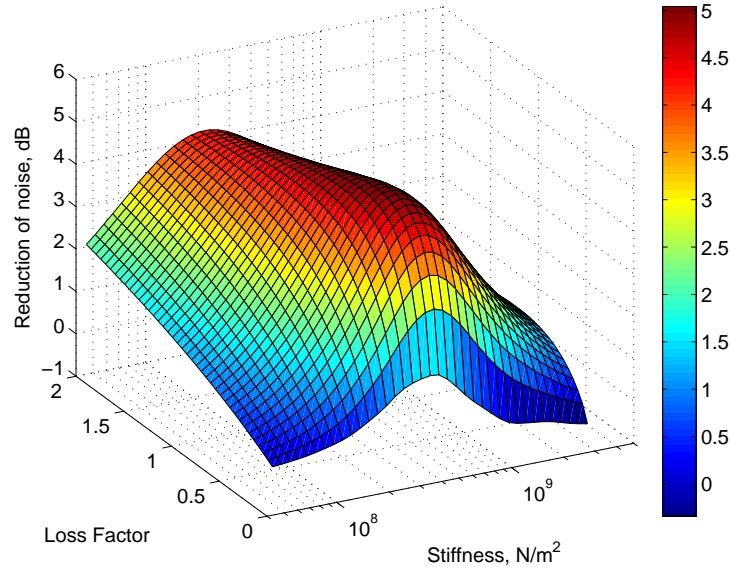
$$\frac{dG'}{dx} = \frac{2G''}{\pi} \tag{3.9}$$

where $x = \log_e(f)$ and f is frequency. The loss factor η can be written as

$$\eta = \frac{G''}{G'} \tag{3.10}$$
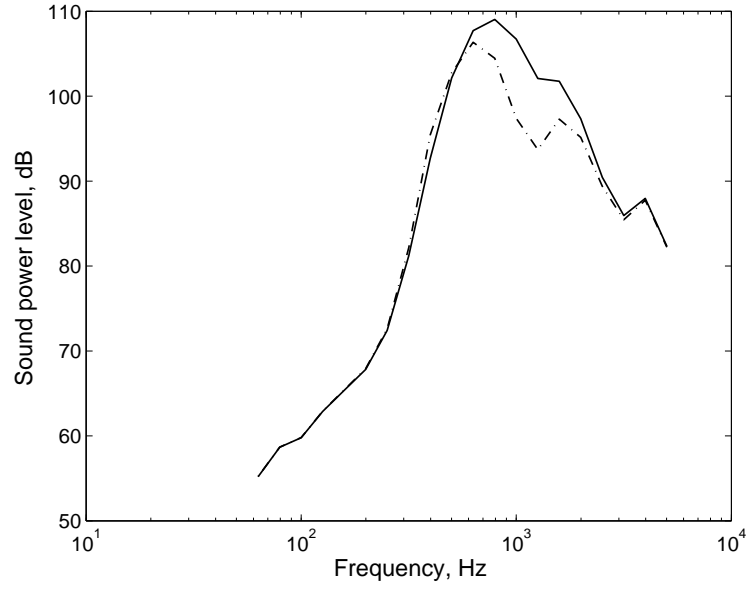
Figure 3.16: *The predicted vertical component of rail noise based on the Timoshenko model with and without absorber. The input parameters are as in Table 3.2, tuning frequency 1000 Hz, η_a=0.35. (a) (—) vertical untreated (113.2 dB(A)); (b) (− · −) vertical treated track (109.2 dB(A)).*

Figure 3.17: *Reduction in rail vertical component of noise in dB(A) for a range of loss factor of 0.01 and 2.0, and a range of stiffness (corresponding to tuning frequencies between 250 and 2000 Hz).*
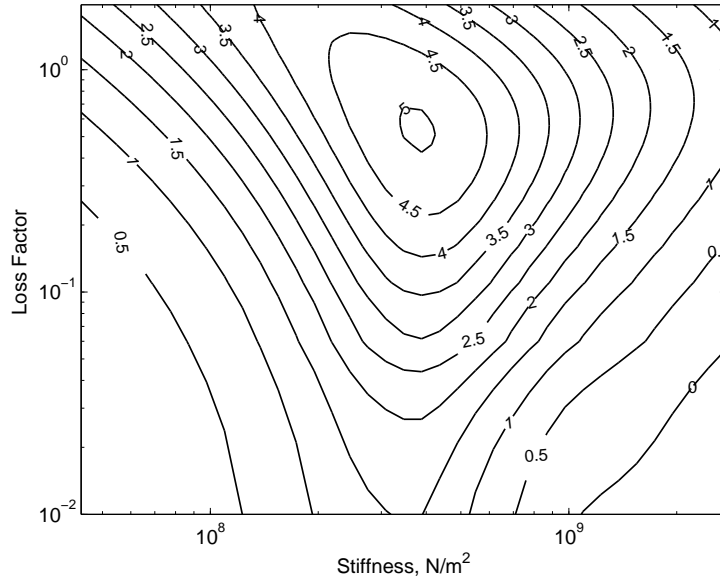
Figure 3.18: *Contour plot of reduction of rail vertical component of noise in dB(A) for a range of loss factor and stiffness (corresponding to tuning frequency between 250 and 2000 Hz).*

Substituting this into Equation (3.9) gives,

$$\frac{dG'}{dx} = \left(\frac{2\eta}{\pi}\right) G''$$
(3.11)

Although the loss factor is generally dependent on frequency and temperature, as seen in Chapter 2, insight can be gained by assuming a constant value of η. Then, the solution to Equation (3.11) is

$$G' = G_0 e^{\left(\frac{2\eta x}{\pi}\right)} = G_0 f^{\left(\frac{2\eta}{\pi}\right)}$$
(3.12)

for some constant G_0. Thus the ratio between G' at two frequencies f_1 and f_2 is

$$\frac{G'(f_2)}{G'(f_1)} = \left(\frac{f_2}{f_1}\right)^{\frac{2\eta}{\pi}}$$
(3.13)

An example of the result of the above equation can be seen in Figure 3.19. This shows the ratio of G' over one decade of frequency versus loss factor. It shows that the ratio of G' increases with increasing loss factor.

Next this frequency-dependence has to be converted into a temperature-dependence. According to the principle of time-temperature superposition described in section 2.3.3 (Ferry, 1970), it is possible to superimpose the curves of G' against $\log_{10} f$ at different
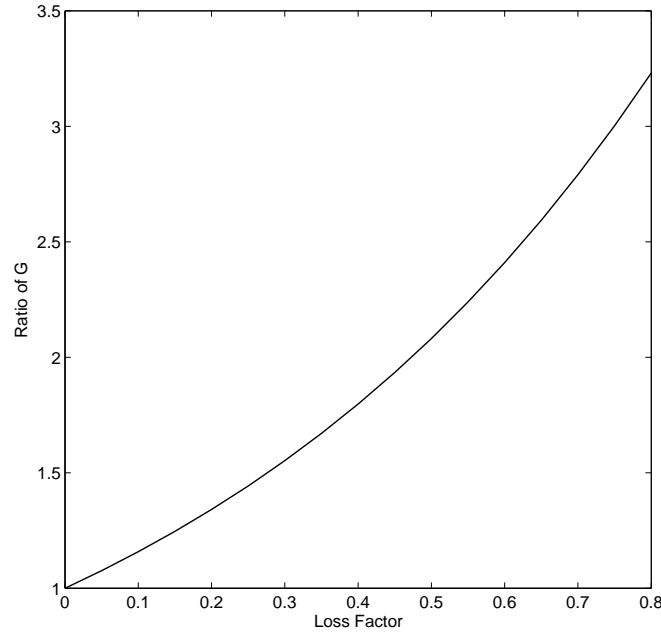
Figure 3.19: *The ratio of G' over one decade of frequency for various loss factors.*

temperatures by adding a temperature-dependent factor $\log_{10} \alpha(T)$, called a shift factor, to $\log_{10} f$. This applies strictly only for a thermorheologically simple material. The shift factor should be the same for all frequencies for a curve measured at a given temperature.

The Williams-Landel-Ferry (WLF) model (Williams *et al.*, 1955) described in section 2.3.3 can be used to generate the relationship between f and T. This model is found to apply to a wide range of elastomeric materials, (Ferry, 1970; Williams *et al.*, 1955). The WLF model predicts the shift factor as

$$\log_{10} \alpha(T) = \frac{-8.86(T - T_s)}{101.6 + T - T_s} \tag{3.14}$$

where T_s is a reference temperature, applying to a given material. It can be estimated approximately as $T_g + 50$, where T_g is the glass transition temperature of the material (Williams *et al.*, 1955). Equation (3.14) is valid over a range $T_s - 50 < T < T_s + 50$.

Then, the ratio of storage modulus at two temperatures T_1 and T_2 and for a given frequency is given by,

$$\log_{10} \left(\frac{G'(T_1)}{G'(T_2)} \right) = \frac{2\eta}{\pi} \left(\frac{8.86(T_2 - T_s)}{101.6 + T_2 - T_s} - \frac{8.86(T_1 - T_s)}{101.6 + T_1 - T_s} \right) \tag{3.15}$$

Figure 3.20 shows the shift factor for different values of T_s predicted according to equation (3.14) for temperatures between -20℃ and 40℃. These have been normalised by

dividing $\alpha(T)$ by the shift factor at 10℃. The slopes of these curves increase with increasing T_s and decreasing temperature.
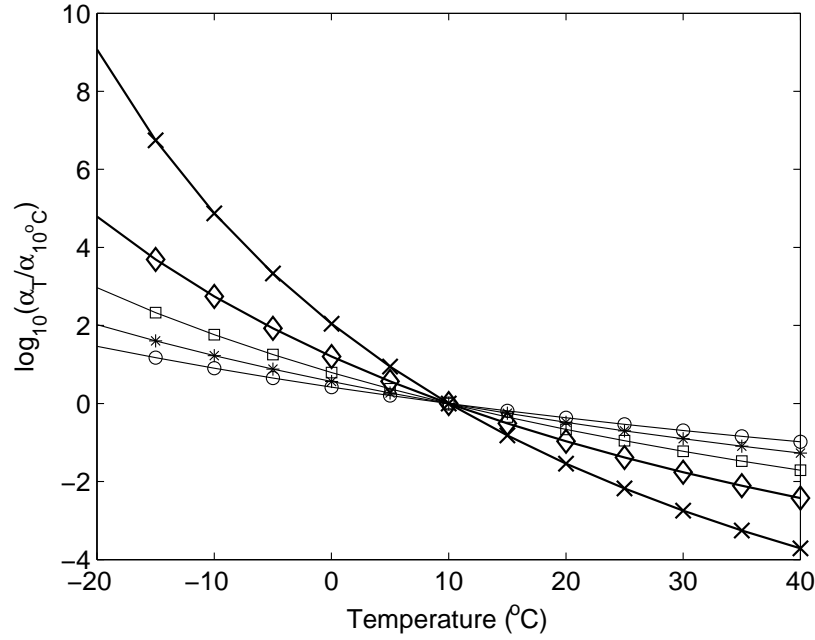
Figure 3.20: *Logarithm of reduction factor $\alpha(T)$ plotted against temperature for various T_s which are normalized at 10℃. The curves represent (∘) T_s=-40℃; (∗) T_s=-20℃; (□) T_s=0℃; (◇) T_s=20℃; (×) T_s=40℃.*

It is now necessary to select a value of T_s. Taking, for example, a value of T_g of -70℃, corresponding to butyl rubber, T_s will be about -20℃. Figure 3.21 shows the variation of G' with temperature for various loss factors, for a value of T_s of -20℃. The value of G' is shown relative to the value at 10℃. The slope of increases as the loss factor increases.

Figures 3.22, 3.23 and 3.24 show the influence of T_s on the stiffness for various values of temperature and loss factor. For a T_s of -40℃, the change of stiffness is smaller across the temperature range than for T_s of -20℃ and 0℃. Again, for higher values of loss factor, the change of stiffness with temperature becomes larger.

3.5 Effect of temperature-dependence on reduction of noise

If a constant loss factor is assumed, the temperature variation of the stiffness can be introduced into the noise predictions using the above model. Dynamic properties at 10℃ are used as nominal input parameters in the prediction of noise reduction. These are based on a stiffness of 4.36×10^8 N/m^2, corresponding to a tuning frequency of 800 Hz. The stiffness is then varied according to the ratio in Figure 3.21 as temperature varies and according to equation (3.13) as frequency varies.
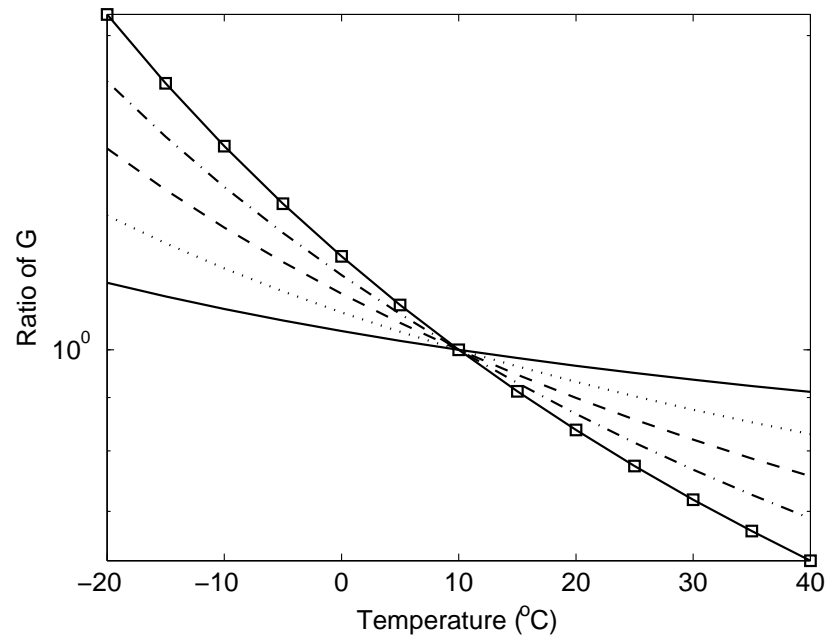
Figure 3.21: *The ratio of G plotted against temperature for a T_s of -20℃ for temperature normalisation at 10℃. The curves represent (—) η=0.05; (· · ·) η=0.1; (−−) η=0.2; (− · −) η=0.4; (□) η=0.8.*
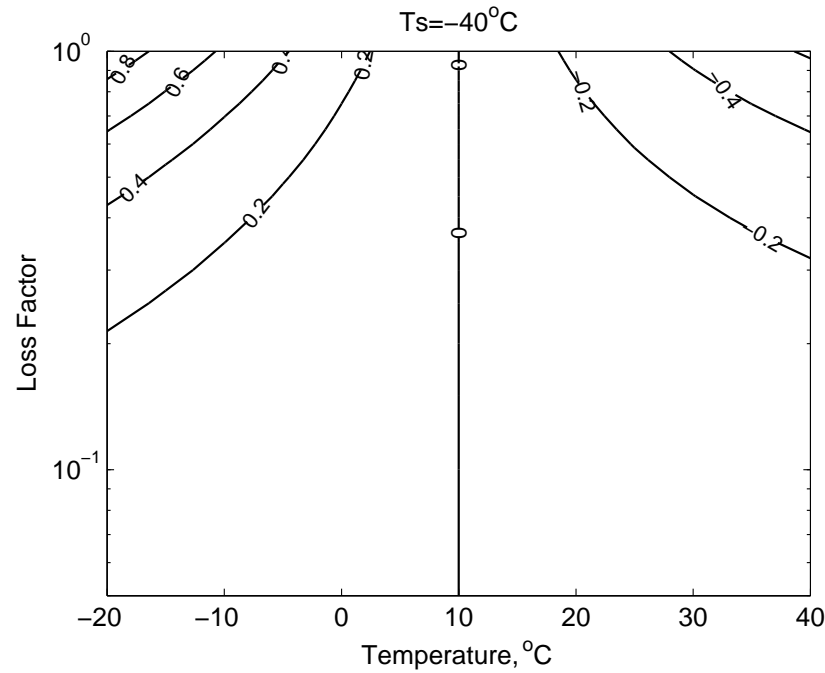
Figure 3.22: *Contour plot of $\log_{10}$ stiffness relative to that at 10℃ against temperature and loss factor. T_s=-40℃.*
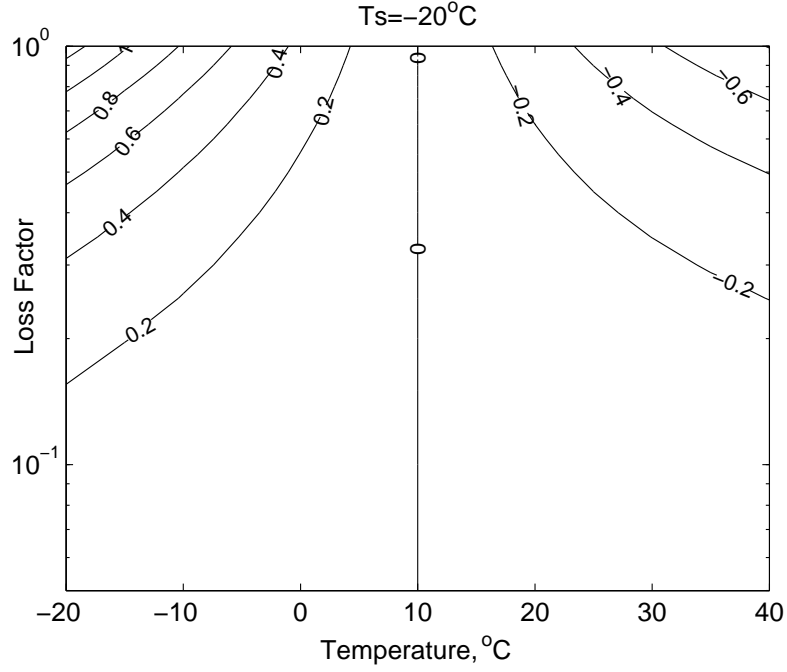
Figure 3.23: *Contour plot of* $\log_{10}$ *stiffness relative to that at 10℃ against temperature and loss factor.* T_s=-20℃.
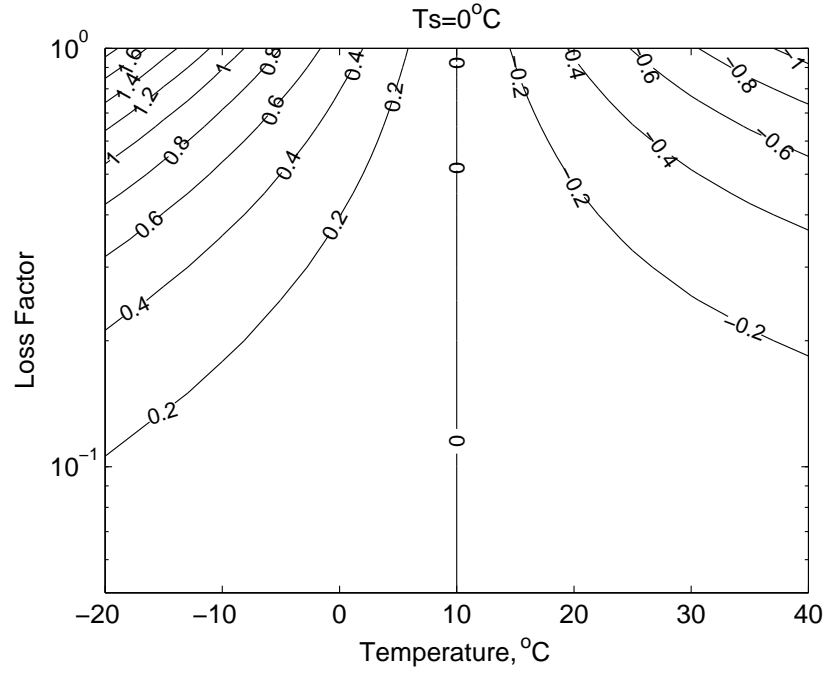
Figure 3.24: *Contour plot of* $\log_{10}$ *stiffness relative to that at 10℃ against temperature and loss factor.* T_s=0℃.
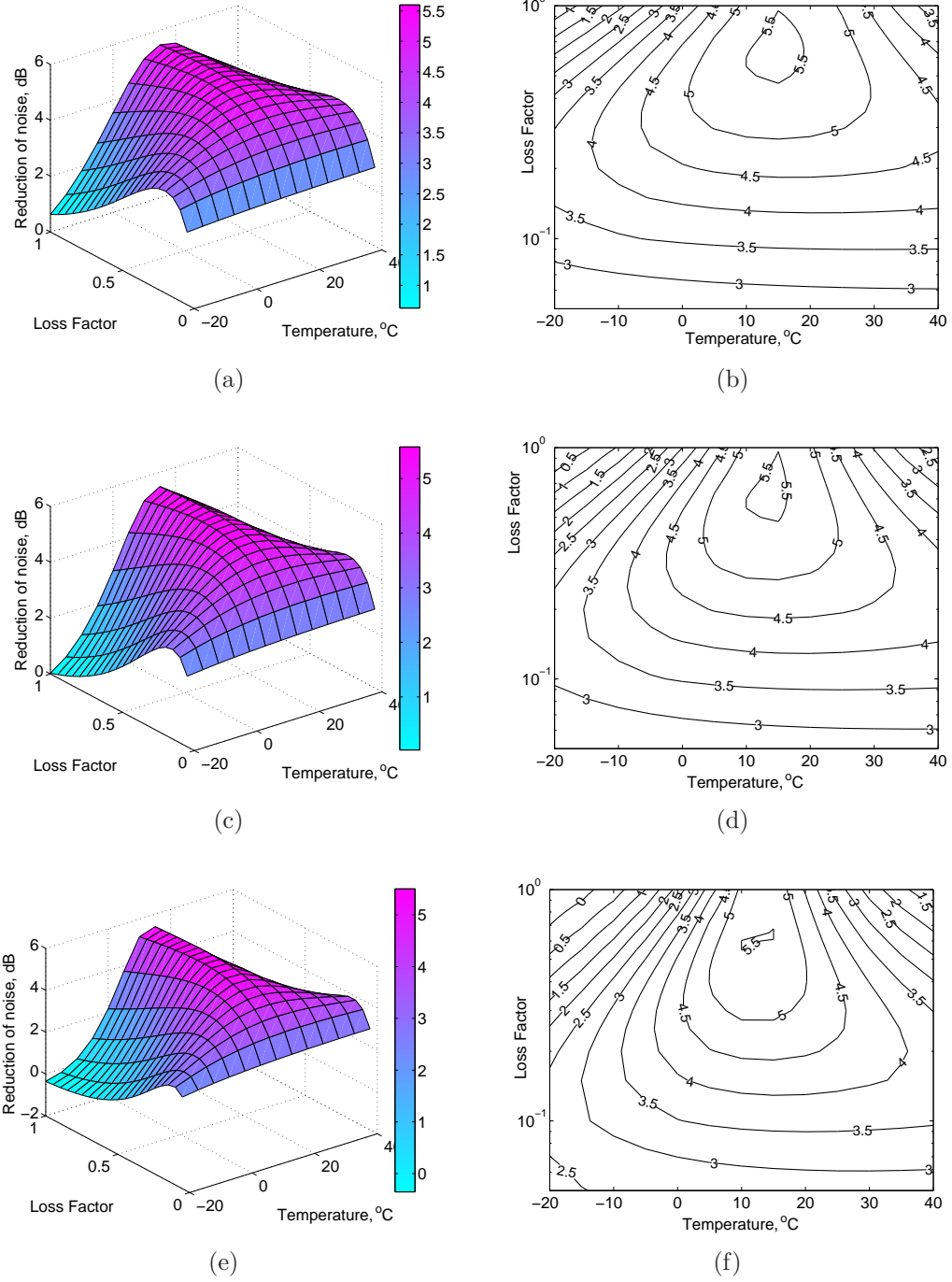
Figure 3.25: *The reduction of vertical rail noise in dB(A) at various temperatures and loss factors. The parameters used are as in Table 3.2 with $S_a = 4.36 \times 10^8 N/m^2$ at 10℃ (a & b) T_s=-40℃, (c & d) T_s=-20℃ and (e & f) T_s=0℃.*

Figure 3.25 shows the reduction of the vertical rail noise as a contour plot against temperature and loss factor and also as a 3D mesh plot. Results are shown for three values of T_s. In all cases, low loss factors give less noise reduction but give results which are less sensitive to the change of temperature than for higher loss factors. For example, for T_s=-20℃ (Figure 3.25(d)), a loss factor of 0.3 allows a maximum reduction of 5.0 dB to be achieved and this remains above 3.5 dB between -10℃ and 40℃. However, when the loss factor is increased to 1.0, although the maximum noise reduction is 5.5 dB, the results are much more strongly dependent on temperature due to the higher variation of the stiffness. Generally, a loss factor around 0.25 to 0.4 appears to give the best results across the range of temperatures considered.

The values of T_s assumed also affect the results. The lowest value of T_s (-40℃) gives less variation of noise reduction across the temperature range while a T_s of 0℃ gives a higher variation. This follows from the stiffness variation seen in Figure 3.20. The choice of T_s in the analysis is somewhat arbitrary, but -20℃ is realistic for a common workable material such as butyl rubber.

The results in Figure 3.25 show only the effect on the overall A-weighted sound level. To illustrate the frequency dependence of the noise reductions, Figures 3.26 to 3.28 show results for three values of loss factor and several temperatures. These are based on T_s=-20℃. The shifting of these curves across the frequency range as temperature varies becomes larger at higher loss factors. Similarly, the bandwidths of the peaks become wider as the loss factor increases. For example in Figure 3.26, the curve representing 20℃ has a maximum reduction of noise of 13 dB but the bandwidth is very narrow. On the other hand, the equivalent curve in Figure 3.28 has a lower reduction of noise of about 8 dB but the bandwidth is larger.

3.6 Two-frequency absorber system

3.6.1 Masses in parallel

In a previous study by Thompson *et al.* (2007), it was shown that using an absorber with two tuning frequencies, the loss factor peak in the decay rate curve can be broadened, giving a greater noise reduction for the same overall mass. Such a system has been implemented here using the same procedure as above. In the nominal arrangement (at 10℃) the tuning frequencies are selected as 630 and 1350 Hz corresponding to the optimum determined by Thompson *et al.* (2007). Firstly, the decay rate of the track is determined
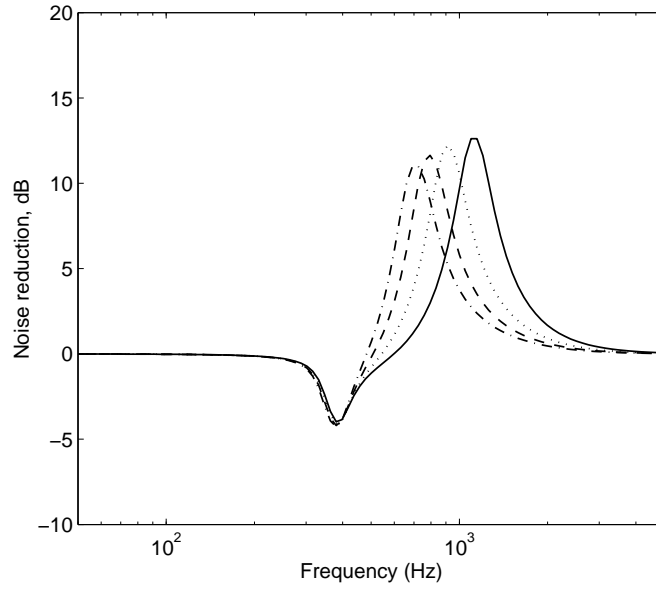
Figure 3.26: *Plots of noise reduction at various temperatures for loss factor of 0.2 and T_s=-20℃. The curves represent (—) -20℃, (· · ·) 0℃, (— — —) 20℃ and (-··-) 40℃*
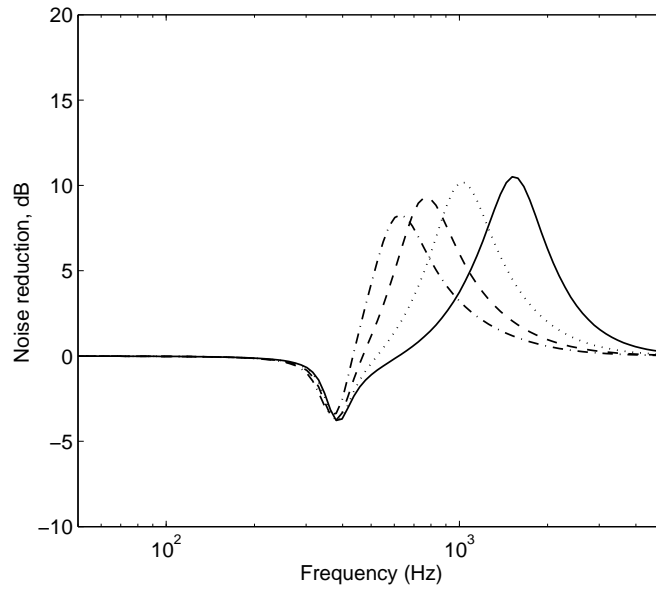
Figure 3.27: *Plots of noise reduction at various temperatures for loss factor of 0.4 and T_s=-20℃. The curves represent (—) -20℃, (· · ·) 0℃, (— — —) 20℃ and (-··-) 40℃*
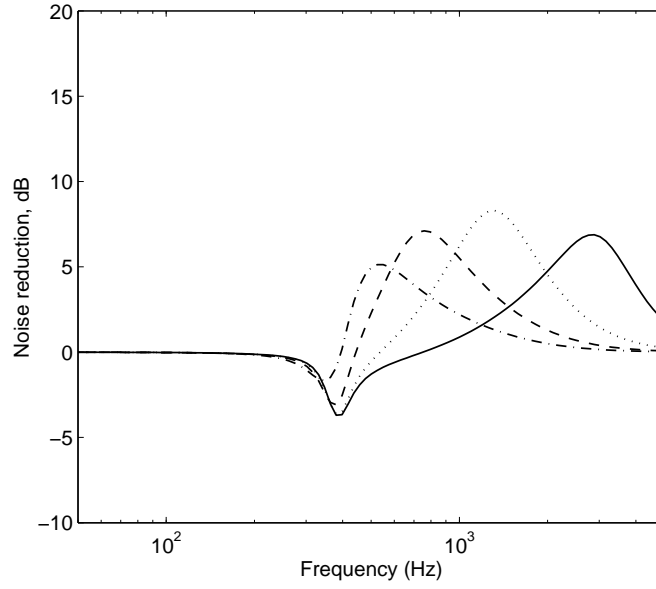
Figure 3.28: *Plots of noise reduction at various temperatures for loss factor of 0.8 and T_s=-20℃. The curves represent (—) -20℃, (···) 0℃, (− − −) 20℃ and (-··-) 40℃*

for an arrangement in which the masses are placed in parallel, giving a dynamic stiffness,

$$S_{dyn}(\omega) = \left(S_{a1} - \frac{S_{a1}^2}{S_{a1} - \mu_1\omega^2}\right) + \left(S_{a2} - \frac{S_{a2}^2}{S_{a2} - \mu_2\omega^2}\right) \tag{3.16}$$

where S_{a1} and μ_1 represent the stiffness and mass applying to the system tuned to 630 Hz and S_{a2} and μ_2 for stiffness and mass tuned to 1350 Hz. The overall mass of 17.5 kg/m is divided into 10 kg/m and 7.5 kg/m respectively and the decay rates are calculated using the Timoshenko beam model.

The results are shown in Figure 3.29 for materials with a loss factor of 0.2, 0.4 and 0.8. In the results for a loss factor of 0.2 the twin peaks in the decay rate can be seen more clearly than for higher loss factors. These peaks are more stable with changes in temperature. For a loss factor of 0.8, at temperature 10℃, the two peaks are very broad, and at low or high temperature, they shift out of the frequency range of interest.

Figure 3.30 shows the noise reduction for a range of temperatures and loss factors. Compared with the single absorber with the same overall mass, Figure 3.25(c) and (d), a greater noise reduction is achieved and this is sustained over a wide range of temperatures, especially for loss factors between 0.2 and 0.4.
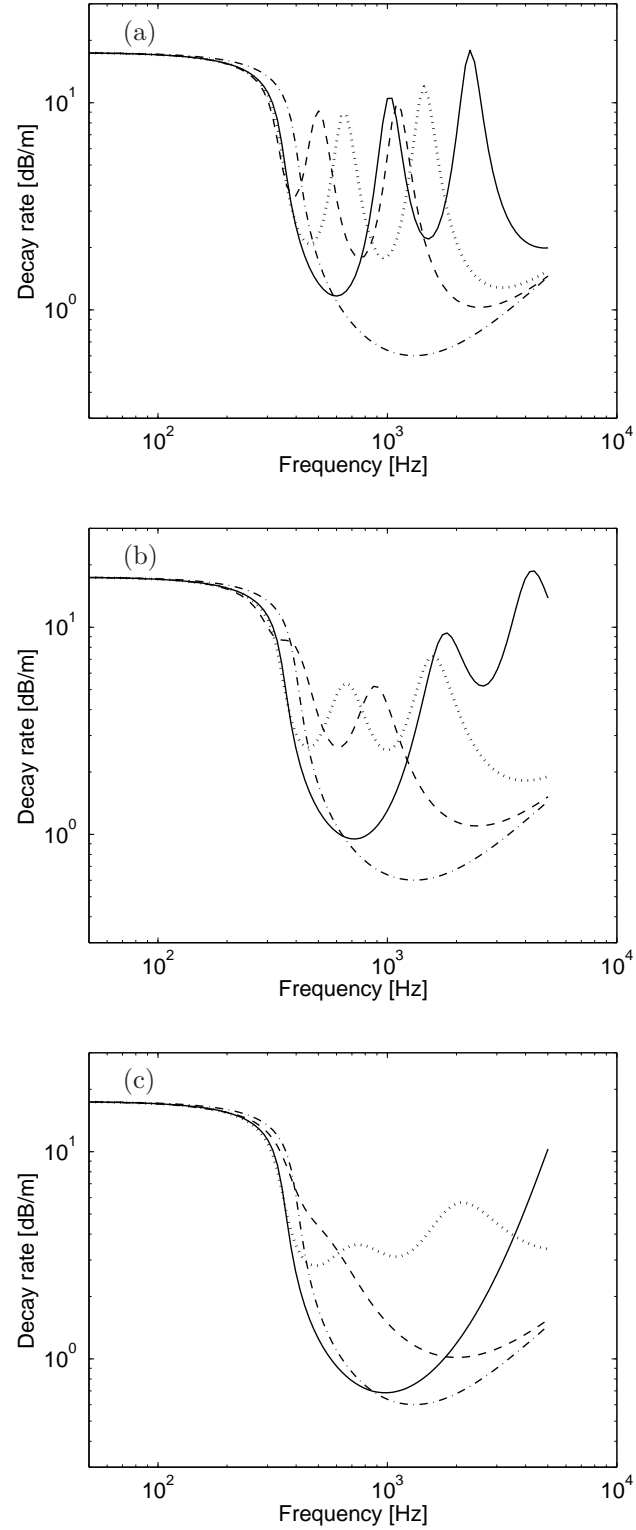
Figure 3.29: *Decay rate of track with two-mass absorber in parellel for temperatures (—) T=-20℃, (· · ·) T=10℃, (— — —) T=40℃, (— · —) no absorber. Results normalised at 10℃ and T_s=-20℃. The decay rates are for various loss factors: (a) η=0.2, (b) η=0.4 and (c) η=0.8.*
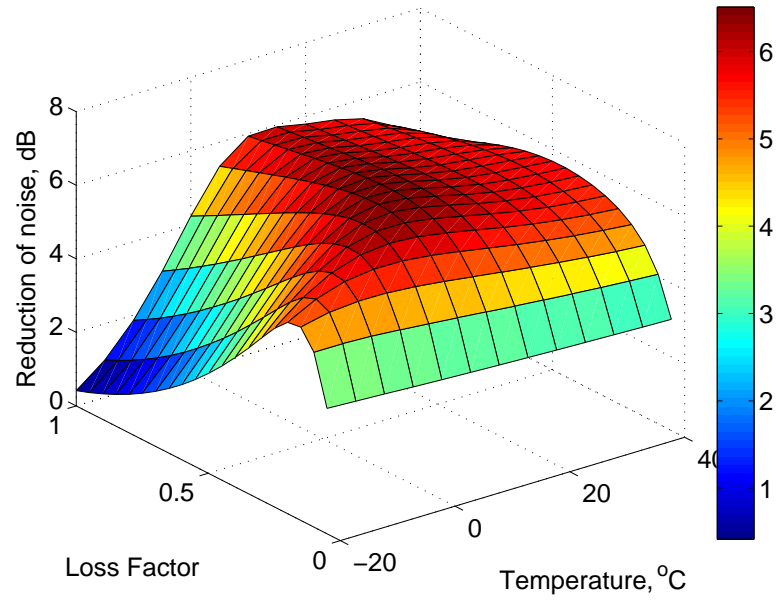
(a)
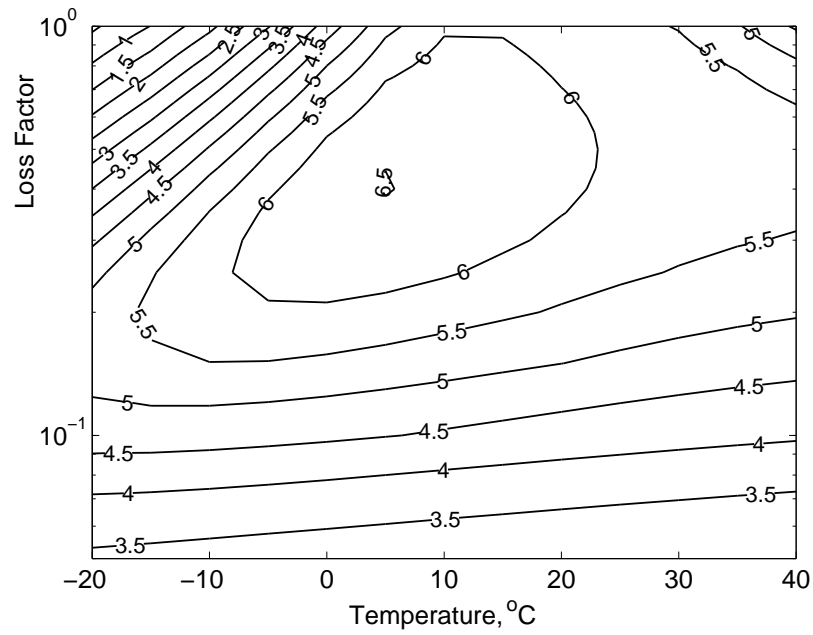
(b)

Figure 3.30: *The reduction of A-weighted rail noise level in dB for two-mass absorber with masses in parallel, T_s=-20℃.*

3.6.2   Stacked masses

Figure 3.31 shows a two-tuning frequency system with stacked masses. The corresponding dynamic stiffness is derived as

$$S_{dyn}(\omega) = S_{a1} - \frac{(S_{a1}^2)}{B} \tag{3.17}$$

where $B = (S_{a1} + S_{a2} - \mu_1\omega^2) - \left(\dfrac{S_{a2}^2}{S_{a2} - \mu_2\omega^2}\right)$. The absorber masses are chosen as $\mu_1 = 10.7$ kg/m and $\mu_2 = 6.8$ kg/m. The corresponding stiffness is at 10℃ are $S_{a1} = 5.62 \times 10^8 N/m^2$ and $S_{a2} = 1.46 \times 10^8 N/m^2$ to give tuning frequencies of 630 Hz and 1350 Hz.
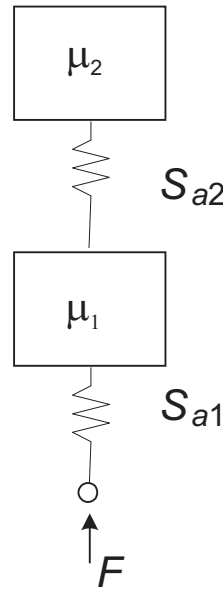
Figure 3.31: *Schematic diagram of stacked masses.*

The results are shown in Figure 3.32. As before, two clear peaks can be seen for $\eta = 0.2$, Figure 3.33 shows the results for a range of temperatures and loss factors. Compared with the results in Figure 3.30, the maximum noise reduction is slightly greater but it is not sustained at higher temperatures quite so well due to the fact that the second peaks are smaller in Figure 3.32 than in Figure 3.29.

3.6.3   Calibration of results for measured material properties

The two-tuning frequency model is next used with measured material properties in order to establish the confidence of predicting the noise reduction from the measured data using the Timoshenko track model. For this purpose, measured data of nitrile rubber (NBR), marked as sample 23 in Jones (2005) and Ahmad (2005), is used and a comparison is made
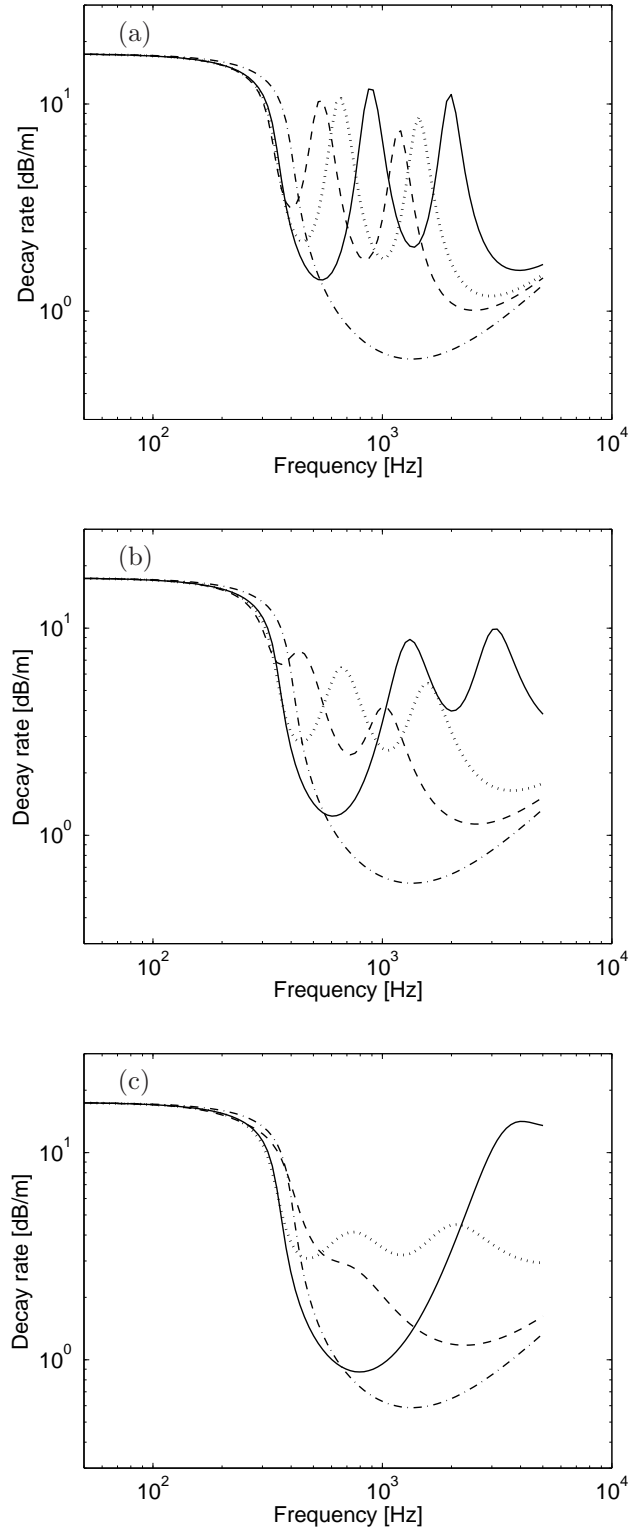
Figure 3.32: *Decay rate of track with stacked mass absorber for temperatures (—) T=-20℃, (⋯) T=10℃, (− − −) T=40℃, (− · −) no absorber. Results normalised at 10℃ and Tₛ=-20℃. The decay rates are at various loss factor: (a) η=0.2, (b) η=0.4 and (c) η=0.8.*
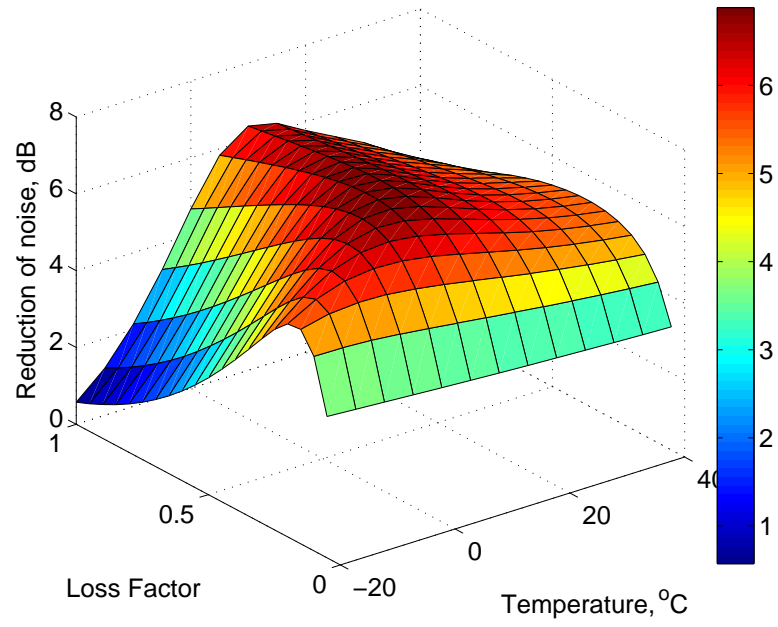
(a)
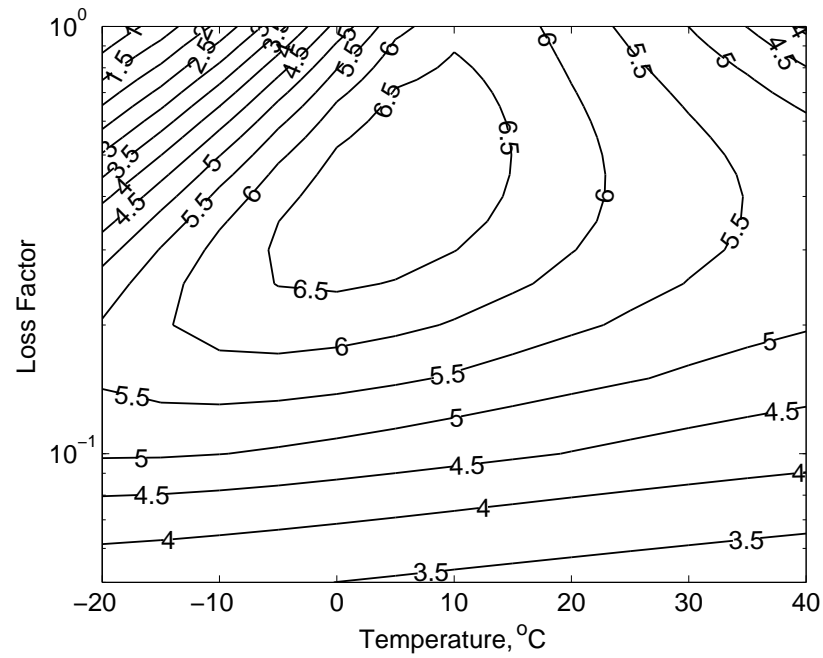
(b)

Figure 3.33: *The reduction of A-weighted rail noise level in dB for two-mass absorber with stacked masses.*

between the present Timoshenko beam predictions and TWINS predictions from Jones (2005), which include rail cross-section deformation.

To simplify the measured data, which is not valid at low and high frequencies, a single value of stiffness and loss factor is used for 1000 Hz at each temperature. The frequency-dependence is then determined using Equation (3.13). The shear modulus is converted to a stiffness by a constant factor, chosen to ensure that the tuning frequency at 20℃ matches that found by Jones (2005).

As a check of this procedure, Figure 3.34 shows the estimated stiffness and that measured for a range of frequencies. These show reasonable agreement, with the high frequency data at 40℃ and the low frequency data at -20℃ being known to be unreliable in the measurements.
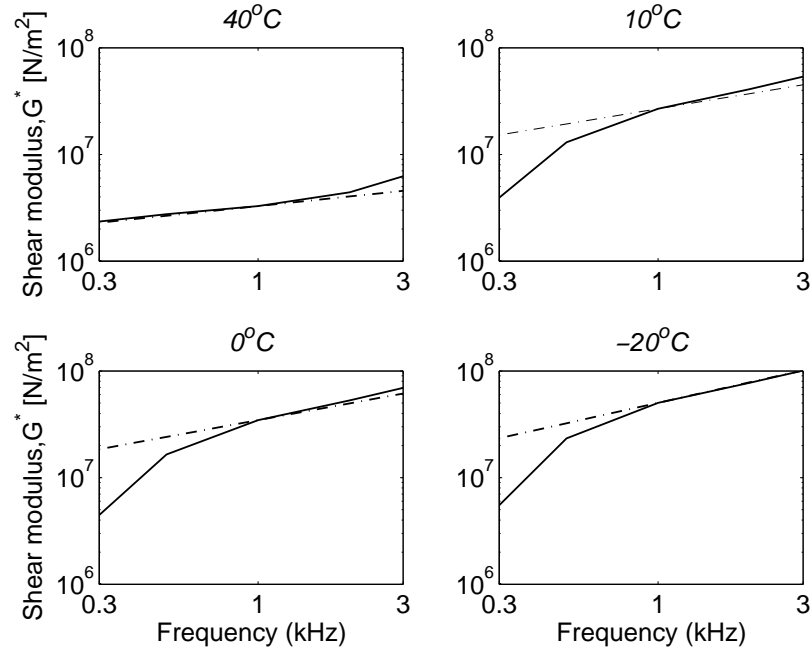
Figure 3.34: *Comparing the shear modulus of $(- \cdot -)$ predicted and $(—)$ measured data of NBR sample 23 at temperatures 40℃, 10℃, 0℃ and -20℃.*

Then, using the measured data of this NBR sample 23, a comparison is carried out between the decay rates predicted using these two track models, the Timoshenko beam and TWINS and the results are shown in Figure 3.35. In each case the support stiffness is omitted. Both methods present a similar trend. At high frequency, above 1000 Hz, the decay rate predicted by the TWINS model is similar to the Timoshenko beam model except at low temperature 0℃.

Figure 3.36 shows the ratio of the two results. Basically, these ratios give a similar trend. The agreement is quite good above 400 Hz. The Timoshenko curves present higher damping behaviour at low frequencies. This may be due to the omission of the shear stiffness in the Timoshenko beam model.
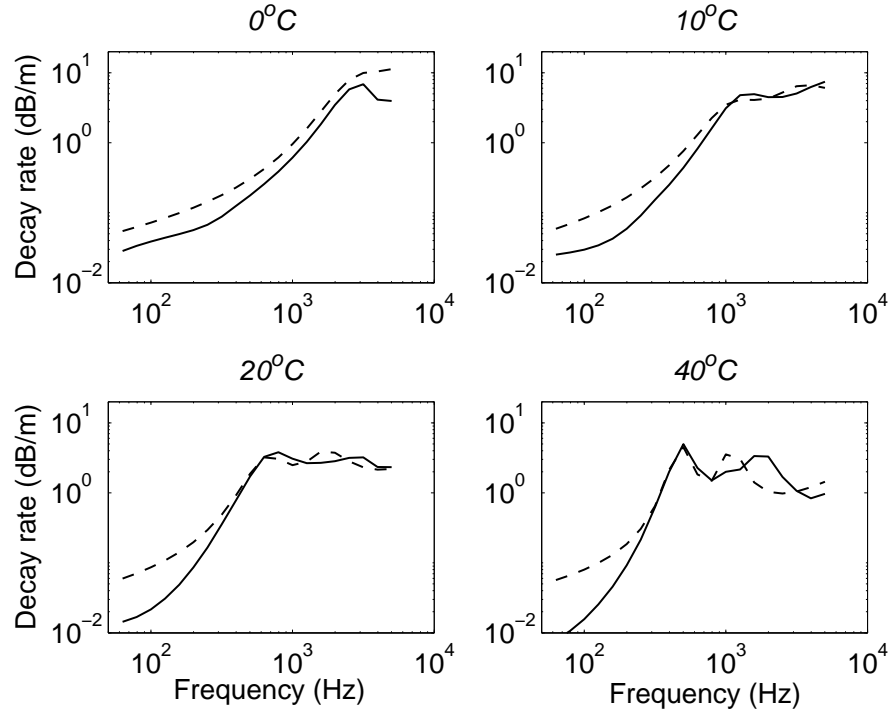
Figure 3.35: *Comparing the decay rate of TWINS (—) and Timoshenko (−−) beam model for NBR sample 23 at various temperatures.*
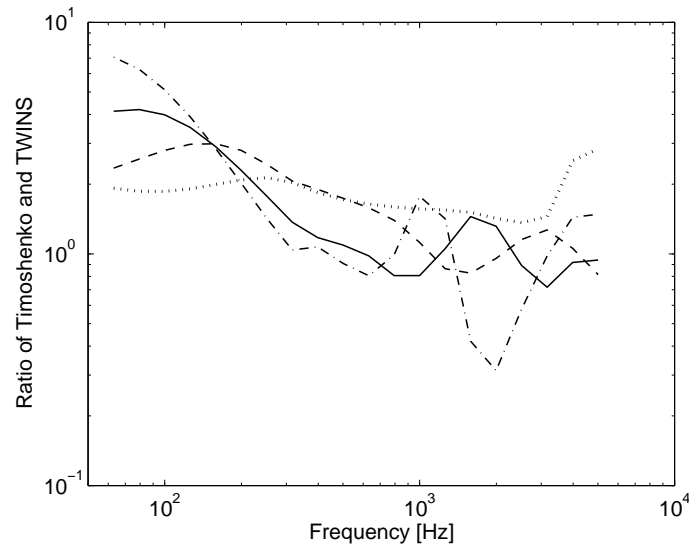
Figure 3.36: *The ratio of TWINS to Timoshenko beam model for NBR sample 23 at various temperatures: (· · ·) 0℃; (−−) 10℃; (—) 20℃ and (− · −) 40℃.*
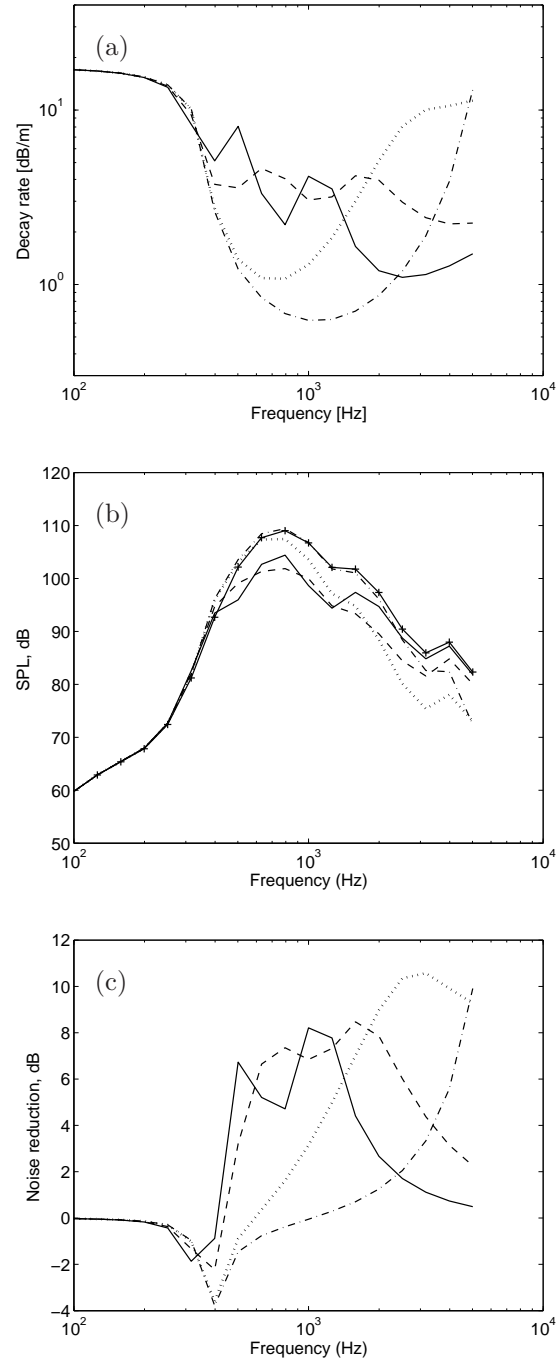
Figure 3.37: *Based on the measured data of NBR sample 23, the Timoshenko beam model is used to predicted the decay rate, sound power level and noise reduction at various temperatures; (—) 40℃, (− − −) 20℃, (⋯) 0℃, (− · −) -20℃ and (+) no absorber. (a) Decay rate, (b) Sound power level and (c) Noise reduction.*
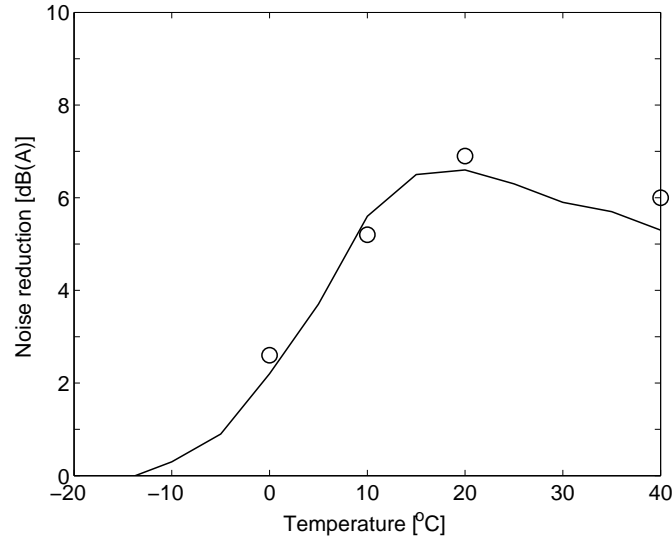
Figure 3.38: *Comparison of noise reduction for the rail between TWINS (○) and Timoshenko beam (—) track model for NBR sample 23.*

The decay rates and noise reductions determined by the Timoshenko beam model for each temperature (0℃, 10℃, 20℃ and 40℃) are shown in Figure 3.37. The decay rate peak at 40℃ and 20℃ occurs between 500 Hz and 3000 Hz. For 0℃ and -20℃ the peak occurs above 2000 Hz which is less relevant to the rail absorber application.

Table 3.3 shows the predicted noise reductions for all the various temperatures for all the NBR samples measured in (Ahmad, 2005), which are based on the properties in Table 3.4. The reduction of noise becomes larger as temperature increases from 0℃. The results for sample 23 are compared with those obtained using TWINS in Figure 3.38. This shows very good agreement. Therefore, this method will be used to choose the optimum material based on the predicted noise reduction found using Timoshenko beam track model.

3.7 Conclusions

In this chapter, a mathematical model of a beam representing the rail was predicted based on Timoshenko beam theory. It was shown that it is necessary to use the Timoshenko beam model rather than an Euler-Bernoulli beam model above about 500 Hz, which is in the range of frequencies where rail noise is dominant. However in this frequency region the support can be simplified to a single layer of stiffness representing the rail pads.

Using the Timoshenko beam model, the optimum loss factor and stiffness of an absorber with a single tuning frequency is determined for a particular wheel/track combination. A loss factor of at least 0.3 and a stiffness of 4.36×10^8 N/m^2 are the appropriate parameters for a mass of 17.5 kg/m, giving a tuning frequency of 800 Hz.

Table 3.3: *The average sound power level reduction for NBR samples at various temperatures predicted using Timoshenko beam model*

Sample	Reduction of noise [dB(A)]												
	-20℃	-15℃	-10℃	-5℃	0℃	5℃	10℃	15℃	20℃	25℃	30℃	35℃	40℃
NBR21	-0.3	-0.2	-0.2	-0.1	0.2	0.5	1.0	1.8	2.5	3.0	3.9	4.7	5.3
NBR22	-0.1	0.0	0.2	0.7	1.2	2.8	4.3	6.0	6.6	6.6	6.3	5.9	5.6
NBR23	-0.2	-0.1	0.3	0.9	2.2	3.7	5.6	6.5	6.7	6.4	6.0	5.8	5.4
NBR24	-0.2	-0.2	-0.1	0.1	0.5	1.0	1.8	2.7	3.4	4.1	4.8	5.1	5.3
NBR25	-0.2	-0.1	0.0	0.4	1.2	1.8	3.0	3.5	4.6	5.5	5.9	6.3	6.5
NBR26	-0.2	0.0	0.2	0.6	1.0	1.4	2.9	4.7	6.0	6.7	6.9	6.8	6.8
NBR27	-0.3	-0.2	0.0	0.6	0.9	1.7	3.2	5.0	6.0	6.7	6.9	6.9	6.9
NBR28	-0.1	0.0	0.2	0.4	0.8	1.5	2.5	3.9	5.0	6.1	6.8	6.9	6.8
NBR30	-0.3	-0.1	0.1	0.8	1.4	2.1	3.3	4.2	5.2	5.9	6.2	6.6	6.6
NBR32	-0.1	-0.1	-0.1	0.1	0.1	0.6	0.8	1.4	1.9	2.4	3.0	3.4	3.9
NBR33	0.0	0.1	0.6	1.5	3.4	5.2	6.4	6.5	5.8	5.4	5.1	4.9	4.8
NBR34	-0.2	-0.1	0.1	0.2	0.6	1.2	2.6	3.5	4.7	6.1	6.7	6.9	6.8

Table 3.4: *Measured shear modulus and loss factor of NBR samples, which were used to predicted the noise reduction in Table 3.3*

Sample		-20°C	-15°C	-10°C	-5°C	0°C	5°C	10°C	15°C	20°C	25°C	30°C	35°C	40°C
NBR21	G [N/m²]	2.93E+08	2.36E+08	2.27E+08	1.73E+08	1.19E+08	7.62E+07	4.95E+07	2.97E+07	2.06E+07	1.69E+07	1.25E+07	9.79E+06	8.15E+06
	η	0.20	0.23	0.28	0.35	0.44	0.53	0.64	0.68	0.64	0.61	0.50	0.42	0.35
NBR22	G [N/m²]	2.02E+08	1.68E+08	1.14E+08	6.88E+07	4.19E+07	1.84E+07	1.03E+07	6.11E+06	3.94E+06	3.43E+06	2.70E+06	2.43E+06	2.17E+06
	η	0.38	0.45	0.56	0.71	0.80	0.94	0.97	0.88	0.78	0.66	0.54	0.42	0.35
NBR23	G [N/m²]	2.53E+08	1.81E+08	1.08E+08	5.36E+07	2.38E+07	1.25E+07	6.84E+06	4.77E+06	3.52E+06	2.84E+06	2.48E+06	2.35E+06	2.08E+06
	η	0.23	0.35	0.56	0.80	0.99	1.03	0.94	0.80	0.64	0.52	0.43	0.38	0.31
NBR24	G [N/m²]	2.78E+08	2.28E+08	1.85E+08	1.25E+08	8.03E+07	4.81E+07	2.96E+07	1.93E+07	1.46E+07	1.16E+07	9.33E+06	8.55E+06	7.94E+06
	η	0.21	0.31	0.36	0.44	0.57	0.62	0.64	0.61	0.55	0.47	0.40	0.36	0.33
NBR25	G [N/m²]	2.56E+08	2.09E+08	1.82E+08	8.28E+07	4.03E+07	2.84E+07	1.72E+07	1.43E+07	1.01E+07	8.05E+06	7.19E+06	6.33E+06	5.81E+06
	η	0.33	0.37	0.45	0.51	0.61	0.65	0.71	0.69	0.61	0.45	0.37	0.32	
NBR26	G [N/m²]	2.17E+08	1.47E+08	1.16E+08	7.22E+07	5.12E+07	3.69E+07	1.76E+07	9.79E+06	6.73E+06	5.34E+06	4.10E+06	3.89E+06	3.93E+06
	η	0.22	0.32	0.44	0.53	0.67	0.70	0.73	0.72	0.65	0.50	0.41	0.35	0.32
NBR27	G [N/m²]	4.32E+08	3.15E+08	1.69E+08	6.87E+07	5.31E+07	3.11E+07	1.58E+07	9.20E+06	6.84E+06	5.45E+06	4.64E+06	4.61E+06	4.49E+06
	η	0.22	0.36	0.45	0.57	0.67	0.69	0.71	0.63	0.52	0.46	0.40	0.36	0.34
NBR28	G [N/m²]	1.74E+08	1.43E+08	1.17E+08	8.84E+07	5.94E+07	3.47E+07	2.08E+07	1.24E+07	9.12E+06	6.63E+06	5.20E+06	4.45E+06	4.02E+06
	η	0.34	0.39	0.46	0.55	0.64	0.71	0.74	0.71	0.65	0.54	0.43	0.36	0.31
NBR30	G [N/m²]	3.82E+08	2.12E+08	1.42E+08	5.51E+07	3.74E+07	2.56E+07	1.52E+07	1.15E+07	8.76E+06	7.10E+06	6.52E+06	5.35E+06	4.51E+06
	η	0.20	0.36	0.45	0.56	0.62	0.71	0.69	0.65	0.60	0.42	0.38	0.30	0.24
NBR32	G [N/m²]	1.46E+08	1.55E+08	1.92E+08	1.32E+08	1.19E+08	7.13E+07	5.70E+07	3.75E+07	2.67E+07	2.09E+07	1.65E+07	1.37E+07	1.15E+07
	η	0.26	0.28	0.30	0.36	0.39	0.51	0.59	0.66	0.61	0.56	0.49	0.42	0.35
NBR33	G [N/m²]	1.78E+08	1.44E+08	7.27E+07	3.53E+07	1.38E+07	7.39E+06	4.56E+06	3.07E+06	2.05E+06	1.75E+06	1.51E+06	1.39E+06	1.44E+06
	η	0.37	0.51	0.70	0.95	1.13	1.08	0.89	0.70	0.56	0.47	0.36	0.32	0.28
NBR34	G [N/m²]	2.26E+08	1.92E+08	1.47E+08	1.10E+08	7.31E+07	4.31E+07	1.95E+07	1.42E+07	9.95E+06	6.57E+06	5.51E+06	4.71E+06	4.19E+06
	η	0.29	0.33	0.44	0.54	0.63	0.79	0.86	0.79	0.69	0.57	0.47	0.40	0.32

In order to calculate the noise reduction, the vertical wave is most important and the absorber has to be optimised for this component. Lateral waves also contribute to the noise but are less pronounced than the vertical component. It is expected that the absorber will also reduce the lateral component but this has been neglected in the analysis for simplicity.

The reduction of noise is influenced by changes of temperature. Knowing that the stiffness of the elastomer in the absorber is very sensitive to temperature, an approximate technique has been adopted to estimate this effect. By assuming a constant loss factor, the variation in stiffness across the temperature range can be estimated assuming only a value for the temperature, T_s as used in the WLF equation. A value of -20℃ has been adopted for butyl rubber. It is shown that the noise reduction can be maintained within 1 dB of the maximum effect in a range -10℃ to 40℃ for most values of loss factor. To achieve the maximum noise reduction over a range of temperatures, it appears that the loss factor should be between about 0.25 and 0.4.

Introducing an absorber with two tuning frequencies, a better performance can be obtained in which the reduction of noise is larger and is sustained over a wider range of temperatures. The results from the Timoshenko beam track model are shown to be comparable with previous results from TWINS. Predictions have been made using the two-mass absorber for a range of materials measured previously. It is found that the effectiveness of the noise reduction is more pronounced for temperatures above 10℃, but below this temperature the effectiveness of the absorber is much less. This is because the loss factors of these materials are too high, making them very sensitive to temperature. Therefore, it appears that new materials with a more moderate loss factor (in the range of 0.25 to 0.4) are required to satisfy requirements for the rail absorber in the range of temperatures -20℃ to 40℃.

However, it is clear that the performance of the rail absorber at different temperatures should not be treated with equal weight. More weight should be given to those temperatures occuring more frequently during a year. Therefore, the effect of such distributions of temperature will be considered in the next chapter.

Chapter 4

Estimating the weighted noise reduction for a range of rail temperatures

4.1 Introduction

Due to the variability of weather and climate the rail temperature varies considerably in the course of a year. This will also have an effect on the performance of the rail absorber. In the previous chapter, the effect of the temperature on the reduction of rail noise has been established. In this chapter the statistical distribution of rail temperatures is investigated and used to develop a weighting procedure with which to account for temperature variations.

To cover a wide range of situations in Europe, temperature distributions from three different countries, the United Kingdom (UK), Sweden and Italy, have been evaluated. The temperature data for the UK was collected at a site at Leominster over a 12-month period from October 2003 to September 2004 (Chapman, 2007). Both the rail and air temperatures were sampled every 10 minutes over a whole year, although the data was incomplete. To obtain a distribution for Sweden and Italy, use has been made of air temperature data published by European Climate Assessment and Dataset (2007). For Sweden, data was obtained for Fulum covering the period from January to December 2000 in the form of the maximum and minimum temperature each day. Similarly, the temperature data in Italy were obtained for Brindisi from January to December 2005 as maximum and minimum temperature each day throughout the particular year.

The objective of this chapter is to develop a method to estimate a weighted noise reduction based on the rail temperature distribution for any location. This method will subsequently
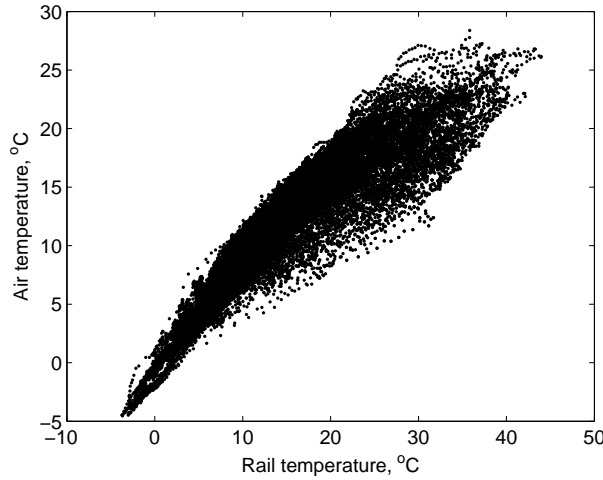
Figure 4.1: *Air versus rail temperature for a Leominster site, UK. The data was obtained at 10 minutes intervals.*

be used to assess various elastomeric materials in order to determine the optimum material for any given situation.

4.2 Temperature distribution at Leominster, United Kingdom

Data for a site at Leominster in the UK have been published by Chapman (2007). The raw data has kindly been supplied to us by the author. The rail temperature was collected every minute for each day throughout the year, whilst the air temperature was obtained every 10 minutes. For consistency the rail temperature has also been used at 10 minute intervals. Unfortunately some data are missing due to malfunction of the equipment, including all results for December and January.

Figure 4.1 shows the rail temperature plotted against air temperature. This shows a complicated relation due to the effects of sunlight (see Chapman (2007)). Figure 4.2 shows the maximum and minimum daily air temperature extracted from this data which illustrates the seasonal variations as well as the periods with missing data. The data (at 10 minute intervals) for each month were then arranged into frequency distributions with a 5℃ resolution. For example, the curves for June and October are shown in Figure 4.3.

The frequency distributions for the whole year were generated by adding the distributions for each month. In this way each month was treated equally and missing data within a particular month did not bias the data. In the case of two months with no data (December and January), approximate distributions were generated by using the frequency
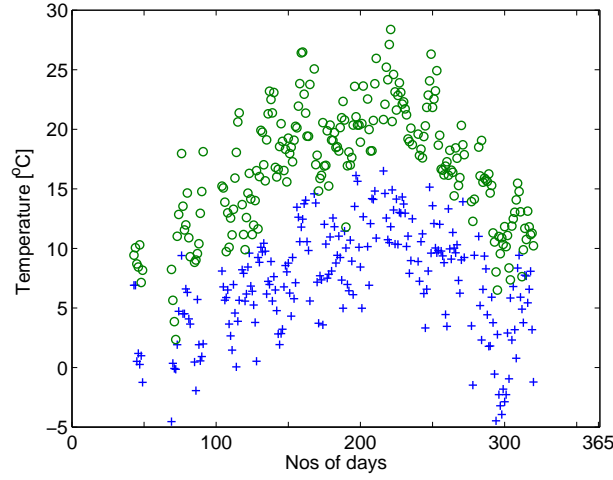
Figure 4.2: *The maximum (o) and minimum (+) air temperature at Leominster, UK for each day in a year. The data were recorded for the period October 2003 to September 2004 but are plotted against day number (1= 1 January, 365 = 31 December).*

distributions for October and March, respectively, in each case shifted by -5℃. The resulting distribution of rail temperature for the whole year is shown in Figure 4.4 along with that for air temperature.

(a)   (b)
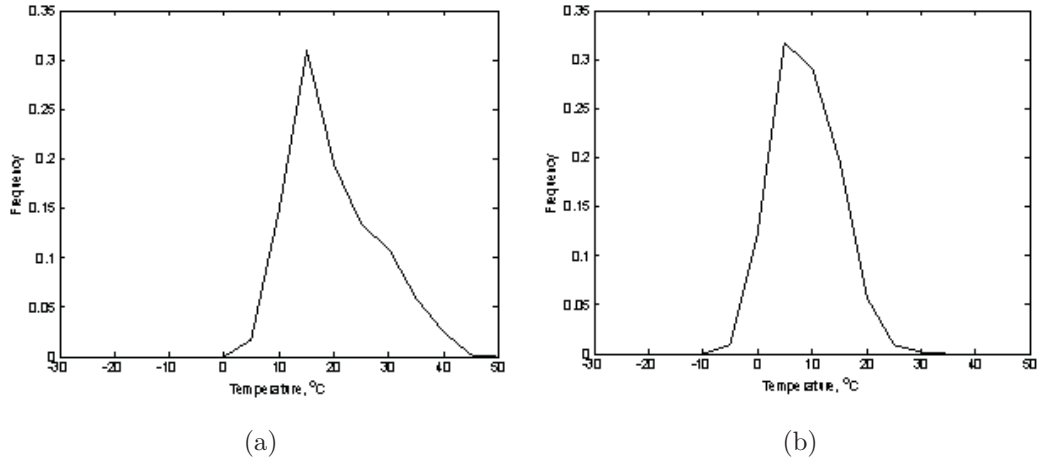
Figure 4.3: *Distribution of rail temperature at Leominster site, UK. (a) June and (b) October.*

This distribution of rail temperature can be used as a weighting for the noise reduction obtained at each temperature using the model of the previous chapter. Thus most account should be taken of the effect at 10℃, and relatively little effect taken of -10℃ and 40℃. At this site no temperatures below -10℃ (±2.5℃) were recorded.
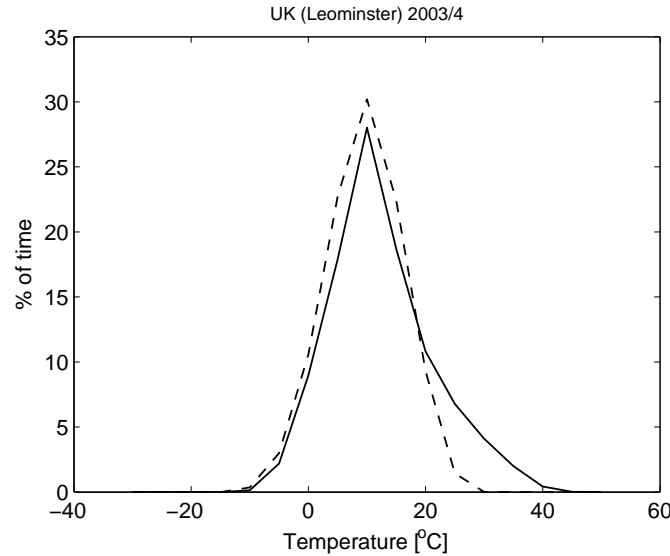
Figure 4.4: *Distribution of rail temperature (—) and instantaneous air temperature (−−) throughout the year for Leominster, UK.*

4.3 Estimation of rail temperature distribution in Sweden and Italy

For the locations in Sweden and Italy, measurements are not available for every 10 minutes of the day as at Leominster. Only maximum and minimum temperatures for each day are available. Such data is quite commonly given.

Figures 4.5 and 4.6 show distributions of the maximum and minimum daily air temperature for Sweden and Italy. At the site in Italy, the temperature range is 0℃ to 35℃. The distributions of minimum and maximum temperature are similar apart from a constant shift. For Sweden the temperature distributions contain a large 'tail' at low temperatures. The range of temperatures here is between -30℃ and 25℃. The data from the UK site has been converted to daily maximum and minimum temperatures (Figure 4.2) as well, so that comparisons can be made. Figure 4.7 shows the frequency distribution of these maximum and minimum air temperatures.

As the temperature data from Sweden and Italy do not include rail temperature, the rail temperature distribution obtained from the UK site will be used as a guide to estimate the rail temperature distribution for Sweden and Italy. To do that, it is convenient to take the points mid-way between the maximum and minimum air temperature for each day of the year.

Figure 4.8 shows the distribution of these daily mid-points of temperatures for all three countries. The UK has the narrowest distribution. The curve for Italy is shifted more towards high temperature, with the peak shifted by about 5℃ compared with the UK.
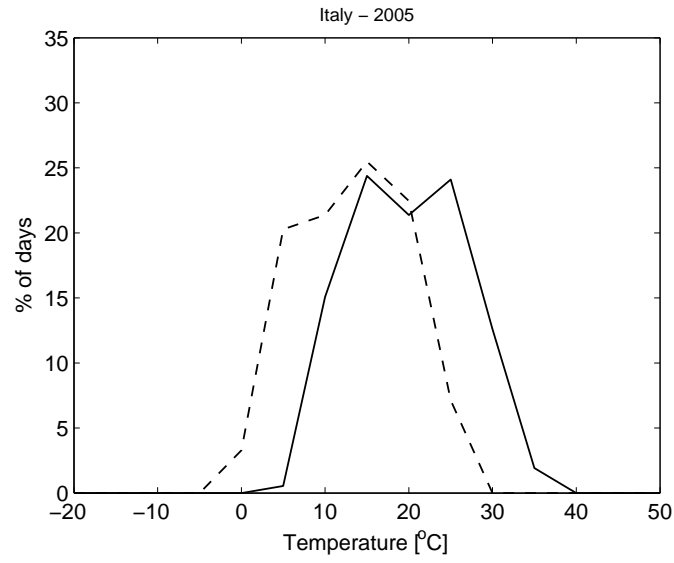
Figure 4.5: *Maximum (—) and minimum (−−) daily air temperature throughout the year 2005 in Italy.*
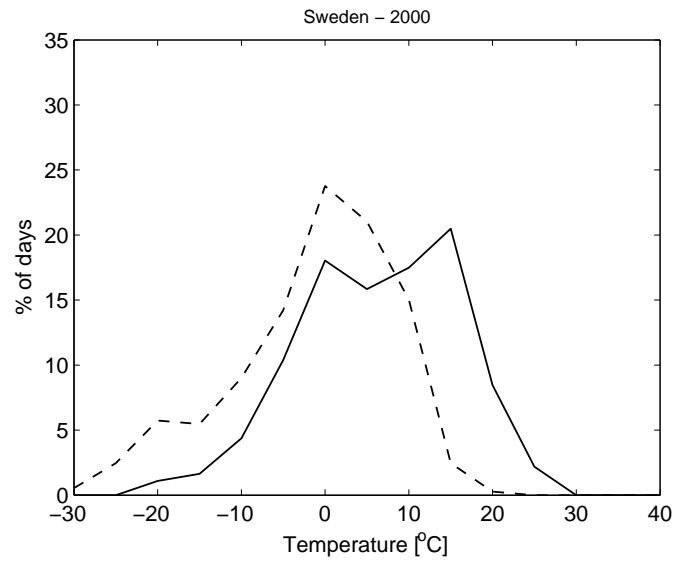
Figure 4.6: *Maximum (—) and minimum (−−) daily air temperature throughout the year 2000 in Sweden.*
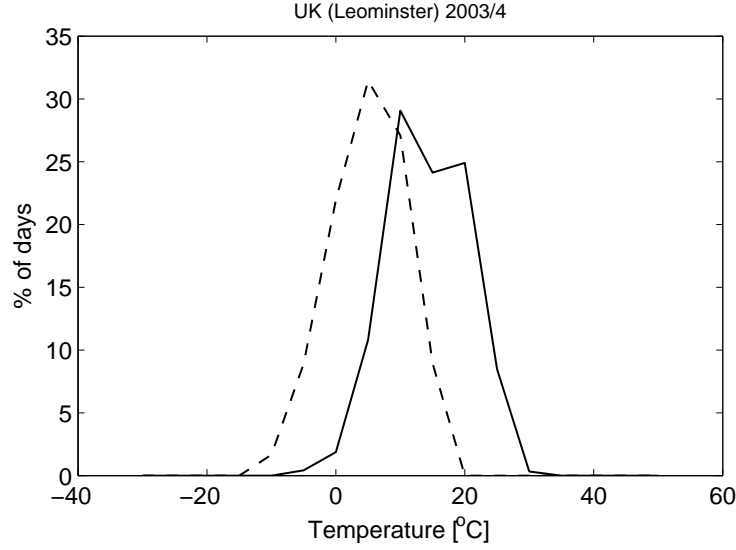
Figure 4.7: *Maximum (—) and minimum (−−) air temperature for each day throughout the year*

The curve for Sweden has a larger tail towards the lower temperatures.
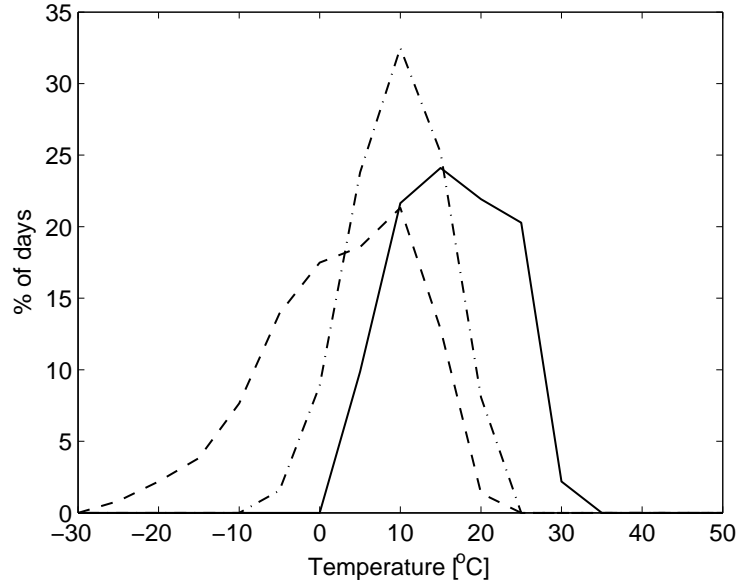
Figure 4.8: *Middle point of max and min of daily temperature throughout the year for UK (− · −), Sweden (−−) and Italy (—).*

Based on the distributions obtained in Figure 4.4 and 4.8, plausible rail temperature distributions that are consistent with the available air temperatures can be determined. This has been done by plotting the frequency distributions as cumulative distributions, as shown in Figure 4.9. By considering the shift between the daily mid point air temperature and the full distribution of rail temperatures at the UK site (Figure 4.9(a)), plausible distributions for the rail temperature in Sweden and Italy were determined as shown in Figure 4.9(b) and 4.9(c). The results of the estimation are shown in Figure 4.10 as a

frequency distribution. The rail temperature for the UK is in the range -10℃ to 40℃, Italy in the range 0℃ to 50℃ and Sweden in the range of -25℃ to 35℃.

(a)

(b)   (c)
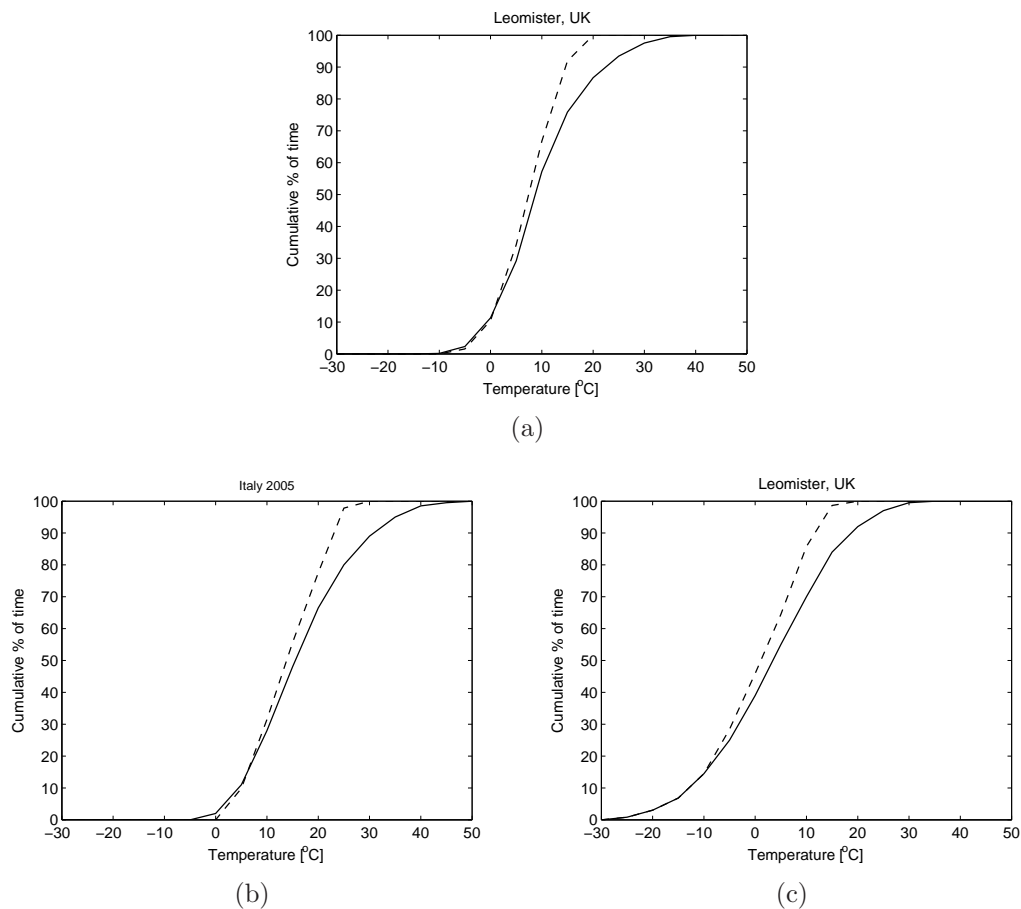
Figure 4.9: : (a) The cumulative frequency distribution of daily mid-point air temperature (−−) and instantaneous rail temperature (—) for the UK. For Italy (b) and Sweden (c) the daily mid-point air temperature is used to estimate a rail temperature distribution based on a similar shift factor.

4.4 Weighted noise reduction based on temperature weighting

The temperature distributions in Figure 4.10 can be used as weighting functions. They are listed in Table 4.1. The most common temperature for the UK is around 10℃ which has the largest weighting value (0.28). For Sweden, the largest weighting is 0.16 at 5℃ and for Italy it is 0.2 at 15℃. Since material properties have been measured in the range -20℃ to 40℃, the weighting for -25℃ is added to that at -20℃ for Sweden and the weighting for 45℃ and 50℃ are added to those at 40℃ for Italy.
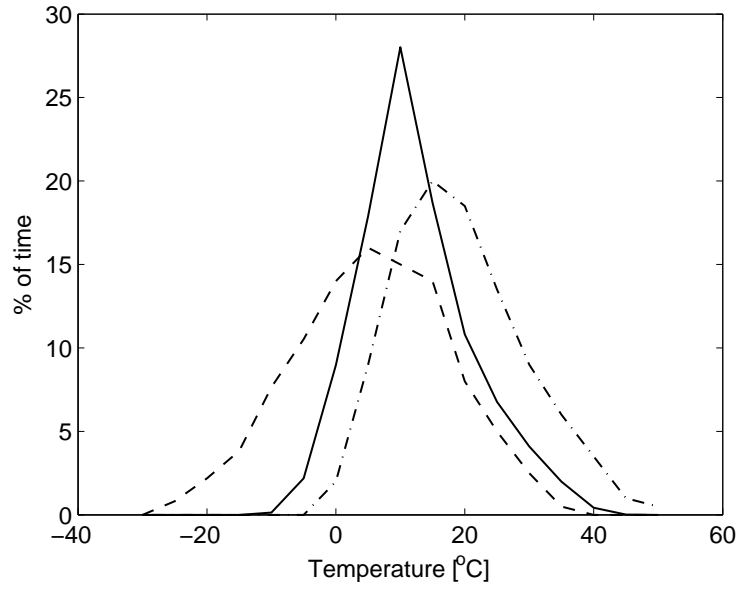
Figure 4.10: *Rail temperature distribution for UK (—) and estimated for Sweden (−−) and Italy (− · −).*

For a single frequency absorber, the weighted noise reductions have been determined for notional materials as follows. For a given loss factor and stiffness at 10℃ (which can also be expressed in terms of the tuning frequency at 10℃), the corresponding stiffnesses are determine at each temperature in the range -20℃ to 40℃. For each of these temperatures the rail decay rate is determined and hence the noise reduction achieved by the absorber. The results for each temperature are then weighted using the factor in Table 4.1 to give a weighted noise reduction.

$$\Delta L_{A,T} = \sum_{i=1}^{n} (w_{T,i} \times \Delta L_{A,i}) \tag{4.1}$$

where $\Delta L_{A,T}$ is the average weighted noise reduction with respect to temperature, $w_{T,i}$ is the weighting factor for temperature i and $\Delta L_{A,i}$ is the A-weighted noise reduction for temperature i.

Figure 4.11 shows the results using the UK weighting for a notional material with a constant loss factor. These are shown for a range of loss factors and stiffnesses that are fixed at 10℃. This shows that the maximum benefit is found for a nominal tuning frequency of 800 Hz and loss factors between 0.25 and 0.75. Figure 4.11(b) shows the results for the nominal tuning frequency of 800 Hz plotted against loss factor which confirms this.

Figure 4.12 shows the equivalent results for the Swedish weighting. Figure 4.12(a) shows that the greatest weighting noise occurs for a tuning frequency of about 700 Hz at 10℃. As this material gets stiffer at lower temperatures, this will mean that the tuning frequency
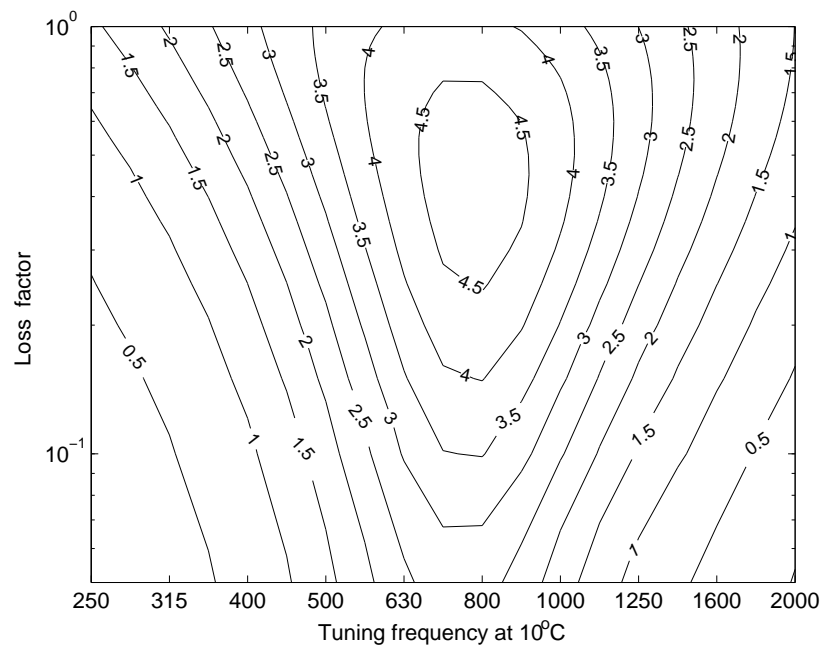
(a)
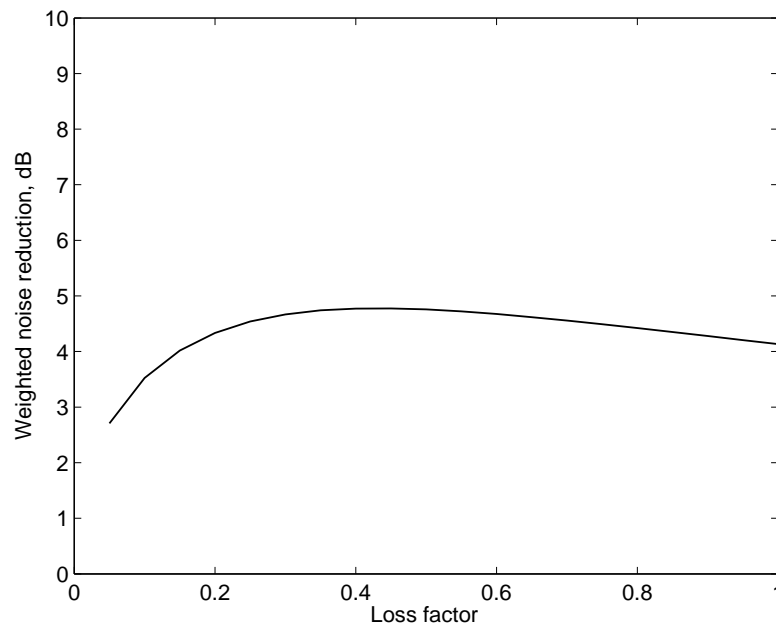
(b)

Figure 4.11: *(a) The contour plots of reduction of A-weighted track noise level in dB against tuning frequencies and loss factor for UK temperature weighting. (b) The effect of various loss factors on the weighted noise reduction for tuning frequencies of 800 Hz at 10℃.*

Table 4.1: *Weighting factors applied for each temperature for UK, Sweden and Italy.*

Temp (℃)	Temperature Weighting UK	Temperature Weighting Sweden	Temperature Weighting Italy
-20	0	0.030	0
-15	0	0.038	0
-10	0.0013	0.077	0
-5	0.022	0.105	0
0	0.090	0.140	0.020
5	0.179	0.160	0.090
10	0.280	0.150	0.170
15	0.187	0.140	0.200
20	0.108	0.080	0.185
25	0.068	0.050	0.135
30	0.041	0.025	0.090
35	0.020	0.005	0.060
40	0.004	0	0.050

will be around 800 Hz for the most common temperature of 5℃. The maximum benefit is slightly reduced due to the wider spread of temperatures, particularly low temperatures, included in the weighting.

Figure 4.13 shows the weighted noise reduction for Italy. This shows the opposite trend, with the maximum benefit for a slightly stiffer material, which gives a tuning frequency of 800 Hz at 15℃. The maximum benefit is similar to the result for the UK.

4.5 Weighted noise reduction of blended nitrile rubber (NBR)

For two-frequency absorber described in Section 3.6.2, the measured data of NBR samples (Ahmad, 2005) see also Table 3.4, have been used to determine the weighted noise reduction using a similar approach to that used in Section 4.4. Based on the UK weighting, Table 4.2 lists the noise reduction for NBR. The maximum noise reductions for temperature range considered are between 4 and 7 dB. The temperatures at which the maximum noise reduction occurred are between 15℃ and 40℃. Based on the temperature weighted results, the noise reduction for different blends of NBR can be predicted using a least-squares regression as shown in Figure 4.14. The optimum area is at the bottom left corner of the plot, where the proportion of carbon black and the blend ratio of NBR are low. These points correspond to compounds 23 and 33.. Similar trends are found for UK, Sweden and Italy.
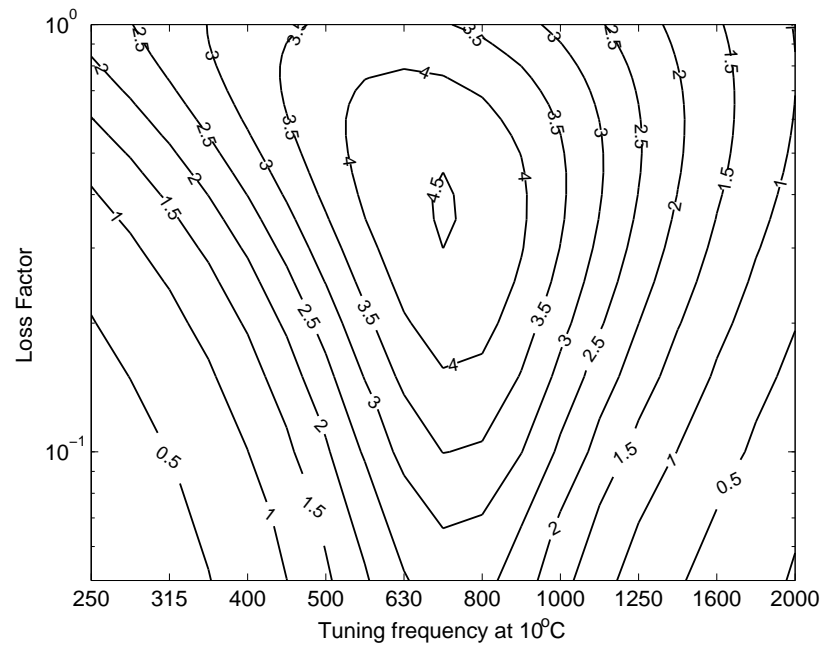
(a)
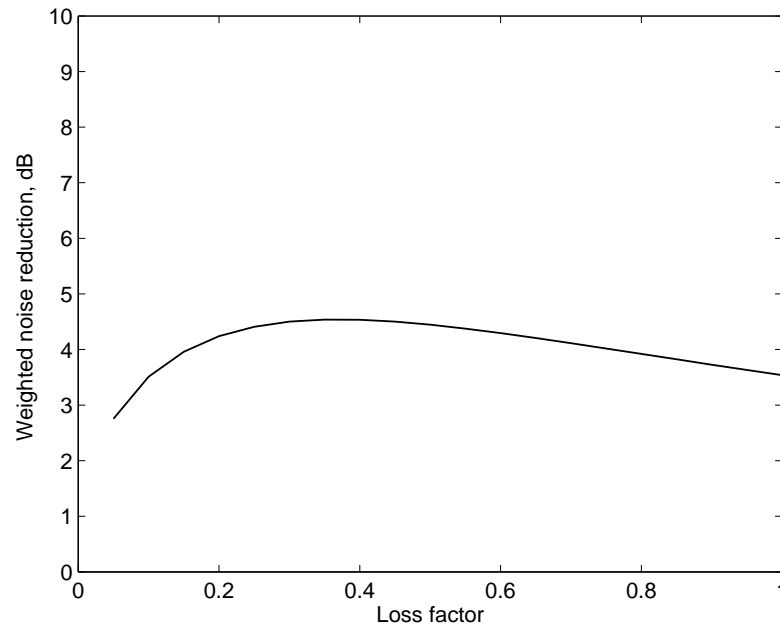
(b)

Figure 4.12: *(a) The contour plots of reduction of A-weighted track noise level in dB against tuning frequencies and loss factor for Sweden temperature weighting. (b) The effect of various loss factors on the weighted noise reduction for tuning frequency of 700 Hz at 10℃.*

(a)

(b)
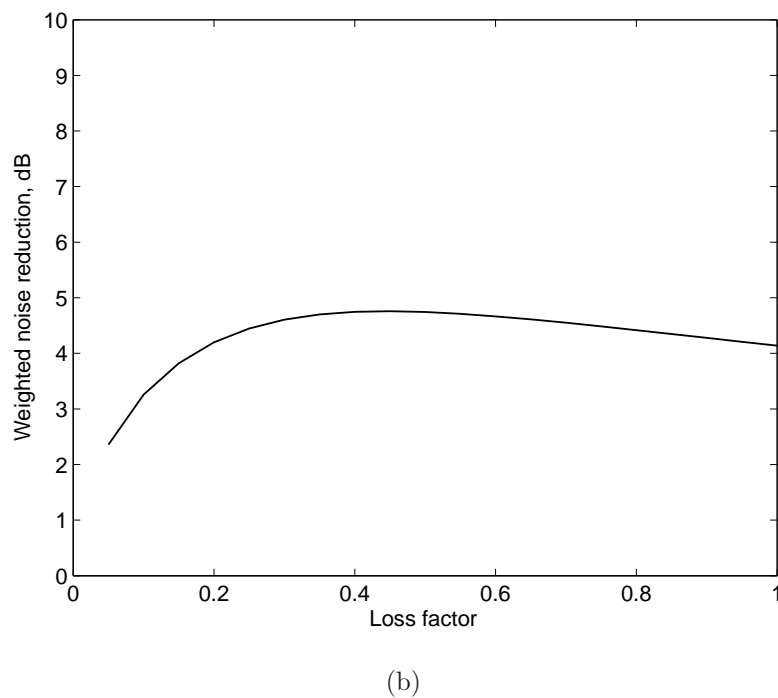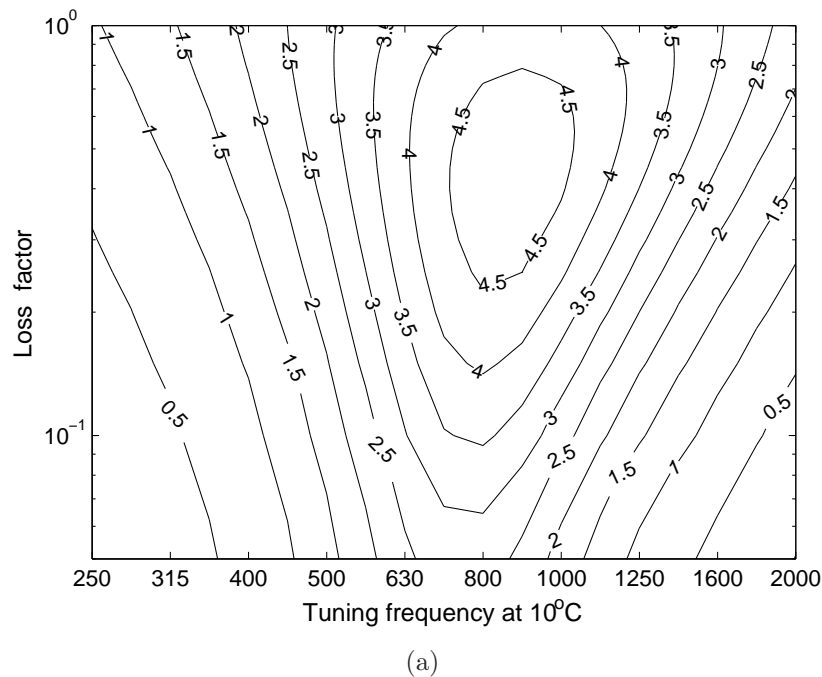
Figure 4.13: *(a) The contour plots of reduction of A-weighted track noise level in dB against tuning frequencies and loss factor for Italy temperature weighting. (b) The effect of various loss factors on the weighted noise reduction for tuning frequency of 900 Hz at 10℃.*

Table 4.2: *Predicted noise reduction for NBR blends as measured in (Ahmad, 2005).*

Compound Samples/Particulars	21	22	23	24	25	26	27	28	30	32	33	34
Polymer	100	100	100	100	100	100	100	100	100	100	100	100
Carbon black	50	10	10	50	30	30	30	30	30	60	0	30
Blend ratio	1.17	1.17	-1.17	-1.17	0	0	0	0	-1.65	1.65	-1.65	1.65
Max. $\triangle$L, dB(A)	5.3	6.6	6.7	5.3	6.5	6.9	6.9	6.9	6.6	3.9	6.4	6.9
T_{max} $\triangle$L, dB(A)	40	25	20	40	40	30	30	35	35	40	15	35
T-weighted (UK) $\triangle$L, dB(A)	1.5	4.5	5.2	2.2	3.2	3.6	3.8	3.9	3.6	1.2	5.6	3.0
T-weighted (Sweden) $\triangle$L, dB(A)	1.0	3.2	3.8	1.5	2.3	2.6	2.7	2.2	2.6	0.8	4.2	2.1
T-weighted (Italy) $\triangle$L, dB(A)	2.3	5.5	5.9	3.1	4.2	5.0	5.1	4.5	4.7	1.8	5.7	4.3
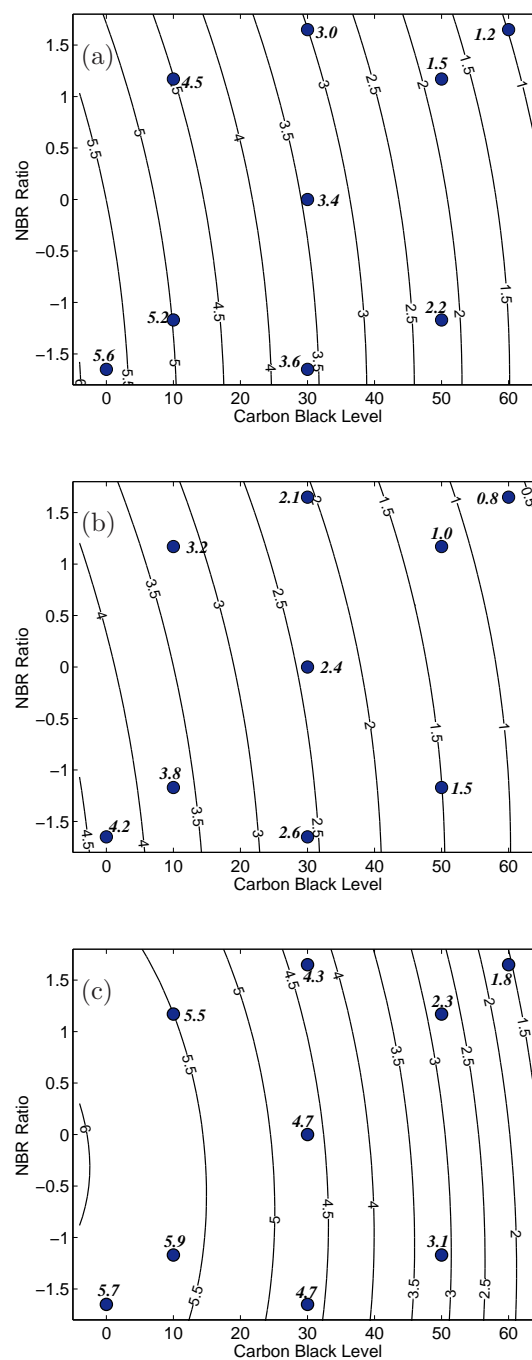
Figure 4.14: *The temperature weighted noise reduction in dB(A) for NBR, based on temperature weighting of (a) UK, (b) Sweden and (c) Italy.*

4.6 Conclusions

A method is presented from which plausible rail temperature distributions can be obtained from the daily maximum and minimum air temperature data, this being the form of data most commonly available. These distributions are not required to be highly accurate, only to give an indication of the distribution of temperature over a year. The results obtained are not very sensitive to the details of these distributions.

The rail temperature distributions obtained for the UK show that the temperature ranges between -10℃ and 40℃ with the most common temperature around 10℃. For Italy the range is higher, between 0℃ and 45℃ whilst for Sweden it is between -25℃ and 35℃, with a longer tail towards low temperatures.

These distributions can be used as weighting functions for the noise reduction to ensure that the rail absorber design is focussed on the temperatures that occur most commonly at a given location. For the UK site, the most common temperature is at 10℃ so the maximum noise reduction is required at this temperature. For Italy a slightly stiffer material is required to give the maximum noise reduction at around 15℃, while for Sweden a slightly softer material is required.

For the right choice of material, the weighted noise reductions for UK, Italy and Sweden are almost similar. For the best performance a loss factor of around 0.4 is required, although the results are not very sensitive to the damping.

The temperature-weighted noise reduction allows the suitability of a given material for the rail absorber to be expressed as a single number. This will allow optimisation of materials to be carried out more readily than in (Ahmad, 2005) where several metrics were considered simultaneously.

Chapter 5

Analysis of dynamic stiffness test rig

5.1 Introduction

An existing test rig has been used previously to measure the dynamic properties of viscoelastic materials for the rail absorber (Ahmad, 2005). The test rig used was developed by ISVR and was shown in Figure 1.12. This test rig uses an electrodynamic shaker (coil and magnet) to excite samples of viscoelastic material in shear. A force transducer mounted on a high impedance foundation measures the blocked force. Through the development and testing of the material for the rail absorber in the past, it has been well demonstrated that the measurement of dynamic shear modulus and loss factor can be obtained over a fairly broad frequency range. Furthermore, such a simple and functional design makes this test rig compact and mobile allowing it to be used outside the laboratory.

However, some disturbances have been seen in the data gathered, which may be caused by unwanted vibration of the test rig. Consequently the frequency range of valid data is limited, particularly when stiff samples or very soft samples are measured. When measuring over a range of temperatures, these effects are found at low and high temperatures respectively.

The test rig will inevitably have resonances due to the mass and stiffness characteristics of the seismic mass, test jig, magnet and frame. The surface of the bench, where the test rig is placed, may also have a certain stiffness which may affect the measurement.

The primary objective of this chapter is to describe and understand the test rig system for the measurement of dynamic properties (shear modulus and loss factor). It is important to understand the limitations of the test rig and the influence of its design parameters on the reliability of the dynamic properties obtained. By using simple dynamic models in

combination with diagnostic measurements, understanding of the vibration behaviour is obtained and modifications to the test rig are proposed.

5.1.1 Measurement method

The test rig is used to measure the complex dynamic shear modulus, G^*, over a wide frequency range (target range: 300 to 3000 Hz) for low amplitude excitation. To determine the effect of temperature in the target range -20℃ to 40℃, the test rig is placed in a temperature cabinet at TARRC (inner size: $0.2 \times 0.30 \times 0.55$ m) and the dynamic test carried out as before.

Four rectangular samples are used in the tests with dimensions 20 mm × 15 mm and 10 mm thickness. They are held between a central steel shaft and an outer steel yoke as shown in Figure 1.13. The largest face is in contact with the yoke and the central shaft. A bolt, connected to the yoke on either side, allows a pre-compression to be applied. However, this preload is minimal for current measurements, which are for application to a damper in which the resilient element is not loaded. A random signal is input to the electro-magnetic shaker to excite the central part. The force transmitted through the element is sensed by a force transducer (Kistler 9041) mounted between the jig and the seismic mass and motion of the test jig at the input side is sensed by an accelerometer (B&K 4393) mounted under the central part.

An analyser is used to calculate Fourier transforms of force and response signals and from them estimates of the auto- and cross-power spectral densities, frequency response function and coherence. The measured frequency response function (FRF) is a complex function of frequency which has both amplitude and phase. It describes the ratio of the Fourier transforms of the system output $V(f)$ to the system input $U(f)$ as a function of frequency, as given by the following equation.

$$H(f) = \frac{V(f)}{U(f)} = \frac{Output}{Input} \tag{5.1}$$

In practice this is obtained from the power spectral density (PSD) of the input, S_{uu}, and the cross-spectral density (CSD) between input and output S_{uv}.

$$H(f) = \frac{S_{uv}}{S_{uu}} \tag{5.2}$$

In the present case the displacement of the central shaft is the input and the blocked force is the output. The shear stiffness is derived from the transfer function between the

vertical acceleration, $\ddot{X}$ of the central shaft and the force, F, transmitted to the high impedance foundation. The shear modulus is derived from the following equation (5.3) (Thompson *et al.*, 1998) and (Thompson *et al.*, 2000).

$$G^*(\omega) = \frac{-\omega^2 F}{\ddot{X}} \frac{h}{4ab} \tag{5.3}$$

where the samples have dimensions $a \times b$ and thickness, h and ω is the circular frequency. The factor of 4 in the denominator is due to the use of four samples. The ratio $F/\ddot{X}$ is measured as FRF according to equation(5.2).

5.1.2   Vibration problems

It is expected that the shear modulus should show a smooth, monotonic increase in its real part with increasing frequency or decreasing temperature. The loss factor should also have a smooth dependence on frequency and temperature. Figure 5.1 illustrates typical results obtained by Ahmad (2005). At 40℃ and 20℃ the modulus behaves reasonably smoothly up to about 1 kHz, although showing some variations at lower frequency. A resonance appears at about 1.5 kHz and the loss factor becomes erratic at higher frequencies. However at 0℃ and -20℃, where the material is considerably stiffer, strong resonant behaviour is seen below 500 Hz with large fluctuations in both amplitude and phase, while the results at high frequency appear reasonable until a higher frequency.

Due to these problems, the dynamic properties cannot be obtained reliably over the whole range of temperature and frequency required. Therefore, investigations have been carried out to determine the source of this behaviour and if possible to rectify it.

5.1.3   Approach

The first step is to understand the sources of the behaviour seen in the measurements. To facilitate this, simple lumped parameter models will be considered and compared with diagnostic measurements on the test rig. These will be used to identify the assumptions made in using the rig and the expected frequency range of validity. Additional measurements will then be used to identify the effects of the frame supporting the magnet.

(a)

(b)
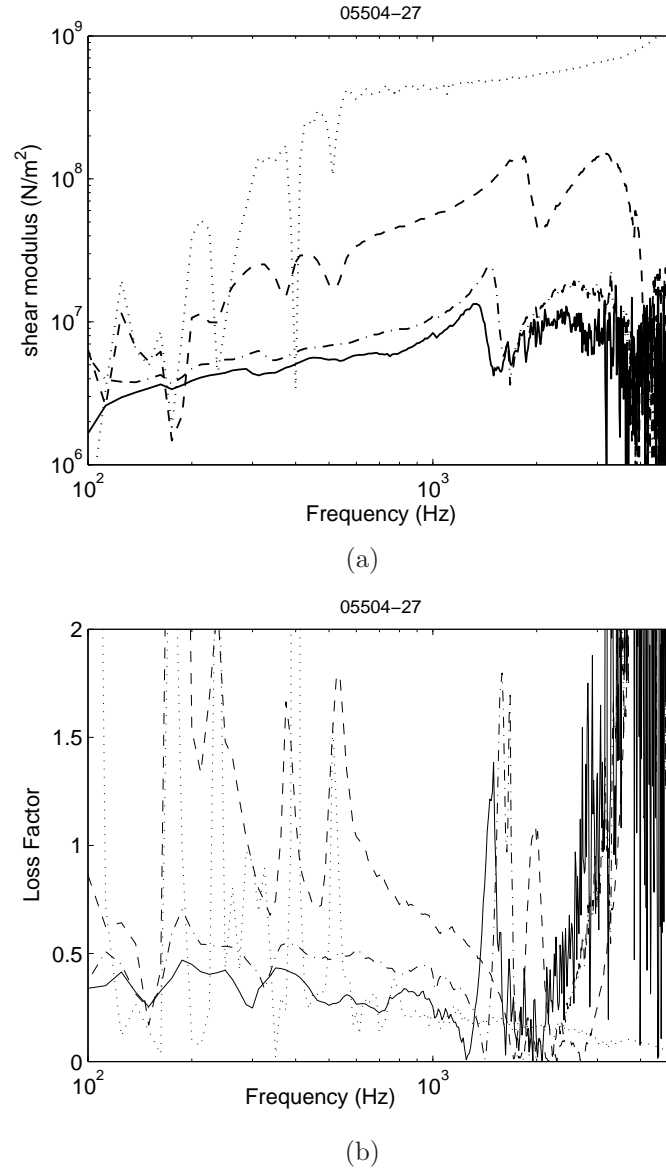
Figure 5.1: *Example of (a) shear modulus and (b) loss factor of NBR blend for temperatures (—) 40℃, (− · −) 20℃, (− −) 0℃ and (· · ·) -20℃ (Ahmad, 2005).*

5.2 Modelling of test rig

5.2.1 Single degree-of-freedom (SDOF) model

The seismic mass of the test rig is not a rigid termination. In order to account for the effect of its finite impedance it is modelled first as a single degree-of-freedom (SDOF) system consisting of a mass m, spring (stiffness) K, and damping loss factor, η, as shown in Figure 5.2. The stiffness and damping represent the bench on which the seismic mass is situated which is not perfectly rigid. By fitting this simple model to a measurement of the response of the seismic mass, the stiffness and damping of the bench can be estimated.

When the system is excited by a force $f(t)$, it undergoes a dynamic displacement $x(t)$. For harmonic motion at frequency ω, $f(t) = Fe^{i\omega t}$, and $x(t) = Xe^{i\omega t}$, where both X and F are complex and the frequency response function in terms of mobility is found as (Ewins, 1997)

$$Y(\omega) = \frac{\dot{X}}{F} = \frac{i\omega}{(K(1+i\eta) - \omega^2 m)} \tag{5.4}$$

The (undamped) natural frequency ω_n of the system is given by:

$$\omega_n = 2\pi f_n = \sqrt{\frac{K}{m}} \tag{5.5}$$
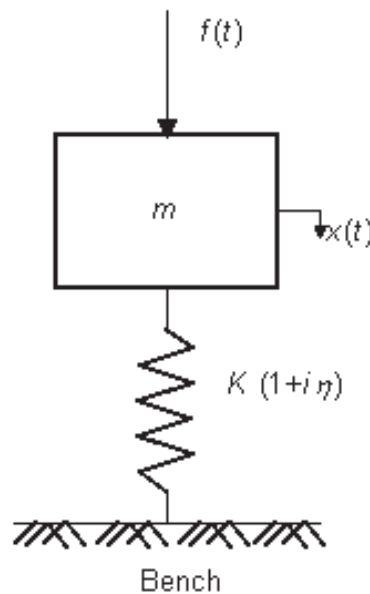
Figure 5.2: *Single degree-of-freedom model consisting of spring element (K) with hysteretic damping, and mass element (m).*

An impact test has been carried out on the seismic mass from the test rig, situated on the bench in the ISVR Dynamics Group laboratory. The bench consists of a wooden top of thickness 40 mm on four substantial legs. A B&K accelerometer type 4393 of mass 2.4 g and impact hammer model 086D80 were used in this experiment. To perform the impact test, the seismic mass was detached from the frame and placed on the bench. The impact hammer was used to strike the seismic mass at its centre while the response acceleration was measured at a fixed reference point. The measurement was based on an average of five strikes. The frequency resolution used is 3.1 Hz with a maximum frequency of 5000 Hz. A rectangular window is used. For comparison, a similar experiment was performed but this time with the mass sitting on a soft cushion.

The results are shown in Figure 5.3. The solid line represents the response of the mass on the bench and the dotted line shows that of the mass on the soft cushion. Above about 100 Hz both measurements give similar results, characterised by a mass line. The mobility tends to $-i/m\omega$ corresponding to the mass of the seismic mass, which was measured independently as 12.28 kg.

When mounted on the cushion the resonance frequency is below 10 Hz, at about 8 Hz. From equation (5.5), this corresponds to a stiffness of 30 kN/m. On the bench two resonances are seen (35 and 59 Hz), possibly corresponding to bounce and pitch modes. Below these resonances the mobility has stiffness behaviour of the form allowing the bench stiffness K to be estimated as 1.69×10^6 N/m. However, below 20 Hz the coherence drops due to noise contamination of the data.

Figure 5.3 also shows the predicted mobility from equation (5.4) for this value of stiffness. This shows similar behaviour to the measurement below 30 Hz and above 60 Hz. The loss factor used is 0.2.

5.2.2   Multi degree-of-freedom (MDOF) model

Having determined the effect of the bench on the seismic mass, a three-degree-of-freedom model can be formed to represent the test rig, as shown in Figure 5.4. At this stage the effect of coupling through the frame is ignored.

Referring to Figure 1.12, the three masses involved are the mass of the central part (m_1 = 0.05 kg), the mass of the outer yoke (m_2 = 0.250 kg) and the seismic mass (m_3 = 12.28 kg). The stiffnesses involved are the stiffness of the material under test (K_1 = various), the force transducer ($K_2 = 7.5 \times 10^9$ N/m obtained from manufacturer's data) and the bench ($K_3 = 1.69 \times 10^6$ N/m) which is obtained from section 5.2.1. For a given material, the stiffness and damping values K_1 and η_1 also change due to the temperature. The damping loss factor for the force transducer and the bench are assumed to be 0.2.
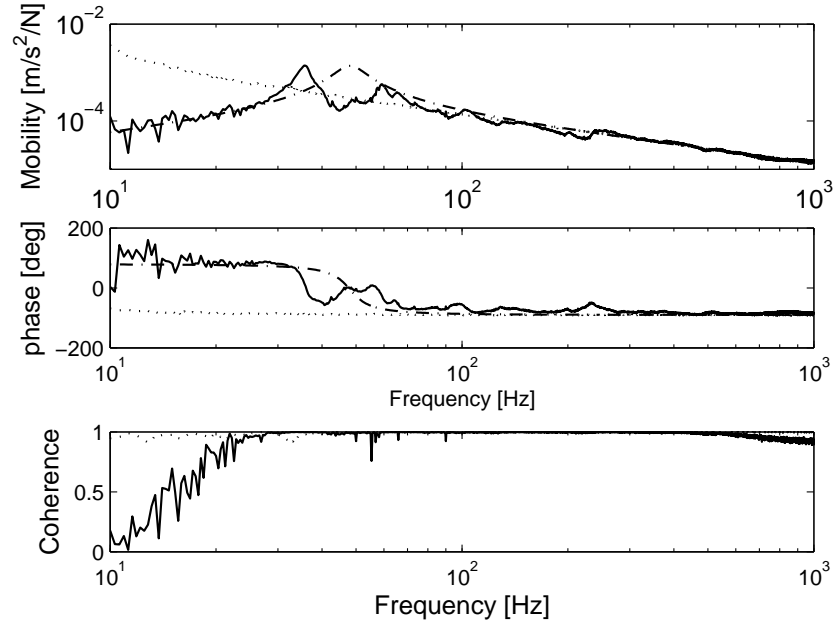
Figure 5.3: *Mobility of seismic mass placed on to the bench (—) and on soft cushion (· · ·). Also shown is prediction (− · −) using the single degree of freedom model.*
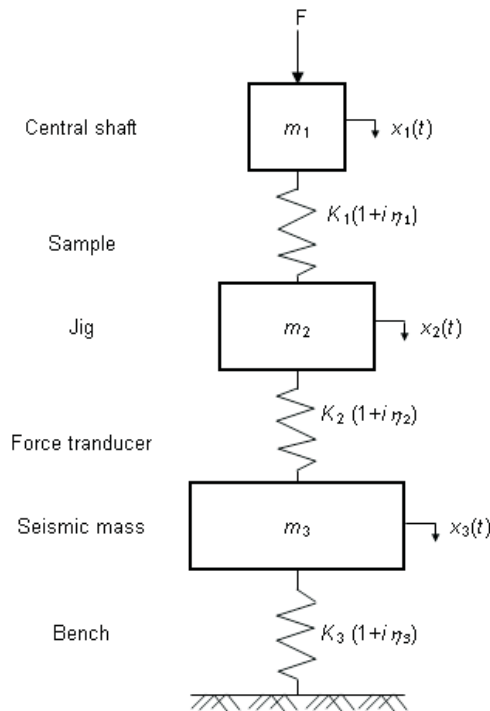
Figure 5.4: *Multi (three) degree of freedom system representing test rig.*

128

For harmonic motion at frequency ω, the equations of motion can be written in matrix form

$$\begin{bmatrix} \bar{K}_1 - m_1\omega^2 & -\bar{K}_1 & 0 \\ -\bar{K}_1 & (\bar{K}_1 + \bar{K}_2) - m_2\omega^2 & -\bar{K}_2 \\ 0 & -\bar{K}_2 & (\bar{K}_2 + \bar{K}_3) - m_3\omega^2 \end{bmatrix} \begin{bmatrix} X_1 \\ X_2 \\ X_3 \end{bmatrix} = \begin{bmatrix} F \\ 0 \\ 0 \end{bmatrix} \tag{5.6}$$

where damping has been included by replacing K_i by $\bar{K}_i = K_i(1 + i\eta_i)$.

In order to determine the movement of the three masses due to the excitation force F, equation (5.6) can be inverted

$$\begin{Bmatrix} X_1 \\ X_2 \\ X_3 \end{Bmatrix} = \begin{bmatrix} \bar{K}_1 - m_1\omega^2 & -\bar{K}_1 & 0 \\ -\bar{K}_1 & (\bar{K}_1 + \bar{K}_2) - m_2\omega^2 & -\bar{K}_2 \\ 0 & -\bar{K}_2 & (\bar{K}_2 + \bar{K}_3) - m_3\omega^2 \end{bmatrix}^{-1} \begin{Bmatrix} F \\ 0 \\ 0 \end{Bmatrix} \tag{5.7}$$

This can be solved using Matlab for each frequency. The values for K_1 are chosen as 0.12×10^6 N/m, 0.6×10^6 N/m, 3.0×10^6 N/m and 15.0×10^6 N/m, which represent a range of typical values corresponding to values of G of 1.3×10^6 N/m^2, 6.4×10^6 N/m^2, 32×10^6 N/m^2 and 161×10^6 N/m^2 (compare Figure 5.1).

5.2.3 Simulation of stiffness measurement

Figure 5.5 shows the predicted response of the various parts of the test rig. The first mode occurs at 56 Hz at which all masses move in phase at the same amplitude on the stiffness of the bench. As frequency increases, the movement of m_1 becomes decoupled from m_2 and m_3 between 100 and 300 Hz. It is evident that by stiffening K_1, the second resonance is shifted upwards in frequency.

The simulation results can be used to estimate the stiffness that would be measured by the rig. The measured stiffness is defined by the ratio of the force measured by the force transducer to the displacement of m_1 as shown in the following equation:

$$K_m = \frac{\bar{K}_2(X_2 - X_3)}{X_1} \tag{5.8}$$

where $\bar{K}_2$ is the stiffness (sensitivity) of the force transducer (including damping).
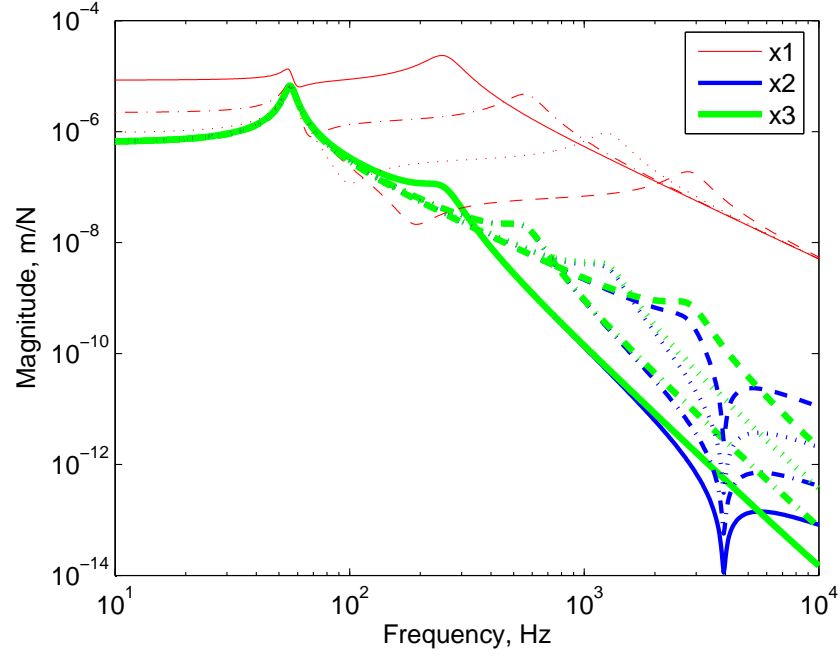
(a)
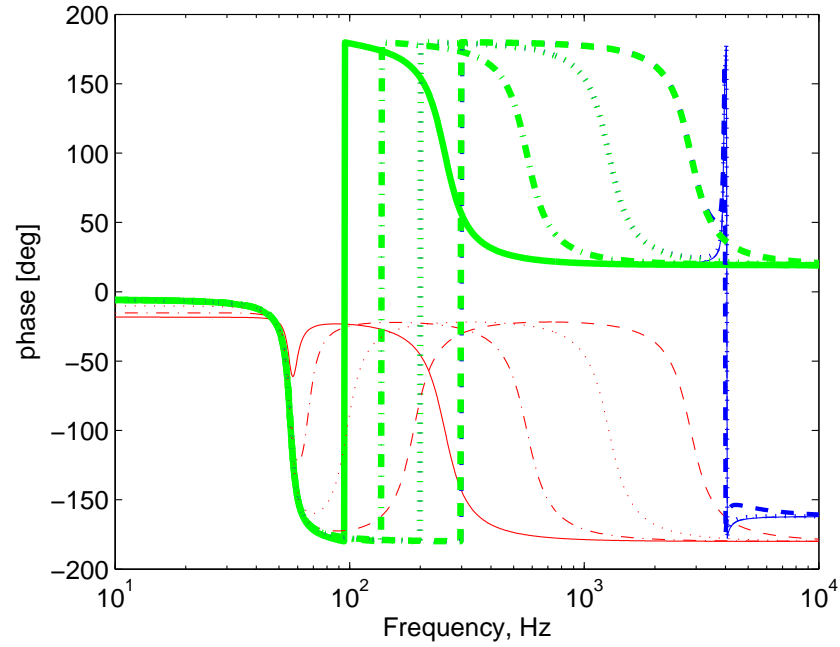
(b)

Figure 5.5: *(The (a) displacement and (b) phase of x_1 (thin line), x_2 (thicker line), x_3 (the thickest line) for $K_1 = 0.12$ MN/m (—), 0.60 MN/m (— · —), 3.0 MN/m ($\cdots$) and 15.0 MN/m (——).*

130

(a)

(b)
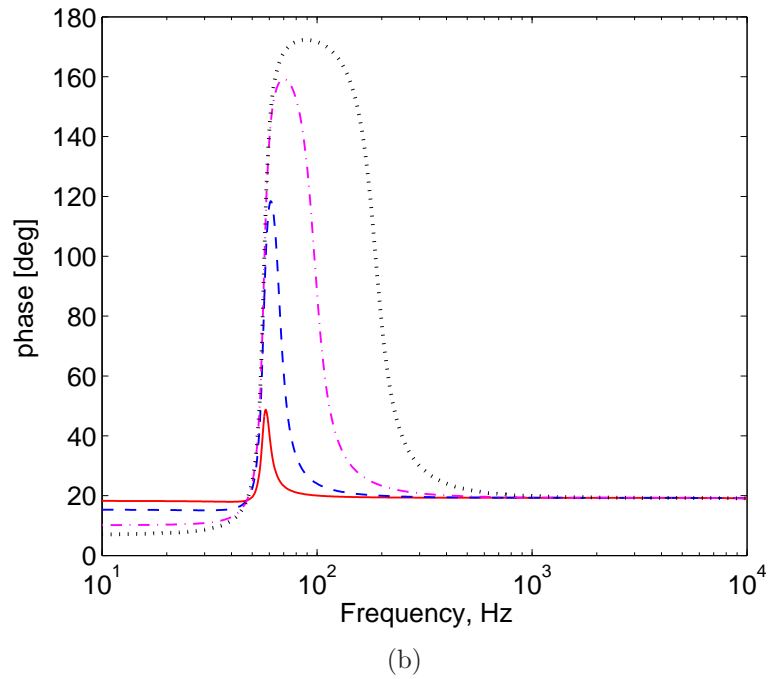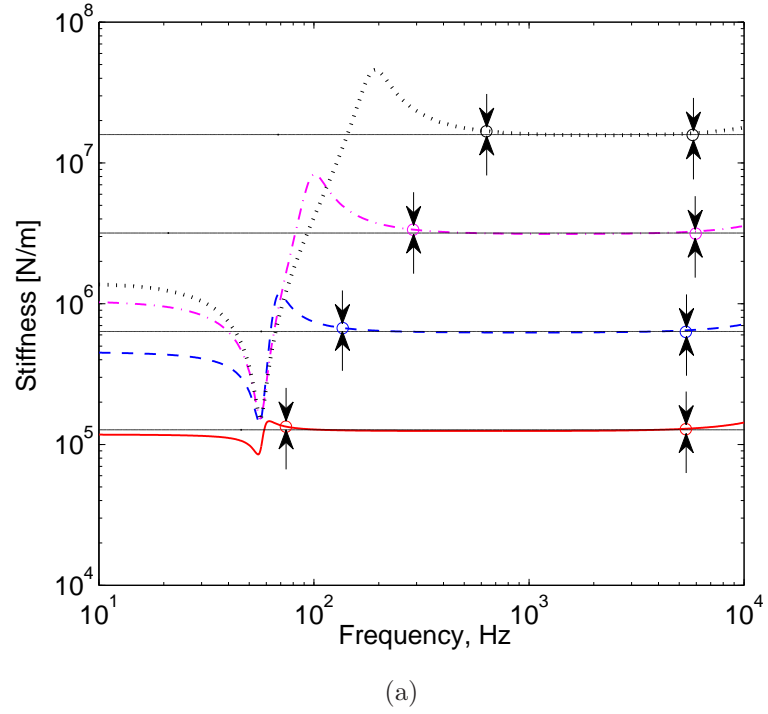
Figure 5.6: *Comparison of simulated measured stiffness K_m, and real stiffness (horizontal line) for various sample stiffnesses (K_1) without the effect of frame. The circles, "$\circ$", mark the low and high frequency limit of valid measurement for each stiffness. Sample stiffnesses are (—) $K_1 = 0.12 \times 10^6$ N/m, (— —) $K_1 = 0.60 \times 10^6$ N/m, (— · —) $K_1 = 3.0 \times 10^6$ N/m and (· · ·) $K_1 = 15.0 \times 10^6$ N/m.*

Results are shown in Figure 5.6 for the different values of K_1. A peak is found in the range 80 to 500 Hz. In this frequency region the apparent stiffness is too large and the measured loss factor becomes very large or even negative. Such effects are seen in the measured results in Figure 5.1, especially at low temperature where the stiffness is high. From Figure 5.6, as the stiffness increases, the peak moves into the frequency range of interest (300-3000 Hz) and the range over which reliable results can be obtained becomes narrower.

At low frequencies, the resonance at 56 Hz is found as a dip in the apparent stiffness as seen in Figure 5.6. Below this frequency the stiffness measured tends to that of the bench (K_3: 1.69 MN/m) for large values of K_1. The range of reliable data is identified by finding the frequency range in which stiffness is within 1 dB (12 %) of the correct value. The lower limit of this range is marked by an arrow where the measured stiffness starts to deviate from the real stiffness. Thus, the 1 dB lower limit is at 78 Hz, 130 Hz, 284 Hz and 600 Hz for the values of K_1 between 0.12 MN/m and 15 MN/m. The 1 dB upper limits are also marked by an arrow and occur between 5600 and 7700 Hz.

The lower and upper limits are shown as a function of K_1 in Figure 5.7. The upper limit shows very little change in frequency as stiffness varies. Similarly, when the stiffness is less than 1×10^5 N/m the change in lower limiting frequency is very small. However, above 1×10^5 N/m the change in this frequency is considerable.
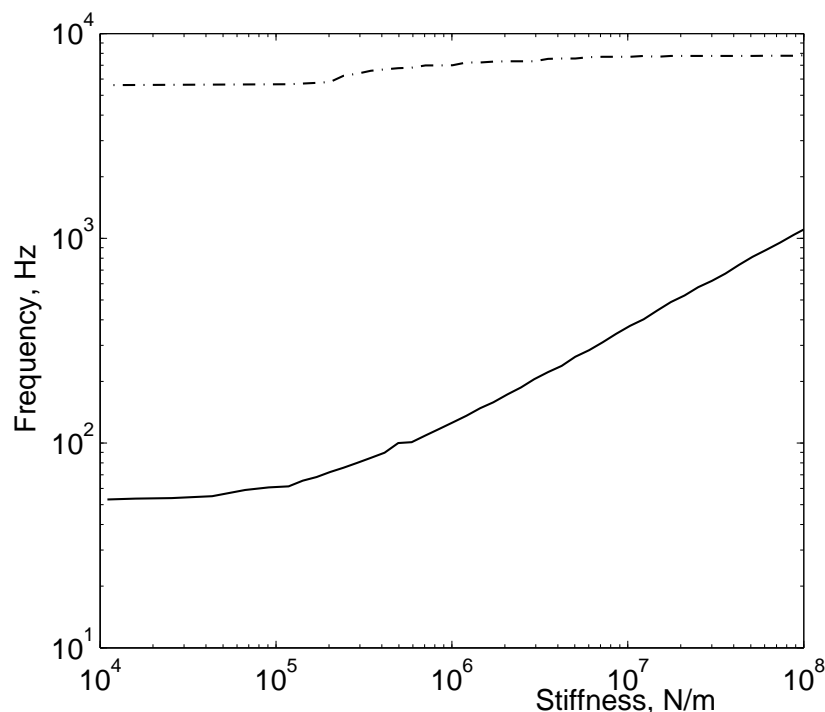
Figure 5.7: *Plot of 1 dB lower (—) and upper (− · −) frequency limit obtained from 3 DOF model for various stiffness.*

5.3   Effect of frame

In practice the magnet of the exciter is held by a frame which is connected to seismic mass. This may provide an additional excitation of the seismic mass which may be detected by the force transducer. To investigate this possibility, simple FRF measurements were taken on the test rig.

5.3.1   Measurement of transfer functions

The test set up is shown in Figure 5.8. The test rig was mounted on the bench, with the force transducer and jig omitted. An impact hammer was used to excite the system on the seismic mass. Two accelerometers were mounted on the seismic mass (position 1) and frame (position 2) as shown in Figure 5.8. The average of five strikes by the hammer on the seismic mass was recorded. The results are presented in the form of mobility.

Figure 5.9 and 5.10 show the point and transfer mobility curves of the system. For the point mobility measurement of the seismic mass a good coherence is found in the range 30 - 3000 Hz. The mobility curves show the first pair of modes at 38 and 58 Hz, which agrees with the earlier measurements. However, the experimental results show that there is another mode at 203 Hz. This mode does not appear in the numerical analysis or in the measurements on the seismic mass, and is therefore likely to be an effect of the frame.

The transfer mobility results have a coherence which is less good but still acceptable. At low frequency it can be seen that both frame and seismic mass move in phase. The same resonance frequencies can be seen as for the input mobility, with large amplitude at 203 Hz, while at high frequency a lot more resonances occur on the frame than on the seismic mass.

The results obtained for the point mobility of the seismic mass with and without the frame are compared in Figure 5.11. It is evident that the frame introduces additional resonances in the range 100-300 Hz, particularly at 203 Hz.

5.3.2   Simulation including effect of frame

The results from the impact test are given in Figure 5.12 in the form of transmissibility Y_{12}/Y_{11}. The transmissibility curve is close to 0 dB at low frequencies indicating rigid motion. Resonance frequencies caused by the frame can be seen at 200 Hz and above 1 kHz.
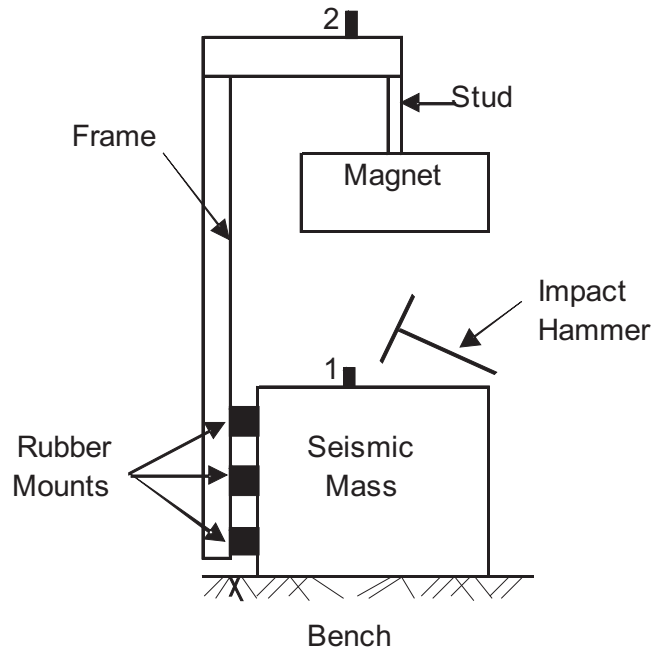
Figure 5.8: *FRF measurements of the test rig, which consists of seismic mass, magnet and frame.*
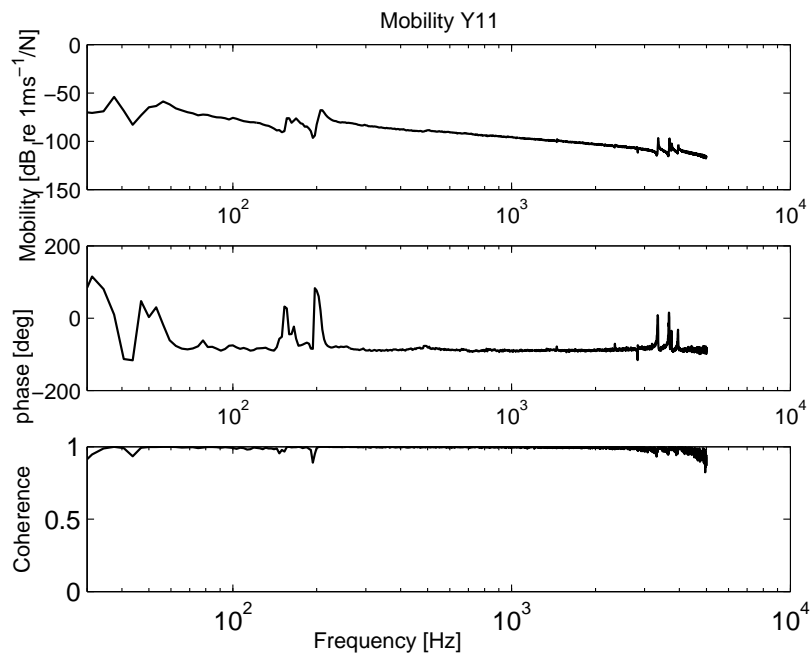
Figure 5.9: *The point mobility of the test rig where the excitation force and response are at the seismic mass.*
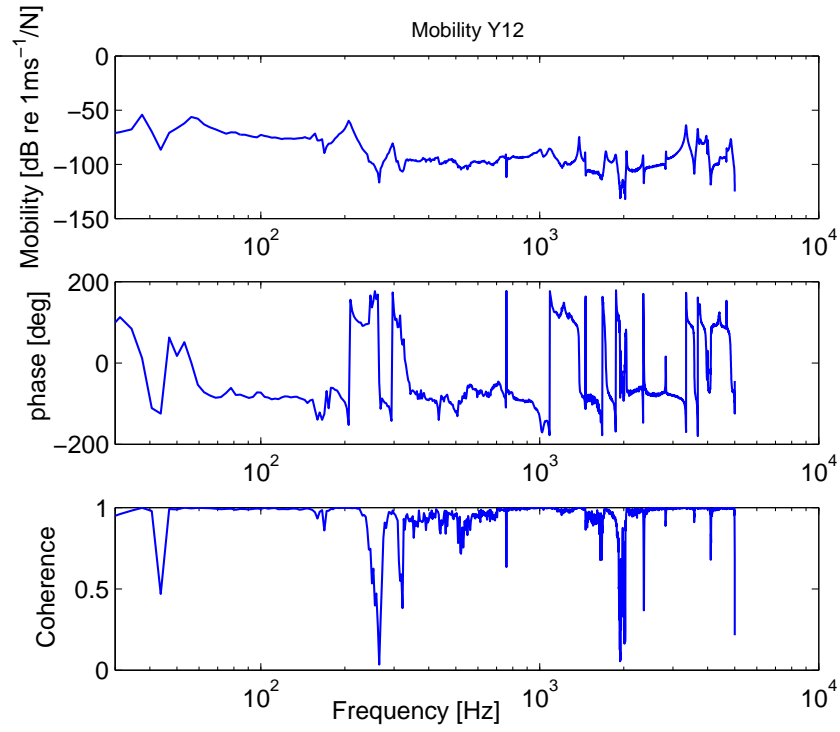
Figure 5.10: *The transfer mobility of the test rig where the excitation force is at seismic mass and response is at the top of the frame.*
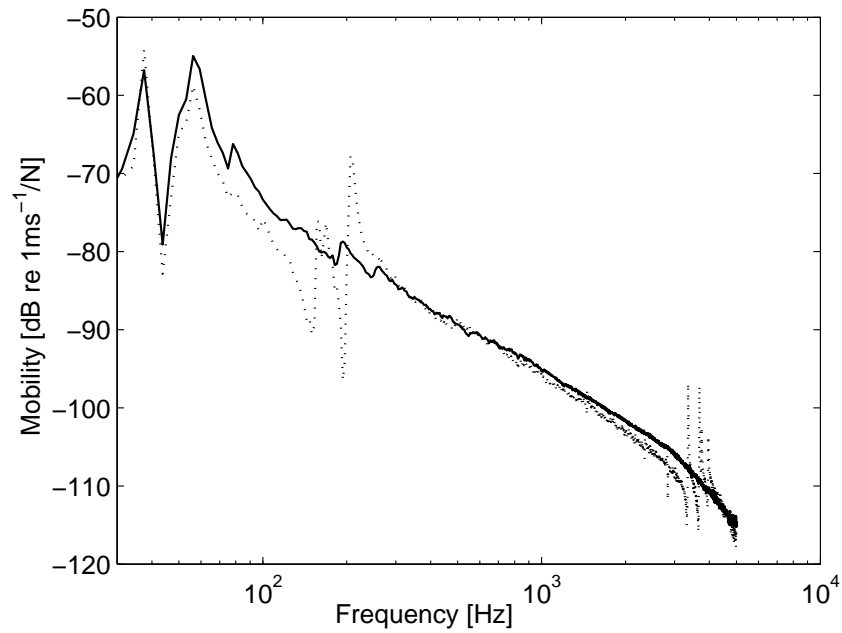
Figure 5.11: *Comparison of point mobility of the seismic mass with $(\cdots)$ and without $(—)$ the effect of frame.*

Having determined the behaviour of the frame, this can be added to the lumped mass-spring system. This will be incorporated in the three-degree of freedom system to investigate the effect of including the frame in the system.

When a current excites the coil, a force, F (positive downwards) acts on the mass, m_1. A similar force, $-F$ acts on the frame. This gives a response of $-FY_{12}$ at the seismic mass where Y_{12} is the transfer mobility shown in Figure 5.10. This is the same as if a force $F_{eq} = (-F)Y_{12}/Y_{11}$ were acting directly on the seismic mass. Thus the frame can be included into the three-degree-freedom model as follows:

$$
\left\{ \begin{array}{c} X_1 \\ X_2 \\ X_3 \end{array} \right\} = \left[\begin{array}{ccc} K_1 - m_1\omega^2 & -K_1 & 0 \\ -K_1 & K_1 + K_2) - m_2\omega^2 & -K_2 \\ 0 & -K_2 & (K_2 + K_3) - m_3\omega^2 \end{array} \right]^{-1} \left\{ \begin{array}{c} F \\ 0 \\ F_{eq} \end{array} \right\} \quad (5.9)
$$

Moreover, the effect of changing the frame can be simulated by varying the transmissibility.

Figure 5.13 presents the results based on the measured transmissibility. The curves have a similar trend to those in Figure 5.6, except that there are several additional resonances occurring in the frequency range around 200 Hz and above 1000 Hz due to the effect of the frame. As shown in Table 3.1, the lower limits are 59, 157, 286 and 606 Hz. Compared with Figure 5.6, the lower limit of Figure 5.13 is slightly higher except for the stiffness of $0.12 \times 10^6 N/m^2$. The lower frequency limit, however, is not significantly affected by the frame. It can also be seen that for soft samples the upper frequency limit is reduced by transmission through the frame. As a result, the system without the effect of the frame gives a wider range of reliable data as presented in Table 5.1. Figure 5.14 shows the predicted 1 dB lower and upper limits obtained when the effect of frame is included.

Table 5.1: *Comparison of lower and upper limit of stiffness measurement with and without the effect of frame.*

Stiffness (N/m)	Without effect of frame		With effect of frame	
	Lower limit (Hz)	Upper limit (Hz)	Lower limit (Hz)	Upper limit (Hz)
0.12×10^6	78.0	5600	59.0	1000
0.60×10^6	130	6700	157	1100
3.00×10^6	284	7100	286	2800
15.0×10^6	600	7700	606	3300

(a)

(b)
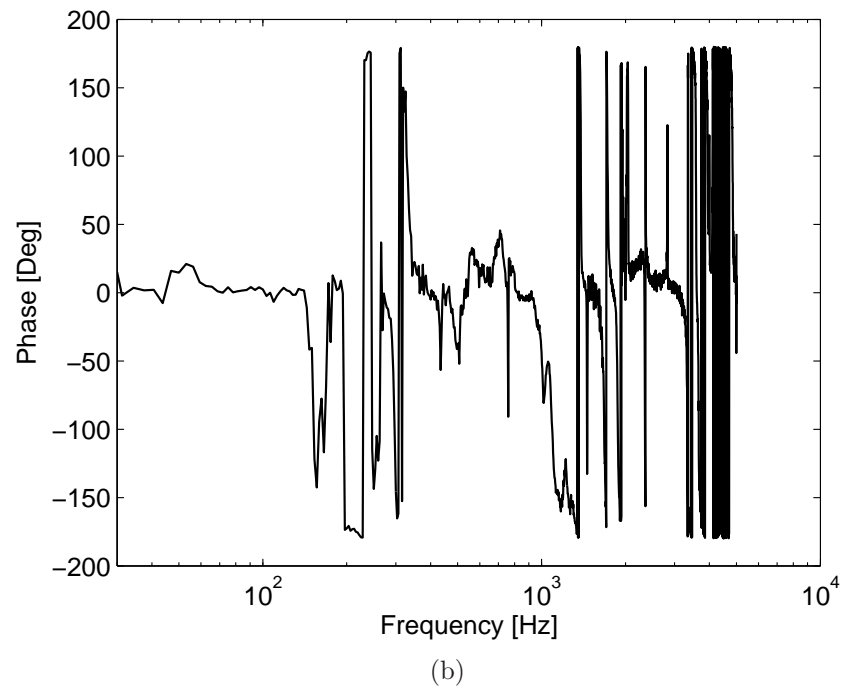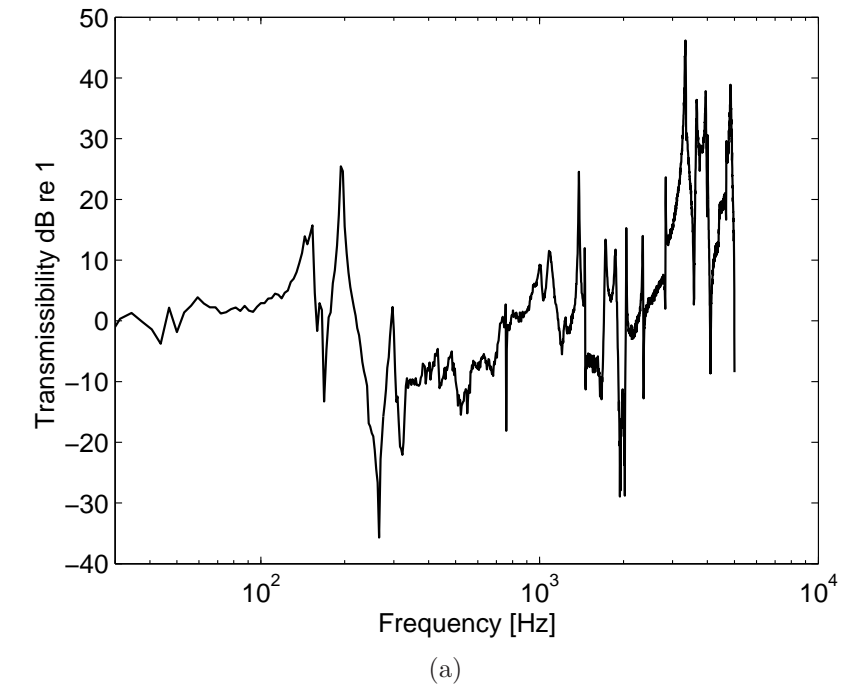
Figure 5.12: *The ratio of transfer to input mobility of the impact test (a) transmissibility and (b) phase angle.*
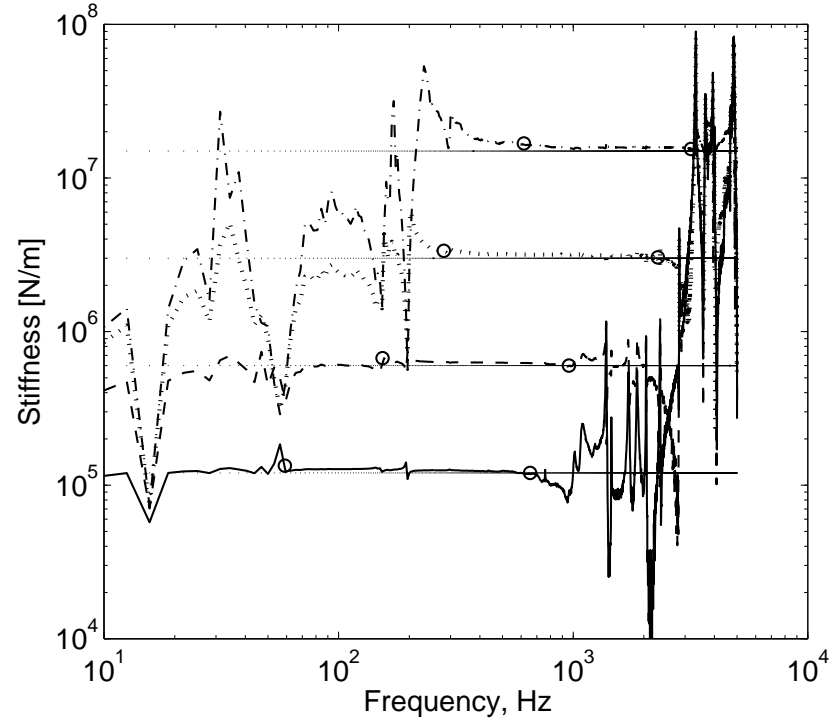
(a)
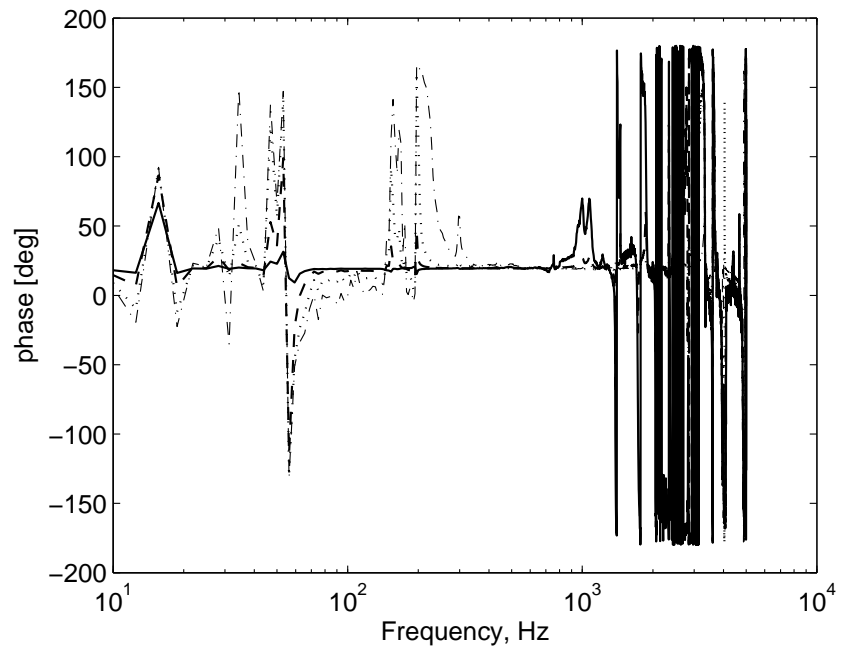
(b)

Figure 5.13: *Comparison of measured stiffness (K_m) and actual stiffness including the effect of the frame for (a) stiffness curve (b) phase curve. The circle "∘" marked the lower and higher limit for each stiffnesses; (—) $K_1 = 0.12 \times 10^6$ N/m, (−−) $K_1 = 0.60 \times 10^6$ N/m, (− · −) $K_1 = 3.0 \times 10^6$ N/m and (· · ·) $K_1 = 15.0 \times 10^6$ N/m.*
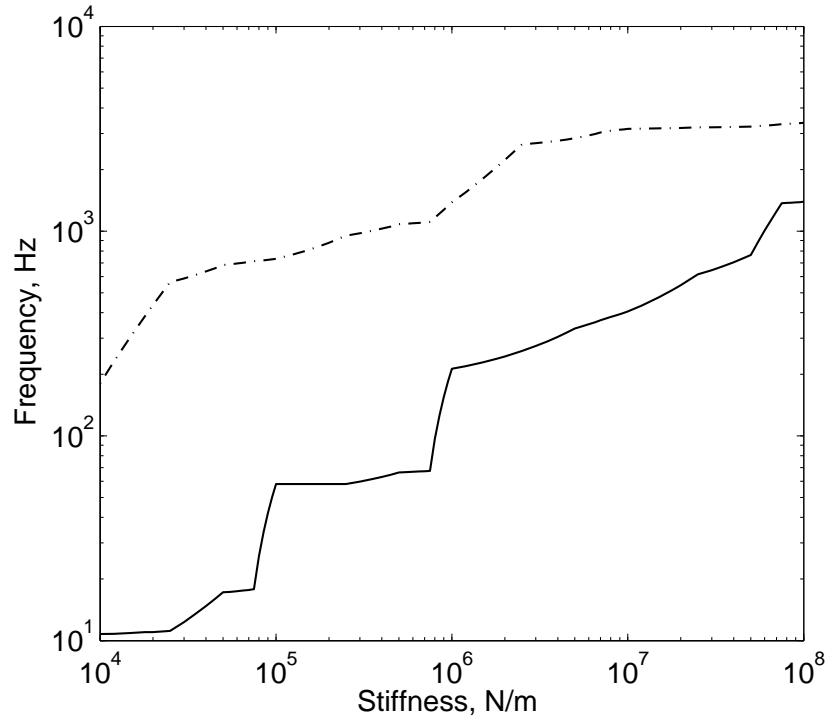
Figure 5.14: *The plot of frequency versus stiffness for various stiffness of 1 dB lower (—) and upper (− · −) frequency limit including the effect of frame.*

5.4   Sample thickness

The above analysis has identified, at least qualitatively, the source of erratic behaviour in the measured stiffness below 500 Hz as being associated with limitations in the test rig. The resonant behaviour seen above 1 kHz, particularly for soft samples, however, is likely to have a different cause. In this section the effect of internal resonances in the rubber samples is considered.

5.4.1   Analytical model

First a simple analytical model is used to identify the likely frequency range of internal resonances of the rubber samples. For simplicity, consider a rod of length L and area A as shown in Figure 5.15. A force F_1 is applied to the upper surface, which deflects by x_1. The force F_2 is transmitted to the lower surface, which is assumed blocked.

The input (K_{11}) and transfer (K_{12}) stiffnesses are given by Gardonio & Brennan (2004).

$$K_{11} = \frac{F_1}{x_1} = \frac{EA}{L}\left(\frac{kL}{\tan kL}\right) \tag{5.10}$$

139
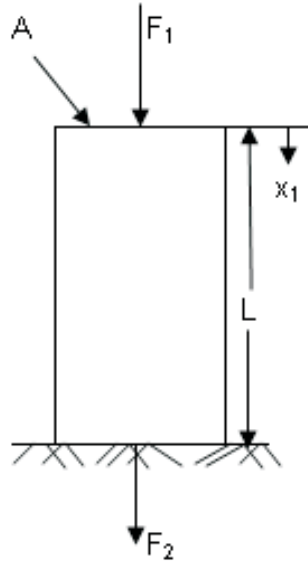
Figure 5.15: *Cross-section of the rod.*

$$K_{12} = \frac{F_2}{x_1} = \frac{EA}{L} \left(\frac{kL}{\sin kL} \right) \qquad (5.11)$$

where E is Young's modulus, A is the cross sectional area and L is the length. The wavenumber k, can be derived from $k = \omega/c$, where the wave speed c, is given by $c = \sqrt{E/\rho}$.

Since the sample is tested under shear deformation, E in the above equations can be replaced by the shear modulus G, and L becomes the thickness of the sample h.

$$K_{11} = \frac{F_1}{x_1} = \frac{GA}{h} \left(\frac{kh}{\tan kh} \right) \qquad (5.12)$$

$$K_{12} = \frac{F_2}{x_1} = \frac{GA}{h} \left(\frac{kh}{\sin kh} \right) \qquad (5.13)$$

The speed shear wave,

$$c = \sqrt{\frac{G}{\rho}} \qquad (5.14)$$

Figure 5.16 shows results for K_{11} and K_{12} for a density, ρ, of 1100 kg/m³, sample thickness h of 10 mm and a shear modulus, G, of 5×10^6 N/m². The first peak K_{11} and K_{12} occurs at 3370 Hz, corresponding to a wavelength of $2h$. The transfer stiffness (K_{12}) starts to

(a)

(b)
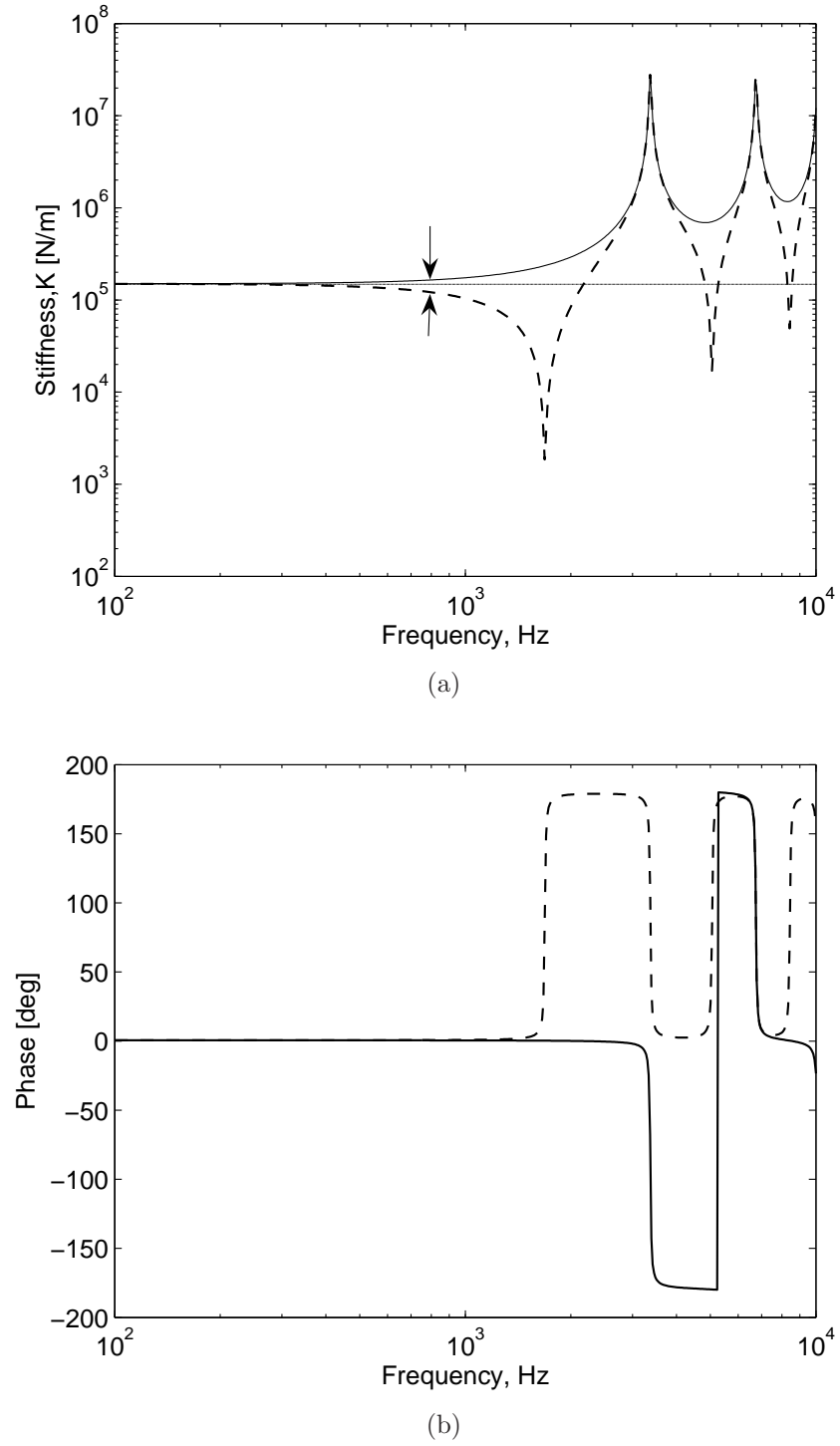
Figure 5.16: *(a) The input and transfer stiffness (b) the phase angle of sample under shear. The curves represented by (−−) K_{11} and (—) K_{12}.*

deviate from the constant stiffness at around 800 Hz, where the difference is 1 dB. This can be used to determine the upper limit of reliable data. This is marked by an arrow.

The resonance frequency can be estimated as follows. For the above parameters the shear wave speed is 67.4 m/s. The peaks in the stiffness occur when $kh = \pi, 2\pi, 3\pi, \cdots$ or when the wavelength $\lambda = 2h, h, 2h/3$, etc. The dips in the point stiffness occur for $kh = \pi/2, 3\pi/2, 5\pi/2, \cdots$. For a sample of thickness 10 mm, the wavelength ($\lambda = 2h$) at the first peak should be 20 mm. Then, the frequency can be estimated from $f_t = c/\lambda = 1/2h\sqrt{G/\rho}$ which gives 3370 Hz as seen in Figure 5.16.

The 1 dB limit can be found analytically as follows. The static stiffness $K = \dfrac{GA}{h}$. K_{12} is within 1 dB of K if

$$1 \geq 20\log_{10}\left(\left|\frac{K_{12}}{K}\right|\right) = 20\log_{10}\left(\frac{kh}{\sin kh}\right) \tag{5.15}$$

which gives

$$\frac{\sin kh}{kh} \geq 0.89 \tag{5.16}$$

For small values of kh,

$$\frac{\sin kh}{kh} \approx 1 - \frac{(kh)^2}{6} + \cdots \tag{5.17}$$

Thus

$$\frac{(kh)^2}{6} \leq 0.11 \tag{5.18}$$

or $(kh) \leq 0.81$. This corresponds to a frequency

$$f_{1dB} = \frac{ck}{2\pi} = \frac{0.81}{2\pi h}\sqrt{\frac{G}{\rho}} \tag{5.19}$$

Compared with the resonance frequency f_t, the 1 dB limit occurs at a factor of $0.81/\pi$, or about 0.26, times f_t.

Using the above equation will give 870 Hz for the above parameters, as seen in Figure 5.16. The above equations are also used to estimate the limits for the range of input parameters considered above.

A range of sample thicknesses between 1 and 10 mm is considered as well as allowing the shear modulus to vary between 1×10^5 and 1×10^8 N/m^2. Firstly, the 1 dB high frequency limit was predicted using equation (5.19). As shown in Figure 5.17, a sample thickness less than 2 mm gives a high frequency limit above 3000 Hz even with a shear modulus of 1×10^6 N/m^2. For a sample size of 10 mm and G between 5×10^6 and 2×10^7 N/m^2, the upper limit is found to occur between 1000 and 2000 Hz. As the sample thickness is reduced, the high frequency limit increases, which causes the range of reliable data to become wider.
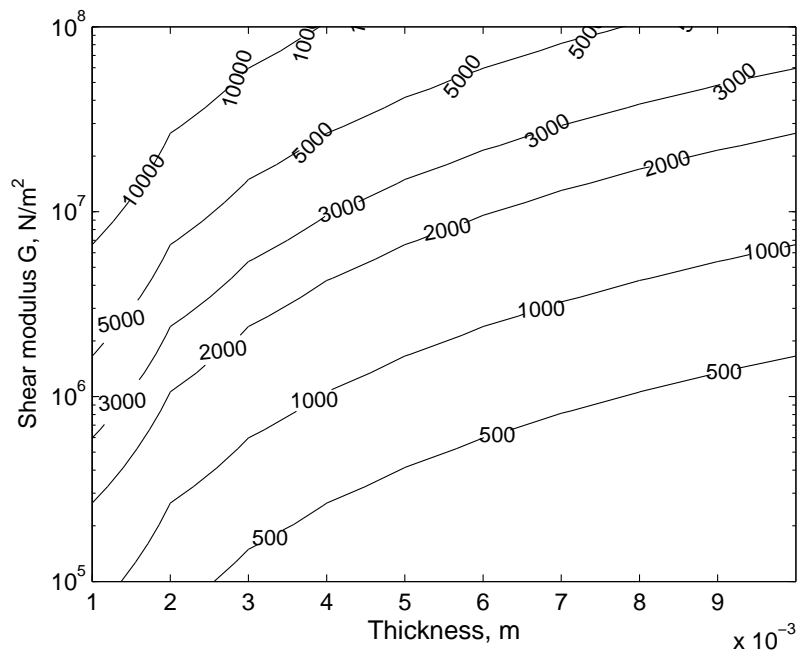
Figure 5.17: *Contour plot of 1 dB high frequency limit for various shear modulus and sample thicknesses due to internal resonances of the samples.*

Secondly, Figure 5.18 shows the corresponding lower frequency limit obtained as in section 5.2 but again for a range of sample thicknesses. Here the target is ≤ 300 Hz. All selected sample thicknesses have the low frequency limit below 300 Hz for a shear modulus below 5×10^6 N/m^2. The low frequency limit increases as the sample thickness is reduced.

For comparison, Figures 5.19 and 5.20 show the contour plots of the 1 dB high and low frequency limits obtained including the effect of the frame. The upper limit here is due to the connection through the frame, not the internal resonances of the samples. It has a weaker dependence on thickness and on G than the above results (Figure 5.17). For small values of G the internal resonances determine the upper limit but for large G the frame effect is dominant. The low frequency limit contours have a similar trend to those without the effect of the frame.
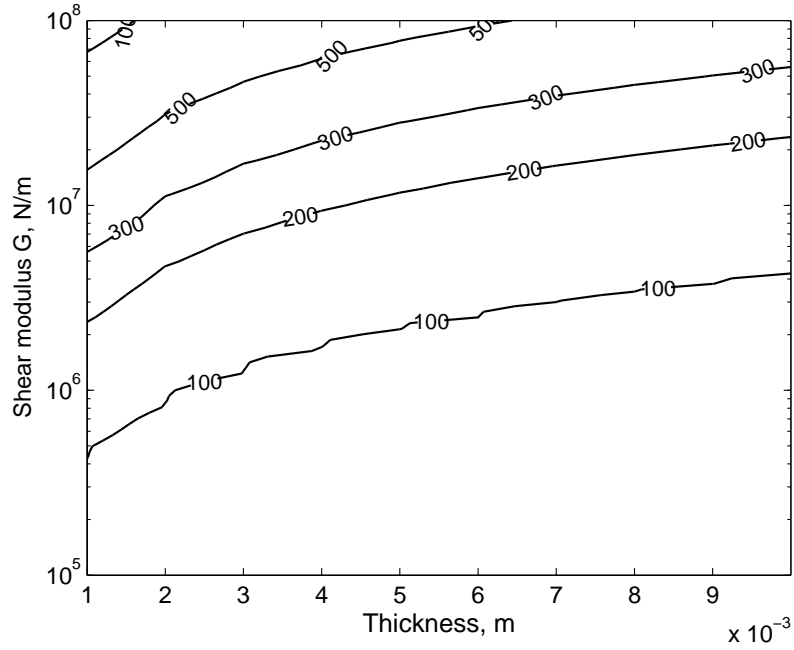
Figure 5.18: *Contour plot of 1 dB low frequency limit for various thicknesses and shear modulus due to dynamic behaviour of the test rig.*
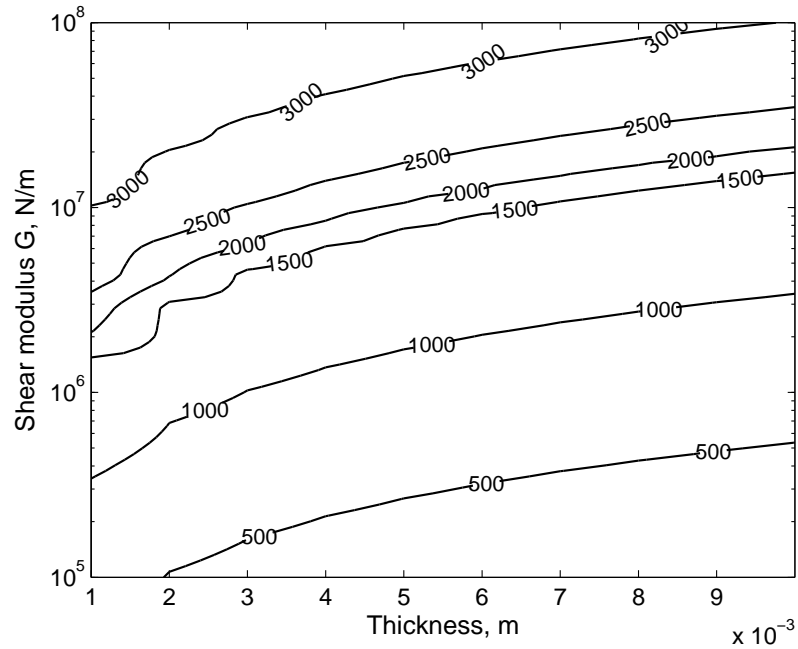
Figure 5.19: *Contour plot of 1 dB high frequency limit for various thicknesses and shear modulus due to dynamic behaviour of the rig including the effect of frame.*
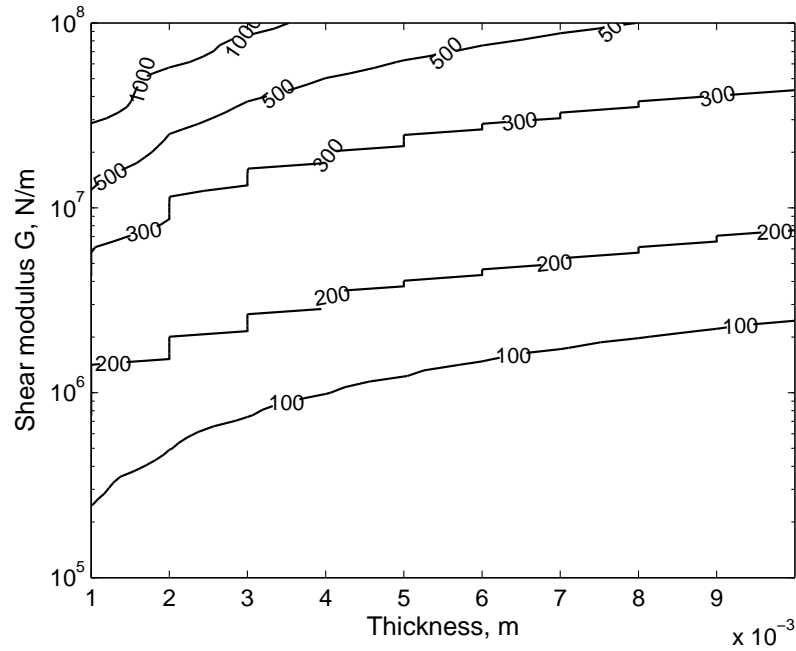
Figure 5.20: *Contour plot of 1 dB low frequency limit for various thicknesses and shear modulus due to dynamic behaviour of the rig including the effect of frame.*

5.4.2   Experiment

An experiment has been carried out to verify the effect of sample thickness on the internal resonance frequency. Samples from butyl rubber were vulcanized using a compression-moulding technique in a steam press at a pressure of 40 tons at 160℃ for 30 minute with a curing determined in a Monsanto rheometer. The vulcanized rubber took the form of sheets of 228.6×228.6 mm with several thicknesses. Then, the samples were cut to the dimensions of 20×15 mm according to the thickness required.

Experiments were carried out at approximately 20℃ on three different materials, categorized by their hardness of 32, 59 and 63 IRHD. Three different thicknesses of sample, 2, 5 and 9 mm, were used to investigate the effect of thickness. The test set up shown in Figure 1.12 was used. The rig was excited by a random signal. The results are shown in Figures 5.21, 5.22 and 5.23.

Figure 5.21 shows the shear modulus and loss factor obtained for samples of hardness 32 IRHD at the three different thicknesses. The results at 2 mm thickness appear smooth between about 500 and 3000 Hz whereas those for 5 and 9 mm are smooth over a lower frequency range. Differences can be seen in the shear modulus obtained, for example the stiffness around 500 Hz is found as $1.5 - 2.3 \times 10^6$ N/m^2, which may have been caused by variations in the pre-compression force applied to the sample while running the test. The loss factor drops to 0 at around 3.4 kHz for 9 mm thickness and 4.2 kHz for 5 mm thickness, in each case followed by a sharp rise. It is clear from this figure that

145
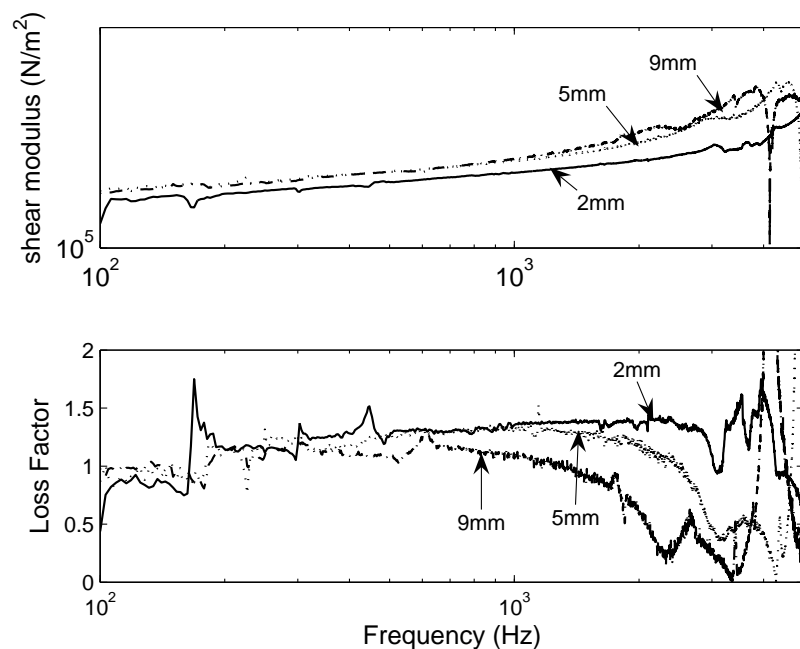
Figure 5.21: : Shear modulus and loss factor of various sample thickness for sample hardness 32 IRHD.
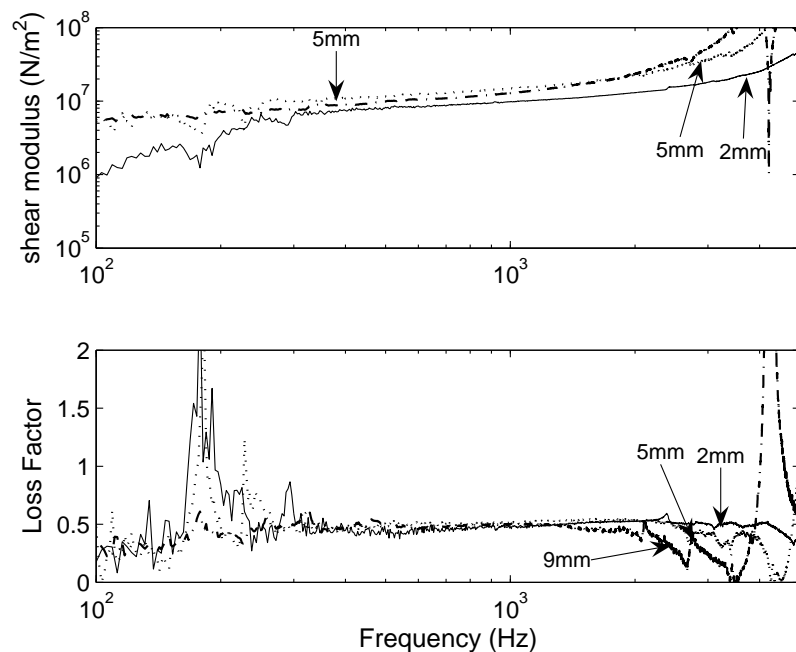
Figure 5.22: : Shear modulus and loss factor of various sample thickness for sample hardness 59 IRHD.

146
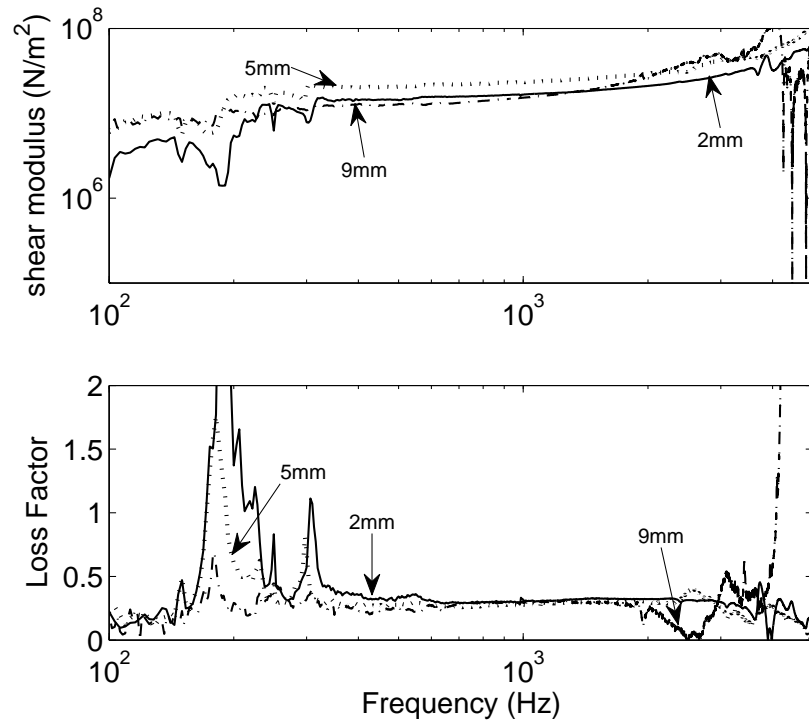
Figure 5.23: *Shear modulus and loss factor of various sample thicknesses for sample hardness 63 IRHD.*

the resonance frequency increases as sample thickness is reduced, as predicted. From Figure 5.17 for $G \approx 2.3 \times 10^6$ N/m^2, the upper limit should increase from about 700 Hz for 9 mm thickness to over 2000 Hz for 2mm. This is consistent with the measured results as seen in Figure 5.21.

The shear modulus and loss factor for samples of hardness 59 IRHD are shown in Figure 5.22. The shear modulus for three different thicknesses of sample at 500 Hz is found as $4.7-5 \times 10^6$ N/m. The shear modulus curve for 2 mm samples is smooth from 350-5000 Hz, however the curves for 5 and 9 mm samples are only smooth in the range 250 to 3500 Hz. The loss factor for 2 mm is above 0.35 from 350 to 4.5 kHz while for samples of 5 and 9 mm it drops to 0 at around 2.6 and 2.2 kHz.

Figure 5.23 shows corresponding result for the 63 IRHD material. This is much stiffer than that 32 IRHD material with the shear modulus around 500 Hz found as $1.4-2.0 \times 10^7$ N/m^2. In these results a lower limit of around 350 Hz can be seen at 2 mm reducing to 250 Hz at 5 mm and 9 mm. The high frequency behaviour suggests reliable data at 2 mm up to 3.5 kHz but at 9 mm this reduces to 2 kHz. The results at 5 mm appear anomalous, in particular at high frequency where the data appear reliable up to more than 5 kHz. This curve does not follow the same trend as 2 and 9 mm.

The results shown in the experiments have similar trends to those from the analytical method, although as the materials have frequency dependent properties it is not possible

to identify a 1 dB limit. Table 5.2 shows the measured stiffnesses and moduli and the corresponding predicted lower and upper limits for sample thicknesses of 2, 5 and 9 mm for these materials. As the material becomes stiffer, the lower frequency limit increases as well as the upper limit. For example, a 2 mm sample of 63 IRHD has a range of reliable data wider than for 59 and 32 IRHD. However, as the sample thicknesses increases from 2 mm to 9 mm, the range of reliable data become narrower especially for the soft material.

Table 5.2: *The lower and upper limit of various hardnesess and thicknesses of elastomeric samples.*

Sample Hardness (IRHD)	Sample Thickness (mm)	Stiffness at 500 Hz ($\times 10^6$) (N/m)	Measured G^* at 500 Hz ($\times 10^6$) (N/m²)	Analytical	
				f_{1dB} Lower limit (Hz)	f_{1dB} Upper limit (Hz)
32	2	0.93	1.55	57.2	2400
	5	0.57	2.38	54.3	1200
	9	0.33	2.46	53.3	700
59	2	4.72	7.87	80.2	5400
	5	2.71	11.3	67.8	2600
	9	1.31	9.80	59.3	1300
63	2	8.64	14.4	100	7400
	5	4.80	20.0	80.2	3500
	9	1.68	12.6	61.4	1500

5.5   Rig modification

Having diagnosed the vibration problems of the test rig, the next step is to identify whether modifications are possible to extend the range of validity.

5.5.1   Change of sample size

The first modification already considered, is changing the sample thickness. The shape of the sample is maintained (20 × 15 mm) but the thickness is changed from 10 mm to 2 mm. Based on the above analysis (Figures 5.17 and 5.18), a sample thickness of 2 mm will give a wide range of reliable data. Furthermore, the results from the experiments have also shown that a sample thickness of 2 mm has a wider range of validity than a sample thickness of 5 and 9 mm. To achieve valid measurements between 300 and 3000 Hz the shear modulus should be between 2.5 and 12 MN/m². For stiffer materials a larger thickness should be used, or the low frequency limit will be increased.

Another consideration is to change the width and length of the rectangular sample. Several sizes are selected, as shown in Table 5.3. The maximum sizes that can be fitted to the test jig are 20×20 mm. To investigate the effect on the range of data validity, the lower limit is fixed to 300 Hz and the corresponding stiffnesses determined. As shown in Figure 5.7, the stiffness for a limit of 300 Hz is 6.92×10^6 N/m. The shear modulus is derived from this stiffness using $G = Kh/4A$. The upper limit is calculated using equation (5.19). This shows that decreasing the sample size will increase the upper limit significantly. As a result, the range of reliable data increases as the sample sizes are reduced.

Similarly, Table 5.4 shows the effect of changing the sample size on the lower and upper frequency limits, based on a constant shear modulus of 5×10^6 N/m^2. The stiffness values are calculated from $K = G(4A)/h$ and the corresponding lower limit is determined from Figure 5.7. The upper limit is derived from equation (5.19). As a result, the lower limit decreases with reduction of sample size while the upper limit remains constant. Therefore, the ranges of reliable data increase as the sample sizes are reduced. However, using smaller samples may lead to other practical difficulties so this has not been pursued further.

Table 5.3: *The shear modulus and 1 dB upper limit at a given 1 dB lower limit of various sizes of sample.*

Thickness (mm)	Width (mm)	Length (mm)	G (MN/m^2)	K (MN/m)	Analytical Lower limit (Hz)	Analytical Upper limit (Hz)
2	20	20	8.65	6.92	300	5700
2	15	20	11.5	6.92	300	6600
2	10	20	17.3	6.92	300	8100
2	10	10	34.6	6.92	300	11400

Table 5.4: *The 1 dB lower and upper limit of various sizes of sample at a given shear modulus.*

| Thickness (mm)	Width (mm)	Length (mm)	G (MN/m^2)	K (MN/m)	Analytical Lower limit (Hz)	Analytical Upper limit (Hz)
2	20	20	5.0	4.0	231	
2	15	20	5.0	3.0	205	4300
2	10	20	5.0	2.0	167	
2	10	10	5.0	1.0	124	

5.5.2 Change of seismic mass

The 3-DOF system (Figure 5.4) is used to determine the effect of changing the seismic mass (m_3) from its current value of 12.28 kg. Simulated results are shown in Figure 5.24 for a sample stiffness $K_1 = 3$ MN/m and seismic mass (m_3) of 12.28, 24.0 and 48.0 kg. The first peak of the predicted stiffness is shifted to a lower frequency as the mass is increased. Correspondingly, increasing the mass of the seismic mass will decrease the lower frequency limit; this will increase the range of reliable data for a given value of K_1. Figure 5.25 shows equivalent results including the effect of the frame. Therefore, making the seismic mass (m_3) heavier than its current value will reduce its vibration due to the effect of the frame and bench.

From the results observed, a larger seismic mass should improve the range of reliable data. However, the restrictions imposed by the size of the temperature cabinet should be considered. The current seismic mass is cylindrical and has a diameter of 0.126 m and height of 0.126 m. Increasing the diameter, the maximum size that can be accommodated is 17.69 kg (0.1509 m diameter with the same height). This is not sufficient to reduce the lower frequency limit significantly. A rectangular block of dimensions $0.13 \times 0.20 \times 0.126$ m would give a mass of 25.71 kg. Increasing this to $0.18 \times 0.26 \times 0.136$ m would give 36.08 kg. Such improvements are worth considering, although the rig would become much more difficult to handle. A practical limit for one person to lift is probably around 25 kg. Care would also be needed to avoid sharp edges.

5.5.3 Stiffness of the bench

The stiffness of the bench K_3 was also varied in the simulations to investigate its effect on the resonance peak as well as the range of reliable data. Selected K_3 values are 0.67×10^5, 0.67×10^6 and 0.67×10^7 N/m. The middle of these three corresponds to the measured value. Results from the experiment showed that the effect of changing the value of K_3 depends also on the value of the sample stiffness K_1. Results are shown in Figure 5.26.

Figure 5.26(a), for $K_1 = 0.6$ MN/m, shows that increasing the value of K_3 will shift the resonance peak toward higher frequencies. At this particular value of K_1 the lower frequency limits for these three values of K_3 are at 98 Hz, 103 Hz and 140 Hz. However, increasing the values of K_3 will have no effect on the lower limit when K_1 is high (Figure 5.26(c)). The lower limit occurs at 475 Hz for all the values of K_3. A similar trend occurs in Figure 5.26(b) for an intermediate stiffness. Similar results can also be seen in Figure 5.27, which includes the effect of the frame.
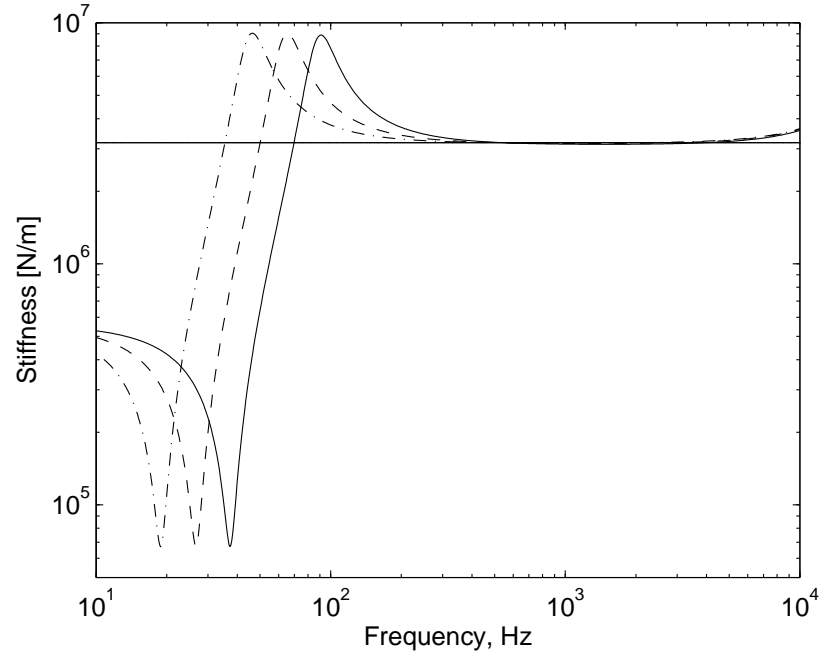
(a)
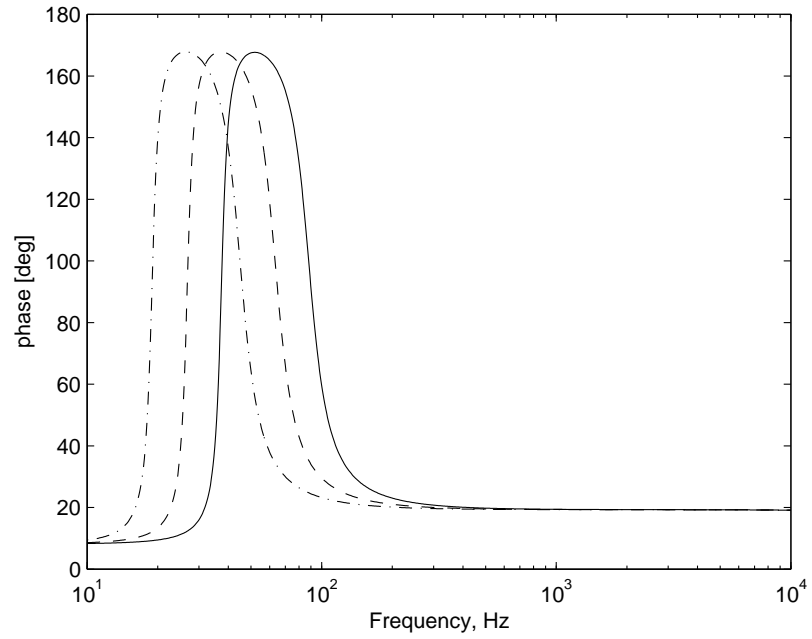
(b)

Figure 5.24: *Predicted effect of various values of mass (m_3) on measured stiffness ($K_1 = 3.0 \times 10^6$ N/m) - without the effect of frame. The various masses are (—) m_3=12.28 kg, (− −) m_3=24.0 kg and (− · −) m_3=48.0 kg.*

(a)

(b)
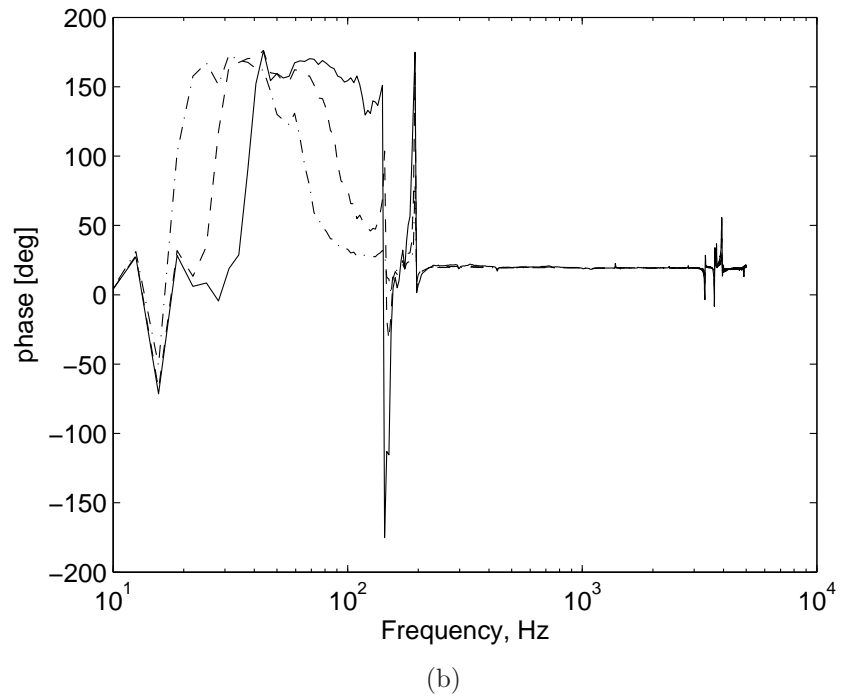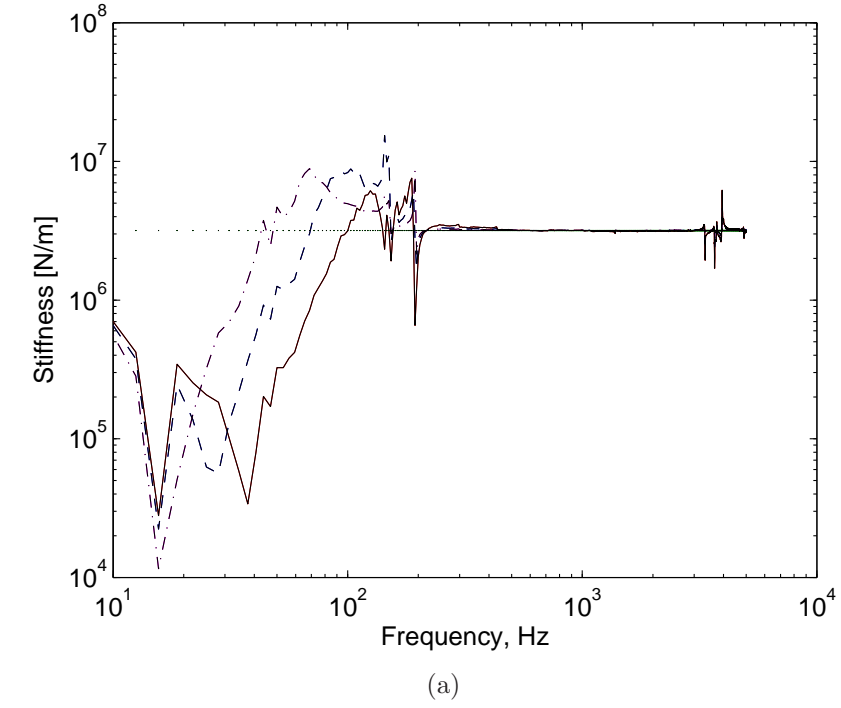
Figure 5.25: *Predicted effect of various values of mass (m_3) on measured stiffness for $K_1 = 3 \times 10^6$ N/m - including the effect of frame. The various masses are (—) m_3=12.28 kg, (— —) m_3=24.0 kg and (— · —) m_3=48.0 kg.*
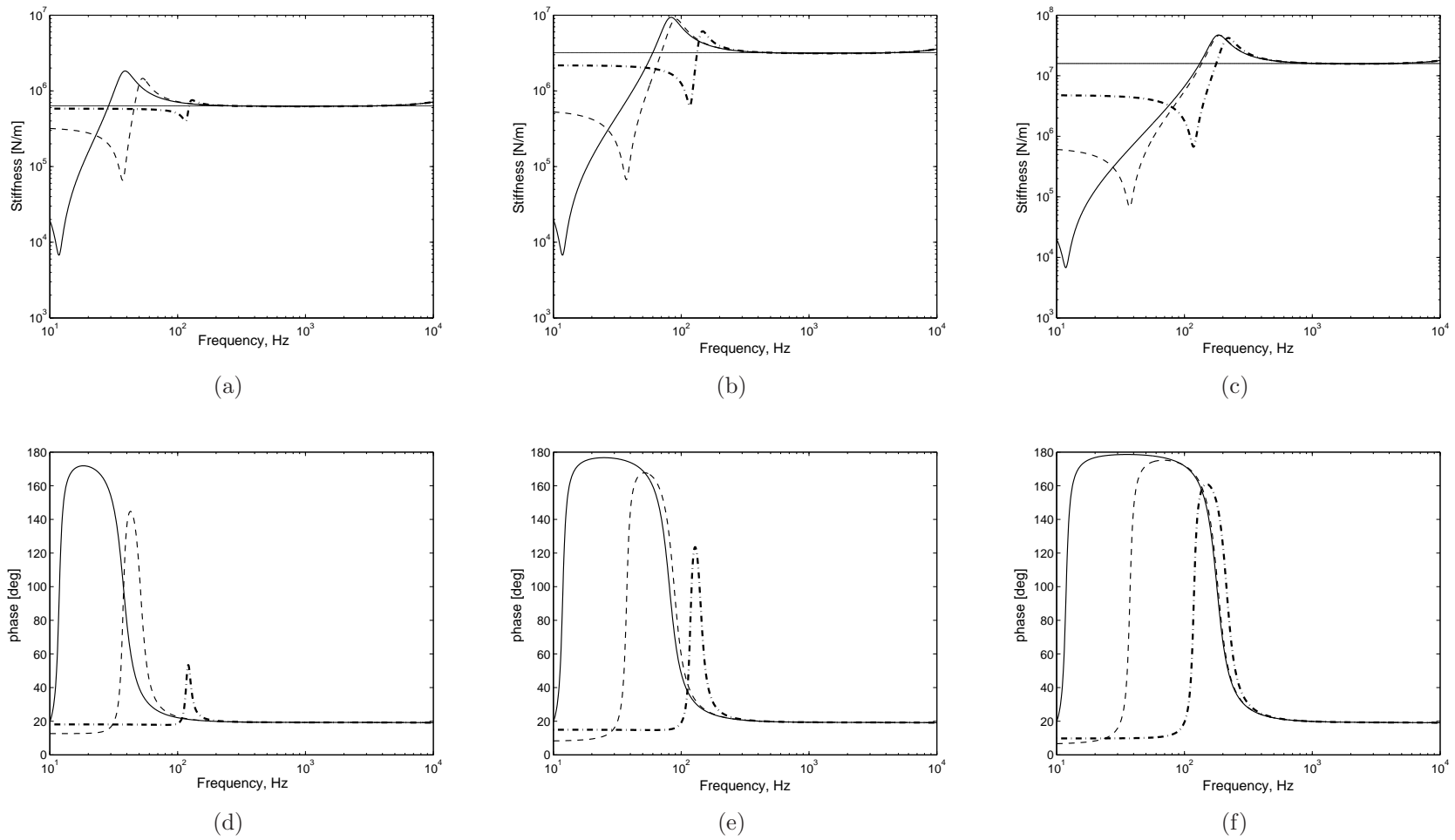
Figure 5.26: *Predicted effect of various stiffnesses (K_3) on the measured stiffness for different sample stiffnesses K_1 (a&d) 0.6 MN/m, (b&e) 3 MN/m and (c&f) 15 MN/m. The various stiffnesses are (—) K_3=0.674 × 10^5 N/m, (−−) K_3=0.674 × 10^{6}N/m and (···) K_3=0.674 × 10^7 N/m.*
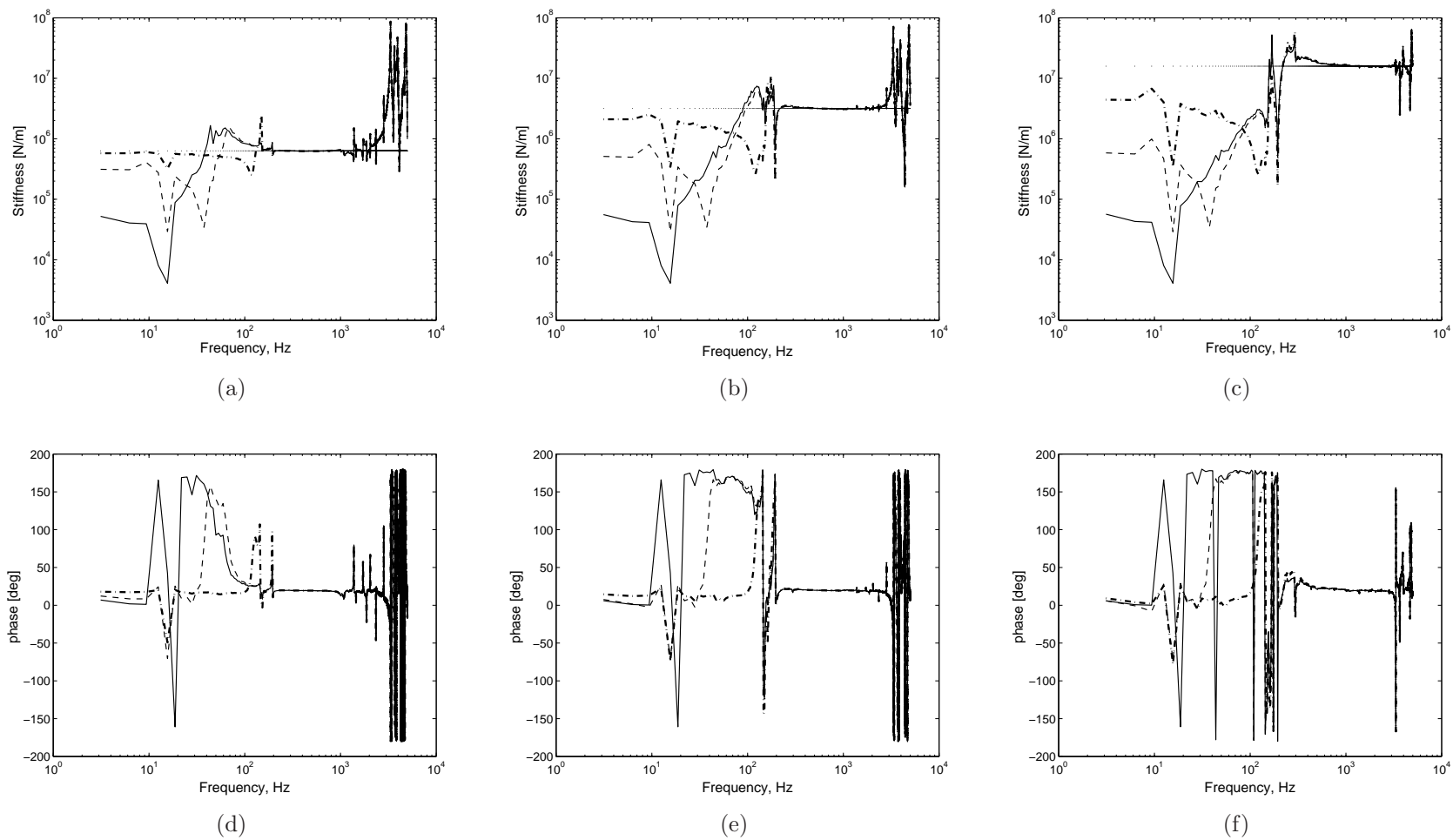
Figure 5.27: *Predicted effect of various stiffnesses (K_3) on the measured stiffness for different sample stiffnesses K_1 (a&d) 0.6 MN/m, (b&e) 3 MN/m and (c&f) 15 MN/m - including the effect of frame. The various stiffnesses are (—) K_3=0.674 × 10^5 N/m, (−−) K_3=0.674 × 10^6 N/m and (···) K_3=0.674 × 10^7 N/m.*

5.5.4 Modification of the beam

Another possibility is to stiffen the beam of the current test rig to avoid resonance effects. Changing the current L-shape beam to a U-shape could increase its rigidity, but this may introduce other problems. To give a simple estimate of the effect of stiffening the beam, the 3-degree of freedom system is used with the transmissibility Y_{12}/Y_{11} set to unity. Figure 5.28(a) and 5.28(c) shows the results of the simulation where the range of reliable data increases as the stiffness increases. A similar trend can also be seen in Figure 5.13. Although the effects of resonances have been removed, significant transmission occurs at high frequency, which affects the measurement especially for soft samples.

On the other hand, Figure 5.28(b) and 5.28(d) shows simulation results of the 3-degree of freedom system with the ratio of position 2 to position 1 set to 0.1 to represent a softer frame. This gives a better performance in terms the range of valid data. However, this model is very simplified and only intended to show the sensitivity of the results to the frame transmissibility.

5.5.5 Separate beam

Another method to prevent the vibration from the magnet being transmitted to the seismic mass via the beam is by separating the frame from the seismic mass. An experiment was carried out and the test set up is shown in Figure 5.29. The frame was detached from the seismic mass and they were placed on different surfaces to avoid vibration transmission between them. Figures 5.30 and 5.31 show the shear modulus and loss factor obtained both with the frame connected and with it separated for sample thickness 2 and 9 mm. The shear modulus and loss factor presented are for the material of hardness 63 IRHD at different sample thicknesses (see section 5.4.2 for comparison).

Separating the frame from the seismic mass improves the data at low frequency. This is shown in the following figures, the fluctuations in the data around 200 Hz for the test rig with attached frame are shifted to 100-150 Hz for the test rig with separate frame. A similar effect can also be seen in the predicted curves in Figure 5.6 and Figure 5.13 for a stiffness of 3×10^6 N/m. Although this experiment demonstrates the reduction of unwanted vibration of the test rig especially at low frequency, it is not workable in terms of testing the sample in the temperature cabinet, which has a restricted size of $0.2 \times 0.3 \times 0.55$ m.

Instead, the installation of soft mounts between the frame and seismic mass may approximate the effect of separating the frame from the seismic mass. However, a resonance will also be introduced. In theory this will reduce the transmissibility above its resonance
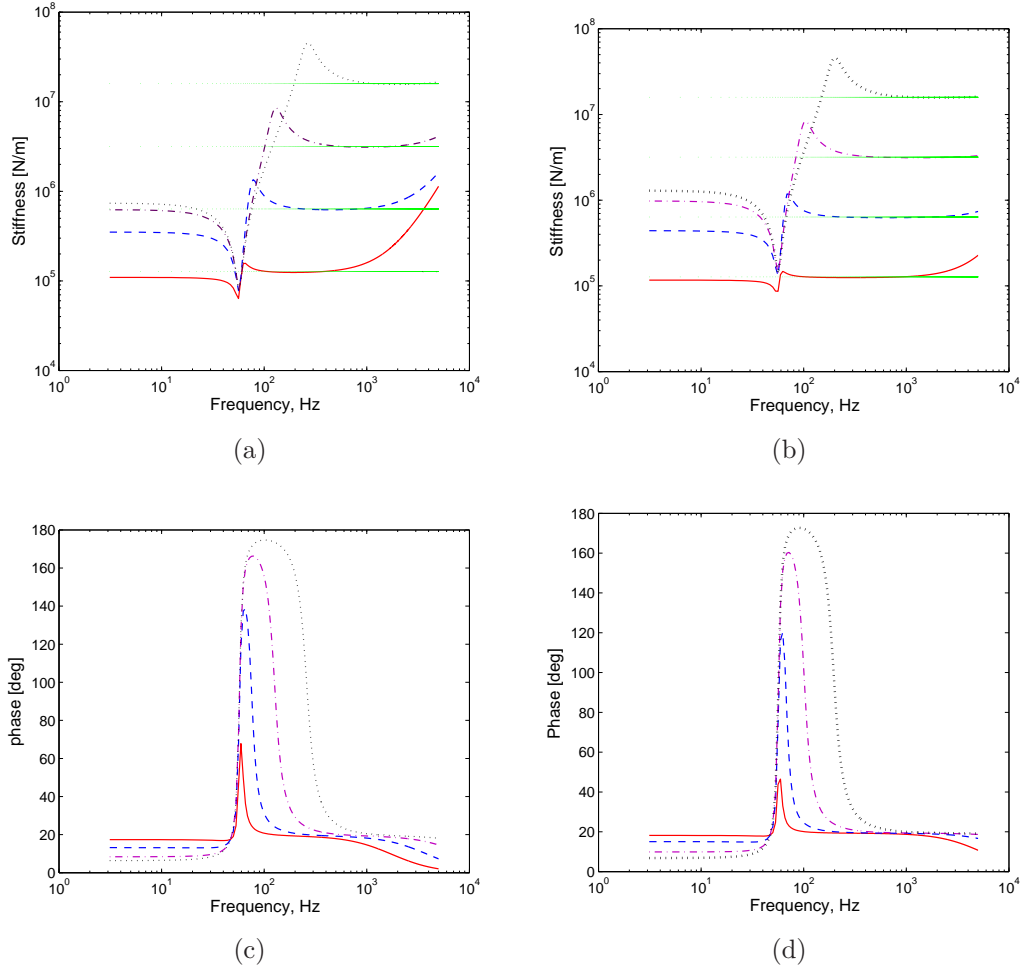
Figure 5.28: *Predictions of measured and real stiffness including the effect of frame where(a & c) Y12/Y11=1 and (b & d) Y12/Y11=0.1. The various stiffnesses are (—) K_1=0.12 × 10^6 N/m, (−−) K_1=0.60 × 10^6N/m, (− · −) K_1=3.0 × 10^6 N/m and · · ·) K_3=15.0 × 10^6 N/m.*

frequency, which should therefore be below 100 Hz. At the same time, it is necessary for the test rig still to fit inside the temperature cabinet. An experiment will be carried out to investigate whether this method is workable.
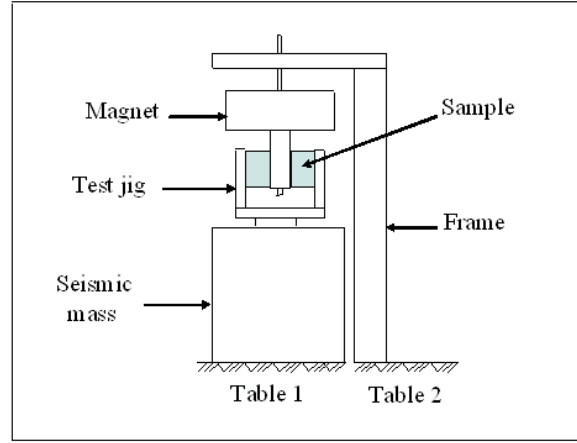
Figure 5.29: *The test set up of FRF measurement for separate frame from seismic mass.*
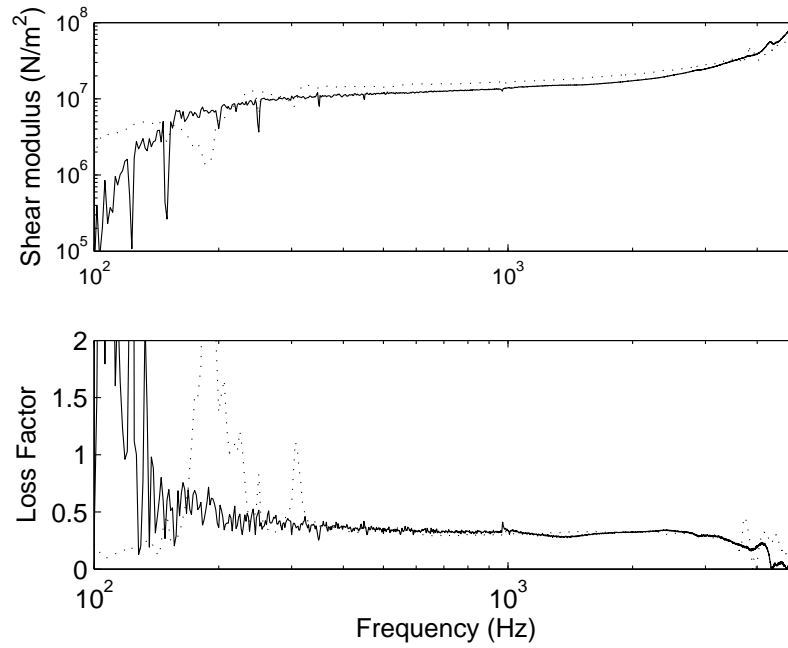
Figure 5.30: *Shear modulus and loss factor obtained with frame attached ($\cdots$) and separated (—) from the seismic mass for rubber sample 2 mm of 63 IRHD.*
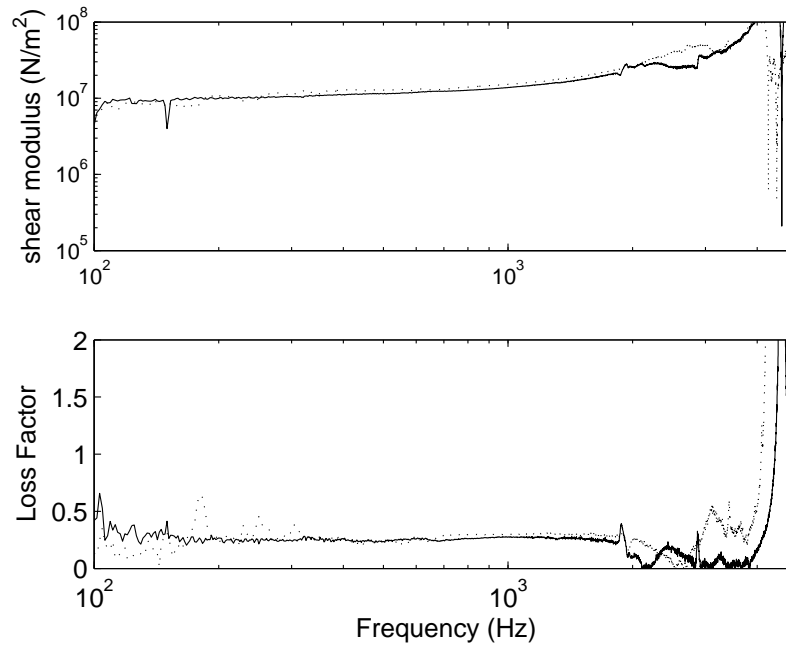
Figure 5.31: *The comparison of shear modulus and loss factor obtained with frame $(\cdots)$ attached and separated $(—)$ from the seismic mass for rubber sample 9 mm of 63 IRHD.*

5.6 Dynamic measurements of modified ISVR test rig

5.6.1 Introduction

Following the analysis of Section 5.5, the ISVR test rig has been modified in an attempt to improve the measurement of dynamic stiffness at low frequency. The seismic mass has been increased from 12 kg to 31 kg by increasing its dimension to $140 \times 200 \times 140$mm and the frame has been isolated from the seismic mass by installing six rubber mounts between the frame and the seismic mass as shown in Figure 5.32.

5.6.2 Effect of change of seismic mass and isolation of frame

Similar mobility tests as in section 5.3 were carried out to determine the improvement of the test rig performance at low frequencies. An impact hammer was used to excite the system on the seismic mass. Accelerometers were located at the excitation position on top of the seismic mass and on top of the frame as before. The average of five strikes by the hammer on the seismic mass was recorded in each case. The results are presented in the form of mobility.
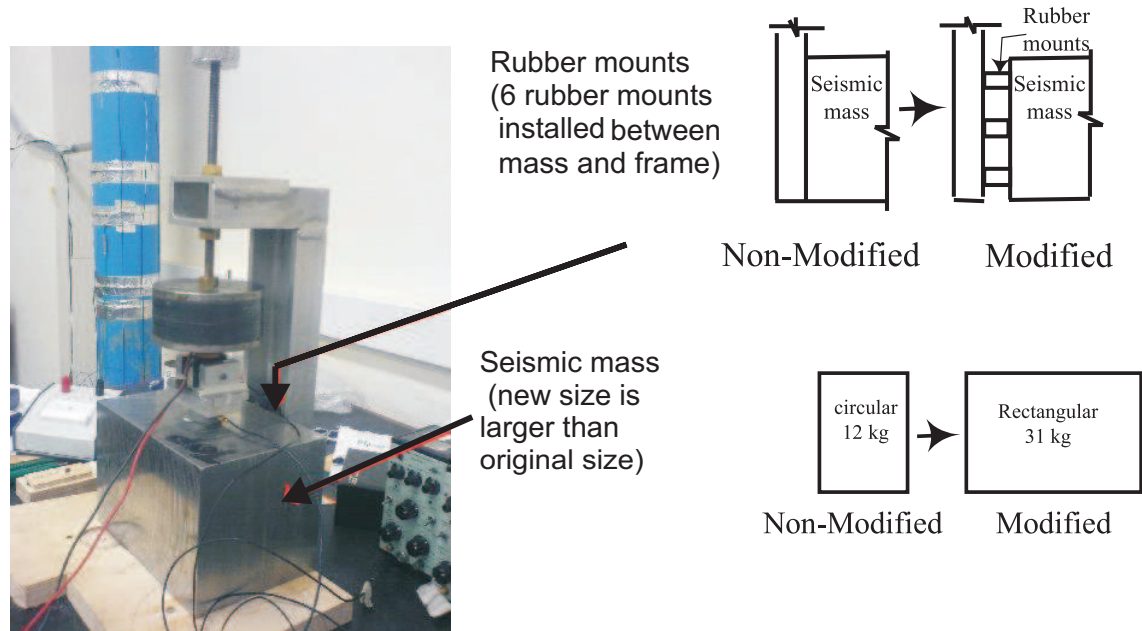
Figure 5.32: *The modified ISVR test rig. The seismic mass is larger than the original size (refer to Figure 1.12) and there are six rubber mounts installed between the seismic mass and frame.*

Figures 5.33 and 5.34 show the point and transfer mobility results for the system. For the point mobility measurement of the seismic mass a good coherence was found in the range 30 - 3000 Hz. The mobility curve shows mass-like behaviour in most of this frequency range. Compared with the non-modified rig the mobility is reduced by about 10 dB corresponding to the increase in mass. Although not a large effect this is the most that could be achieved within practical constraints. In addition the various resonances seen in the mobility of the unmodified rig have been suppressed. This is most likely to be due to the isolation of the frame from the seismic mass.

The transfer mobility shows a considerable reduction due to the isolation of the frame. There is some noise contamination especially above about 100 Hz due to the very low levels of response. The coherence is also poor above 100 Hz. Nevertheless, this result shows that the isolation has been effective.

In Figure 5.35, the results from the impact test are given in the form of transmissibility. The transmissibility curve has a peak at 25 Hz and then falls with a slope of approximately -40 dB/decade over the range 30-200 Hz as expected for a single-degree-of-freedom system. At high frequencies it is contaminated by noise due to the low levels of response.

5.6.3 Stiffness measurements

Tests of various samples have been repeated using the modified rig in order to verify the improvements expected. A similar test method as in section 5.4.2 was adopted. The tests
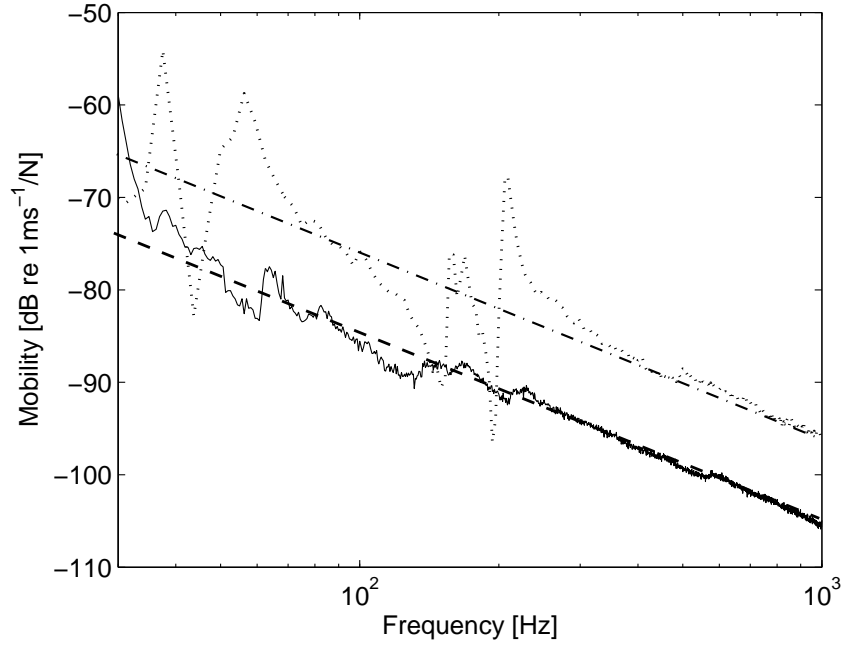
(a)
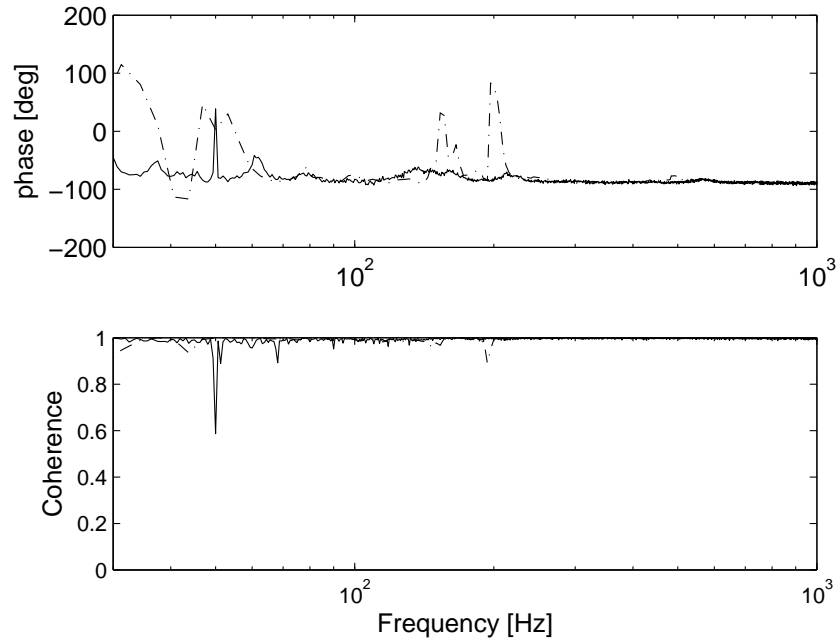
(b)

Figure 5.33: *(a) The point mobility of the test rig where the excitation force and response are at the seismic mass for modified (—) and non-modified (···) test rig and mass line of (−−) for 12 kg and (− · −) for 31 kg. (b) The phase and coherence of the point mobility for modified and non-modified test rig. (—) modified rig; (− · −) non-modified rig.*
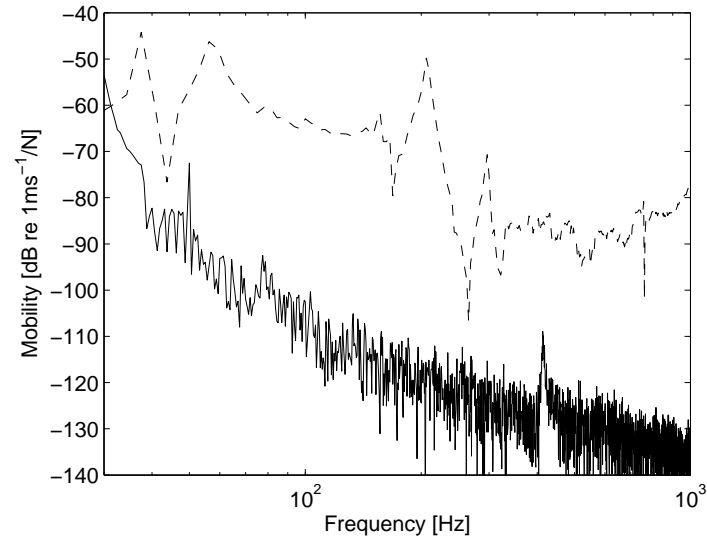
Figure 5.34: *The transfer mobility of the test rig where the excitation force is at seismic mass and response is at the top of the frame. (—) modified rig; (——) non-modified rig.*
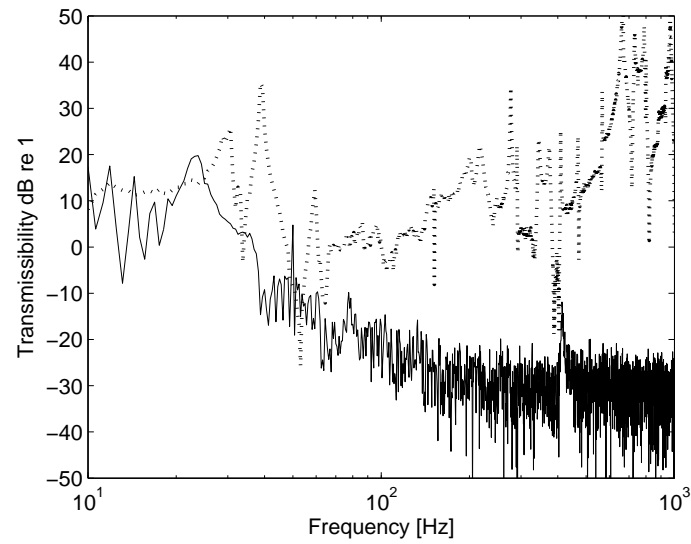
Figure 5.35: *The transmissibility the impact test for modified rig. (—) modified rig; (· · ·) non-modified rig.*

were done at 20℃ for different sample thicknesses and two materials of different hardness. The samples have dimensions 20 mm× 15 mm with thickness 2 mm, 5 mm and 9 mm. The samples are butyl rubber with hardness of 32 IRHD and 63 IRHD as before.

Figures 5.36 to 5.38 show the shear modulus and loss factor measured for different sample thicknesses for the material of hardness 32 IRHD. Results for the modified rig, presented as a solid line curves, are compared with the earlier results for the unmodified rig and results where the frame was disconnected from the seismic mass. The modified rig reduces the erratic behaviour below 500 Hz for these particular samples. For example in Figure 5.36, the results from the modified rig appear consistent down to 200 Hz where the previous results (non-modified and detached rig) show large deviations at 300 Hz especially in the loss factor. This improvement is consistent with the predictions in Section 5.5.2 where an increase in the seismic mass reduces the lower limit of validity.

Figure 5.38 shows resonance behaviour at high frequency above 3000 Hz for all curves which may be caused by the internal resonance of the sample. The modification of the test rig does not give any improvement in data validity at high frequency but this is addressed by the use of thinner samples as in Figure 5.36.

The results show larger differences below 1000 Hz. These are due to inconsistencies in setting up the rig which were not initially identified. It is quite difficult to clamp the rubber sample between the central shaft and the outer yoke, especially for thinner samples, as they tend to slip out during assembly. Moreover, a similar pre-strain should be applied via the bolt which holds the rubber samples to the test jig. It is clear that tests should be repeated in each situation in order to ensure consistency of results.

Figures 5.39 to 5.41 show the shear modulus and loss factor of various sample thicknesses for the material of hardness 63 IRHD. Again the results from the modified rig show improved behaviour, with the phase showing consistent results down to around 150 Hz. There are less problems with inconsistent results.
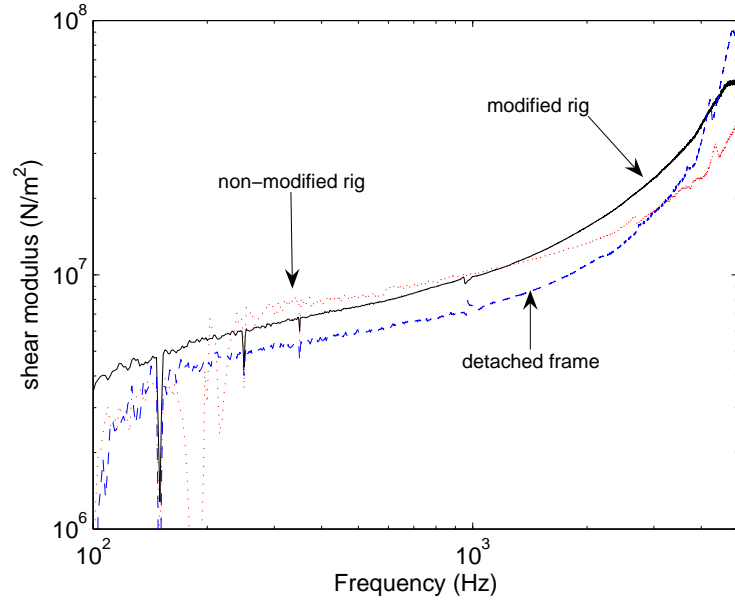
(a)
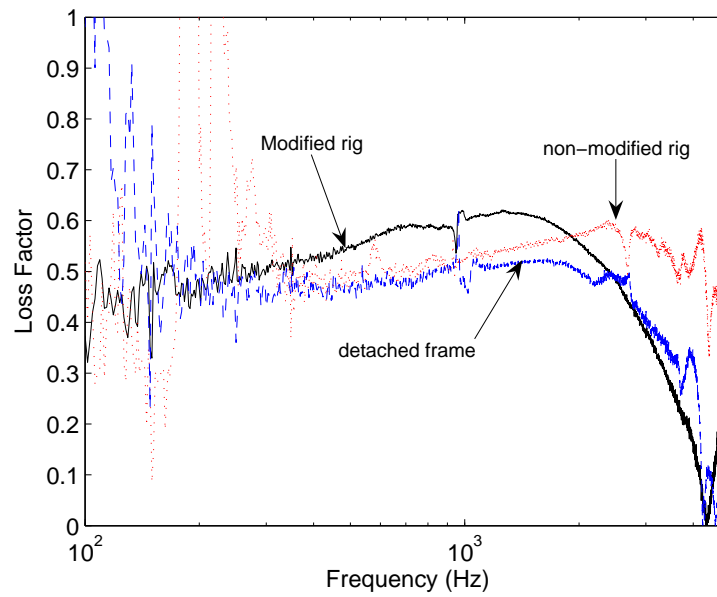
(b)

Figure 5.36: *The shear modulus and loss factor for sample thickness 2 mm (32 IRHD).*
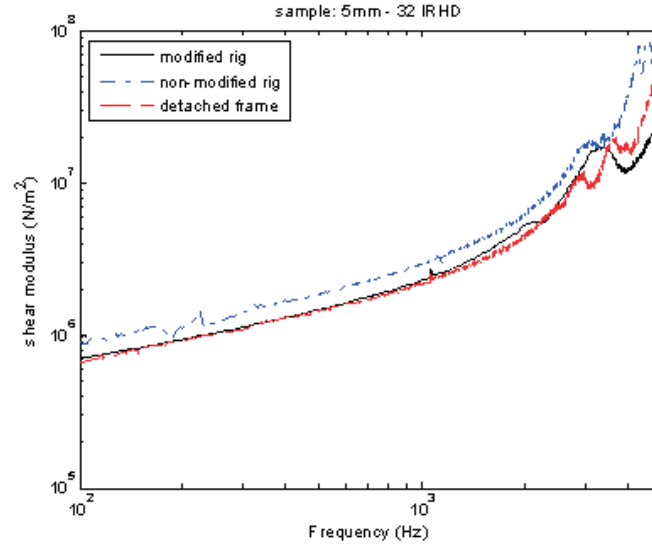
(a)
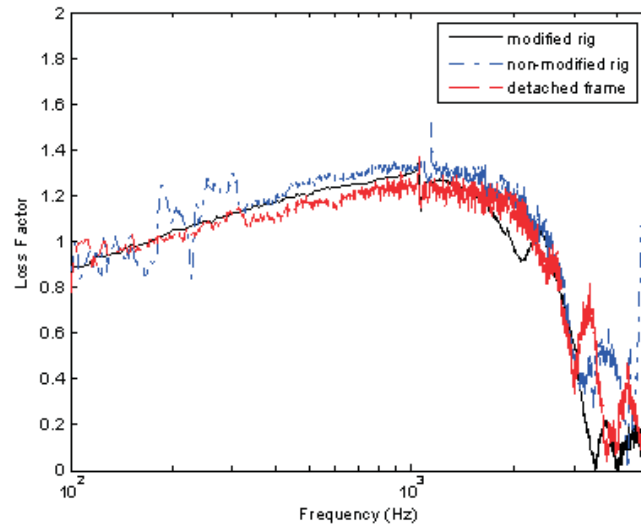
(b)

Figure 5.37: *The shear modulus and loss factor for sample thickness 5 mm (32 IRHD).*
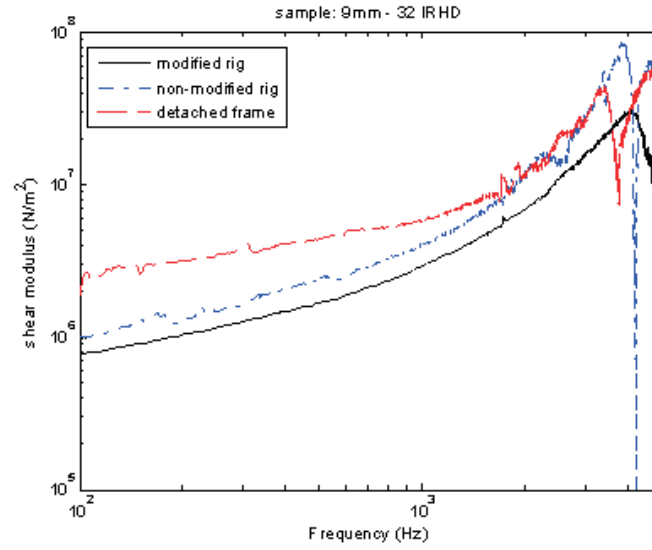
(a)
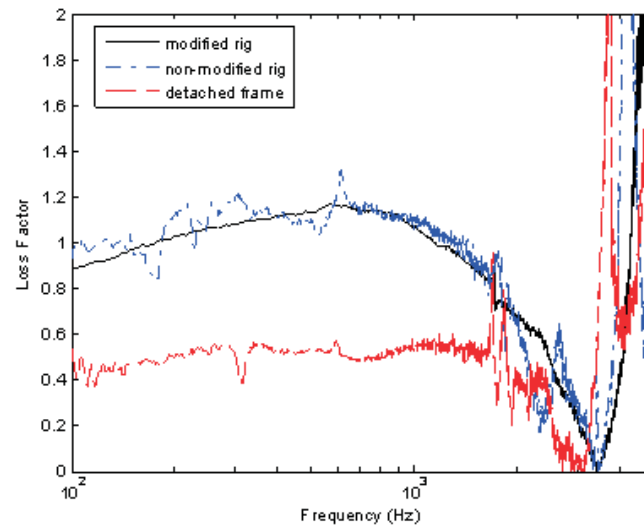
(b)

Figure 5.38: *The shear modulus and loss factor for sample thickness 9 mm (32 IRHD).*
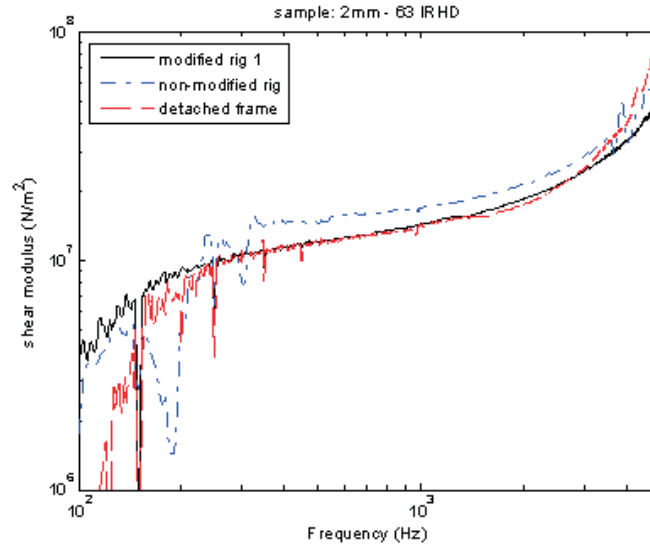
(a)
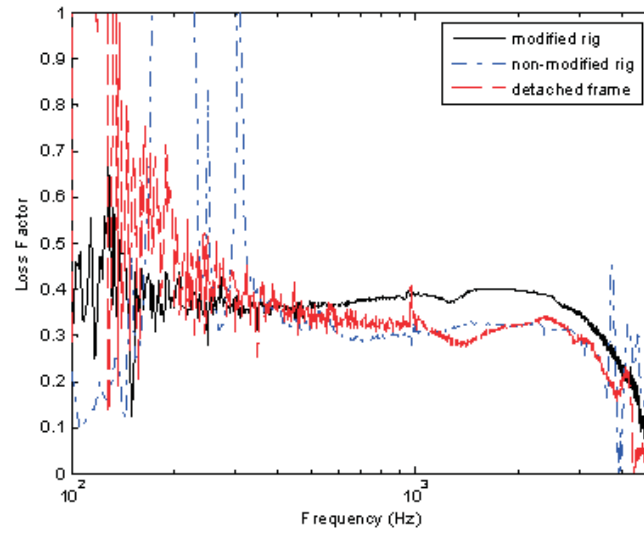
(b)

Figure 5.39: *Shear modulus and loss factor for sample thickness 2 mm (63 IRHD).*
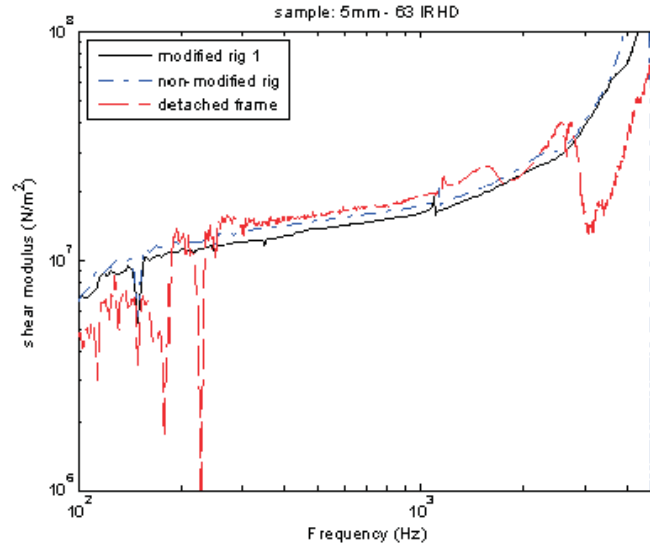
(a)
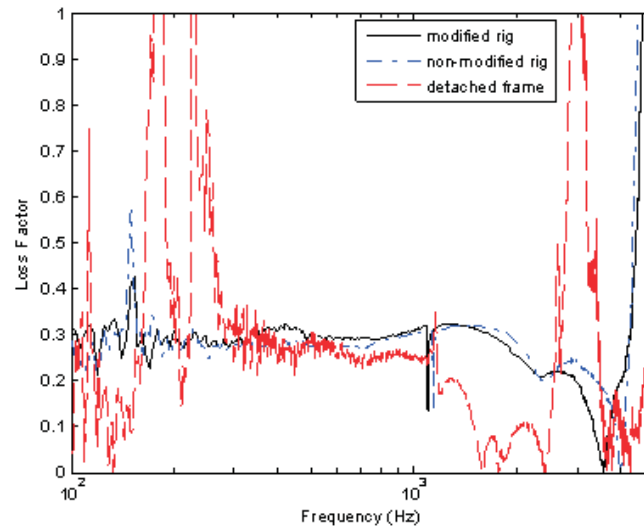
(b)

Figure 5.40: *Shear modulus and loss factor for sample thickness 5 mm (63 IRHD).*

167
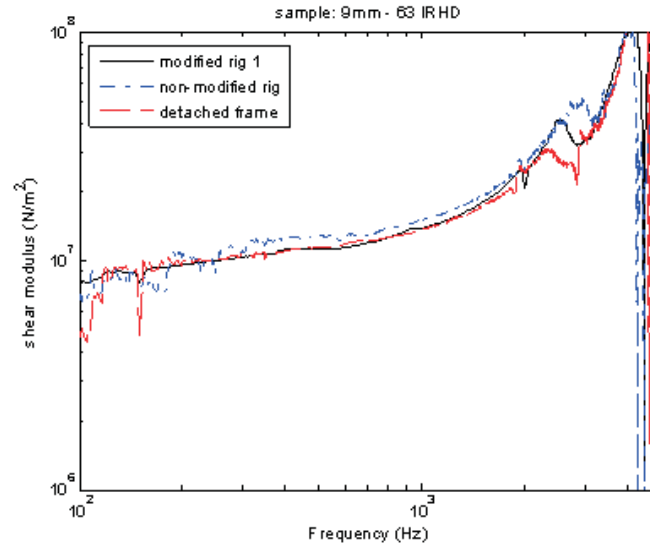
(a)
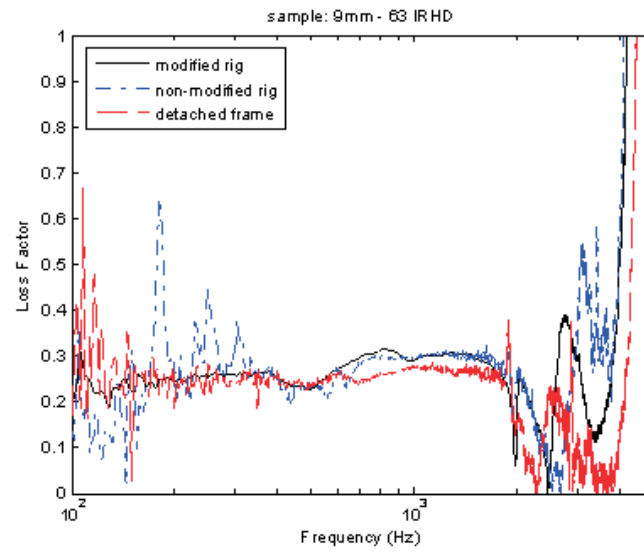
(b)

Figure 5.41: *Shear modulus and loss factor for sample thickness 9 mm (63 IRHD).*

5.6.4   Verification of test method

In order to verify the results from the ISVR test rig, measurements of the shear modulus and loss factor of unfilled Natural Rubber vulcanisates are compared with published data from Ahmadi *et al.* (1992). A duplicate formulation was produced for testing in the ISVR rig and samples 2 mm thick were manufactured. Only results at room temperature are presented.

The results from the ISVR test rig are obtained in shear at room temperature (approximately 18-20°C) over a frequency range 300-3000 Hz for an rms strain amplitude of 0.01%. The results from Ahmadi *et al.* (1992) were obtained in simple shear at three frequencies (0.1, 1 and 15 Hz) at a strain amplitude of 2% and for a temperature range -40°C to 150°C. These results were then transformed using time-temperature superposition to give equivalent results at 22°C as a function of frequency. The transformed results were presented in the original paper. It should be borne in mind that these results are transformed to much higher frequencies than those for which tests were conducted, so that small errors in the time-temperature superposition process cannot be ruled out.

The dynamic shear modulus is shown in Figure 5.42 and the loss factor in Figure 5.43. The shear modulus results are within 20% of each other below 1 kHz. The difference becomes larger as frequency increases due to the internal resonance of the sample, as mentioned in section 5.4.1. Furthermore, the sample is soft, making it more difficult to measure at high frequency. According to Figure 5.19 for a thickness of 2 mm and the present shear modulus the upper limit of validity is expected to be 1000 Hz. The loss factor appears slightly lower in the present results than in those from Ahmadi *et al.* (1992). Nevertheless, ignoring the erratic behaviour in the present test results above 2 kHz, fairly good agreement is seen between the two sets of results, confirming the validity of the current test rig.

5.7   Conclusions

An existing test rig has been analysed from which insight has been gained into the causes of disturbances in the data gathered.

For stiff materials significant fluctuations are found in the data at low frequency, which are caused by an insufficiently high impedance of the seismic mass. Increasing the mass has increased its impedance, thereby reducing the disturbance behaviour around 300-500 Hz and widening the range of valid data.
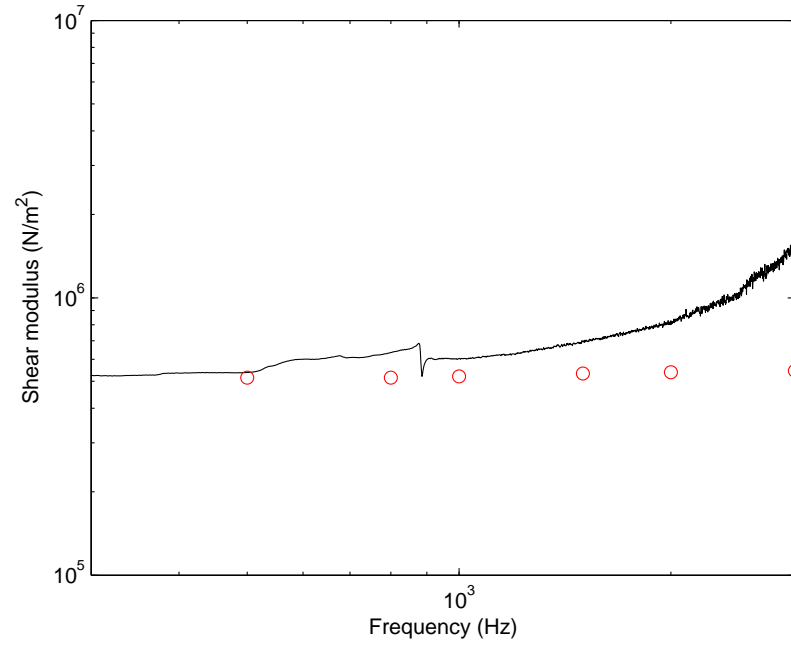
Figure 5.42: *Shear modulus of Natural Rubber at room temperature. (—) from present test rig, (◦) from Ahmadi et al. (1992).*
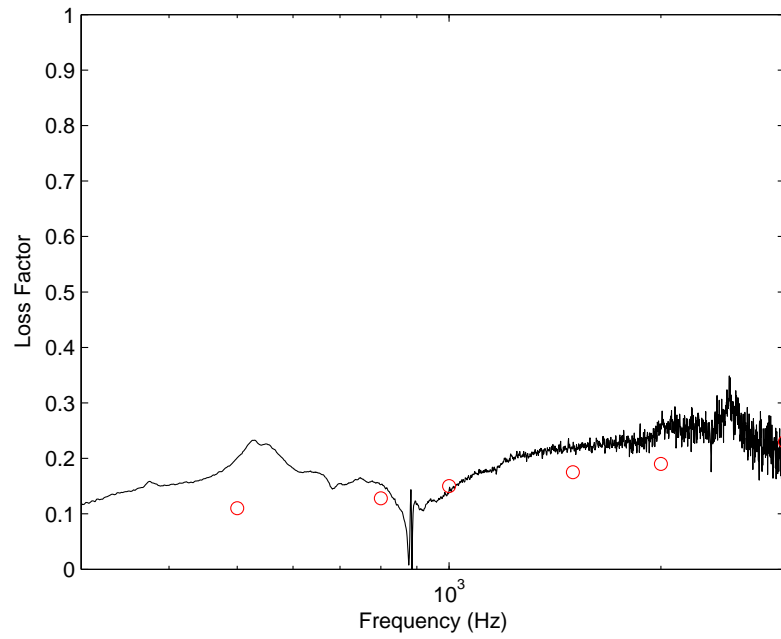
Figure 5.43: *Loss factor of Natural Rubber at room temperature. (—) from present test rig, (◦) from Ahmadi et al. (1992).*

The resonance at low frequency is also affected by the stiffness of the bench, where the test rig is placed during the test. It has been shown that the seismic mass sitting on the bench has a resonance frequency well below 100 Hz. In terms of reliable data, changes to the bench stiffness have negligible effect in the frequency range of interest.

The frame of the test rig also causes a problem of resonance at low frequency (200-300 Hz) as well as high frequency (2000-3000 Hz). This has been avoided by installing a soft mount between the frame and seismic mass to isolate the vibration.

The deviations at high frequency are dominated by internal resonances of the samples. This is resolved by using thinner samples (2 mm). However, this can make matters worse at low temperatures where the stiffness will be even higher. Therefore, the sample thickness must be chosen according to the stiffness of the material. A 2 mm thick sample is suitable for shear modulus in the range 2.5 to 12 MN/m^2. For stiffer materials a thicker sample should be used or the low frequency limit will be greater than 300 Hz.

The installation of the rubber samples between the central shaft and the outer yoke is found to be quite critical. If the samples are not placed consistently the results can differ considerably. It is therefore necessary to repeat the tests for each configuration in order to ensure consistent results.

Measurements have shown that the modifications implemented, i.e. larger seismic mass, isolation of the frame and use of thinner samples, give wider data validity and more accurate measurement of dynamic shear modulus and loss factor.

Chapter 6

Dynamic-mechanical characteristics - butyl rubbers

6.1 Introduction

In Chapter 2 butyl rubber was identified as a good candidate for use in the rail absorber (Sections 2.4 and 2.5). From the predictions of noise reduction carried out in Chapters 3 and 4, it has been found that a damping loss factor between 0.25 and 0.4 gives the best results across the range of temperatures considered. In terms of temperature-weighted noise reductions, a loss factor between 0.3 and 0.8 gives good results. Although butyl has a higher loss factor than this, nevertheless, its high damping and other suitable properties mean that it is worth investigating further.

Butyl rubber is a random copolymer which has a broad peak of loss factor over a range of temperatures. It is widely available but a little more costly than general purpose rubbers such as NR and SBR (Medalia, 1978).

Filler and plasticiser can be used to improve the characteristics of the butyl compound especially at low and high temperatures. Filler is added to the butyl compound to increase the modulus at higher temperatures and plasticiser is added to soften the material at the lower temperatures (Sections 2.4.3 and 2.4.4). The use of both filler and plasticiser together is expected to broaden the transition zone.

6.2 Initial investigation

An initial investigation has been carried out into the dynamic properties of filled butyl rubber. For this, a number of samples were chosen with different loadings of carbon black and oil. This screening experiment (set 1) was intended to determine the best range of compounds in which to focus further investigation. A wide range of proportions of filler and plasticiser were selected in an ad-hoc manner, as listed in Table 6.1.

The compositions selected consist of a polymer of butyl rubber, reinforced with a filler of carbon black and with paraffinic oil as a plasticiser. Composition number 1 allows, first, the characteristic of the polymer itself to be determined without filler or plasticiser. Composition number 6 was used to investigate the effect of filler only with no plasticiser. Composition numbers 4, 7 and 8 allow the effect of plasticiser to be investigated. Here the amount of filler is constant at 20 parts per hundred rubber (pphr), while the amount of plasticiser is varied. Composition numbers 3, 4 and 5 have a fixed ratio of filler to plasticiser. Moreover, the effect of increasing the amount of filler for a given amount of plasticiser can be seen by comparing the pairs 1 and 6, 2 and 7, and 3 and 8.

In addition to the polymer, filler and plasticiser, processing aids and curing agents were also added to enhance the dynamic properties of the compounds. They are zinc oxide, stearic acid, sulphur and two types of rubber accelerator, tetramethylthiuram disulphide (TMTD) and 2-Mercapto benzothiazole (MBT).

Table 6.1: *Ratio of fillers and plasticisers in butyl compounds set 1 (weight in pphr).*

Compound Ingredients	1	2	3	4	5	6	7	8
Polymer	100	100	100	100	100	100	100	100
Filler	0	50	80	20	60	40	20	20
Plasticiser	0	20	40	10	30	0	20	40

To manufacture each sample, the butyl rubber was blended with filler and plasticiser and also the other chemicals using a Banbury internal mixer. Then, the process of adding the sulphur and accelerators was done using a 406.4 mm × 406.4 mm two-roll mill. The compounds were placed in a sheet mould of size 228.6 mm × 228.6 mm with thickness 2 mm and cured in a steam press at 160℃ for 24 minutes. Four rectangular samples of size 20 mm × 15 mm were cut from this sheet for the shear tests.

In addition, a preliminary investigation was carried out of using butyl rubber with a different kind of filler. This filler was graphite flake, which is believed to have the potential to improve the damping performance by increasing the loss factor (Ball & Salyer, 1966). The same manufacturing process was used and this sample was also tested. However, the result obtained was disappointing. In this case, the results for the graphite flake

were no different from the standard filler, in this case carbon black, in terms of damping performance. Therefore, this was not taken further.

6.2.1 Testing procedure

As these initial tests were carried out at an early stage in the project, the unmodified test rig shown in Figure 1.12 was used to test the materials in set 1. The measurement method described in Section 5.1.1 was used to determine the dynamic properties of these butyl compounds.

The measurements were carried out in a temperature cabinet. A white noise signal over the range 0-5 kHz was used to excite the system. The samples were tested at 5℃ increments of temperature between -20℃ and 40℃. The samples were exposed to a particular temperature for 5 to 10 minutes before the measurements were taken. A two-channel FFT analyser was used to analyse the data. The samples of each compound were tested several times refitting them to the rig between each sequence of measurements, to ensure consistent results.

6.2.2 Results and discussion

All samples were measured using the above test procedure. Firstly, results are shown for compound no 1, butyl rubber without any filler and plasticiser, in Figure 6.1. The shear modulus increases with increasing frequency and decreasing temperature. Between -20℃ and 40℃ it increases by a factor of 48 at a frequency of 1000 Hz. The peak loss factors are well above the target value of 0.25 to 0.4. These results are therefore rather high for application to the rail absorber. However, the modulus is close to the target value of 5MN/m² at about 10℃.

Secondly, the effect of adding filler without plasticiser is determined. Figure 6.2 shows results for compound 6 (40pphr) at 1 kHz compared with those for butyl without filler. The shear modulus can be seen to be increased especially at high temperatures but the loss factor is reduced significantly over the temperature range.

Figure 6.3 shows the effect of varying the carbon black content for various loadings of plasticiser. In each case, butyl rubber with no filler or plasticiser - 'pure butyl' is included as a reference. This again shows that increasing the amount of filler increases the shear modulus across the temperature range but significantly reduces the peak of the loss factor.

Results are shown in Figure 6.4 for butyl rubber with various loadings of plasticiser at a fixed loading of filler (20 pphr). As the amount of plasticiser is increased, the shear
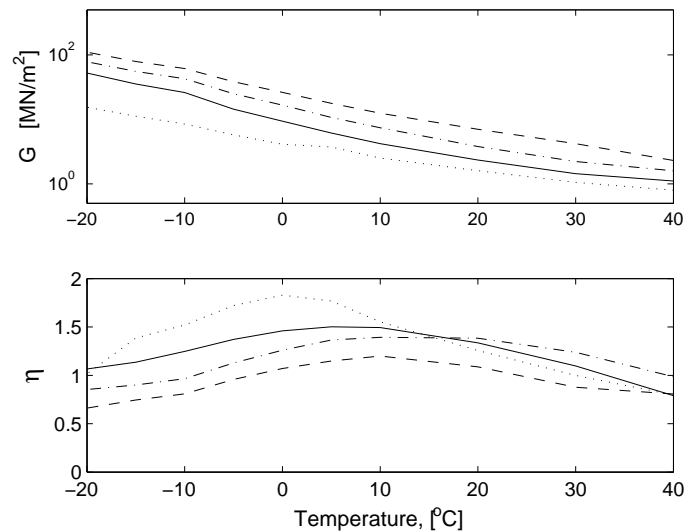
Figure 6.1: *The shear modulus and loss factor of butyl rubber at various frequencies: (· · ·) 0.5 kHz, (—) 1 kHz, (− · −) 2 kHz, (−−) 3 kHz.*
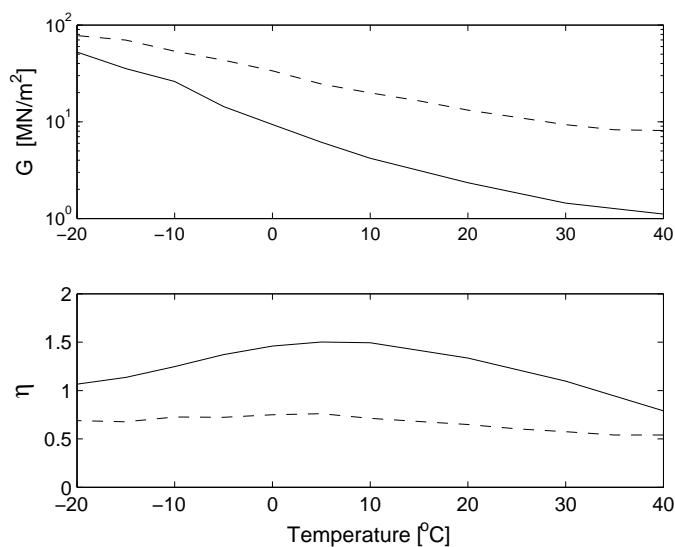
Figure 6.2: *The effect of adding filler to butyl rubber at 1 kHz. (—) filler loading 0 pphr and plasiciser loading 0 pphr ('pure butyl'), and (−−) filler loading 40 pphr and plasticiser loading 0 pphr (compound 6).*

(a)

(b)
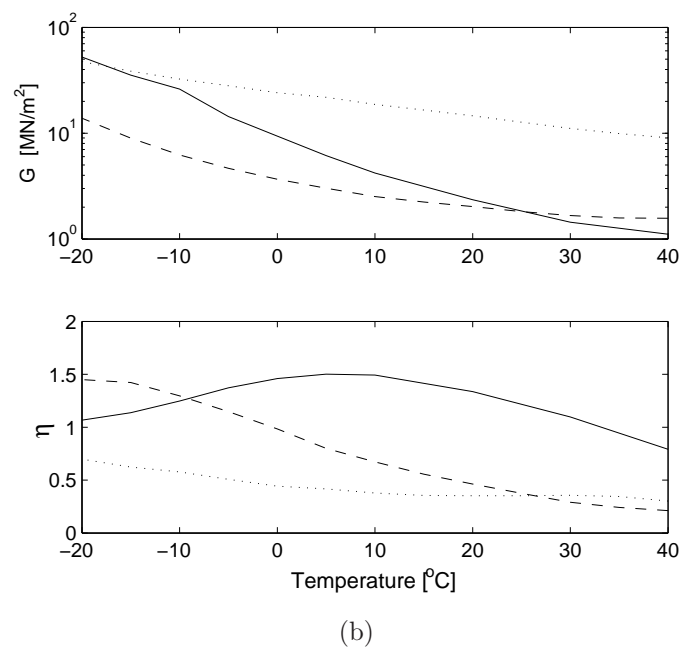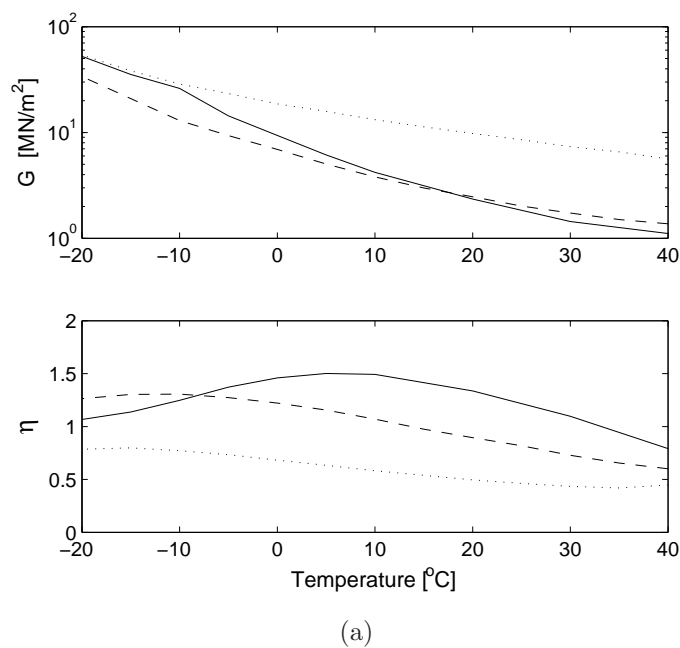
Figure 6.3: *Effect of increasing filler with constant plasticiser on dynamic properties of butyl rubber at 1 kHz. (a) (−−) compound 7, 20 pphr of filler, (···) compound 2, 50 pphr of filler each with 20 pphr plasticiser and (—) pure butyl. (b) (−−) compound 8, 20 pphr of filler, (···) compound 3, 80 pphr of filler each with 40 pphr of plasticiser and (—) pure butyl.*

modulus is reduced at most temperaturess. The effect is greatest at low temperatures. The loss factor retains a broad peak in most cases, but is reduced at high temperatures for high loadings of plasticiser.

In these results, the shear modulus decreases by 73% at -20℃ between 10 and 40 pphr of plasticiser. Compared with the shear modulus of pure butyl, the shear modulus for 40 pphr plasticiser is reduced by 74% at low temperature and increased by 29% at high temperature.

For large amounts of plasticiser, the addition of filler to the composition does not boost the shear modulus at high temperature. For example, compositions 7 (20 pphr carbon black and 20 pphr plasticiser) and 8 (20 pphr carbon black and 40 pphr plasticiser) which have shear moduli at 40℃ of 1.37 MN/m^2 and 1.57 MN/m^2 are similar to composition 1 (pure butyl) with 1.0 MN/m^2. However, composition 4, which has only a small amount of plasticiser (20 pphr carbon black and 10 pphr plasticiser) shows a significant increase of shear modulus at 40℃ to 3.28 MN/m^2 due to the filler.

The addition of plasticiser affects the height and width of the loss factor peak across the temperature range. As shown in Figure 6.4, the peaks of the loss factor curve are shifted to lower temperatures as the amount of plasticiser is increased. The maximum value of loss factor is very high for unfilled butyl: composition 1 has a loss factor of 1.5 at 5℃ at 1000 Hz. A similar value can be seen for composition 8 (20 pphr carbon black and 40 pphr plasticiser) but the peak occurs at -20℃ and the loss factor falls below 0.25 at 40℃. Hence increasing the amount of plasticiser will still give a high peak value of loss factor but will lower the shoulder of the curve. However a smaller amount of plasticiser gives a broad loss factor peak over the temperature range with a lower maximum value.
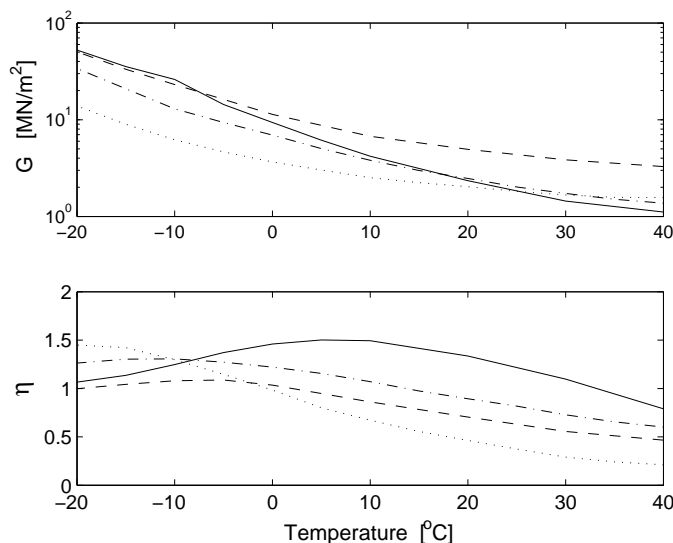
Figure 6.4: *Effect of plasticiser for constant loading of filler on dynamic properties of butyl rubber at 1 kHz. The propotions of filler and plasticizer in pphr are (−−) 20/10 (compound 4), (− · −) 20/20 (compound 7), (· · ·) 20/40 (compound 8) and (—) 0/0.*
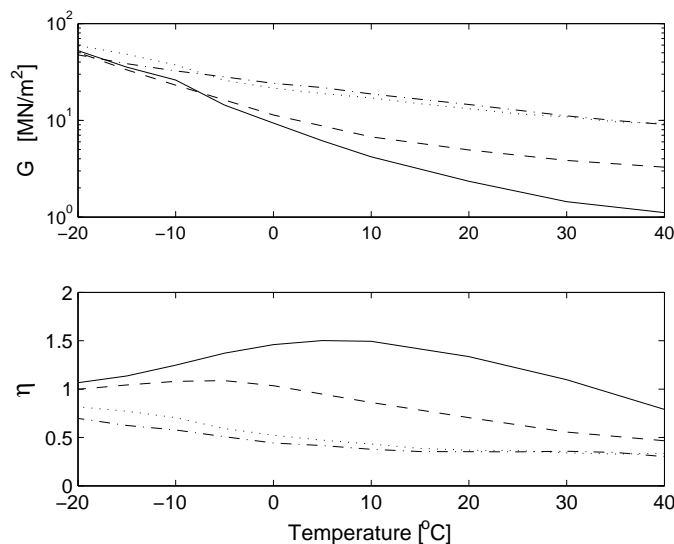
Figure 6.5: *Effect of increasing the filler and plasticiser loadings in fixed ratio and compared to pure butyl in pphr are(—) 0/0, (− −) 20/10 (compound 4), (· · ·) 60/30 (compound 5), (− · −) 80/40 (compound 3).*

Figure 6.5 shows the effect of increasing the carbon black and plasticiser levels in a fixed ratio. Pure butyl rubber is again shown for reference. As the carbon black and plasticiser loadings are increased, the shear modulus increases at higher temperatures but the loss factor reduces for all temperatures. It seems that at higher amounts of carbon black and plasticiser the dynamic properties change only very little, compounds 3 and 5 giving similar results. All loss factors are above 0.35. The slope of the shear modulus curve across the temperature range for 60/30 and 80/40 is less than for 20/10 but the shear modulus found is too high for direct use in the rail absorber application.

All the results of shear modulus and loss factor for this set of samples are shown in Figure 6.6, as a function of temperature at 1000 Hz. Two compounds in this preliminary study have promising dynamic properties; they are compound no 4 (20/10) and 7 (20/20). Their shear moduli fall between 3 and 7 MN/m² for temperatures between 10℃ and 40℃, and 5℃ and 15℃ respectively. Other compounds are either too stiff or too soft in this temperature range. However, all the compounds have values of shear modulus at -20℃ that are much too high.

Although Nashif *et al.* (1985) and Fletcher & Gent (1973) give results for a similar material (butyl), their results do not agree with each other as shown in Figure 2.42. These results are compared with those for butyl rubber 0/0 from the current measurements in Figure 6.7. The shear modulus of butyl rubber 0/0 is stiffer than the butyl studied by Fletcher & Gent (1973) but softer than that from Nashif *et al.* (1985), especially for temperatures less than 10℃. The loss factor peak occurs at 10℃ in the present measurements but at 0℃ and -10℃ in the results from the literature.
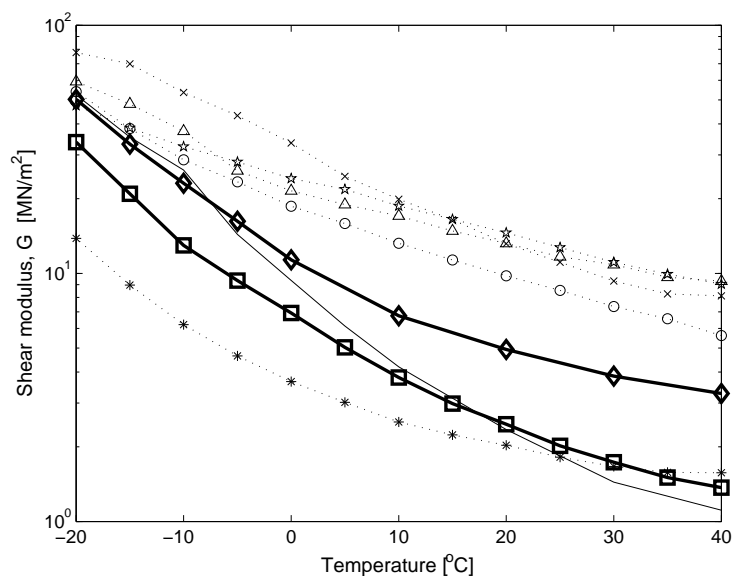
(a)
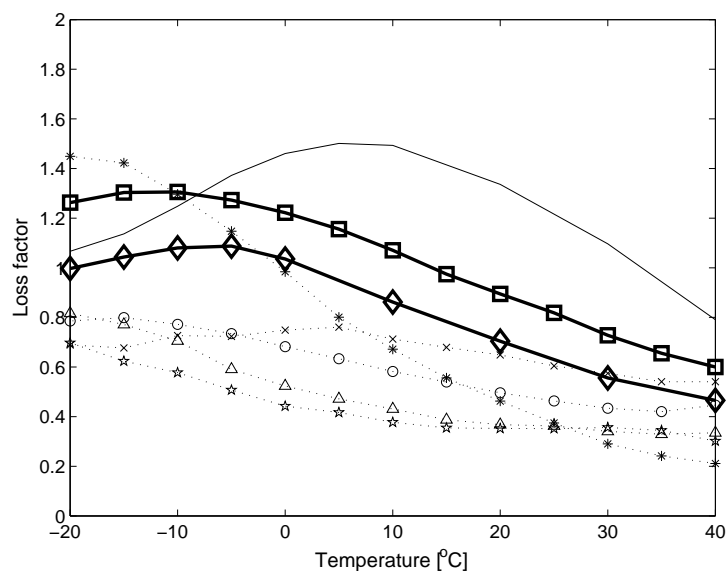
(b)

Figure 6.6: *The shear modulus and loss factor of butyl rubber for all the samples in set 1: (a) Shear modulus and (b) Loss factor. The butyl rubbers in weight, pphr are (—) 0/0 (compound 1), (◦) 50/20 (compound 2), (⋆) 80/40 (compound 3), (◇) 20/10 (compound 4), (△) 60/30 (compound 5), (×) 40/0 (compound 6), (□) 20/20 (compound 7) and (∗) 20/40 (compound 8).*

179
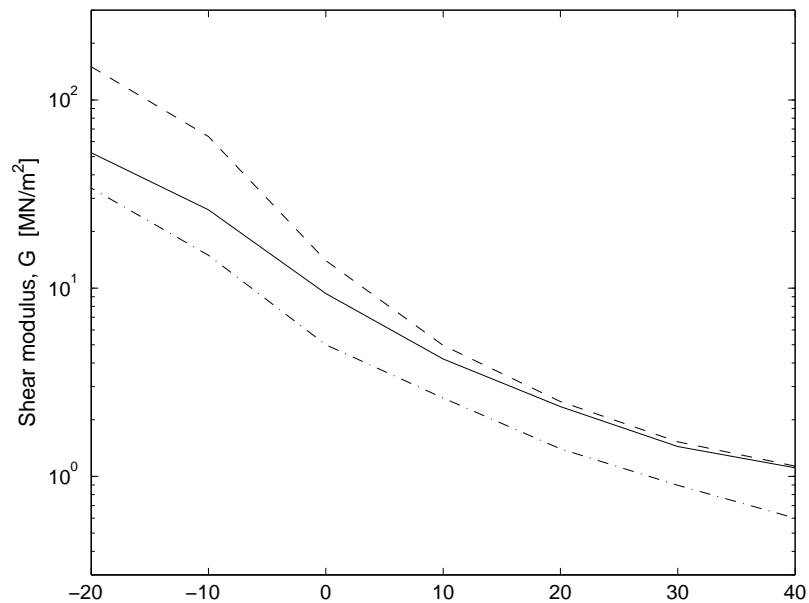
(a)
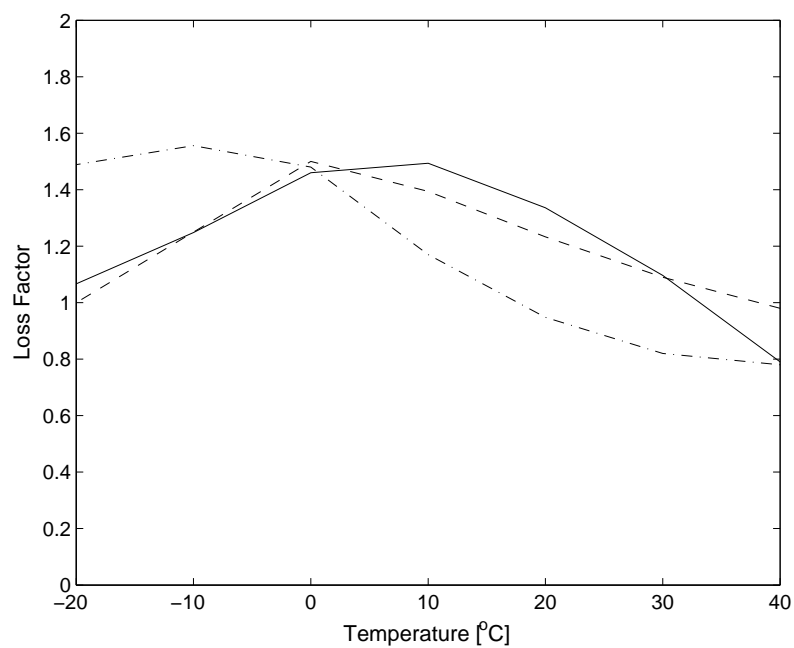
(b)

Figure 6.7: *(a) Shear modulus and (b) Loss factor at 1 kHz of butyl rubber (—) 0/0 (compound 1) are compared to butyl rubber which were studied by Nashif* et al. *(1985) (−−) and Fletcher & Gent (1973) (⋯).*

180
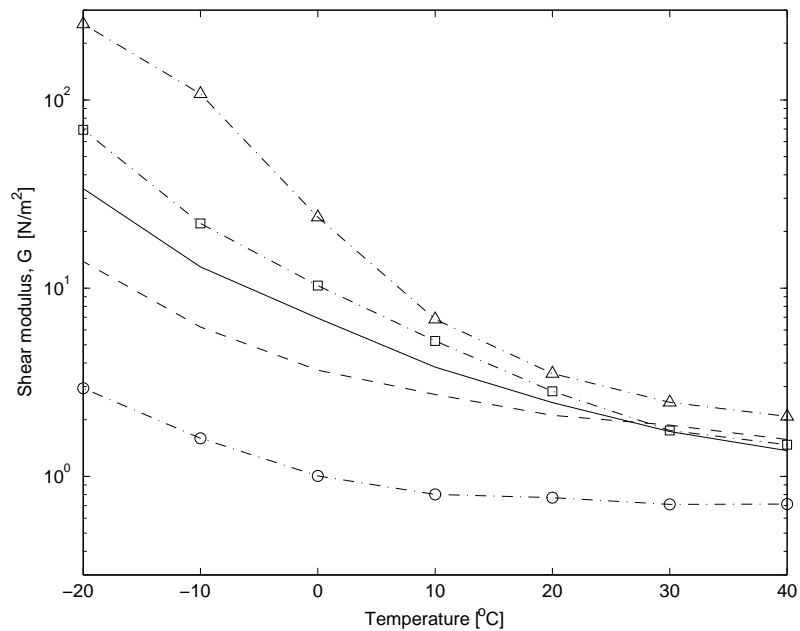
(a)
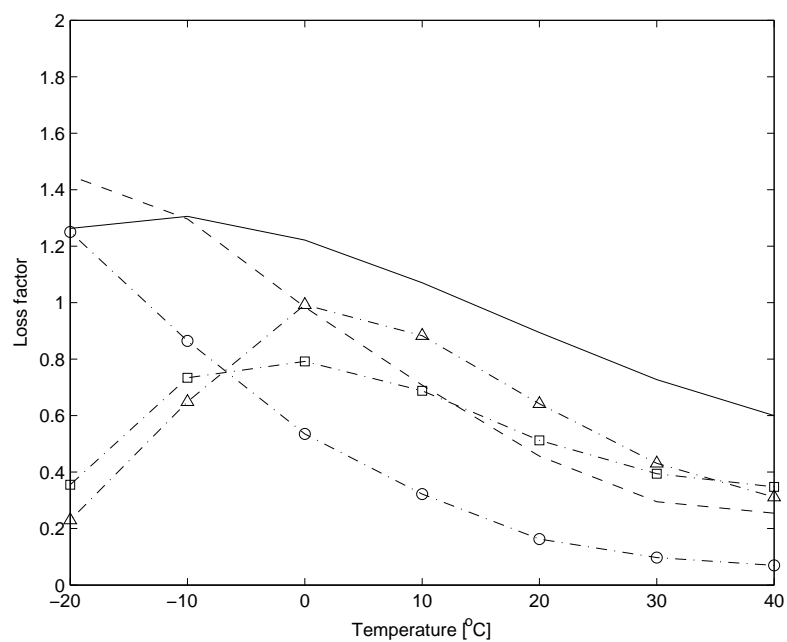
(b)

Figure 6.8: *(a) Shear modulus and (b) Loss factor at 1 kHz of butyl rubber (—) 20/20 (compound 7) and (−−) 20/40 (compound 8) are compared to (∘) NR , (□) PU (sample 7f) and (△) NBR blend (sample 23).*

Figure 6.8 shows the comparison of dynamic properties of best compounds, no 7 (butyl 20/20) and no 4 (20/40) with various other rubbers from the literature review in Chapter 2. From this comparison, butyl 20/20, butyl 20/40 and PU have properties closer to the requirement than the others. Compared with PU, the shear modulus of both butyl rubbers is slightly lower but as the temperature decreases, the shear modulus of both butyl rubbers increases at a lower rate than PU.

Most of the materials considered in this initial set have loss factors above the requirement (see Figure 6.8). Adding oil loading to butyl rubber has broadened the transition region and shifted the loss factor peak towards low temperatures.

Table 6.2 shows the temperature-weighted noise reductions for each of these materials predicted using the two-frequency absorber and model in Section 4.4. These are similar for the two butyl compounds and PU. Figure 6.9 shows the noise reductions plotted as function of temperature. This shows that the 20/40 butyl compound in particular is more effective at low temperatures than PU. Apart from NR, all these materials give noise reductions between 4 and 6 dB for temperatures above 5℃. At 10℃, the most common temperature found for the UK, 20/20 butyl gives the best noise reduction.

Table 6.2: *The average temperature-weighted noise reduction of butyl compounds set 1 and compared to NR, PU and NBR blend.*

No.	Samples	Avg. temp.-weighted noise reduction (based on UK weighting in dB(A))
1	B0/0	5.5
2	B50/20	4.0
3	B80/40	2.7
4	B20/10	5.7
5	B60/30	3.0
6	B40/0	2.9
7	B20/20	6.0
8	B20/40	6.0
	NR	3.4
	PU (sample 7*f*)	6.0
	NBR blend (sample 23)	5.2

The temperature-weighted average noise reductions for the materials in set 1 are shown in Figure 6.10. The noise reduction appears higher when the carbon black level is less than 40 pphr and the oil level above 10 pphr. In order to study this region in more detail, a more systematic approach is taken in the next section.
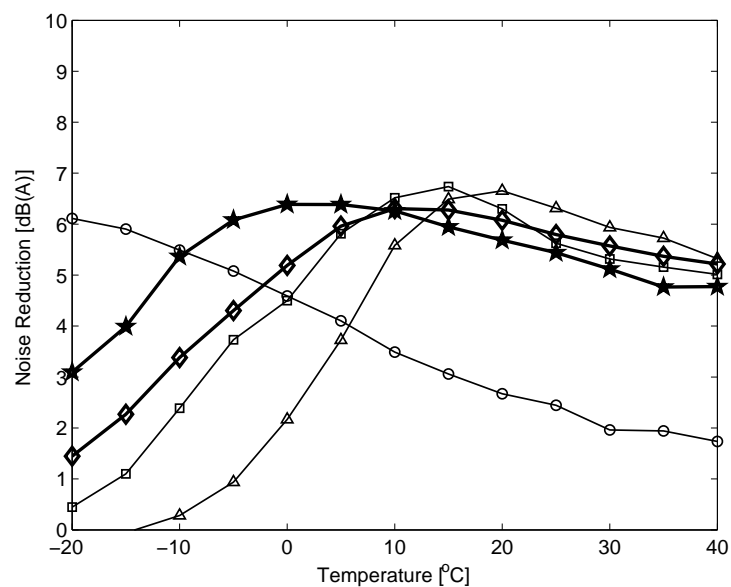
Figure 6.9: *The comparison of noise reduction of butyl (◇) 20/20 (compound 7) and (⋆) 20/40 (compound 8) to (○) NR, (□) PU and (△) NBR blend.*
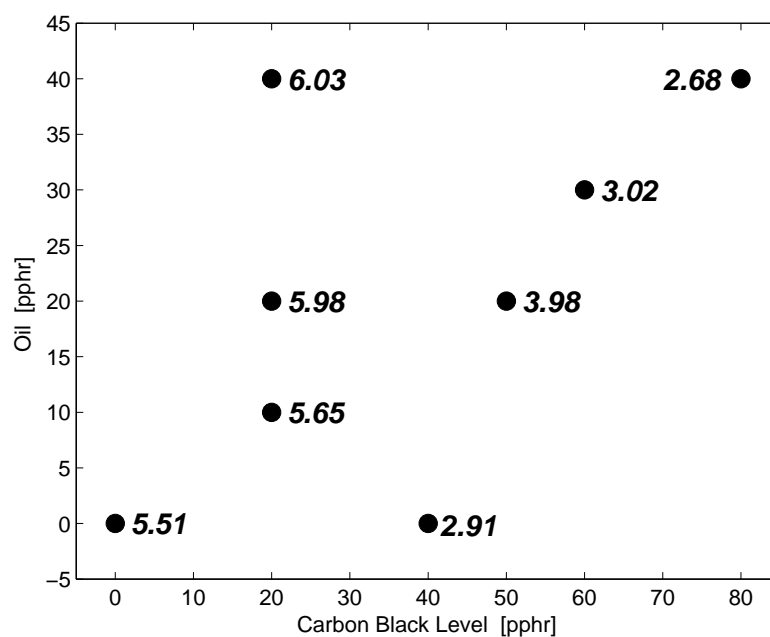
Figure 6.10: *The temperature-weighted noise reductions (dB(A)) for butyl rubber set 1.*

183

6.3 Design of experiment (DOE)

Following the initial experiments, an experimental design (DOE) procedure has been followed to determine the dependance on filler and plasticiser more systematically. The function of DOE is to characterize the relationship between one or more measured responses and a number of input variables (Montgomery, 1997). Using regression analysis, contour diagrams and response surfaces can be plotted allowing the optimum region to be identified. From this process an optimum formulation can be found using only a small number of actual mixes, thereby speeding up the study as well as reducing the cost of experiments.

There are several types of experimental design, such as full and fractional factorial designs, and response surface design including central composite design. The full factorial creates 2^k sample points with all possible combinations of the minimum and maximum values of the control parameters where k is the number of factors. Similar to full factorial, the fractional factorial uses a fraction, $1/2$ or $1/4$, of the runs specified by the full factorial design. The central composite design is a response surface design which determines different factor level combinations that provide the optimum response and identifies the optimum region. Appendix A describes these experimental design methods in more detail.

In this case, two variables, the proportions of filler and plasticiser, will be studied. Their variable level setting combinations will constitute the design points (experimental runs) of this design experiment for which Central Composite Design is used.

6.3.1 Central Composite Design

The use of Central Composite Design (CCD) (Montgomery, 1997) to study the effects of the properties of filler and plasticiser is illustrated in Figure 6.11. The CCD provides information on the direct additive effects of the studied variables (combinations of filler and plasticiser) and enables estimates of the location of a maximum or minimum in the experimental domain. To do this, the factorial terms (corner points) are added to star points.

The CCD for two variables requires 11 experimental runs. The dots in Figure 6.11 identify 11 design points (4 corner points, 4 star points and 3 centre points) and the numbers in the rectangles represent the order of experimental runs. Appendix A3 gives more details on the particular form of CCD which is used in this study.

For this study, two independent factors, representing carbon black (X_1) and oil (X_2) were investigated to determine the response variable. As discussed in Appendix A3 the
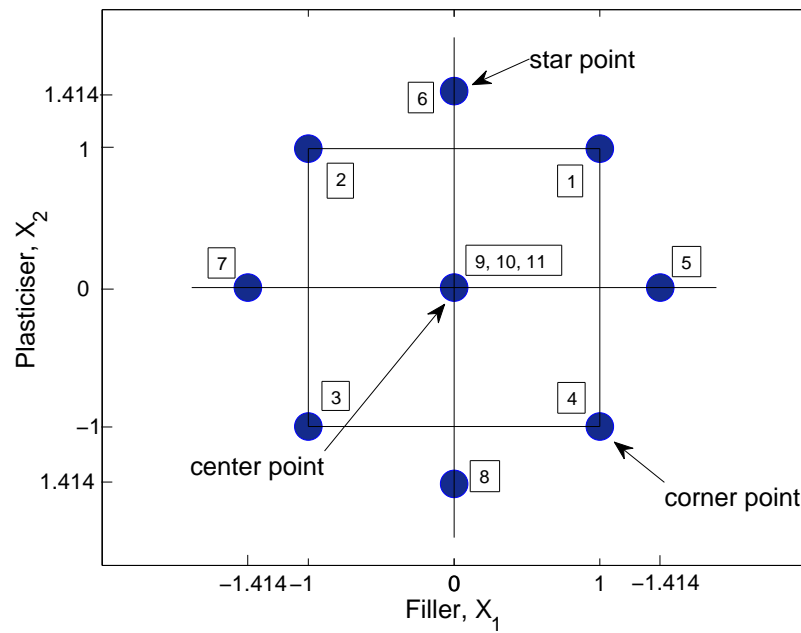
Figure 6.11: *The central composite design for two variables.*

proportions of filler and plasticiser were converted to 'coded' levels for use in DOE. These are listed in Table 6.3.

The response variable Y was chosen as the temperature-weighted noise reduction, as developed in Chapter 4.

Table 6.3: *Coding scheme two independent variables of the CCD.*

runs	Coded X_1	Coded X_2	Uncoded X_1,	Uncoded X_2
11	+1	+1	34	34
12	-1	+1	6	34
13	-1	-1	6	6
14	+1	-1	34	6
15	+1.414	0	40	20
16	0	+1.414	20	40
17	-1.414	0	0	20
18	0	-1.414	20	0
19a	0	0	20	20
19b	0	0	20	20
19c	0	0	20	20

6.3.2 Modelling

The influence of these two variables X_1 and X_2 will be evaluated using a second-order polynomial multiple regression model. For this, the 11 design points in the CCD are used

to estimate regression coefficients as given by

$$Y_i = \beta_0 + \beta_1 X_{i1} + \beta_2 X_{i2} + \beta_{12} X_{i1} X_{i2} + \beta_{11} X_{i1}^2 + \beta_{22} X_{i2}^2 \tag{6.1}$$

where Y_i is the variable being predicted (noise reduction) and X_1 and X_2 are the predictor variables in the equations. A total of six coefficients are determined using a least-squares fit to the data at the 11 design points.

Once the response equations are generated these can be used to allow predictions to be made for combinations not actually evaluated. MATLAB software is used for conducting regression analysis and generating contour plots and three-dimensional response surface diagrams.

6.3.3 Material composition - set 2

A second set of butyl formulations was chosen based on the DOE approach. A wide range of proportions of filler and plasticiser was selected as listed in Table 6.4. Figure 6.12 shows these combinations (rectangular markers) as well as the combinations considered in the initial study (circles). This new set was centred on 20/20 which was found to give a high noise reduction in Figure 6.10. Although butyl 20/40 gave the highest noise reduction, it was anticipated that the higher loading of oil in the compound may give problems in mixing. Therefore, 40 pphr was selected to be the maximum loading of oil and the maximum loading of filler was also 40 pphr.

Table 6.4: *Ratio of fillers and plasticisers in butyl compounds set 2 (weight in pphr).*

Compound Ingredients	11	12	13	14	15	16	17	18	19a	19b	19c
Polymer	100	100	100	100	100	100	100	100	100	100	100
Filler	34	6	6	34	40	20	0	20	20	20	20
Plasticiser	34	34	6	6	20	40	20	0	20	20	20

Unfortunately, the mixing of these materials was unsuccessful. The materials became very sticky, especially the compounds with a high level of plasticiser such as samples 11, 12, 16 and 17. It was found that the oil did not blend smoothly with the butyl rubber and filler. Several actions were carried out to improve the mixing process. For example, adding the oil gradually to the butyl compound, lowering the mixing temperature to 20℃, reducing the rotor speed and increasing the mixing time. After taking these actions, some improvement was seen in the mixing process. However, the material was still sticky and hardly manageable and the dispersion of the curative in the compound was questionable. Therefore, no further work was carried out on this set of materials.
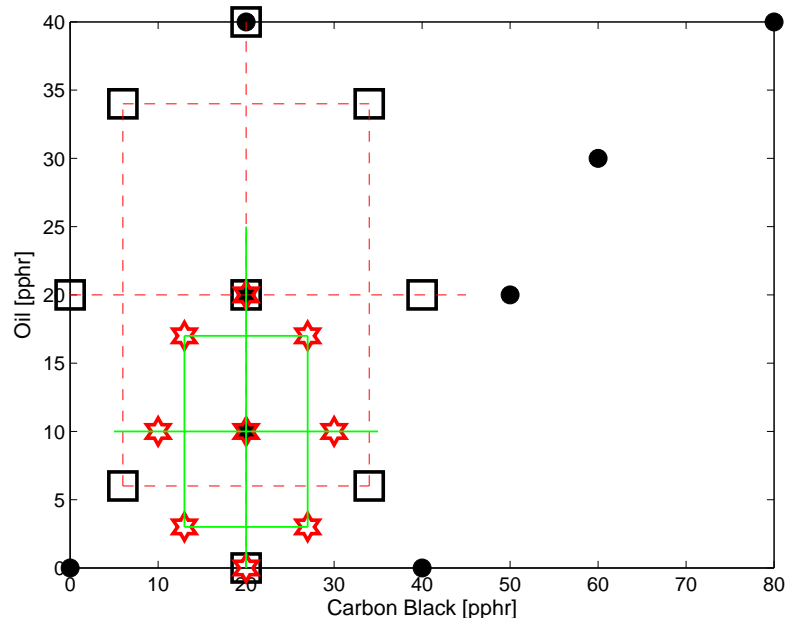
Figure 6.12: *The Central Composite Designs (CCD) for the butyl compound. Three sets of compounds have been studied, circles (set 1), rectangles (set 2) and stars (set 3).*

6.3.4 Material composition - set 3

Due to the problems that occurred in producing set 2, the range of the DOE area was reduced to produce a new set of butyl compounds as shown in Figure 6.12 (stars at each point). The levels of filler and plasticiser are listed in Table 6.5, from which it is seen that the levels of plasticiser were reduced by half from those of set 2 and the range of filler was also reduced. A similar mixing process was adopted and this batch of butyl rubbers was successfully mixed. The cure characteristics of the compounds were determined in a Monsanto Rheometer. A similar vulcanizing process was carried out to that used previously.

Table 6.5: *Ratio of fillers and plasticisers in butyl compounds set 3 (weight in pphr).*

Compound Ingredients	21	22	23	24	25	26	27	28	29a	29b	29c
Polymer	100	100	100	100	100	100	100	100	100	100	100
Filler	27	13	13	27	30	20	10	20	20	20	20
Plasticiser	17	17	3	3	10	20	10	0	10	10	10

6.4 Results and discussions

The samples were tested for dynamic characteristics over temperature range -20℃ to 40℃ and for frequencies up to 5000 Hz. The tests were carried out using the modified ISVR

test rig. A test procedure similar to that described in Section 5.1 was adopted to measure the dynamic properties. To measure the dynamic properties at various temperatures, the test rig was placed in the temperature cabinet.

Figure 7.2 shows example results for samples at the centre of the CCD, 29a, 29b and 29c. The shear modulus and loss factor obtained follow the same trend as previous results in set 1. The shear modulus changes between -10℃ and 40℃ by a factor 13 at 1000 Hz. There are broad peaks in the loss factor curves but they are above the target range 0.25 and 0.4 at all temperatures and frequencies. These loss factors are mostly quite high, which means the modulus is quite sensitive to changes in temperature, as can be seen.

The shear moduli presented are repeatable for the selected temperatures. This means that the results presented can be considered to be reliable. In addition, the measured shear modulus is compared with values predicted using Equation (3.13) as presented in Figure 6.14. In these results the measured value of modulus and loss factor at 1 kHz are used to determine the modulus at other frequencies. Both measured and predicted values are similar over much of the frequency range. However, as seen in Figure 6.13(a) the measured values at 300 Hz are unreliable at low temperatures.

The shear modulus and loss factor for all samples at 1000 Hz are plotted in Figure 6.15. The slope of the shear modulus versus temperature is high, the ratio between the shear modulus at -10℃ and 40℃ being between 15 and 26. Having such a large slope means that the noise reduction can be expected to vary considerably across the temperature range, especially below 0℃.

Using the measured data of sample 26 (20/20), the decay rate of the two-frequency absorber is estimated for various temperatures and compared with the undamped behaviour. This is shown in Figure 6.16. The decay rates vary significantly from low to high temperatures. The peaks at the tuning frequency are above 5 kHz at -20℃. They move down to lower frequencies as the temperature increases.

Based on this decay rate, the noise reductions of the rail damper as a function of temperature are calculated and summarised in Table 6.6. For all samples the maximum noise reduction is between 6.1 and 6.7 dB(A). The best results are found for butyl sample 25 (30/10), at 35℃. Although sample 25 has the highest noise reduction, it will not perform well as the average temperature for the UK is about 10℃. For this, it is therefore preferable to use the temperature-weighted noise reduction. This is also presented in Table 6.6.

From this estimation, samples 21 (27/17), 22 (13/17), 26 (20/20) and 27 (10/10) give the most significant noise reductions. As shown in Figure 6.17 the shear modulus and loss factor of these samples have similar trends as those for samples in set 1. For instance,
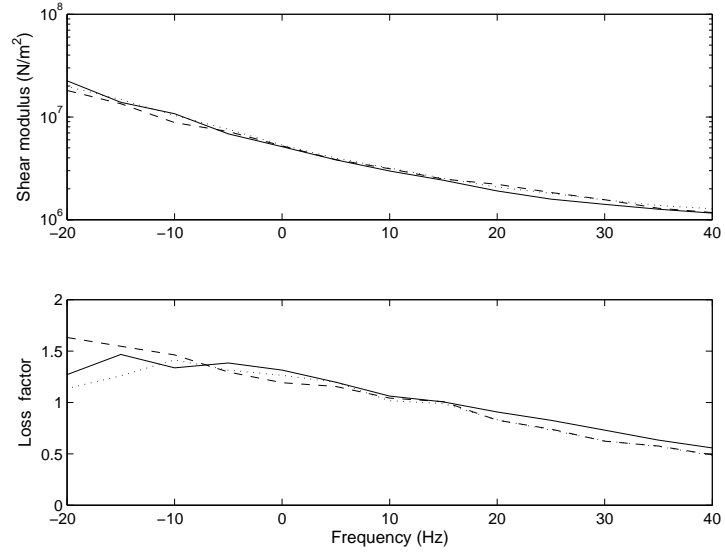
(a)
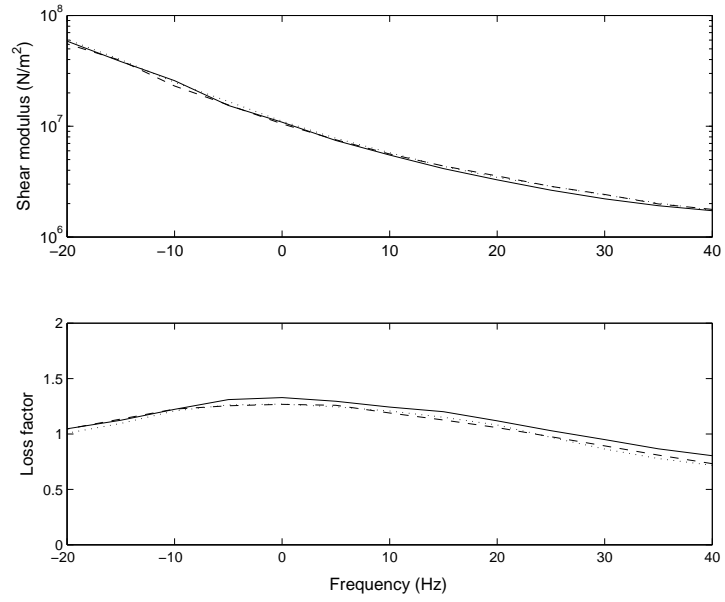
(b)

Figure 6.13: *The shear modulus and loss factor of butyl rubbers at the centre point, (—) 29a, (···) 29b and (−−) 29c which are measured at (a) 0.3 kHz and (b) 1 kHz.*
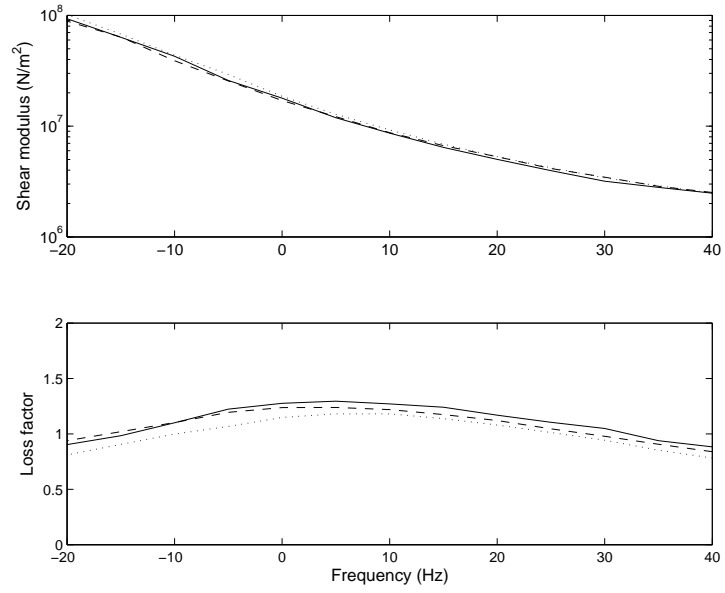
(c)
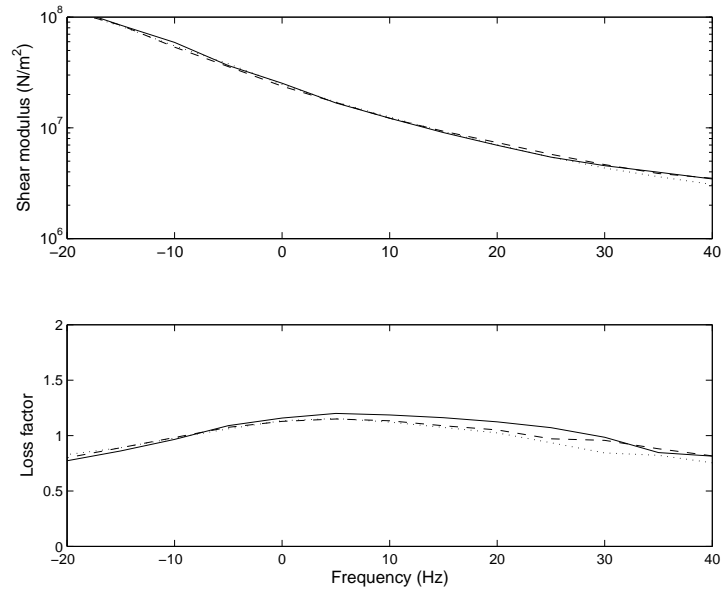
(d)

Figure 6.13: *(Continued). (c) 2 kHz and (d) 3 kHz.*

190
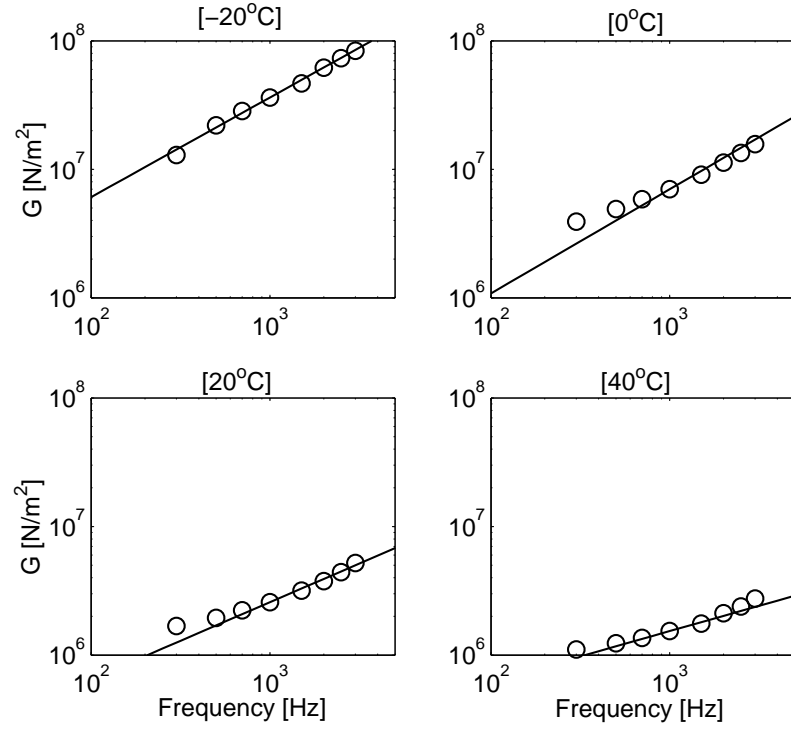
Figure 6.14: *The comparison of measured (○) and predicted (—) values of shear modulus for butyl sample 26 (20/20), which is are based on Eq. (3.13). The measured shear modulus and loss factor are taken at 1 kHz.*

Table 6.6: *The noise reductions for butyl rubber in set 3.*

Particulars	21	22	23	24	25	26	27	28	29a	29b	29c
Filler [pphr]	27	13	13	27	30	20	10	20	20	20	20
Plasticiser [pphr]	17	17	3	3	10	20	10	0	10	10	10
Max. noise reduction [dB(A)]	6.4	6.2	6.3	6.6	6.7	6.3	6.1	6.4	6.2	6.3	6.3
Occurance temp. [℃]	20	10	20	35	35	15	15	30	20	20	20
Temp.-weighted noise reduction [dB(A)]	5.7	5.9	5.6	4.2	4.8	5.9	5.7	4.5	5.5	5.5	5.5
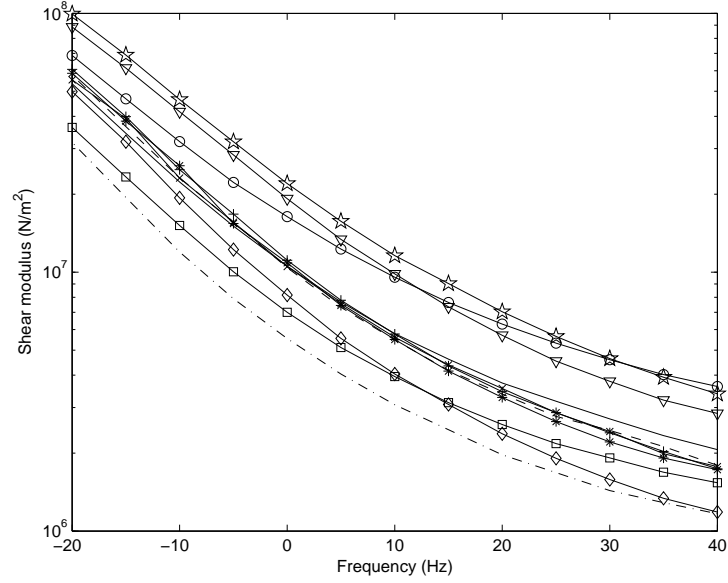
(a)
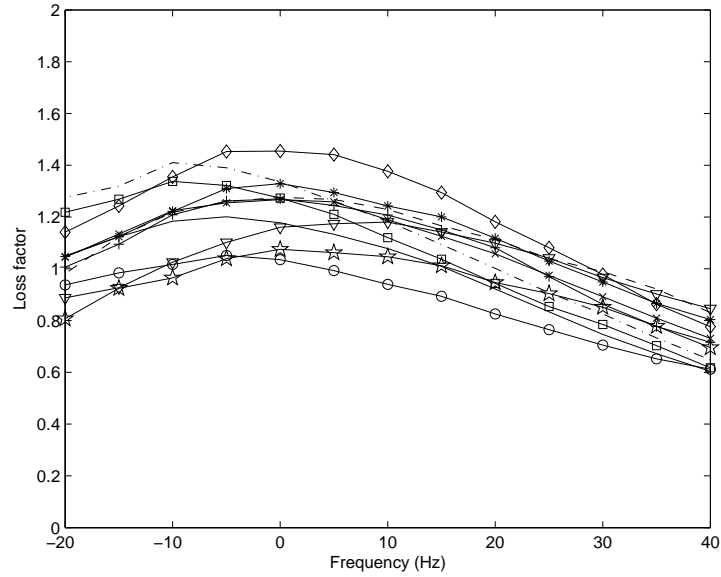
(b)

Figure 6.15: *(a) The shear modulus and (b) loss factor of butyl rubber for all samples in set 3. The samples are (—) 21 (27/17), (− · −) 22 (13/17), (−−) 23 (13/3), (⋆) 24 (27/3), (∘) 25 (30/10), (□) 26 (20/20), (◇) 27 (10/10), (▽) 28 (20/0), (∗) 29a (20/10), (+) 29b (20/10), (×) 29c (20/10).*
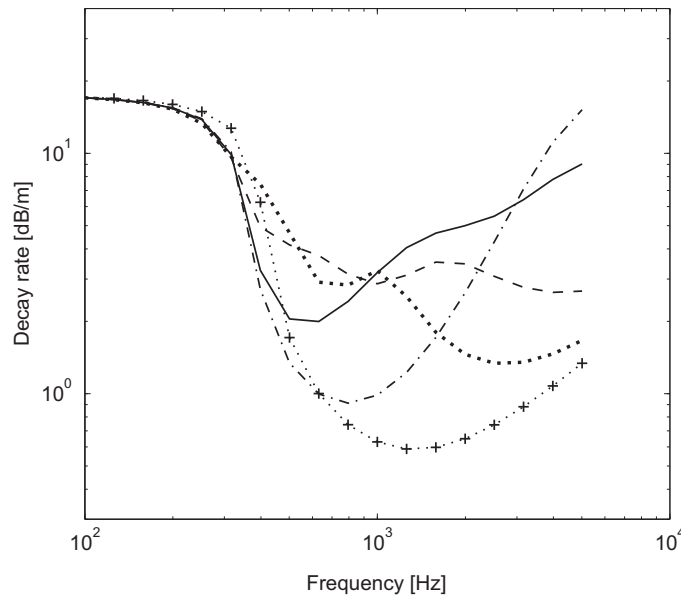
Figure 6.16: *The decay rate of sample 6 (20/20) using Timoshenko beam (2-stacked mass) model for various temperatures. (· · ·) 40℃, (− −) 20℃, (–) 0℃, (− · −) -20℃ and (+) undamped*

samples 21 (27/17) and 22 (13/17), which have same levels of plasticiser but changing level of filler, result in an increase in shear modulus and a decrease in loss factor as the level of filler is increased. Samples 26 (20/20) and 27 (10/10), have the same ratio of filler to plasticiser. Increases in both variables do not change the shear modulus much but the loss factor of sample 27 (10/10) is higher for temperatures above -5℃ than for sample 26.

Figure 6.18 shows the reduction of noise for these four compounds at various temperatures. These materials are effective for temperatures greater than 0℃ and less so as temperature reduces. This is due to the high slope of the shear modulus. The maximum noise reduction is shifted to the left as the level of filler is increased; its peak value is also reduced slightly. As the temperature decreases, these butyl compounds lose their effectiveness as the stiffness becomes too high and the tuning frequency also becomes too high.

Figure 6.19 summarises the temperature-weighted noise reduction found, along with the regression surface. The best compounds in the study have plasticiser greater than 10 pphr and filler between 10 and 20 pphr of which samples 22 (13/17) and 26 (20/20) gave the best results. As shown in Figure 6.18, the 20/20 compound is good at temperatures 0℃ to 40℃. However, most of the compounds have similar values of shear modulus at -20℃ where they lose their effectiveness. Therefore, a different approach is required to solve this problem, particularly for use in colder environments such as Sweden.

Finally, the butyl rubber combination (20/20) in set 3 was compared with butyl sample (20/20) in set 1 in Figure 6.20 in terms of predicted noise reduction. They have similar
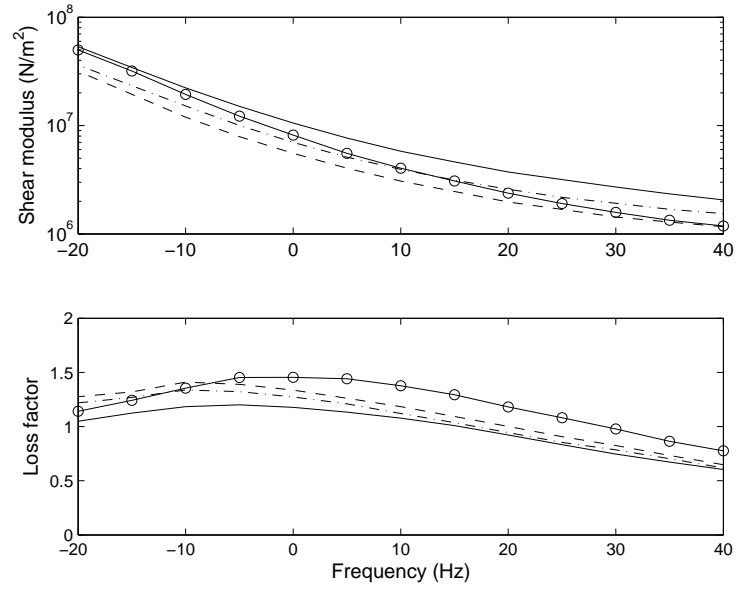
Figure 6.17: *The shear modulus and loss factor for butyl samples (—) 21 (27/17), (−−) 22 (13/17), (− · −) 26 (20/20) and (· · ·) 27 (10/10) for various temperatures.*
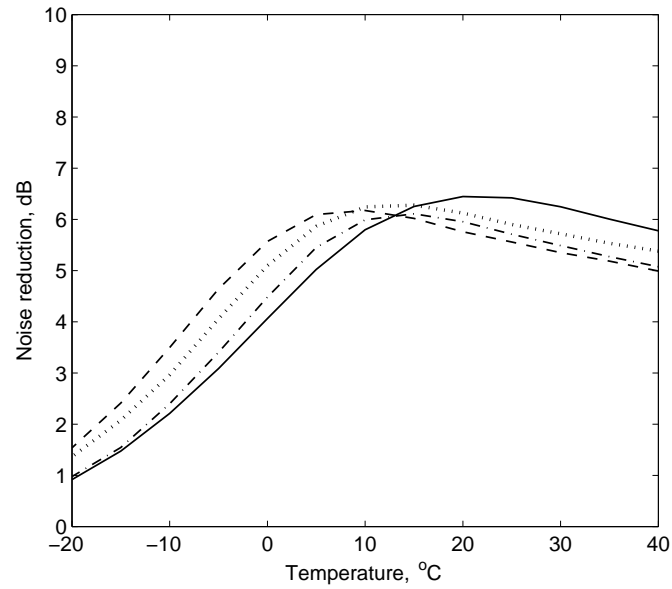
Figure 6.18: *The reduction of A-weighted noise level for butyl samples (—) 21 (27/17), (−−) 22 (13/17), (· · ·) 26 (20/20) and (− · −) 27 (10/10) for various temperatures.*
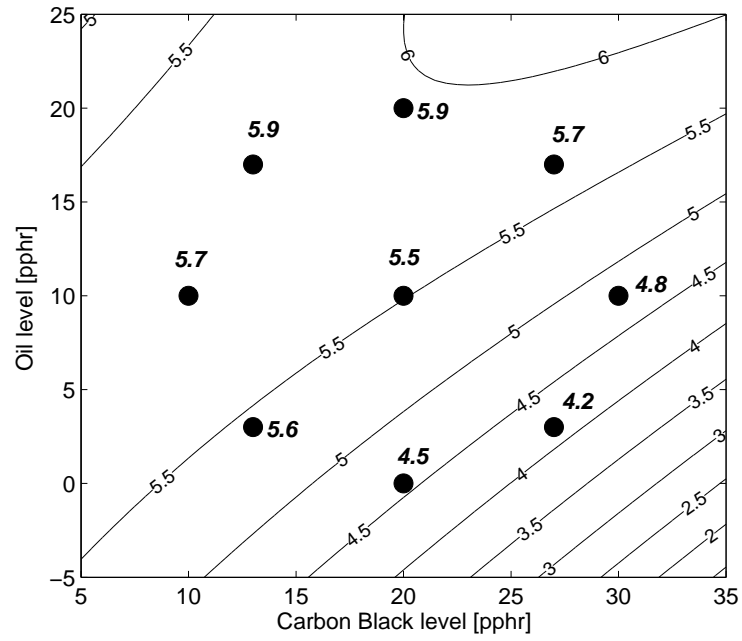
(a)
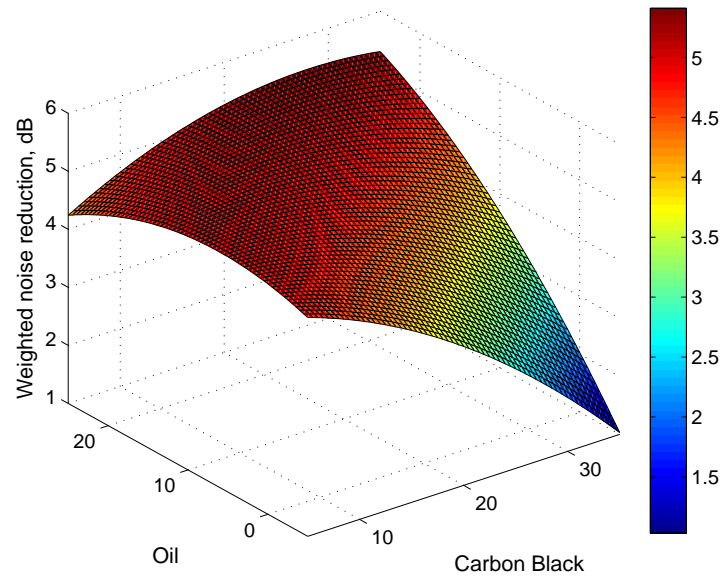
(b)

Figure 6.19: *(a) Contour plot and (b) Response surface of temperature-weighted noise reduction (dB(A)) plotted against filler and plasticiser levels for butyl rubber set 3.*

trends and only slight differences, which may due to the influence of the test rig. The materials in set 1 were tested using the unmodified test rig, whereas the materials in set 3 were tested using the modified test rig. Generally, however their results are comparable.

The best results from set 3 show that the maximum weighted noise reduction of 5.9 dB(A) can be achieved for temperature range -20℃ and 40℃. Based on the contour plot, the noise reduction of this butyl rubber can be improved by combining filler and plasticiser in the range of 15 - 35 pphr and 10-25 pphr respectively.
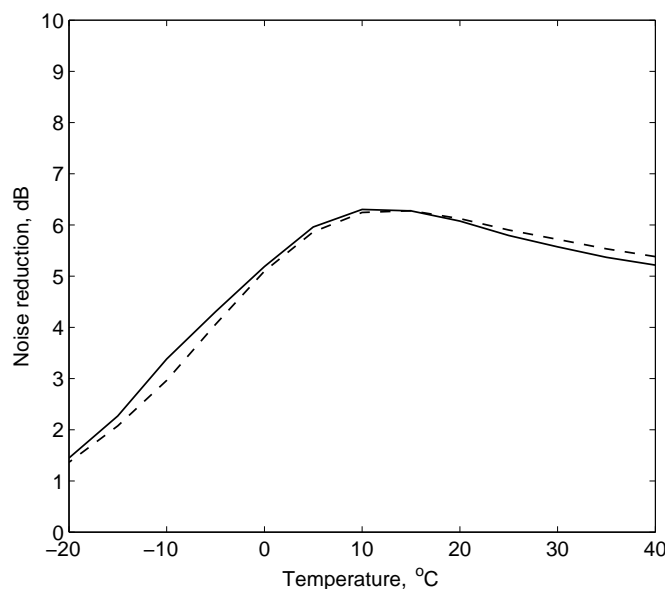
Figure 6.20: *The reduction of A-weighted noise level for butyl sample 6 in set 1 (—) (20/20), 26 in set 3 (−−) (20/20) for various temperatures.*

6.5   Conclusions

The introduction of plasticiser and filler helps to improve the dynamic properties of butyl rubber in the temperature range considered. The filler increases the shear modulus at the higher temperatures but decreases the loss factor peak and increases the tail of the loss factor curve at low and high temperatures which keeps the loss factor above 0.25. The plasticiser decreases the shear modulus at low temperatures. The plasticiser also helps to increase the peak value of the loss factor and broaden the transition region, but a large amount of plasticiser will lower the tail of the loss factor curve and thereby decrease the value of loss factor at high temperatures.

The experimental design approach has been used to evaluate different levels of filler and plasticiser in butyl compositions. The DOE approach is efficient and gives enough information of the variable effects for a small number of experiments.

Butyl rubber in combination with 20 pphr filler and 20 pphr plasticiser is found to be the best material tested so far. When comparing this butyl rubber with the other potential rubbers, it is seen that the butyl rubber is suitable for use in the rail absorber giving high noise reductions between 0℃ and 40℃. For butyl, the best combinations which gave temperature weighted noise reduction for the UK above 5.5 dB(A) are samples 21 (27/17), 22 (13/17), 26 (20/20) and 27 (10/10). However the loss factors are generally rather higher than desirable if a wider temperature range is to be considered. Consequently in the next chapter an alternative material is considered.

Chapter 7

Dynamic-mechanical characteristics II- Ethylene-propylene-diene monomer (EPDM)

7.1 Introduction

In the previous chapter it has been found that butyl rubber with 20 pphr carbon black and 20 pphr oil gives the best temperature weighted noise reduction of 5.9 dB(A). However, it complied only partly with the target specification for the rail absorber. The dynamic properties of this butyl are satisfactory over the range of temperature from 40℃ to 0℃. Below 0℃, however, the effect fell considerably so the material become too stiff.

In this chapter an alternative material is investigated: Ethylene-propylene-diene monomer (EPDM) rubber. This rubber is a thermorheologically simple material (Ginic-Markovic *et al.*, 2000) allowing the time temperature superposition principle to be used. It was observed that the slope of its stiffness with temperature is smaller   (Ginic-Markovic *et al.*, 2000) than the butyl compounds, which means it is less sensitive to changes of temperature. Nevertheless, its damping is reasonably high though lower than butyl. For these reasons, EPDM rubber is considered for further investigation.

As stated in Chapter 2, unfilled EPDM has a low stiffness and low tensile strength (Eggers & Schmmer, 1996). It must therefore be reinforced to achieve useful properties. In this investigation high loadings of filler are employed to ensure the required reinforcement for strength and mechanical properties. In addition, high loadings of plasticiser are also used to improve wetting and incorporation of the very high filler loadings as well as to plasticise the polymer. To tie the EPDM chains together, additives are added in the vulcanization process.

This chapter focuses on the effect of various loadings of carbon black and oil in the EPDM compounds on their dynamic stiffness and damping across the temperature range considered. The dynamic shear test is used as in the previous chapter. The measured shear modulus and loss factor are used to determine the weighted noise reduction based on the UK temperature distribution, from which the optimum formulation will be sought.

7.2 Initial investigation - EPDM set 1

An initial investigation was carried out with two mixes of EPDM to get an idea of the performance properties of the final EPDM compound and also the processing behaviour of the compound. These two mixes of EPDM compounds, with filler and plasticiser, are listed in Table 7.1. Carbon black filler type N330 was added to the EPDM compounds to reinforce and increase both hardness and stiffness. High viscosity paraffinic oil, Sunpar 2280, is employed to improve heat resistance and minimize shrinkage. As shown in the table, mix 2 has half the amount of carbon black and oil compared with mix 1. However, mix 2 also includes another type of filler called nanofil 9 which was believed could modify the mechanical properties, especially by broadening the transition region.

These mixes were processed using a Plasticorder internal mixer with rotor speed 80 rpm at 50℃ mixing temperature. Due to the high temperature stability, these compounds were cured using DiCumyl Peroxide (DCP). To determine the curing times and condition, rheometer tests were carried out which indicated similar processing properties as butyl, with slightly longer curing times because of the large amounts of carbon black. The EPDM compound was vulcanized in a steam press at 160℃ for 30 minutes.

A similar test procedure to that described for the butyl compounds in Chapter 6 was used. The dynamic properties of these initial mixes were only measured at 20℃ as a function of frequency and tested using the unmodified test rig. The results are shown in Figure 7.1. The more highly loaded compound produced a higher shear modulus. Both compounds had similar loss factors of around 0.25 to 0.3.

Comparing these dynamic properties of EPDM with the results for the butyl compounds (Chapter 6), the shear modulus of the EPDM compounds is higher. However the loss factor for the EPDM compounds was closer to the required value for the rail absorber. The effect of nanofil 9 in the EPDM compound did not help much in this area, so it was not considered worthwhile for further material development.

Table 7.1: *Ratio of fillers and plasticisers in EPDM compound initial test - set 1 (material weight in pphr).*

	Mix No.(pphr)	
Materials	1	2
EPDM	100	100
Carbon black (N330)	240	120
Oil (Sunpar 2280)	160	80
Nanofil 9	-	10
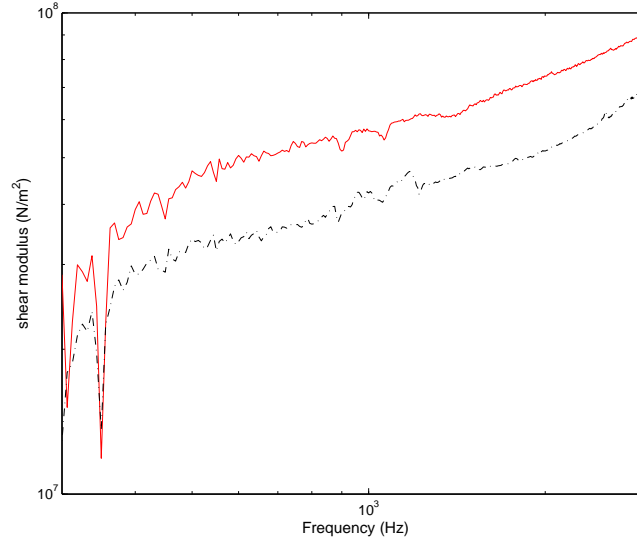
(a)
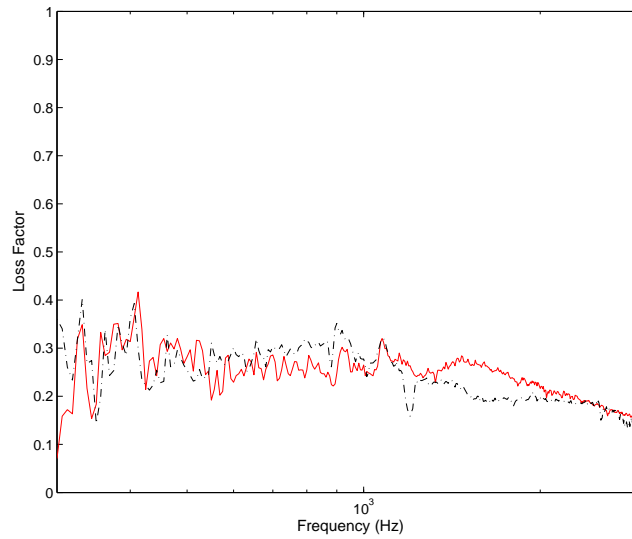
(b)

Figure 7.1: *(a) The shear modulus and (b) loss factor of EPDM; (—) mix 1 with high level of carbon black and oil, and (− · −) mix 2 with lower level of carbon black and oil including nanofil 9.*

7.3 EPDM composition - set 2

7.3.1 Compounds

To extend this work, a range of different EPDM compounds has been produced, varying in their proportions of carbon black and oil. This is based on a DOE approach similar to that used in Chapter 6. Nine proportions of carbon black and oil were chosen covering a wide range, as shown in Table 7.2. In order to incorporate all the particles and the curing agent DCP into the EPDM rubber compound, a Plasticodar internal mixer and a two-roll mill machine were employed. A rotor speed of 70 rpm and processing temperature of 60℃ were used.

However, these EPDM compounds had early scorch or premature vulcanization problems due to heat unavoidably generated during the vulcanization process. The conflict of EPDM with finer particle size blacks and large loads of filler with the peroxide cure, may also cause the scorch thereby producing uneven surfaces on the finished product. These EPDM compounds could not be processed further.

Table 7.2: *Ratio of fillers and plasticisers in EPDM compound set 2 (material weight in pphr).*

Materials	Mix No. (material weight in pphr)										
	11	12	13	14	15	16	17	18	19a	19b	19c
EPDM	100	100	100	100	100	100	100	100	100	100	100
Filler	216	104	104	216	240	160	80	160	160	160	160
Plasticiser	188	188	132	132	160	200	160	120	160	160	160

To overcome this problem, a sulphur cure was used instead of the peroxide cure in the EPDM compounds. Similar proportions of carbon black and oil were used, as shown in Table 7.2. Other ingredients such as zinc oxide and stearic acid are also included in all sulphur-vulcanized EPDM compounds as part of the vulcanization system. A similar mixing and vulcanization process was used except the curing agents, sulphur, mercaptobenzothiazole (MBT) and tetramethyl thiuram disulphide (TMTD) were added to the EPDM compound in a two-roll mill machine.

The dynamic test was performed on the modified ISVR test rig for a temperature range 40℃ and -20℃ and frequency range up to 5 kHz. The tests were carried out three times at each temperature in each case from 40℃ to -20℃ with an interval of 5℃.

7.3.2   Results and discussion

Figure 7.2 shows example results for samples 19a, 19b and 19c at the centre point of the CCD. This shows that shear modulus and loss factor at 0.3, 1, 2 and 3 kHz. The loss factor is within the target range and it is almost constant above 0℃, increasing at lower temperatures. The results for these three samples are similar except for 0.3 kHz where slightly erratic data is observed.

The shear modulus and loss factor for all samples are plotted in Figure 7.3 against temperature, based on the measurements at 1000 Hz. The ratio between the shear modulus at -10℃ and that at 40℃ is between about 2.5 and 3.4. Having this kind of slope will result in much less variation in the noise reduction across the temperature range than for butyl. However, the shear modulus is mostly much higher than the target values. As seen in the figure, two samples, 17 (80/160) and 12 (104/188), have the lowest shear modulus. These samples are among the lowest proportions of the carbon black. The loss factor of sample 17 increases more rapidly at low temperature whereas the loss factor of sample 12 stays low until -5℃.

As a check of the consistency of the results presented, the measured data is compared with predictions, calculated using equations (3.13) based on the modulus and the loss factor at 1 kHz. Figure 7.4 shows results for sample 17 (80/160). The predicted value is similar to the measured results.

7.3.3   Decay rate and noise reduction

Comparing the shear modulus and loss factor results for EPDM illustrated in Figure 7.3 with these in Figure 6.15 for the butyl compounds, the loss factor for EPDM is much lower than for butyl while the modulus varies less rapidly with temperature. The effect of these results can be seen in the decay rates predicted for the rail absorber based on EPDM and butyl.

Figure 7.5 shows the decay rate for EPDM sample 17 (80/160) at various temperatures with the undamped track shown for comparison. At 20℃, both peaks of the decay rate occur at a slightly lower frequency than intended (630 and 1350 Hz) and at 0℃ these peaks occurred at slightly higher frequency. Hence the shear modulus of this material is close to the target value. Sharp peaks are found in the decay rate around 6.5 dB/m (20℃), due to the low loss factor of the EPDM. In contrast, butyl rubber has a high value of loss factor which results in a wider peak of decay rate but the peak is lower at around 2.5 dB/m, as shown in Figure 6.16.
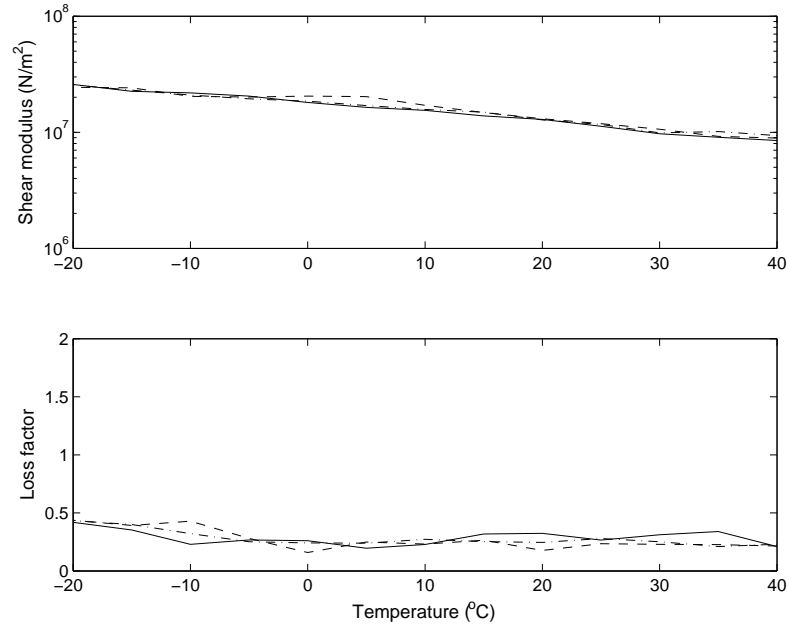
(a)
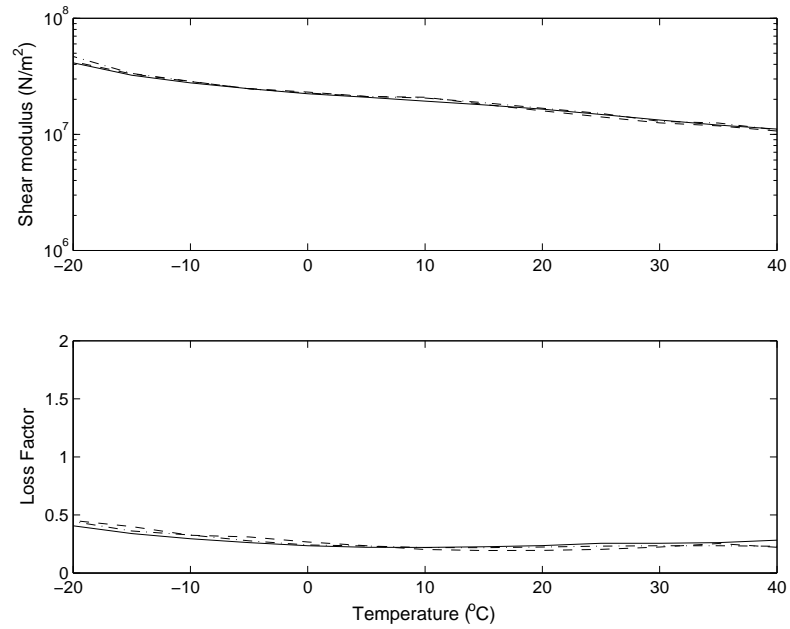
(b)

Figure 7.2: *The shear modulus and loss factor of EPDM rubbers at the centre point, (—) 19a, (···) 19b and (− −) 19c which are measured at (a) 0.3 kHz and (b) 1 kHz.*
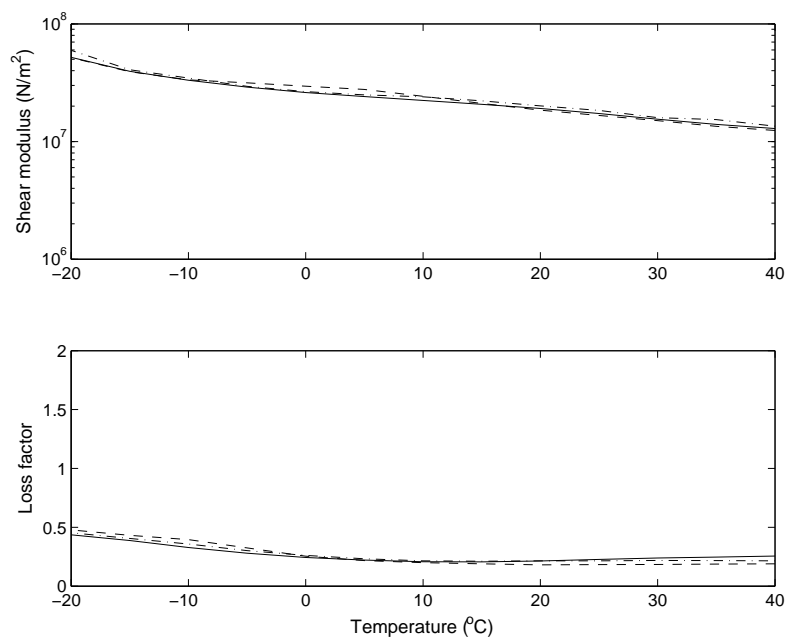
(c)
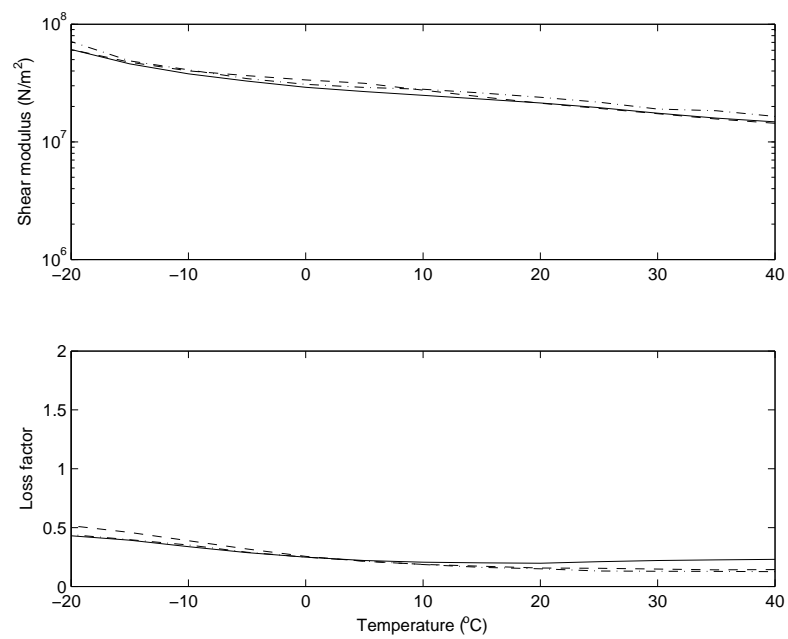
(d)

Figure 7.2: (Continued). (c) 2 kHz and (d) 3 kHz.
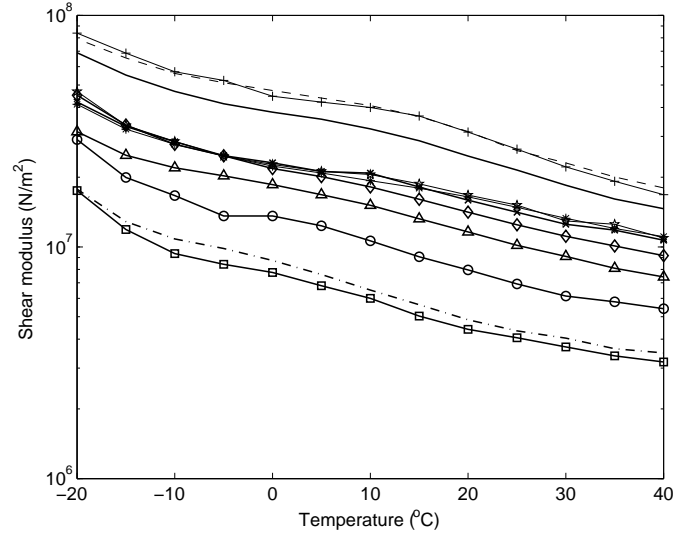
(a)
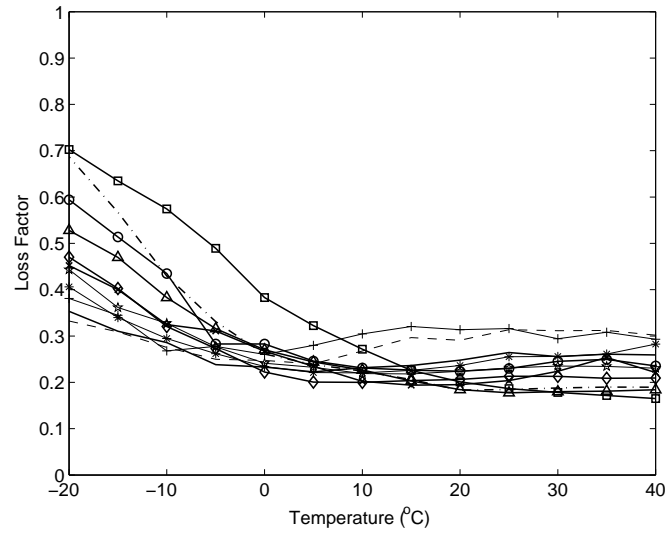
(b)

Figure 7.3: *(a) The shear modulus and (b) loss factor of EPDM at various frequencies across the temperature range; (—) sample 11 (216/188), (···) sample 12 (104/188), (○) sample 13 (104/132), (+) sample 14 (216/132), (−−) sample 15 (240/160), (△) sample 16 (160/200), (□) sample 17 (80/160), (◇) sample 18 (160/120), (∗) sample 19a (160/160), (⋆) sample 19b (160/160), (×) sample 19c (160/160).*
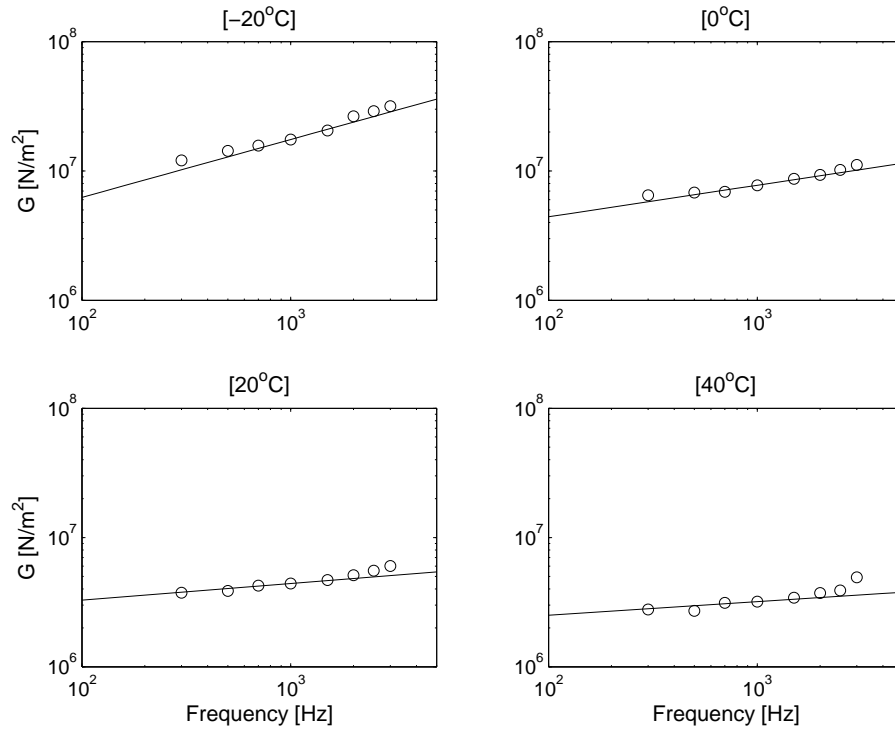
Figure 7.4: *The comparison of measured (◦) and predicted values (–). The measured values taken at 1 kHz of EPDM sample 17 (80/160) and predicted values are based on equations (3.13).*
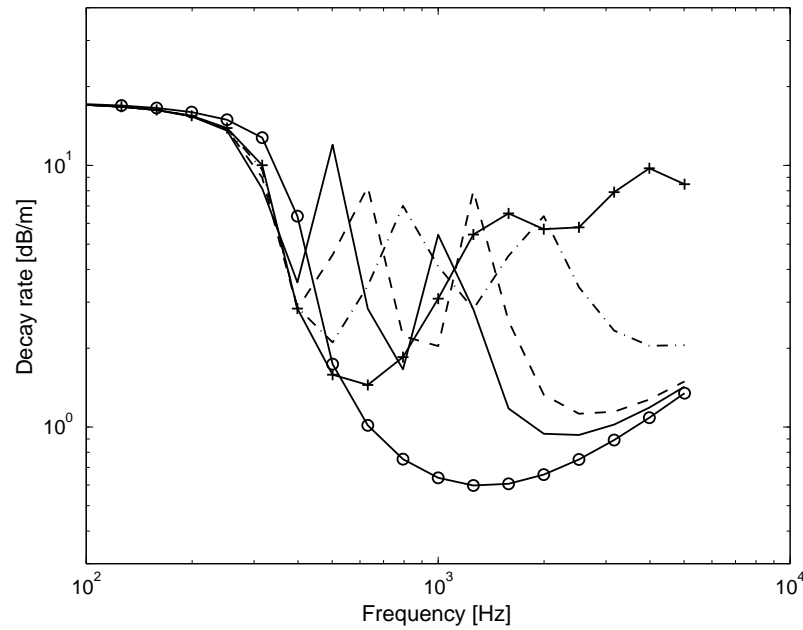
Figure 7.5: *The decay rate of sample 17 (80/160) using Timoshenko beam (two-stacked mass) model for various temperatures. (–) 40℃, (– –) 20℃, (– · –) 0℃, (+) -20℃ and (◦) undamped*

206

Based on these decay rate values, the noise reductions for all EPDM samples are calculated and the maximum noise reduction and the temperature at which it occurs are listed in Table 7.3. As expected, EPDM sample 12 (104/188) and 17 (80/180) are the best, followed by sample 13 (104/132) and 16 (160/200). Their results are plotted against temperature in Figure 7.6. For sample 12 (104/188) and 17 (80/180) the noise reductions are more pronounced at low temperatures, below 10℃, whereas for sample 13 (104/132) and 16 (160/200) the maximum noise reduction occurs at higher temperatures above 10℃. The maximum noise reduction for samples (12 (104/188) and 17 (80/180)) is 6.5 and 6.8 dB(A) respectively, both occurring at 5℃. For comparison, the maximum noise reductions for butyl material (Figure 6.18) are slightly smaller 6.7 dB(A) and occurred above 10℃.

Table 7.3: *The noise reduction of EPDM compound.*

Particulars	11	12	13	14	15	16	17	18	19a	19b	19c
Filler	216	104	104	216	240	160	80	160	160	160	160
Plasticiser	188	188	132	132	160	200	160	120	160	160	160
Max. noise reduction [dB(A)]	4.2	6.5	6.5	3.8	3.6	6.2	6.8	5.9	5.5	5.3	5.4
Occurrence temp. [℃]	40	5	25	40	40	40	5	40	40	40	40
Temp. weighted noise reduction [dB(A)]	2.0	6.1	5.6	1.7	1.6	4.2	6.2	3.4	3.2	3.1	3.1
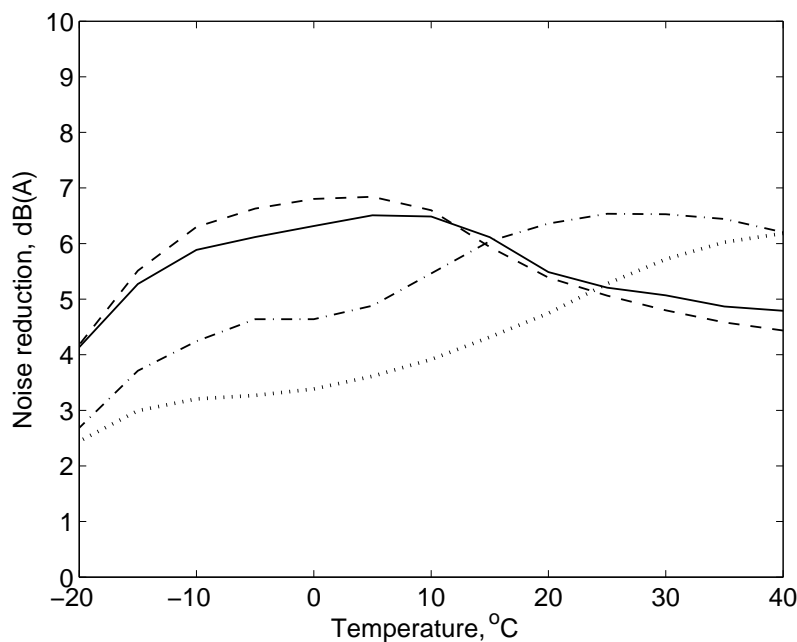
Figure 7.6: *The noise reduction in dB(A) for EPDM (–) sample 12 (104/188), (– · –) 13 (104/132), (· · ·) 16 (160/200) and (– –) 17 (80/160).*

From the overall data gathered, the temperature weighted noise reduction was evaluated and is listed in Table 7.3 and plotted in Figure 7.7(a). At all temperatures, compounds

with high proportions of carbon black do not give significant noise reduction. This is because the materials are too stiff, as seen in Figure 7.3. The results are relatively insensitive to the proportion of oil. The best performance is found for low carbon black loading and high oil loading. This is confirmed in the contour plot shown in Figure 7.7, which was calculated from regression analysis using a second-order polynomial function as described in Appendix A. From Figure 7.7(b), it is clearly seen that the best area to develop further for the rail absorber is with relatively small amounts of carbon black and medium or large amounts of oil (top left corner).

This regression analysis implies that by extrapolating to lower filler proportions still large noise reduction are possible. However, this seem unlikely, as the optimum will be based on G=5MN/m^2 below which the reduction will be smaller.

To verify the amount of carbon black and oil required for the optimum noise reduction, Figure 7.8(a) show the shear modulus plotted against proportion of carbon black for three levels of oil, (○) low level, (□) medium level and (△) high level. The shear modulus is at 1 kHz and 10℃. It is observed that a linear relation is found between the amount of carbon black and shear modulus relatively independent of the amount of oil. Using linear regression analysis, the contour of log shear modulus against the proportions of carbon black and oil is plotted in Figure 7.8(b). The log shear modulus increases with carbon black but is only weakly dependent on the amount of oil. This shows that points at the top left corner of the contour plot are most likely to meet the target requirement.

Referring to Figure 7.6, it appears that it should be possible to arrange for the maximum noise reduction to lie at a sligtly higher temperature than for samples 12 and 17 by increasing the carbon black content slightly and thereby increasing the shear modulus. However, from Figure 7.3 it can be seen that these two samples also have higher loss factors below 10℃ which may also contribute to their good performance.

Comparing this contour plot for EPDM in Figure 7.7 with that for butyl (Figure 6.19), they have a similar trend in that low amounts of filler and high amounts of oil give the best results. The maximum noise reduction occurs at different temperatures; the maximum noise reduction for EPDM is below 10℃ and for butyl is above 10℃. This is shown in Figure 7.9. Overall, the EPDM compound gave a slightly higher reduction of noise than butyl and its effectiveness is stable over a wider temperature range.

7.3.4   Comparison of EPDM with other materials

The studies of butyl and EPDM compounds have shown that both rubbers can give significant noise reduction when used in the rail absorber but their maximum benefit occurs at different temperatures. In Figure 7.10, EPDM sample 17 (80/60) and butyl
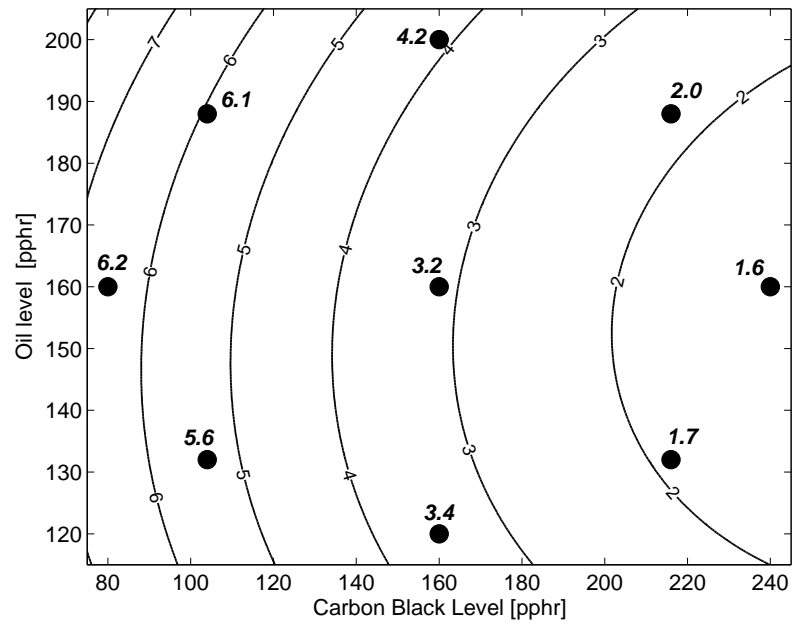
(a)
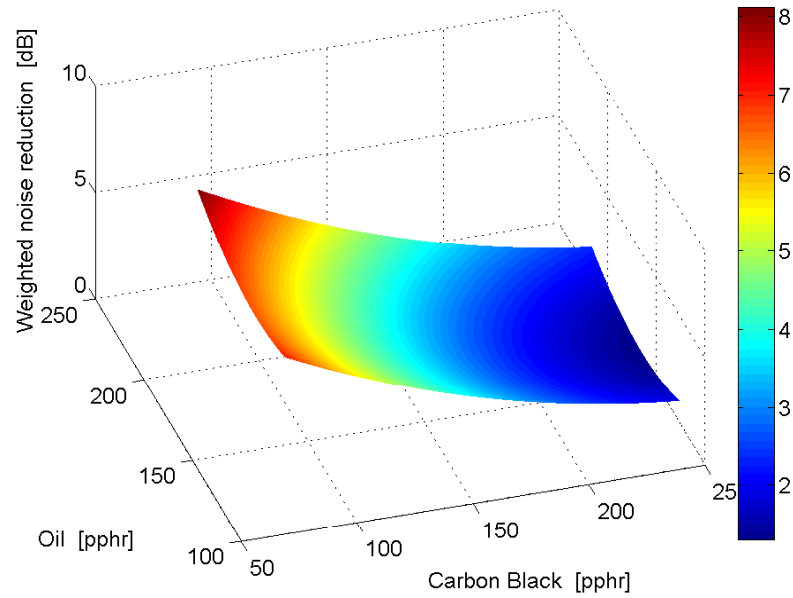
(b)

Figure 7.7: (a) Contour plot and (b) Response surface of temperature-weighted noise reduction (dB(A)) plotted against filler and plasticiser levels for EPDM compounds.
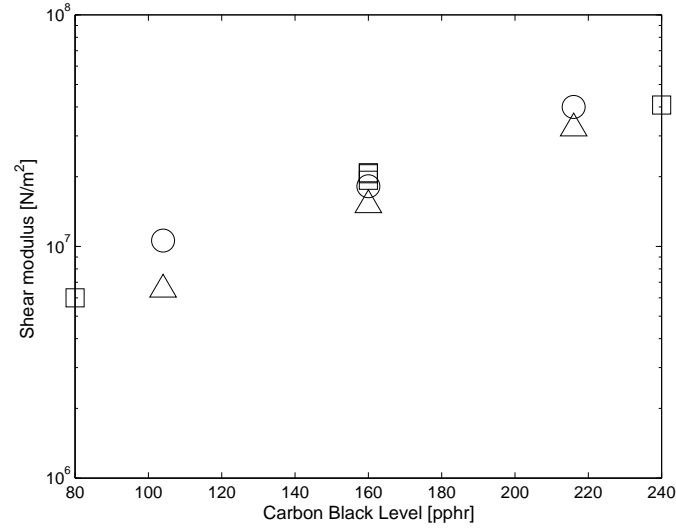
(a)
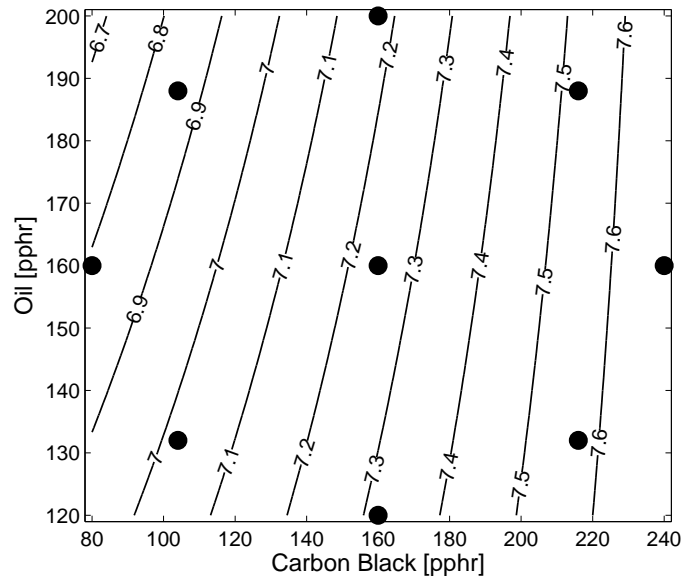
(b)

Figure 7.8: *(a) The relationship of shear modulus at 1 kHz and 10℃ carbon black for different levels of oil. The levels of oil are (○) low, (□) medium and (△) high. (b) The contour of log shear modulus in terms of carbon black and oil. (●) represent the point of mixes in the range of carbon black and oil.*
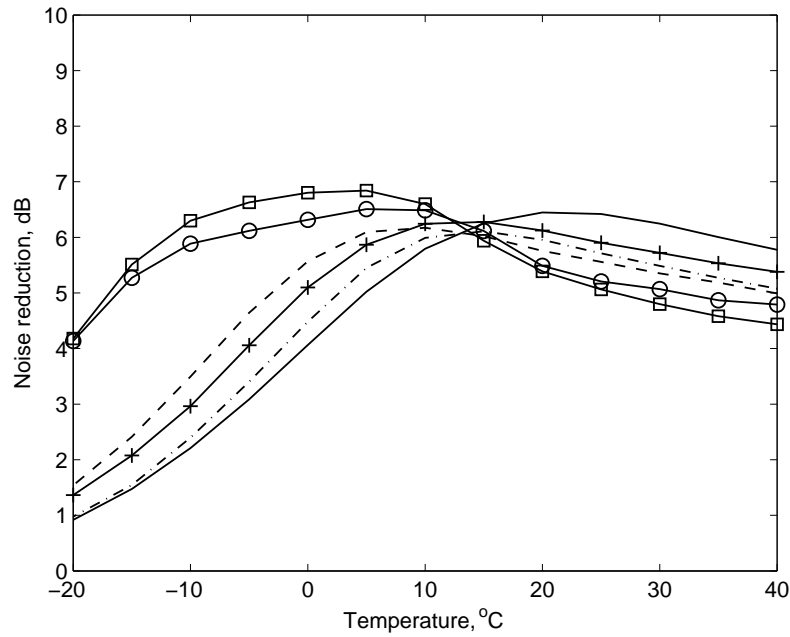
Figure 7.9: *The noise reduction for EPDM and butyl compounds in dB(A). EPDM sample (○) 12 (104/188) and (□) 17 (80/160) and butyl (—) sample 21 (27/17), (−−) 22 (13/17), (+) 26 (20/20) and (− · −) 27 (10/10).*

sample 26 (20/20) are compared with other materials: PU, NR and NBR blend. This shows that the EPDM rubber gives a high reduction of noise and the effectivess is less sensitive with temperature, whereas the other materials (apart from NR) all show a strong decrease in performance at low temperature.

The temperature-weighted noise reduction for each of these materials has been evaluated for the three countries studied in Chapter 4. The temperature-weighted noise reduction is calculated using the weighting factors listed in Table 4.1 and the results are presented in Table 7.4 for the best EPDM and butyl compounds, together with PU, NBR blend and NR. The modulus of the PU material and NR have been measured for the same range of temperatures. These are presented in Appendix B. The results for NBR are from Ahmad (2005) as shown in Table 3.4. EPDM rubbers clearly give higher reductions of noise, at about 6.2 dB(A) for both the UK and Sweden. Conversely, butyl rubber is most applicable for higher temperatures, such as found in Italy, with a noise reduction of 6.0 dB(A), and for the UK the noise reduction is about 5.9 dB(A). In addition, PU gave a similar value of noise reduction for the UK and Italy at 6.0 dB(A). The NBR blend is only satisfactory at higher temperatures. NR rubber is less effective compared with the rest of the materials considered, as it is too soft and has a lower loss factor except at low temperatures. Its maximum noise reduction is only 4.0 dB(A) for Sweden, although from Figure 7.10 it can be seen that at -20℃ it gives a reduction of 6 dB(A).
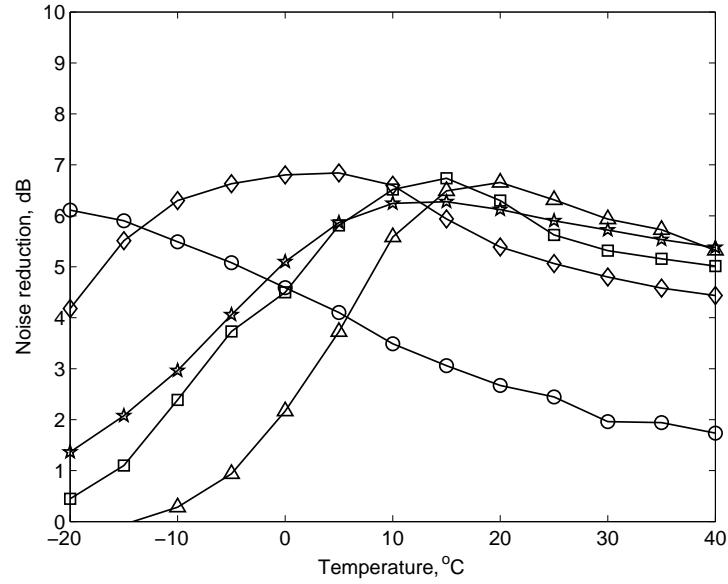
Figure 7.10: *The noise reduction in dB(A) for (⋄) EPDM sample 17 (80/160) and (⋆) butyl sample 26 (20/20) compared to (□) PU (sample 7f), (○) NR and (△) NBR blend (sample 23).*

Table 7.4: *The temperature-weighted noise reduction in dB(A) of various materials for UK, Italy and Sweden.*

Material	Sweden	UK	Italy
EPDM 12(104/188)	6.0	6.1	5.7
EPDM 17(80/160)	6.2	6.2	5.7
Butyl 21(27/17)	4.7	5.7	6.0
Butyl 22(13/17)	5.3	5.9	5.8
Butyl 26(20/20)	5.2	5.9	6.0
Butyl 27(10/10)	4.8	5.7	5.8
PU (sample 7*f*)	5.1	6.0	6.0
NBR blend (sample 23)	3.8	5.2	5.9
NR	4.0	3.4	2.9

7.4 Conclusions

In general, the results from the dynamic tests carried out show that the shear modulus of the EPDM compounds is higher than for the butyl compounds. For temperatures greater than 0℃, the EPDM compounds are three times stiffer than the butyl compounds. However, as temperature decreases, the shear modulus of butyl becomes higher than EPDM. Compared with butyl, the slope of the shear modulus of EPDM with temperature is more gradual. The loss factor of EPDM is consequently much lower than for butyl, in the range of 0.2 to 0.3, increasing at low temperatures. This loss factor is more suitable than that of butyl, although it is at the low end of the required range.

To give an optimum noise reduction in the rail absorber, the EPDM compound should have a loading of carbon black of around 80 pphr and a high loading of oil. Two samples, 12 and 17 are found to be the best EPDM compounds so far, with a potential temperature-weighted reduction of noise of up to 6.2 dB(A).

Both EPDM and butyl rubber, gave a significant noise reduction in the temperature range required. However, their maximum benefit occurs at different temperatures. The EPDM compounds are more suitable for low temperatures, less than 10℃, whereas the butyl rubber is more suitable for higher temperatures, above 10℃. For application to the rail absorber, in terms of temperature-weighted noise reduction, the EPDM is most suitable to be used in the UK and Sweden. Butyl and PU are better for application in warmer climates such as Italy.

EPDM can be tailored for any situation by varying the amount of filler. The results are less sensitive to the oil content. This suggests it could also be possible to find a suitable EPDM rubber with slightly higher filler content for the optimum noise reduction for Italy.

Chapter 8

Conclusions and further work

A methodology has been developed for obtaining an effective viscoelastic material for application to damping devices allowing for their temperature and frequency dependance. The particular application considered is a rail damper but the same approach could be used for many other applications.

A simple model is used to predict the noise reduction of the damping device for a given set of material properties. These properties are measured as a function of frequency for various temperatures. An annual distribution of temperatures is used to form a weighting function for the noise reduction at different temperatures. The temperature-weighted noise reduction can be used as a cost function to allow optimisation of the material for the damping device at any given location.

Based on the information gathered from the literature review, two viscoelastic materials, butyl and EPDM, were used as a basis for the development of optimal formulations. A DOE approach has been used with two variables which relate to the proportions of filler and oil added to the formulations. The results obtained from these materials in terms of temperature-weighted noise reduction show that the behaviour of the rail damper can be improved by using these new materials, especially for colder locations. In summary, the high damping material optimization methodology offers good potential in saving product development cost and time.

8.1 Polymer properties

The glass transition temperature, T_g is a useful physical property that can be measured and reflects the behaviour of a polymer. In the transition region, the damping goes through a sharp peak but the modulus decreases rapidly. The glass transition temperature is important because it determines the temperature range in which a material can be

used effectively as a damping material. For single-phase polymer, the time-temperature superposition principle can be used.

Fillers and materials with strain-crystallisation can be used to increase strength and perhaps increase the breadth of the transition region. This should broaden the operable temperature and frequency range of the damping system. The use of a plastisicer in a polymer will lower the melt viscosity, thus lower the T_g and reduce the modulus at low temperature.

From seven candidate rubbers identified, butyl rubber, EPDM, PU and NBR appear to be practical for the rail absorber application. Of these, butyl rubber and EPDM were selected to be studied further. This selection was not only based on their dynamic properties but on other criteria such as cost-effectiveness, material availability and processing method.

8.2   Method of prediction

Knowing the polymer properties together with appropriate mathematical models, the noise reduction for the rail absorber can be predicted efficiently. The track vibration was calculated using a Timoshenko beam model and the change in decay rates was used to estimate the noise reduction. This approach was validated by comparison with previous results calculated using a more detailed finite element model in TWINS.

In this prediction method, the reduction of noise is estimated from the increase in the decay rate of the vertical wave in the track. This wave is more pronounced in the radiated noise and the absorber is optimised for this component of vibration. To simplify the analysis, the lateral component was neglected, since its effect is small compared with vertical component.

The reduction of noise is influenced by changes in temperature. Knowing that the stiffness of the elastomer in the absorber is very sensitive to temperature, an approximate technique has been adopted to estimate this effect. By assuming a constant loss factor, the variation in stiffness across the temperature range can be estimated assuming only a value for the temperature, T_s as used in the WLF equation. A value of -20℃ has been adopted as typical. It is shown that the noise reduction can be maintained within 1 dB of the maximum effect in a range -10℃ to 40℃ for most values of loss factor. To achieve the maximum noise reduction over a range of temperatures, it appears that the loss factor should be between about 0.25 and 0.4.

An absorber with two tuning frequencies gives a better performance than a single- frequency absorber. The reduction of noise was larger and was sustained over a wider range

of temperatures. From the prediction based on measured material properties, using a standard two-mass absorber, it is found that in most cases the reduction of noise is acceptable for temperatures above 10℃, but below this temperature the effectiveness of the absorber is much less. This is because the loss factors of these materials are too high, making their stiffness very sensitive to temperature. Therefore, new materials with a more moderate loss factor (in the range 0.25 to 0.4) are required to improve the performance of the rail absorber in the range of temperature -20℃ to 40℃.

Knowing that the noise reduction varies with changes of temperature, a method was developed to predict the average noise reduction over a long time period using the temperature distribution throughout the year. These distributions are not required to be highly accurate, only to give an indication of the distribution of temperature over a year. They can be used as weighting functions for the noise reduction to ensure that the rail absorber design is focussed on the temperatures that occur most commonly at a given location.

The rail temperature distributions obtained for the UK show that the temperature varies between -10℃ and 40℃, with the most common temperature around 10℃. For Italy the range is higher, between 0℃ and 45℃ whilst for Sweden it is between -25℃ and 35℃, with a longer tail towards low temperatures. For the UK, it is important that a large noise reduction is obtained at 10℃ (the most common temperature in UK). For Italy a slightly stiffer material is required to give the maximum noise reduction at around 15℃, while for Sweden a slightly softer material is required. The best performance for each of these countries was found using a loss factor of around 0.4, although the results are not very sensitive to the exact value of the damping. The temperature-weighted noise reduction allows the suitability of a given material for the rail absorber to be expressed as a single number. This allows optimisation of materials to be carried out more readily than in previous work (Ahmad, 2005) where several metrics were considered simultaneously.

8.3 Test rig

An existing test rig for the measurement of dynamic stiffness has been analysed and sources of disturbance to the measured data have been identified. The problems occur at low frequency when the test piece is stiff and at high frequency when the test piece is soft.

For stiff materials, the erratic behaviour is caused by an insufficiently high impedance of the seismic mass. Increasing the seismic mass from 12 kg to 31 kg has reduced the

disturbance behaviour around 300-500 Hz, widening the range of valid data. The bench stiffness does not have a significant effect.

The frame of the test rig also contributes a problem of resonance at around 200 Hz as well as a short-circuiting effect at high frequency. These were avoided by installing six soft mounts between the frame and seismic mass to isolate the vibration.

The disturbance at high frequency was dominated by the internal resonances of the samples. This problem is resolved by using thinner samples (2 mm). However, the thinner samples make matters worse at low temperature where the stiffness will be even higher. Therefore, the sample thickness must be chosen according to the stiffness of the material.

The modifications to the seismic mass, the isolation of the frame from the seismic mass and the use of thinner samples gives wider data validity and more accurate dynamic measurement of shear modulus and loss factor. Nevertheless, it has been found to be quite difficult to install the rubber samples between the central shaft and the outer yoke in a way which is consistent. It is therefore necessary to repeat the tests for each material in order to ensure consistent results.

8.4   Material development

Two potential materials were chosen for further development, butyl and EPDM rubber. Both materials had properties which agreed partially with the requirements for the rail absorber. The introduction of plasticiser and filler to both rubbers helps to improve the dynamic properties in the temperature range considered.

The use of filler increases the shear modulus at the higher temperatures but decreases the loss factor peak. This increases the tail of the loss factor curve at low and high temperatures, which helps to keep the loss factor above 0.25 for a wider temperature range. The plasticiser, a paraffinic oil, decreases the shear modulus at low temperatures. The plasticiser also helps to increase the peak value of the loss factor and broaden the transition region, but a large amount of plasticiser will tend to lower the tail of the loss factor curve and thereby decrease the value of loss factor at high temperatures.

A design of experiments (DOE) approach has been used to select a number of compounds for testing. The DOE approach is efficient and gives enough information of the effects of several variables for a small number of experiments. The DOE was used to investigate the dynamic properties for different combinations of filler and plasticiser for both rubbers. It is seen that the butyl rubber is suitable for use in the rail absorber giving high noise reductions between 0℃ and 40℃. As the temperature decreases, however, this material

loses its effectiveness. The optimum combination of filler and plasticiser is in the range of filler around 5-20 pphr and plasticiser of 5-25 pphr.

The shear modulus of EPDM is much higher than butyl but its loss factor is lower (around 0.2 to 0.3). For temperatures greater than 0℃, the EPDM compound is three times stiffer than butyl. However, as temperature decreases, the shear modulus of the butyl compounds becomes higher than EPDM as the slope of the shear modulus of EPDM with temperature is more gentle than for butyl. To give optimum noise reduction in the rail absorber, the EPDM compound should have a loading of carbon black of about 80 to 100 pphr. The proportion of plasticiser was found to be less critical but was in the range 120 to 200 pphr.

The EPDM and butyl rubber compounds gave a significant noise reduction in the temperature range required. However, their maximum benefit occurs at different temperatures. For low temperature, below 10℃, the EPDM compounds are more suitable than butyl, whereas butyl is suitable for higher temperatures above 10℃. For application to the rail absorber, in terms of temperature-weighted noise reduction, EPDM is most suitable to be used in the UK and Sweden. Butyl and PU are best for application in warmer climates such as Italy.

EPDM can be tailored for any situation by varying the amount of filler. This suggests it could also be possible to find a suitable EPDM rubber with slightly higher filler content for the optimum noise reduction for Italy.

8.5   Recommendation for further work

There remain many areas that can be improved and investigated for developing high damping materials for application to damping devices.

As a first improvement of the models used for assessing the noise reduction due to rail vibration absorbers, the noise radiation from the absorber mass should be investigated. In this work, the vibration of the absorber mass has been neglected in the prediction model and the noise reduction has been calculated from the change in track vibration. This is valid for current absorber designs, as the absorber mass is small compared with the rail and, where the damping is high, the vibration of the absorber mass will not be much greater than that of the rail. However, for different designs with larger masses and where smaller damping loss factors are considered, the radiation of noise from the absorber mass may become significant. The Boundary Element Method (BEM) could be used to investigate this issue to improve the prediction model and therefore obtain a more accurate result.

It should be noted that the noise reductions obtained apply to a single value of rail pad stiffness. For other pad stiffnesses the results will differ.

The effect of temperature on the rail pad stiffness should also be taken into account. In this work, only a single value of rail pad stiffness is used in the prediction of the noise reduction. The rail pad stiffness varies with temperature, but more slowly than the elastomer in the rail damper. Refinements of the predictions could be made by taking this effect into account.

For further improvement of track noise treatments, a better knowledge of the temperature distribution for various countries should be obtained. So far, the temperature distributions for Italy and Sweden have been estimated from data available in terms of minimum and maximum temperature per day over a year. More comprehensive data of rail temperature sampled throughout the day over a whole year, would help in giving accurate weighting factors for the calculation of temperature-weighted noise reduction. The analysis could also be applied to climates where the variations in temperature are greater.

The methodology which has been developed in this thesis could be applied to other applications of damping materials where temperature dependence is important. In this work, only a limited range of temperatures has been considered but in other cases a wider temperature range may be required. Examples include dampers for railway wheels, constrained layer damping treatments for a wide range of applications, damping devices in building and automotive applications, etc.

In railway rolling noise, radiation from the wheel is dominant at frequencies above about 1500 Hz. Train wheel vibration can be treated by applying wheel dampers, which limit the amount of vibration. Wheel dampers come in many different forms. A plate damper, for example, is a simple screen mounted on one side of the wheel. The application temperature for these dampers can exceed 200℃ especially when the train uses block brakes. Therefore, further uses of the methodology to find suitable materials and the effect of temperature on meeting the required target will be worth investigating.

Another damping device which can be explored in terms of its temperature dependence is a constrained layer damping treatment (CLD). These devices are a viscoelastic layer which is attached to the structural member with a constraining plate attached to force it into shear. This approach has been widely studied before, for example in an automotive application, where the CLD is used to reduce the noise radiation from the vibrating floor panel (Balmes & Germes, 2002). Studies from Balmes & Germes (2002) have included the effect of temperatures (0℃- 40℃) on the CLD. However, the methodology developed have could be used to optimise its performance through material design.

Tall buildings are sometimes fitted with various energy absorption devices including viscoelastic tuned dampers to mitigate the dynamic responses of the building structures due to wind- and earthquake-excitation (Min *et al.*, 2004; Shukla & Datta, 1999). Temperature and frequency are two factors that affect the performance and hence the effectiveness of these viscoelastic dampers. The study by (Min *et al.*, 2004) shows that the loss factor is very sensitive to changes of temperature. Therefore, using the methodology developed here it will possible to design a more effective viscoelastic damper for building structures.

In addition, for automotive applications, tuned mass dampers are used for example in halfshafts and driveshafts, gear levers, steering wheels, exhaust systems, etc (Aubert & Howle, 2007). They are used to address undesirable vibration responses in vehicles. There are many factors that affect the performance of the dampers which include tuning for temperature variations. The use of the present methodology may help to determine the suitable material to improve the performance of these dampers.

Appendix A

Design of experiments

A.1 What is design of experiment?

When an experiment is performed in which more than one parameter can be varied, it is important to determine the influence of those multiple parameters, including their interaction, in an efficient way.

A design of experiment (DOE) is a statistical method leading to structured and organized experiments for determining the relationship efficiently between the factors (Xs) and the outputs of a process (Ys) (Montgomery, 1997). The DOE involves several elements such as the systematic variation of input quantities, the observation of the resulting effect on output quantities and a mathematical model (i.e. regression analysis) which is used to predict the output for the combinations of input parameters that were not run. The observation and experiments in DOE are planned to illuminate the effect of any change in the process.

The purpose of DOE is to determine the relationship between the different factors (including these interactions effects) and to find a region of optimum for the outputs. This can be done by choosing a set of combinations of various independent parameters at which some dependent variable is sampled (e.g., noise reduction). From this, the mathematical model is applied to predict the value of the dependent variable at other combinations of the independent variables which are not covered. Alternatively, interest may be focused on adjusting the values of key input factors to maximise/optimise the quality of the output.

In general, the DOE can be used in many situations such as comparative experiments,

screening experiments and response surface modelling (RSM). Comparative experiments are used to choose one among several factors that suit the goal of the experiment. Screening experiments are used to select or screen out a few important effects among less important ones. Response surface modelling is used to find the optimum of the output and also to 'fine tune' the process to meet the target of the experiment. Among these three approaches, the RSM is the most suited to the target of the present study. Besides that, the DOE is used to enhance and speed up the process of development of better products and reduce the experimental work, costs and consumption of resources during research study as the number of experiments run can be kept small.

To complete the DOE process, a regression model is required to determine the effect between the variations. It is used to predict values of the dependent variables from one or more independent variables. The selection of the regression model depends on whether the data approximately fit a straight line, for a linear regression, or a more complex form such as a quadratic regression. The most common mathematical models fit the experimental data using either linear or quadratic regression (NIST/SEMATECH, 2008). The following equation is for the simple linear regression that fits data of dependent variable Y for given a single independent variable X.

$$Y = a + b_1 X \tag{A.1}$$

where b_1 represents the slope of the regression line and a is the intercept.

A model that takes account of more than one independent variable is called a multiple regression model. For two independent variables the form of the linear regression model is

$$Y = a + b_1 X_1 + b_2 X_2 + b_3 X_1 X_2 \tag{A.2}$$

where a is the intercept, $b_1, ..., b_3$ are the regression coefficients, X_1 and X_2 are the independent variables and $X_1 X_2$ represents interaction effects.

A quadratic (second-order) regression model can be used where it is suspected that the response surface has curvature. For two independent variables the equation is written as

$$Y = a + b_1 X_1 + b_2 X_2 + b_3 X_1 X_2 + b_4 X_1^2 + b_5 X_2^2 \tag{A.3}$$

where Y is the dependent variable, X_1 and X_2 are the independent variables, a is the intercept, $b_1, \cdots, b_5$ are the regression coefficients. The cross term $X_1 X_2$ is included to

account for the interaction effects between X_1 and X_2.

A.2 Choosing an experimental design

A.2.1 Set objectives

The DOE begins by setting objectives. This is important in order to choose the correct experimental design for determining the required results. In the present case the objective is to find the best combination of filler and plasticiser in a rubber mix, to achieve a high noise reduction in a rail damper.

A.2.2 Selection of variables and levels

The next step is to develop a process model, as shown in Figure A.1, to select the process factors for the study. The process model consists of both controlled input factors and output responses, and uncontrolled co-factors which may be discrete or continuous. The variables in this process may be many, depending on the objective of the experiment. In the present study, the controlled input variables are the proportion of filler and plasticiser, the output response in this case is the noise reduction. The shear modulus and loss factor can also be considered as outputs. There are also a number of "uncontrolled" factors such as temperature and humidity and discrete effects such as the assembly of the sample in the test rig. The machine operators may also have an influences. The mathematical model will be used to link the outputs and inputs.
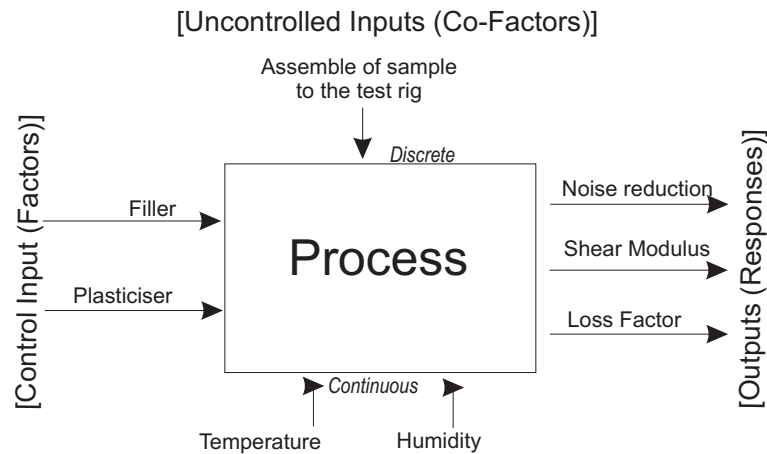
Figure A.1: *An example of process model for DOE based on (NIST/SEMATECH, 2008).*

Then it is necessary to select the number of design levels for each factor. The number of design levels depends on the experimental design model. The most popular experimental

designs are two-level designs. These are ideal for screening designs, as they are simple and economical (Montgomery, 1997). Figure A.2 illustrates two-level-designs, which have only a "high" and a "low" setting for each factor, X_1 and X_2. The standard notation to denote the high and low levels are +1 and -1. These are called the design code. This figure also shows four experimental points with design codes (1,1), (-1,1), (1,-1) and (-1,-1). It is recommended to add centre points in the two-level design (centre points are located in the middle of the design between high and low levels), with a design code of (0,0).
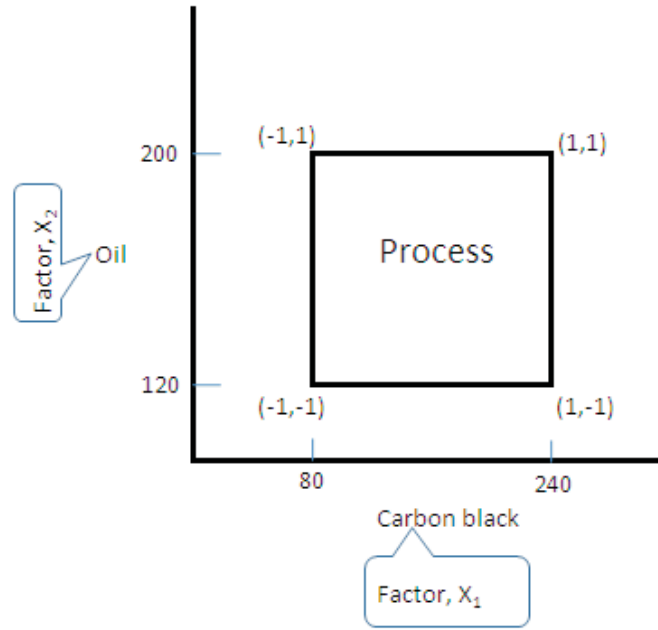
Figure A.2: *An example of the 2 factors in 2-level experimental design.*

A.2.3   Selection of experimental design

The selection of the experimental design is based on the objectives of the experiment and the number of factors to be studied. There are several choices of experimental design that can be used to investigate two or more factors, for example factorial designs and central composite design.

Factorial design uses discrete possible levels for each of two or more factors. Two-level factorial designs considering each factor and their interactions are the most popular.

A full factorial design considers each combination of each factor at two or more levels, as shown in Figure A.3. For simplicity only, the two-level design will be discussed. For two-level designs each input factor is considered at 'high' and 'low' levels or '+1' and '-1' respectively. The number of runs required for a full factorial design can be determined as

2^k, where k is the number of factors. As the number of factors increases the number of runs rapidly becomes larger. Therefore, the full factorial designs are not recommended for 5 or more factors (NIST/SEMATECH, 2008).
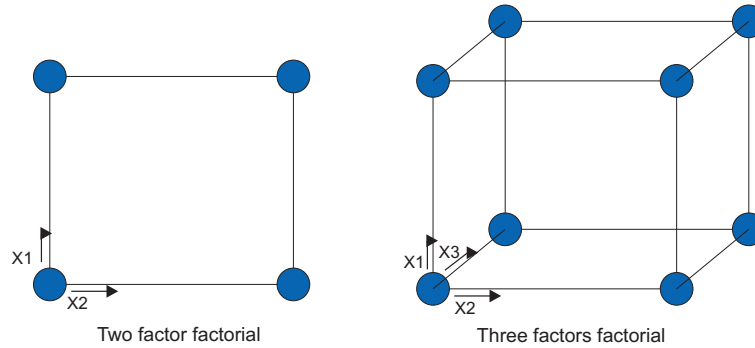
Figure A.3: *An example of the 2 factors in 2-level experimental design.*

If the number of experiments for a full factorial design is too many to be run, a fractional factorial design may be considered. Fractional factorial design uses only a fraction of the runs required by a full factorial design. A number of runs is selected based on an evaluation (or assumption) of which factors and interactions have the most significant effects. Similar to the full factorial design, fractional factorial design can also be used with three or more levels. In general, 1/2 or 1/4 of runs from the full factorial design are used for the fractional factorial design.

Although the use of fractional factorial design is more economical than full factorial design, it will not be able to evaluate the impact of some of the factors independently. The results estimated by fractional factorial design may therefore not be as good as for full factorial design.

Full or fractional factorial designs are rarely used for more than two-level designs. The response surface methodology usually requires more detail than a two-level design can provide so alternatives such as central composite design are preferred.

A.2.3.1 Central composite designs

The central composite design (CCD) is an experimental design used to study the combined effects of seveal variables. The CCD uses five levels, $-\alpha$, -1, 0, +1, $+\alpha$. The combinations considered include the factorial design points (corner) (Figure A.4(a)i), star points (Figure A.4(a)ii) and centre points. This allows estimation of curvature or quadratic terms. The corner points are formulated on the basis of full or fractional factorial design with the distance from the centre of the design space to a factorial point (a_i) of ± 1 unit for each factor. The star points represent new extreme values (low and high) for each factor in the design and the distance from the centre of the design space to a star point (b_i)

is $\pm\alpha$ with $|\alpha| \geq 1$ (NIST/SEMATECH, 2008). There are twice as many star points in the CCD design as the number of factors k, ie $2k$. The centre point is the median of the values used in the factorial portion. This point is often replicated in order to improve the precision of the experiment, as well as provide a measure of process stability and inherent variability.

There are three types of CCD: circumscribed (CCC), inscribed (CCI) and face-centered (CCF) designs. Figure A.4(b) shows 2D schematic diagrams demonstrating these designs. In each case the prediction region is normally limited to values of the control parameters scaled to $[-1,+1]^k$.

The CCC designs are the original form of central composite design. The star points that lie outside the region of interest for prediction at $[-\alpha, \alpha]$ for all factors. These designs have circular, spherical or hyperspherical symmetry which require 5 levels for each factor.

The CCF designs have star points at the centre of each face of the factorial space, such that $\alpha = \pm 1$. This designs required 3 levels of each factors.

The CCI design is a scaled down version of CCC design with each factor level of the CCC design divided by α. The prediction region in the CCI is in effect expanded to $[-\alpha, \alpha]^k$. This design also requires 5 levels for each factor of these three designs. The CCC and CCI are rotatable designs but CCF is not. A design is rotatable when the variance of the predicted response is the same at all points x that are at the same distance from the centre point. Therefore, the rotatable designs give equal precision of estimations in all directions. This rotatability is needed for RSM, especially for the quadratic model designs.

The number of observations (experimental trials) required for the CCD is determined from the following equation,

$$n_T = 2^{k-f} + 2k + n_0 \tag{A.4}$$

where 2^{k-f} corresponds to the factorial design, where k is the number of factors and f allows for a fractional factorial design, $2k$ is the number of star points and n_0 is the number of replications at the centre point.

The value of α is chosen to maintain rotatability and depends on the number of experimental runs in the factorial design of the central composite design, such that $\alpha = $ [number of factorial runs]$^{1/4}$. An example of α for a two-level factorial designs is

$$\alpha = [2^{k-f}]^{1/4} \tag{A.5}$$
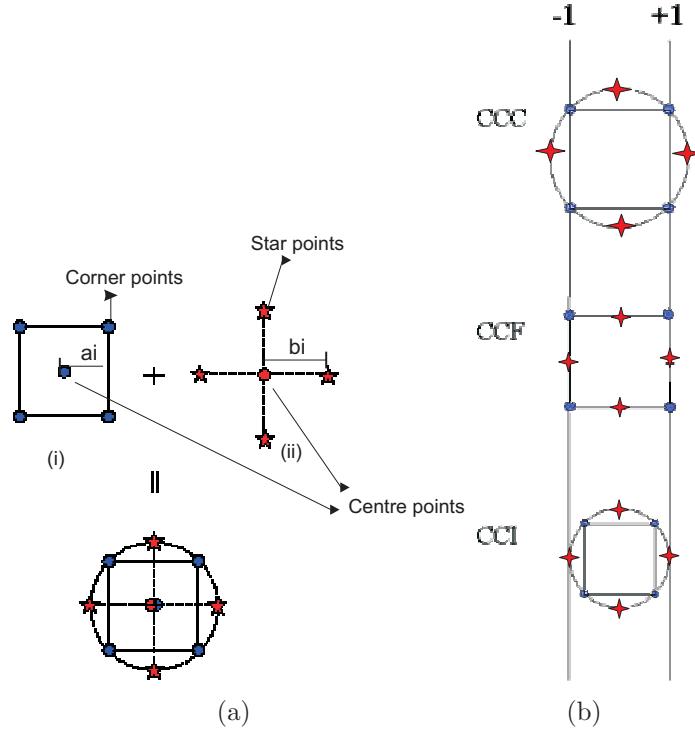
Figure A.4: *(a) The central composite design for two factors illustrates the points designs and (b)Selections of CCD: Circumscribed (CCC)-required 5 levels, new extreme values and rotatable, Inscribed (CCI)-required 5 levels, old extreme retained, rotatable and face centred (CCF)-required 3 levels, old extreme retained, not rotatable. . (NIST/SEMATECH, 2008).*

For a full factorial design with two factors and $n_0=3$, $n_T=11$ and $\alpha=\sqrt{2}$.

A.3 Example of central composite design

In this thesis, to study the influence of two independent factors, carbon black (X_1) and oil (X_2), a five-level central composite design was used to determine the optimum noise reduction. A quadratic model was employed. Each independent factor has five levels which were $-\alpha$, -1, 0, $+1$, $+\alpha$. Using Eq. (A.4), a total of 11 different combinations including three replications at the centre points are used as listed in Table A.1. In this example, corresponding to EPDM, the low and high values of the two independent variables are 104 and 216 for carbon black and 132 and 188 for oil. The coded values of the independent variables were found from the following equation and both coded and uncoded independent variables are given in Table A.1.

$$X_j = \frac{actualvalue - \frac{highlevel+lowlevel}{2}}{\frac{highlevel-lowlevel}{2}} \tag{A.6}$$

Table A.1: *Coding scheme for* 5^2 *factorial design of the CCD. (Example of filler and oil added to EPDM rubber)*

runs	Coded X_1	Coded X_2	Uncoded X_1,	Uncoded X_2
1	+1	+1	216	188
2	-1	+1	104	188
3	+1	-1	216	132
4	-1	-1	104	132
5	+1.414	0	240	160
6	-1.414	0	80	160
7	0	+1.414	160	200
8	0	-1.414	160	120
9	0	0	160	160
10	0	0	160	160
11	0	0	160	160

A quadratic equation (Eq A.3) was used to express the noise reduction as a function of independent variables, carbon black X_1 and oil X_2 where Y represents noise reduction in dB(A).

Appendix B

Dynamic properties of PU and NR

B.1 PU material

Figure B.1 shows the shear modulus and loss factor for the PU material, previously used in the rail absorber. It was tested using the modified ISVR test rig at various temperatures and frequencies. The data at 1000 Hz were used for comparison to butyl and EPDM rubber in this work. The data at 300 Hz are not reliable and should be neglected.
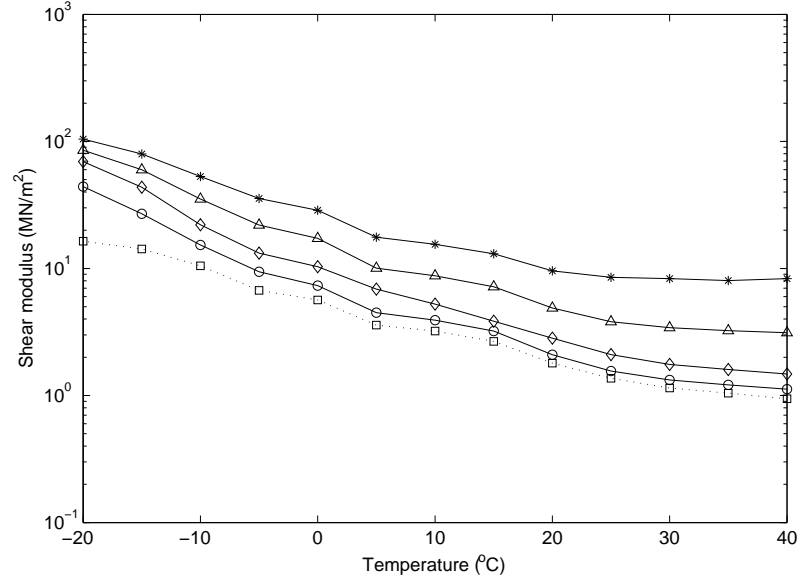
(a)
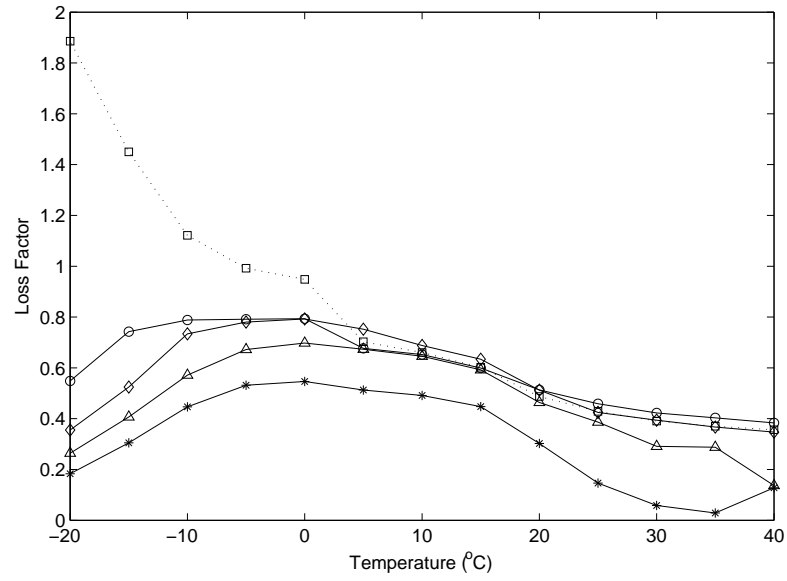
(b)

Figure B.1: *(a) Shear modulus and (b)loss factor of PU material at various frequencies. The curves are (□) 300 Hz, (○) 500 Hz, (◇) 1 kHz, (△) 2 kHz and (∗) 3 kHz.*

B.2   Natural Rubber (NR)

NR samples were also tested using the modified ISVR test rig for a temperature range of 40℃ to -20℃ and a frequency range of 300 to 3000 Hz. Results are shown in Figure B.2. The data at 1 kHz were used as a comparison in this work. The data at above 2 kHz are not reliable because of the internal resonance of the samples.

(a)

(b)

Figure B.2: *(a) Shear modulus and (b) Loss factor of NR at various frequencies. The curves are (□) 300 Hz, (○) 500 Hz, (◇) 1 kHz, (△) 2 kHz and (∗) 3 kHz.*

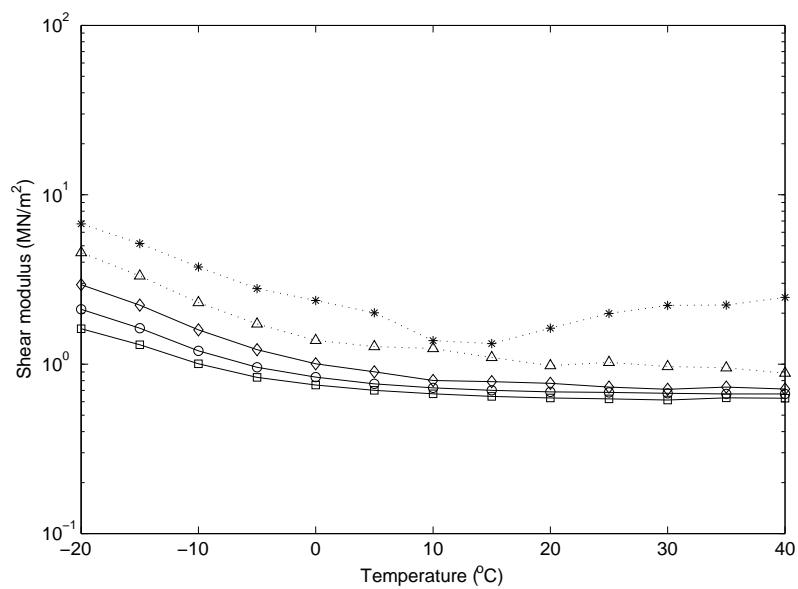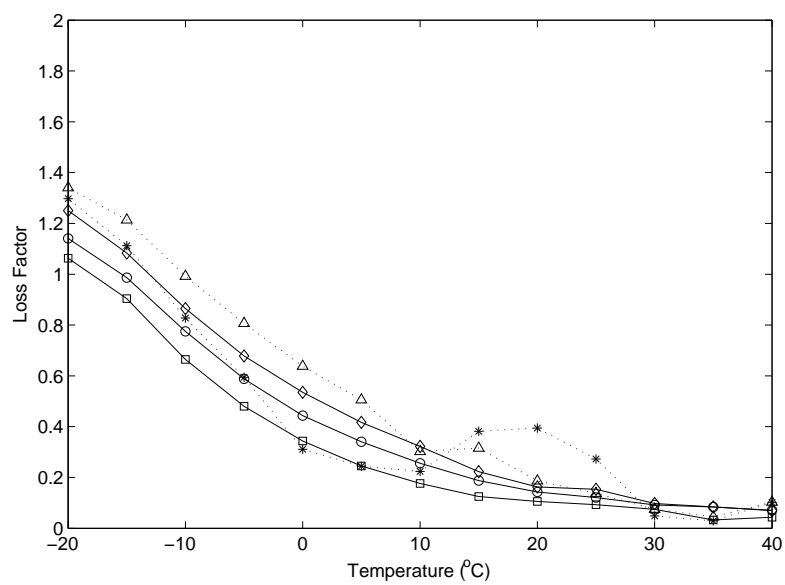# References

AHMAD, N. (2005). *Damping material selection for a rail absorber*. Master's thesis, Institute of Sound and Vibration Research, University of Southampton.

AHMADI, H.R. & FULLER, K.N.G. (1994). *DTA module 51*. Tun Abdul Razak Research Centre.

AHMADI, H.R. & MUHR, A.H. (1994). Use of rubber to suppress ringing of metal components. *Institute of Materials Conference on Quieter Transport with Rubber - Shock, Vibration and Noise Control for the Benefit of User and Environment. University of the West of England, Bristol.*

AHMADI, H.R., FULLER, K.N.G. & MUHR, A.H. (1992). High frequency dynamic properties of natural rubber. *Journal of Natural Rubber Research*, **7**, 181–194.

ALLCOCK, H.R. (1977). Poly(organophosphazenes)-unusual new high polymers. *Angew Chem Int Ed Engl*, **16**, 147–56.

ALLCOCK, H.R. (2002). *Chemistry and application of polyphosphazenes*. Wiley Interscience New Jersey.

ALLCOCK, H.R., MANG, M.N., DEMBEK, A.A. & WYNNE, K.J. (1989). Poly[(aryloxy)phosphazenes] with phenylphenoxy and related bulky side groups. synthesis, thermal transition behaviour and optical properties. *Macromolecules*, **22**, 4179–90.

AUBERT, A. & HOWLE, A. (2007). Design issues in the use of elastomer in automotive tune mass damper.

BALL, G.L. & SALYER, I.O. (1966). Development of viscoelstic composition having superior vibration-damping capability. *Journal of the Acoustical Society of America*, **39**, 663–673.

BALMES, E. & GERMES, S. (2002). Tools for viscoelastic damping treatment design: Application to an automotive floor panel. *ISMA2002, Leuven, Balgium.*, **1**, 461–470.

BEAUBATIE, L. (1997). Absorbeur de bruit pour rails d'une voie ferre, European Patent EP 0 761 879 A1.

BLOW, C.M. (1971). *Rubber technology and manufacture*. Butterworth and Co. Ltd London.

BRANDRUP, J. & IMMERGUT, E.H. (1989). *Polymer Handbook*. Wiley New York.

BRITANNICA (2005). Technical data-thiokol. www.britannica.com.

CHAPMAN, L.T. (2007). Modelling of rail surface temperatures: a preliminary study. *Theoretical and Applied Climatology*, 121–131.

CHOI, S.S., PARK, B.H. & SONG, H. (2004). Influence of filler type and content on properties of styrene-butadiene rubber (sbr) compound reinforced with carbon black or silica. *Polymers for Advance Technologies*, **15**, 122–127.

CHRISTENSEN, R.M. (1971). *Theory of viscoelasticity - an introduction*. Academic Press Inc New York and London.

DERHAM, C.J., KELLY, J.M. & THOMAS, A.G. (1985). Nonlinear NR bearings for seismic isolation. *Nuclear Engineering and Design*, **84**, 417–428.

DIRECTIVE-2002/49/EC (2002). Directive 2002/49/EC of the European Parliament and of the Council-relating to the assessment and management of environmental noise.

DUPONT (2006). Designing with elastomer. www2.dupont.com.

ECKER, R. (1968). Kautsh, Gummi, Kunstst 21(304): Quoted in G. Kraus (1971). *Advanced Polymer Science*, **8**.

EDILON (2007). Edilon tuned rail damper.

EGGERS, H. & SCHMMER, P. (1996). Reinforcement mechanisms in carbon black and silica loaded rubber melts at low stresses. *Rubber Chemistry and Technology*, **69**, 253.

EUROPEAN CLIMATE ASSESSMENT AND DATASET (2007). Temperature distribution. www.eca.knmi.nl.

EWINS, D.J. (1997). *Modal testing: theory, practice and application*. Research Studies Press Ltd England, 2nd edn.

FERRY, J.D. (1970). *Viscoelastic properties of polymers*. John Wiley and Sons-New York, 2nd edn.

FLETCHER, W.P. & GENT, A.N. (1973). Dynamic shear properties of some rubber-like materials. *British Journal of Applied Physics*, **8**, 194–201.

FODIMAN, P. (1996). Line test validation of low noise railway components. WCRR '96. *Colorado Spring (USA)*, 497–502.

FOX, T.G. & FLORY, P.J. (1950). Second-order transition temperatures and related properties of polystyrene. i. influence of molecular weight. *Journal of Applied Physics*, **21**, 581–91.

FOX, T.G. & FLORY, P.J. (1956). Influence of diluent and of copolymer composition on the glass temperature of a polymer system. *Bulletin of American Physical Society*, **1**, 123.

FUJINO, K., SENSHU, K. & KAWAI, H. (1961). Tensile stress relaxation behaviour of partly to completely acetylated polyvinyl alcohol polymers. *Journal of Colloid Science*, **16**, 411.

GARDONIO, P. & BRENNAN, M.J. (2004). *Mobility and impedance methods in structural dynamics In: Fahy, F. and Walker, J. (eds): Advanced Applications in Acoustics, Noise and Vibration:*. Spon Press London.

GAUTIER, P.E. (2000). A review of railway noise research and results since the 5th IWRN in Voss (Norway). *Journal of Sound and Vibration*, **231**, 477–489.

GEORGE, L.B. & IVAL, O.S. (1966). Development of a viscoelastic composition having superior vibration-damping capability. *Journal of Acoustic Society of America*, **39**.

GINIC-MARKOVIC, M., DUTTA, N., DIMOPOULOS, M., CHOUDHURY, N. & MATISONS, J. (2000). Viscoelastic behaviour of filled, and unfilled, EPDM elastomer. *Thermochimica Acta*, **357-358**, 211–216.

GNANARAJAN, T.P., IYER, N.P., NASAR, A.S. & RADHAKRISHNAN, G. (2002). Preparation and properties of poly(urethane-imide)s derived from amine-block polyurethane prepolymer and pyromellitic dianhydride. *European Polymer Journal*, **38**, 487–495.

GRAFF, K.F. (1997). *Wave motion in elastic solids*. Dover Publications, New York (Mineola, NY).

HEMSWORTH, B., GAUTIER, P.E. & JONES, R. (2000). Silent freight and silent track projects. *Internoise 2000 Nice, France*.

HEPBURN, C. (1982). *Polyurethane Elastomer*. Applied Science Publishers London and New York.

HODGSON, W., CLARKE, .J.B., FARRINGTON, D., THOMPSON, D.J. & JONES, C.J.C. (2000). Rail fixings, European Patent EP1015698.

HOFMANN, W. (1963). Nitrile rubber: Rubber chemistry and technology. *A rubber review*, 154–160.

HOFMANN, W. (1989). *Rubber Technology Handbook*. Hanser Publisher New York.

JENCKEL, E. & HERWIG, H.U. (1956). *Kolloid-Z*, **148**.

JONES, C. (2005). A comparison of the performance of two alternative elastomers used in a rail damping device. *ISVR Contract Report No. 05/01 Confidential*.

JONES, C.J.C. (2003). *Description of measurement apparatus*. Institute of Sound and Vibration Research.

JONES, C.J.C. & EDWARDS, J.W. (1996). Development and testing of wheels and track components for reduced rolling noise for freight. Internoise 96, liverpool.

JONES, C.J.C., THOMPSON, D.J., ARMSTRONG, T.D. & THITE, A. (2001a). Measurement of the material properties of additional damping materials for use in rail vibration absorber. Tech. rep., ISVR Contract Report No. 01/05 for the Silent Tract Project. (Confidential).

JONES, C.J.C., THOMPSON, D.J., ARMSTRONG, T.D. & THITE, A. (2001b). Measurement of the material properties of additional damping materials for use in rail vibration absorber. Tech. rep., ISVR Contract Report No. 01/05 for the Silent Tract Project. (Confidential).

JONES, C.J.C., THOMPSON, D.J. & DIEHL, R.J. (2006). The use of decay rates to analyse the performance of railway track in rolling noise generation. *Journal of Sound and Vibration*, **293**, 485–495.

JONES, D.I.G. (1990). On temperature frequency analysis of polymer dynamic mechanical behaviour. *Journal of Sound and Vibration*, **140**, 85–102.

JONES, M.S. (1991). Polyphosphazene elastomers in the oil field. *Rubber World*, **91**, 33–35.

KRAUS, G. (1978). *Sciences and Technology of Rubber*. Academic Press, New York.

KRAUS, G. & ROLLMAN, K. (1971). *Angew. Makromol. Chem.*, **16**, 271.

LAURENCIN, C.T. & NAIR, K.S. (2003). Polyphosphazene nanofibers for biomedical applications: preliminary studies. *Conference NATOASI2003*.

LINDLEY, P.B. (1992). *Engineering design with natural rubber. Natural Rubber Technical Bulletin*. The Malaysian Rubber Producers' Research Association, 5th edn.

MACIOCE, P. (2003). Viscoelastic Damping: Sound and Vibration-101.

MACKEY, D. & JORGENSEN, A. (1999). *Elastomers and synthetic (nitrile rubber)*. Kirk-Othmer Concise Encyclopedia of Chemical Technology, 4th edn.

MEDALIA, A. (1978). Effect of carbon black on dynamic properties of rubber vulcanizates. *Rubber Chemistry and Technology*, **51**, 437–523.

MIEDEMA, H. & VOS, H. (1998). Exposure-response relations for transportation noise. *Journal of the Acoustical Society of America*, **104**, 3432–3445.

MIN, K.W., KIM, J. & LEE, S.H. (2004). Vibration tests of 5-storey steel frame with viscoelastic dampers. *Journal of Engineering Structures*, **125**, 831–839.

MONTGOMERY, D.C. (1997). *Design and Analysis of Experiments*. John Wiley and Sons. New York, 4th edn.

MOORE, G.R. & KLINE, D. (1984). *Properties and Processing of Polymers for Engineers*. Prentice-Hall International, Inc.

MORTON, M. (1995). *Rubber Technology*. Chapman and Hall Publishing Co., New York.

NASHIF, A., JONES, D.I.G. & HENDERSON, J.P. (1985). *Vibration damping*. John Wiley and Sons.

NASHIF, A.D. & LEWIS, T.M. (1991). Data base of the dynamic properties of materials.

NIELSEN, L. (1953). Effects of chemical heterogeneity in copolymers on some physical properties. *Journal of American Chemical Society*, **75**, 1435–1439.

NIELSEN, L. (1962). *Mechanical properties of polymer*. Reinhold Publishing Corporation, New York.

NIST/SEMATECH (2008). e-handbook of statistical methods,sec. 5.3.3.6.1, http://www.itl.nist.gov/div898/handbook/, accessed on 20/06/2008.

OERTLI, J. (2000). Cost-benefit analysis in railway noise control. *Journal of Sound and Vibration*, **231**, 505–509.

PAUL, D.R. & NEWMAN, S. (1978). *Polymer blends*, vol. 1 and 2. Academic Press New York.

PAYNE, A. (1962). The dynamic properties of carbon blackloaded natural rubber vulcanizates. part i. *Journal of Applied Polymer Science*, **6**, 57.

PAYNE, A.R. (1996). *Dynamic properties of rubber*. Proceeding of a conference-use of rubber engineering London.

POISSON, F., LETOURNEAUX, F. & MARGIOCCHI, F. (2006). Complete assessment of rail absorbers performances on an operated track in France. *World Congress on Railway Research, Montral, Canada*.

RAMIREZ, A.C. (1995). Development of high damping elastomer blends. *Malaysian Rubber Producer Research Association*.

REAUSCHLE, D.A., MOUNTZ, D.A., BRISTER, B., CURRY, C.L., SHOEMAKE, K.A., STOREY, R.F. & MAURTIZ, K.A. (1997). *ACS Polymer reprint*, **39**, 381.

ROBERT, T.O. (1990). *Vanderbilt Rubber Handbook*. R.T. Vanderbilt Company Inc, Norwalk CT, 13th edn.

RUBBERMILL (2006). Technical data sheet. www.rubbermill.com.

SALAMORE, J.C. (1996). *Concise polymeric material encyclopedia*. CRC Press.

SARTOMER (2005). Temperatures of Sartomer products.

SCHNEIDER, N.S., SUNG, C.S.P., MATTON, R.W. & ILLINGER, J.L. (1975). Thermal transition behaviour of polyurethanes based on toluene diisocyanate. *Macromolecules*, **8**, 62.

SCHWARZL, F.R. & STRUIK, L.C.E. (1968). Analysis of relaxation measurement. *Advance in Molecular Relaxation Processes*, **1**, 201–255.

SHUKLA, A.K. & DATTA, T.K. (1999). Optimal use of viscoelastic dampers in building frames for seismic force. *Journal of Engineering Structures*, **125**, 401–409.

SMITH, T.L. (1978). Strength of elastomers - a perspective. *Rubber Chemistry and Technology*, **51**, 225–252.

SPERLING, L.H. (1990). Sound and vibration damping with polymer. *American Chemical Society*.

SPERLING, L.H. (1992). *Introduction to Physical Polymer Science*. Wiley, New York.

THOMPSON, D.J. (2007). The theory of a continuous damped vibration absorber to reduce broad-band wave propagation in beams. *ISVR Technical Memorandum No: 986 University of Southampton*.

THOMPSON, D.J. (2008). *Railway noise and vibration: mechanisms, modelling and means of control*. Elsevier, Oxford.

THOMPSON, D.J., HEMSWORTH, B. & VINCENT, N. (1996a). Experimental validation of the twins prediction program for rolling noise, part 1: Description of the model and method. *Journal of Sound and Vibration*, **193**, 123–135.

THOMPSON, D.J., FODIMAN, P. & MAHE, H. (1996b). Experimental validation of the TWINS prediction program for rolling noise, part 2: Results. *Journal of Sound and Vibration*, **193**, 137–147.

THOMPSON, D.J., BRISCOE, A. & JONES, C. (1998). Measurement of material properties of various visco-elastic material-part i: Complex young's modulus at room temperature. Tech. rep., Contract Report No. 98/15 for the Silent Track Project (Confidential) ISVR.

THOMPSON, D.J., BRISCOE, A. & JONES, C. (2000). Measurement of material properties of various visco-elastic material-part 2: Complex moduli for additional materials and temperature dependence. Tech. rep., ISVR Contract Report No. 00/06 Confidential.

THOMPSON, D.J., JONES, C.J., WATERS, T.P. & FARRINGTON, D. (2007). A tuned damping device for reducing noise from railway track. *Applied Acoustics*, **68**, 3–57.

TURI, A. (1981). *Thermal characterization of polymeric materials*. Academic Press, Inc. New York.

UNIFE, UIC, CER & UITP (2001). A joint strategy for European rail research 2020-towards a single european railway system.

VAN DEN DOOL, H. (2007). Rail dampers, rail infrastructure gets quiet. *Internoise 2007, Istanbul*.

VOLLMERT, B. (1973). *Polymer Chemistry*. Springer-Verlag, New York.

WANG, X. & LUO, X. (2004). A polymer network based on thermoplastic polyurethane and ethylene-propylene-diene elastomer via melt blending: morphlogy, mechnical properties, and rheology. *European Polymer Journal*, **40**, 2391–2399.

WARD, I.M. (1983). *Properties of Solid Polymers*. Wiley, Second Edition, Chichester.

WHITBY, G.S., DAVIS, C.C. & DUNBROOK, R.F. (1954). *Synthetic Rubber*. Wiley, New York.

WILLIAMS, M.L., LANDEL, R.F. & FERRY, J.D. (1955). The temperature dependence of relaxation mechanisms in amorphous polymers and other glass-forming liquids. *Journal of the American Chemistry Society*, **77**, 3701–3707.

WOOD, L.A. (1958). Glass transition temperatures of copolymers. *Journal of Polymer Science*, **28**, 319–330.

WU, T.X. & THOMPSON, D.J. (1999). Analysis of lateral vibration behaviour of railway track at high frequencies using a continuously supported multiple beam model. *Journal of the Acoustical Society of America*, **106**, 369–1376.